ENHANCED TRANSVERSE MIXING OF POLLUTANTS IN STREAM WITH SUBMERGED VANES

Ph. D. THESIS

by

HIMANSHU SHARMA

DEPARTMENT OF CIVIL ENGINEERING
INDIAN INSTITUTE OF TECHNOLOGY ROORKEE
ROORKEE – 247 667 (INDIA)
APRIL, 2016

ENHANCED TRANSVERSE MIXING OF POLLUTANTS IN STREAM WITH SUBMERGED VANES

A THESIS

Submitted in partial fulfilment of the requirements for the award of the degree of

DOCTOR OF PHILOSOPHY

in

CIVIL ENGINEERING

by

HIMANSHU SHARMA

DEPARTMENT OF CIVIL ENGINEERING
INDIAN INSTITUTE OF TECHNOLOGY ROORKEE
ROORKEE – 247 667 (INDIA)
APRIL, 2016

©INDIAN INSTITUTE OF TECHNOLOGY ROORKEE, ROORKEE - 2016
ALL RIGHTS RESERVED

INDIAN INSTITUTE OF TECHNOLOGY ROORKEE
ROORKEE

CANDIDATE'S DECLARATION

I hereby certify that the work which is being presented in the thesis entitled "**ENHANCED TRANSVERSE MIXING OF POLLUTANTS IN STREAM WITH SUBMERGED VANES**" in partial fulfilment of the requirements for the award of the degree of Doctor of Philosophy and submitted in the Department of Civil Engineering, Indian Institute of Technology Roorkee, Roorkee, is an authentic record of my own work carried out during a period from July, 2010 to Dec 2015 under the supervision of **Dr. Zulfequar Ahmad,** Professor, Department of Civil Engineering, Indian Institute of Technology Roorkee, Roorkee.

The matter presented in this thesis has not been submitted by me for the award of any other degree of this or any other institute.

Signature of the Candidate

This is to certify that the above statement made by the candidate is correct to the best of my knowledge.

Signature of the Supervisor

Dated: …….

The Ph.D. Viva-Voce Examination of **Mr. Himanshu Sharma**, Research Scholar, has been held on……..

Chairman, SRC **Signature of External Examiner**

This is to certify that the student has made all the corrections in the thesis.

Signature of Supervisor **Head of the Department**

ABSTRACT

Streams have been used for the disposal of various industrial and municipal wastes since long time. Quantitative understanding of mixing of such pollutants in streams is a matter of concern in recent years for the effective control of pollution in the streams. Most of the natural streams are relatively shallow compared with their length and width. When pollutants were disposed off at a point/section of a stream, it mixes quickly over the entire depth and then continues to spread in the longitudinal and transverse flow directions. Thus, it is essential to study how the waste/effluent gets mixed in the flowing stream for the environmental concern and water quality modeling. Excluding the initial distance required to achieve mixing in the vertical direction, the mixing of pollutants can be efficiently modeled by two-dimensional depth-averaged mixing equation, i.e., transverse mixing equation. Transverse mixing is arguably more important in water quality management than either vertical or longitudinal mixing, especially when dealing with the discharge of pollutants from point sources or the mixing of tributary inflows. In such problems, vertical mixing occurs rapidly and is only important very close to the source, whereas, longitudinal dispersion is only important in far-field if the source is unsteady.

In straight open channels, secondary currents are weak compared to curved channels, therefore, spreading of pollutant is higher in curved channels compared to the straight channels (Krishnappan and Lau, 1981; Holley and Nerat, 1983; Boxall et al., 2003; Boxall and Guymer, 2003; Albers and Steffler, 2007; Dow et al., 2009). To increase the secondary current for the enhancement of transverse mixing, it is desirable to have some structure, which can increase the secondary current in that reach. Submerged vanes are suitable structure for this purpose. Transverse mixing has extensively been studied in straight, curved, meandering channels. However, no study related to the effect of artificially-induced secondary current on the transverse mixing has been conducted, so far. The present proposal is intended to study this aspect of the transverse mixing.

Submerged vane is basically an aerofoil structure, which generates the excess turbulence in form of helical flow structure in the flow due to pressure difference between approaching flow side and downstream side of vane (Odgaard and Spoljaric, 1986; Odgaard and Mosconi, 1987; Odgaard and Wang, 1991; Wang and Odgaard, 1993). These vanes are in general placed at a certain angle with respect to the flow directions which is usually equal to $10^o – 40^o$. Submerged vanes utilize vorticity to minimize the drag and produce flow redistribution in the flow such

that longitudinal flow is compelled to get diverted towards the transverse direction (Wang and Odgaard, 1993). Many investigators like Odgaard and Wang (1991a), Wang and Odgaard (1993), Marelius and Sinha (1998), Tan et al. (2005), Ouyang et al. (2008) have studied analytically and experimentally the flow structure around the submerged vanes.

Following were the objectives of the present study:

(i) Development of a numerical scheme for the solution of unsteady transverse mixing equation.

(ii) To study the secondary current induced by installation of series of submerged vanes on the channel beds. To optimize vane size, location, spacing and alignment for obtaining strong secondary current.

(iii) Measurement of concentration profile of tracer injected either side of the channel in the presence of installed vanes and also without it for various flow conditions and vane configurations.

(iv) Determination of mixing coefficients using the measured concentration profiles. Also development of a predictor for enhanced mixing coefficients incorporating the flow parameters, vane sizes and spacing.

(v) Final recommendations for using submerged vanes for the enhancement of transverse mixing to be made.

The governing mass balance equation of transient transverse mixing in streams has been solved using finite volume method invoking the weighted upwind scheme. The developed model takes care of variation of depth of flow, depth-averaged velocity and transverse mixing coefficient across the channel width. The developed model is validated with analytical and experimental data. The numerical model proposed by Ahmad (2008) is extended to determine transverse mixing coefficient from the known concentration profiles at the downstream stations. Satisfactory agreement is found between concentration profiles computed using the proposed finite volume model and the analytical model for constant mixing coefficient and continuous pollutant injection.

Experiments were performed in a recirculating concrete flume of width 1.0 m, depth 0.30 m and length 19 m. The bed slope of the flume was 0.000632. The Rhodamine WT was used as

tracer due to its high detectability and conservative in nature. A tracer injecting system was used to inject dye from one side of the flume that represents a plane source of width 100 mm. The Rhodamine WT dye concentration was measured across the width of the channel and downstream of injection point using Hydro lab MS-5 probe. Micro ADV was used to measure three-dimensional velocity field downstream of the injection location. Three sizes of vanes were used in the experimentations which were 0.02 m × 0.05 m, 0.04 m × 0.1 m and 0.06 m × 0.12 m, whose lateral spacing was 0.05 m, 0.1 m and 0.125 m, respectively. Three flow conditions were maintained in order to perform experimentations for depth of flow of 0.09 cm, 0.1025 m and 0.1241 m. A total 50 runs were taken. Experiments were performed under no, one, two, three and four arrays of vanes for the measurement of dye concentration and three-dimensional velocities.

A computational fluid dynamics (CFD) model was developed on ANSYS-CFX platform to simulate flow pattern and turbulence characteristics around and downstream of a submerged vane and a series of vane rows containing multiple vanes in a single row. *k*-ω turbulence model is used herein. The developed CFD model is validated for the single vane, from the transverse velocity profile measured by Wang and Odgaard (1993) at x = 2H, 8H and 20H for vane size 0.076 m × 0.152 m for depth of flow = 0.152 m. It was observed that for each of transect, the simulated transverse velocity profile matched with the observed transverse velocity profile in a satisfactory manner. It was observed that vorticity has got its maximum value when the angle of attack was 28.7^{o} which was in accordance with the available literature. It was also observed that optimum value of height of vane which induced maximum intensity vortices was 0.4 times depth of flow. It was observed that as the length of vane was increased, the intensity of vorticity also increased subsequently. Simulated flow downstream of a vane indicates that the leading edge of the vane induces high vorticity which decreases exponentially downstream of the vane. The variation of turbulent kinetic energy is also on the pattern of vorticity.

For the multiple vane arrays system, the developed CFD model is validated by comparing simulated longitudinal velocity at three sections *viz.* x = 3H, 8H and 20H with the measured values and validation was also done for measured transverse velocity with the simulated transverse velocity profile. Good agreement in the simulated and observed velocity profiles were observed. Simulated flow pattern around multiple array of vanes indicate that near to the submerged vanes a large vortical field exists. It was observed that when the lateral spacing of vanes in an array was kept at y = 3H (where H = Height of vane), maximum intensity of vorticity was induced in the flow. In order to optimize longitudinal spacing a method was

proposed in which to acquire vorticity of a given strength downstream of a pre-installed vane row, the distance is read from the calibrated graph in lieu of the % vorticity required from the vane row in downstream.

In case of multiple vanes, it was observed that at a distance very near to vane row, each vane row generated a circulation of its own. In the further downstream, vortices coalesce with each other to form a larger field of circulation but effective magnitude of circulation was observed to be less than the magnitude of circulation if it was generated by each vane in individual manner. Moving further downstream, it was observed that circulation field was dissipated and less disturbed flow field was obtained under the action of viscosity. Turbulent kinetic energy was observed to be higher in the case of four arrays of vanes than the one array of vane.

Analysis of measured instantaneous velocity downstream of the zero, one, two, three and four arrays of submerged vanes indicates that in the presence of vanes, flow near to the vane is highly unstable and chaotic. The turbulence is clearly having heterogeneity as going up in vertical direction. The turbulence quantities decrease from bed to flow surface. The variation of all turbulence characteristics was same in all directions and was nearly overlapping to each other for measured instantaneous velocity at three transects in case of plane shear flow.

Variation of transverse velocity along depth for zero one, two, three and four arrays of vanes is also being studied. It is found that as array of vanes increases the transverse velocity increases which signify that transverse mixing shall be higher for higher number of arrays of vanes.

Effect of submerged vanes on tracer concentration profiles was studied experimentally. For this purpose, variation of tracer concentration across the width of the channel at distance of 5 m and 15 m for the depth of flow of 0.09 m, 0.1025 m and 0.1241 m, vane height of 0.02 m, 0.04 m, and 0.06 m and vane rows of 0, 1, 2, 3, and 4 was studied. It was seen that in the case of four vane rows, generation of circulation field was large and was extended to a greater distance; hence the mixing was highest in the case of four arrays of vanes. The number of arrays is proportional to the transverse mixing of the pollutants.

Variation of ratio of transverse mixing coefficients with vane and without vane with ratio of height of vane and depth of flow has been studied. It is found that as the vane size increases there is a drastic increase in the transverse mixing coefficient. This is due to the fact that a high magnitude of transverse circulation is generated in the flow as vane size increases. A predictor to estimate transverse mixing in the presence of submerged vane rows was developed and it

was observed that as the depth of flow was increased the transverse mixing was reduced due to increase in submergence over the vanes. Transverse mixing was observed to be proportional to the height of vane and number of vane rows.

Further, the transverse mixing coefficient for higher arrays/rows of vanes is high. For an example for depth of flow of 0.1241 m, the transverse mixing coefficient for four, three, two and one array of vanes are 23, 17, 13, and 7.5 times, respectively higher than the transverse mixing coefficients with no vane condition. However, such order of increase in the transverse mixing coefficient with vane for lower depth of flow is low. Flow with vane height/depth of flow of the order of 0.25 is not significant for enhancement in the transverse mixing.

Transverse mixing length is an important parameter in the establishment of longitudinal movement of pollutants because it is assumed that after transverse mixing is complete then only the motion in longitudinal will start prominently (Fischer, 1979; Rutherford, 1994). Transverse mixing length was calculated for 98% mixing case and was observed that for 0.06 m vane and depth of flow = 0.1241 m, tracer mixes 11 times faster than its absence. In case of 0.04 m vane and depth of flow = 0.1025 m, this mixing length in presence of vane was around 3.5 times shorter than what has to be without vane. For 0.02 m vane and depth of flow = 0.09 m, tracer was observed to mix 2 times faster than without vanes. This study indicates that submerged vanes can be used for the enhancement of the transverse mixing subjected that morphological changes in the alluvial streams are not noticeable.

ACKNOWLEDGEMENT

To achieve any campaign the hard work, blessing and support is required. I owe it all to the almighty God who showed all his blessing and benevolence on me to complete my research work.

The successful completion of my research work would never have been possible without the grace of God. There is always the benediction of that Almighty; above all that I got such opportunity to make a garland of those precious persons whose blessing and cooperation I got during my research work.

Finally, it gives me immense pleasure to express my profound gratitude to Prof. Zulfequar Ahmad. Words are indeed poor slaves to pen down about Prof. Zulfequar Ahmad sir, a true technocrat and great motivator. He provided me necessary infrastructure and resources to accomplish my research work. The constructive criticism and extensive discussions with Zulfequar Ahmad sir would be unforgettable experience for me that made me buttressed forever. Out of gratitude I can only say "Thank you, Ahmad Sir".

There are scores of IITs now and many other good institutions, but if anyone desires to see a truly secular institution of not only highest academics but of lovely people also, I suggest, please visit Roorkee. I attended two theory courses in first semester and I introduced with Prof. S K Mishra and Dr. V. Sawant. They were ideals who paid intellectual and moral attention to me as a teacher. Similarly, Prof. C.S.P. Ojha, Prof. Deepak Kashyap, Prof. K.S. Hari Prasad and Dr. M.K. Jain sir were always helpful for me. I am really possessed by the greatness of these peoples at IIT Roorkee.

I am very thankful to Dr. Nitin Joshi, Dr. Shakti Suryavanshi, Mr. Gulshan Tirkey, Dr. Rakesh Pratap Singh, Dr. A S Lodhi, Dr. Nilav Karna, Dr. Ankit Chakaravarti, Mr. Umesh Singh, Mr. Nitin Naresh Pandhare, Dr. Rituraj Shukla and many more friends for their sincere help and moral support during entire work. I am very thankful to my other colleagues for their fruitful discussion on various aspects during studies. Also my special gratitude towards Mr. Sandeep Chauhan, who helped me throughout my experimental works and with figures associated with my thesis.

In IIT Roorkee, I have been blessed with a friendly and cheerful group of technical staff namely; Mr. Y. S. Pundir, Mr. Ashok, Mr. Bhairav Singh, Mr. Pramod Kumar, Mr. Arshad Ali, Mr. Rati Ram, Mr. Chhote Lal and all the lab staff of Hydraulic Engineering Laboratory.

I also acknowledge the financial support provided by Department of Science and Technology (DST), Delhi.

I thank God for blessing me with loving, wonderful and caring parents. My gratitude to them cannot be expressed in words. A strong power has always been supporting me during the entire course of my research. I am sure this has been the force of blessings of Parents and Grandparents, which never left me trapped in difficulties. It is their love, blessings, persistent motivation that has brought me up to this stage. I dedicate my words of expression to my father Mr. Bhawani Shanker Sharma who is a retired Ex-IAF men and working as an administrator in Uniara Hospital, Jaipur (Rajasthan). The education, upbringing, moral support, constant patience and a lesson of always being thankful to the God "whatever He gives me could take me out from my crisis moment of life". It is the track of being always honest, which my father showed me to tread upon. I am quite short of words to express my gratitude towards my lovely mother Mrs. Rajeshwari Sharma who is a backbone not only for me but also for my family. Despite of many games played by destiny me and my sibling always had my parents as our guardian angels. In every birth that I take, I wish to be their child. For them I would only say that It was not possible for God himself to come on this earth therefore he took his incarnation in the guise of my parents. I owe my parents for all that what I am today.

Gratitude towards my sibling for their boundless love, constant encouragement and support cannot be expressed in simple words. I am thankful to my younger sister Miss Himadri Sharma, who is an Architect in a private firm having name as ARCADE. It is her constant chiding over phone and giving me the boost to continue my work in an enthusiastic manner. She always relieves my tension with her positive vibes.

Out of this whole episode if any one took the brunt it was my wife; Mrs. Vinita Sharma my companionable life partner. She never drove me up the wall rather supported me always, otherwise it would have been impossible for me to finalize this task. I also want to acknowledge how my child who will come in to the world in near future has put zeal into my mind to complete this thesis.

Above all it's God who strengthened me bodily and spiritually through his word and to Him I owe my lifelong indebtedness.

HIMANSHU SHARMA

LIST OF SYMBOLS

Symbol	Description of Symbol
A_x	Area of element perpendicular to x direction
A_y	Area of element perpendicular to y direction
b	Width of section of injection
B	Width of channel
c	Measured concentration at a point
c_t	Measured concentration in the time-interval “t”.
c'	Fluctuating component of tracer concentration
C	Depth averaged concentration of pollutant
C_D	Coefficient of drag
C_h	Chezy’s coefficient
$C_{i,j}$	Value of concentration at a point (i, j)
C_L	Coefficient of lift
Co	Initial concentration of dye
C_P^o	Concentration at point P at initial time level
C_r	Courant number
C_∞	Cross-sectional mixed concentration of pollutants
ΔC	Concentration excess

d_o	Median size of sediment
D_y	Diffusion factor
e_m	Molecular diffusion coefficient
erf	Error function
e_x	Eddy diffusivities in x-direction
e_y	Eddy diffusivities in y-direction
e_z	Eddy diffusivities in z-direction
ERS	Error in calculation of transverse mixing coefficient
E_x	Depth averaged longitudinal mixing coefficient
E_y	Depth averaged transverse mixing coefficient
E_{yv}	Transverse mixing coefficient with vane rows
f	Friction factor
f_r	Frequency of waves transmitted by ADV
F_L	Lift force
g	Acceleration due to gravity (= 9.81 m/s^2)
h	Depth of flow
h_z	Depth of flow at a point "z" unit above from channel bed.
Δh	Head difference
H	Vane height
H_i	Height of i^{th} vane
i	Unit vector in x-direction

$\mathbf{j}$	Unit vector in y-direction
J_x	Mass-flux across the surface “x”.
k	Turbulent Kinetic Energy
k_s	Roughness height
L	Length of vane
L_c	Crossing distance
L_t	Length scale of turbulence
m	Resistance coefficient
m_{α_o}	Metric coefficient in α_o direction in curvilinear orthogonal system
m_{β_o}	Metric coefficient in β_o direction in curvilinear orthogonal system
M_t	Mass accumulated in control volume in time “t”
$\hat{M}$	Mass inflow rate
n	Direction normal to the unit area
$\mathbf{n}_1$ and $\mathbf{n}_2$	Unit vectors normal to the surfaces A_x and A_y
N	Number of vane rows
p	Pressure acting on any fluid surface
P	Peclet Number
P_k	Production of kinetic energy
q	Cumulative discharge

q_o	Initial value of cumulative discharge at source of injection
Q	Discharge of flow
Qo	Rate of dye discharging
r	Distance from core of the vortex
R_a	Radius of curvature of bend
s	Downstream distance from mid of vane
S	Bed slope
S_{ij}	Strain tensor
t	Simulation time
T_{ad}	Rate of advective transport per unit area
T_o	Submergence of flow over the submerged vane
T_t	Rate of transport of substance by turbulent diffusion per unit area
T_y	Time taken by effluent to get fully mixed in transverse direction
T_z	Time taken by effluent to get fully mixed in vertical direction
u	Component of velocity of flow in longitudinal (x) direction
u_i	Velocity in i^{th} direction
u_v	Velocity of approach towards vane

u_z	Point velocity at height "z" above bed
u_∞	Ambient or free velocity far from vane field
u_*	Shear velocity
u'	R. M. S. value of longitudinal turbulence intensity
u'w'	R. M. S. value of vertical Reynolds stress
U	Average velocity of flow
U_*	Cross-sectional averaged shear velocity
v	Component of velocity of flow in transverse (y) direction
v_i	Transverse velocity components at vane i
v_θ	Tangential velocity
v'	R. M. S. value of transverse turbulence intensity
V_s	Velocity of sound in media
w	Component of velocity of flow in vertical (z) direction
w'	R. M. S. value of vertical turbulence intensity
Δx	Incremental distance in x-direction
y_o	Transverse position of source of injection with respect to left bank
y_P	Point from the wall where log-law and dynamic equilibrium of turbulence were satisfied
Δy	Incremental distance in y-direction
Δz	Incremental distance in z-direction

Greek Letters

α_d	Decay constant of pollutant
α_o	Longitudinal coordinates in an orthogonal curvilinear system
α_t	Temporal weighing factor
β_d	Any source or sink present in pollutant mixing zone
β_o	Transverse coordinates in an orthogonal curvilinear system
δ_{ij}	Kronecker delta
δ_n	Lateral distance between two vanes
δ_s	Longitudinal spacing between rows of vane
$\in$	Concentration at previous time "t"
ϕ	Transportable property
Γ	Vane generated circulation
Γ(s)	Circulation at distance "s"
Γ_o	Circulation at tip of vane
η	Normalized width
φ_i	Phase in i^{th} direction
κ	von Karman constant
λ_i	Interaction factor between vanes
μ	Dynamic viscosity of fluid

v	Kinematic viscosity of fluid
θ	Angle of attack of flow on the vane
ρ	Density of fluid
τ_{ij}	Reynolds stress
ω	Turbulent frequency
ω_s	Length of plane vertical source
ξ	Eddy viscosity
Ω	Control volume

Subscripts

p	Represents quantities for the *pth* adjacent element in Luk et al. (1990)
l	Represent the quantity of the left adjacent elements in Luk et al. (1990)
r	Represent the quantity of the right adjacent elements in Luk et al. (1990)
n	Represents northern point on the control volume in Ahmad (2008)
e	Represents eastern point on the control volume in Ahmad (2008)
w	Represents western point on the control volume in Ahmad (2008)
s	Represents southern point on the control volume in Ahmad (2008)

N	Represents northern point of the control volume in Ahmad (2008)
E	Represents eastern point of the control volume in Ahmad (2008)
W	Represents western point of the control volume in Ahmad (2008)
S	Represents southern point of the control volume in Ahmad (2008)
P	Represents centroidal point of the control volume in Ahmad (2008)

LIST OF FIGURES

LIST OF TABLES

CONTENTS

Chapter 1

INTRODUCTION

1.1 INTRODUCTION

Water is a source for many industrial and domestic needs which include from drinking to cooling of reactors. Need of pure water for these tasks, is as important as management of water quality. Since there happens at many times when any pollutant accidently spills into the water, it gets mixed in water and pollutes it. Understanding the mechanism of mixing of pollutants is necessary for the management of pollutants control in streams. Most of the industrial and domestic wastes are disposed in streams and they take away these disposed off wastes by their moving capability. By discharging such wastes in streams not only affect the water quality but also lead to many ecological and environmental changes. Thus it is essential to study how the waste/effluent gets mixed in the flowing stream for environmental concern and water quality modeling. Whenever any effluent is discharged in any stream, it gets mixed into it rapidly in vertical direction along the depth, known as vertical mixing (Singh, 2005; Singh et al., 2009 & 2010; Zhang and Zhu, 2011a) (also termed as "near-mixing" zone) (Fig. 1.1). After getting mixed in each vertical section the effluent is advected in lateral direction and is allowed to get mixed well in transverse direction due to non-uniformity in velocity distribution in transverse direction and diffusion caused by turbulence in transverse direction. This kind of mixing in lateral direction is known as transverse mixing (Demetrocopolous and Stefan, 1983; Ahmad et al., 2011) (also termed as "mid-field mixing" zone). After having complete mixing of effluent along all the cross-section of the channel, the effluent is advected further downstream direction along the longitudinal direction of flow, this mixing is known as a "far-field" mixing or longitudinal mixing (Azamathulla and Ghani, 2011). Fig. 1.1 depicts the near, mid and far fields under the pollutant discharge and can be clearly seen that vertical mixing ceases in very short distance whereas mid-field and far-field mixing go to longer distances.

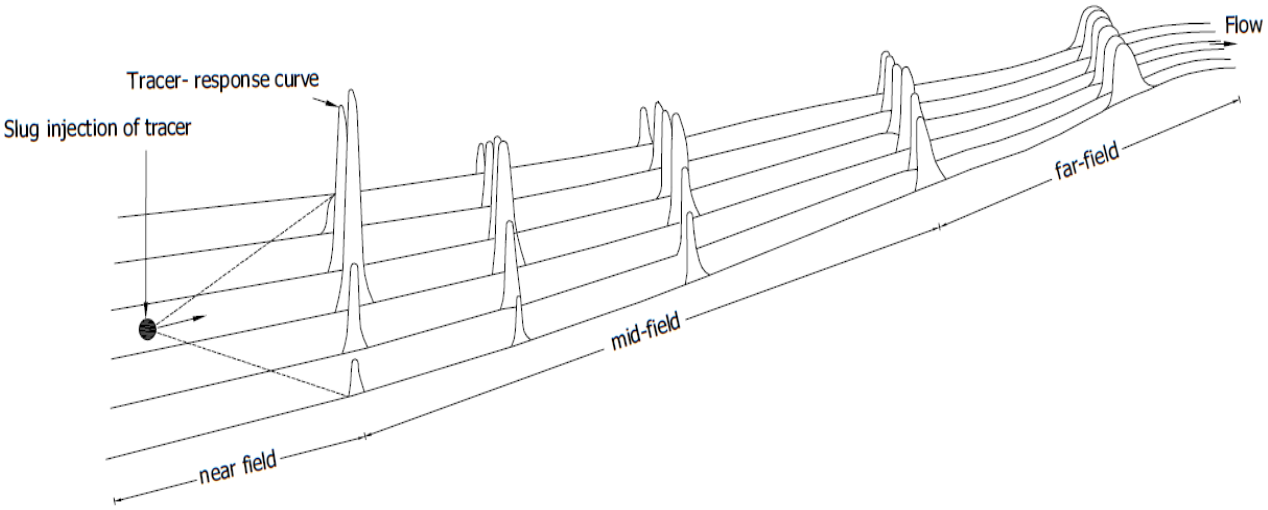

Fig. 1.1 Pollutant mixing process and different mixing field in open channel (Singh, 2005)

In actuality vertical mixing is a very rapid process which is only important in near-source field and can be computed by following relation (Elhadi et al. 1984; Rutherford 1994; Jobson 1997; Biron et al. 2004):

$$\frac{T_y}{T_z} = 310 \tag{1.1}$$

Here, T_y = Time taken by effluent to get fully mixed in transverse direction; T_z = Time taken by effluent to get fully mixed in vertical direction.

In the case of longitudinal mixing it usually goes up to a distance of 100-300 times river width which is a very large distance and generally beyond the concerned reach of the rivers (Rutherford 1994; Jobson 1997; Biron et al. 2004). Hence, transverse mixing can be understood as an important phenomenon to model the water quality in a flowing media from the practical considerations (Rutherford, 1994). Due to the diminishing of vertical gradients of concentration, the mid-field mixing zone is also termed as two-dimensional mixing zone and it is modeled of after depth-averaging the advection-dispersion equation (Fischer et al. 1979; Rutherford 1994):

$$\frac{\partial(hC)}{\partial t} + \frac{\partial(huC)}{\partial x} = \frac{\partial}{\partial x}\left(E_x \frac{\partial(hC)}{\partial x}\right) + \frac{\partial}{\partial y}\left(E_y \frac{\partial(hC)}{\partial y}\right) \tag{1.2}$$

Here, h = Depth of flow; t = Simulation time; C = Depth-averaged concentration of the pollutant; u = Components of velocity of flow in longitudinal (x) and transverse (y) directions, respectively; E_x, E_y = Depth-averaged mixing coefficients in longitudinal and transverse directions, respectively.

Figure 1.2 shows a typical scenario where transverse mixing process prevails the pollutant transport. A tributary having concentration, C_T, meets the main stream having concentration, C_S, and mixing of pollutants starts due to difference in pollutant concentration. Secondary currents are generated due to river-tributary confluence, which prevail the mixing of pollutant in lateral direction, until an equilibrium concentration is reached.

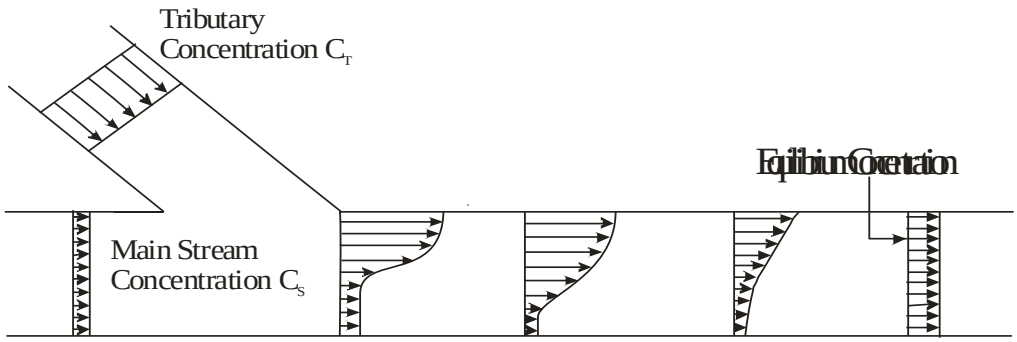

Fig. 1.2 Conceptual sketch showing process of transverse mixing

Several attempts have been made to establish the relationship between the transverse mixing coefficient and bulk channel parameters such as width, depth, shear velocity, friction factor, curvature and sinuosity (Chau, 2000; Webel and Schatzmann, 1984; Lau, 1981; Yotsukura and Sayre, 1976; Beltaos, 1980; Fischer et al 1979; Lipsett and Beltaos, 1978; Azmathullah and Ahmad, 2012; Elder, 1959; Engelund, 1969). From the published data from a number of sources on transverse dispersion in natural channels, Rutherford (1994) proposed empirical formula for the transverse mixing coefficient as shown in Table 1.1. ($\bar{h}$ and U_* = average depth of flow and shear velocity, respectively).

It is evident that in straight open channels secondary currents are weak compared to curved channels, therefore, spreading of pollutant is more in curved channels compared to the straight channels, as secondary currents are much stronger in curved channels (Ward, 1974; Lau and Krishnappan, 1981; Holley and Nerat, 1983; Demuren and Rodi, 1986; Boxall and Guymer, 2001; Boxall and Guymer, 2002; Boxall et al., 2003; Boxall and Guymer, 2003 a & b; Albers and Steffler, 2007; Dow et al., 2009). Thus, it is important to enhance the transverse mixing of

pollutants in straight open channels in order to achieve the proper mixing of pollutants in order to cease lengthwise motion of pollutants as longitudinal mixing and transverse mixing are inverse processes that is increment in one causes decrement in other (Fischer, 1969).

Table 1.1 Transverse mixing coefficient (Rutherford, 1994)

Type of channel curvature	$E_y/U_* \bar{h}$
Straight channel	0.15-0.30
Gently meandering channel	0.30-0.90
Strongly curved channel	1.0-3.0

Hence, in this thesis a new technique i.e., submerged vane that generates transverse secondary circulations, is evolved as transverse mixing enhancing device. This device was developed by Odgaard and his associates (Odgaard and Kennedy, 1983; Odgaard and Mosconi, 1987; Odgaard and Wang, 1991 a & b; Wang and Odgaard, 1993).

Submerged vane is basically an aerofoil structure, which generates the excess turbulence in form of helical flow structure in the flow due to pressure difference between approaching flow side and downstream side of vane (Odgaard and Spoljaric, 1986; Odgaard and Mosconi, 1987; Odgaard and Wang, 1991 a & b; Wang and Odgaard, 1993; Ouyang et al. 2006; Ouyang and Lai, 2013, etc.). These vanes are in general placed at certain angle with respect to the flow directions which is usually in between, $10^o - 40^o$ (Fig. 1.3). Submerged vane was invented for sediment management in rivers and differs from the traditional methods like groins, dikes, etc., which are usually placed normally to the flow and produce flow distribution by drag force and are not so much efficient in controlling the sediment transport.

Submerged vanes utilize vorticity to minimize the drag and produce flow redistribution in the flow such that longitudinal flow is compelled to get diverted towards the transverse direction (Wang and Odgaard, 1993). Many investigators like Odgaard and Wang (1991a), Wang and Odgaard (1993), Marelius and Sinha (1998), Tan et al. (2005), Ouyang et al. (2008) and Ho et al. (2010) have studied analytically and experimentally the flow structure downstream of the submerged vane.

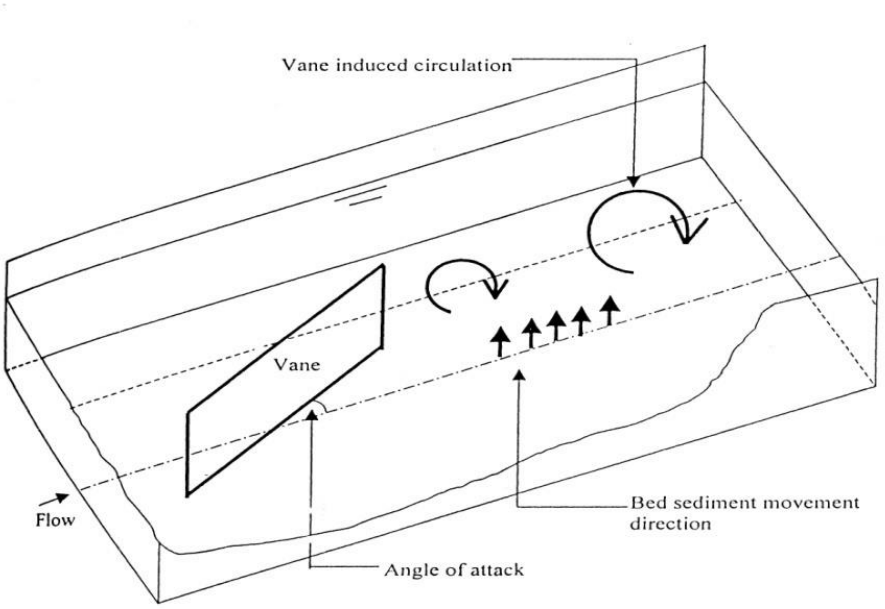

Fig. 1.3 Submerged vane induced transverse circulations

1.2 BRIEF REVIEW OF LITERATURE

(a) Transverse Mixing

As discussed above, transverse mixing is an important process than the vertical and the longitudinal mixing since vertical mixing is a very rapid process and assumed to occur with twice the rate as compared to transverse mixing while longitudinal mixing is assumed to occur after a distance beyond 300 times of width and if the source of pollutant is unsteady in nature (Rutherford, 1994). Hence both are not of that importance as the transverse mixing is. Many studies carried out investigation on transverse mixing process and various factors affecting it (Holley et al., 1972; Holley and Abraham, 1973 a & b; Beltaos, 1975; Yotsoukura and Sayre 1976; Lau and Krishnappan, 1977; Cotton and West, 1980; Lau and Krishnappan, 1981; Holley Jr. and Nerat, 1983; Webel and Schatzmann, 1984; Boxall and Guymer, 2003; Boxall et al., 2003; Seo et al., 2006; Albers and Steffler, 2007; Ahmad, 2008; Zheng et al., 2008; Dow et al., 2009; Baek and Seo, 2010). Fischer (1969) experimentally studied effect of bend on the dispersion of tracers and found that transverse mixing is enhanced in the bend region. Holley et al. (1972) studied the various aspects and factors affecting the transverse diffusion across the river and henceforth introduced the generalized change of moment method. Holley and Abraham (1973) studied the transverse mixing in rivers through laboratory experimentations and also took observations on fixed bed river in the presence of groins as protective work. Engmann and Kellerhals (1974) studied the effect of ice over on the transverse mixing.

Yotsoukura and Sayre (1976) developed a new method called as stream tube method. Krishnappan and Lau (1977) experimentally and numerically studied the effect of varying bottom roughness and cross sections on the transverse mixing process. Cotton and West (1980) studied the transverse diffusion in unidirectional and wide channel. Lau and Krishnappan (1981) numerically solved the two dimensional tracer transport equation and included sinuosity as describing transverse mixing parameters. Holley Jr. and Nerat (1983) experimentally and analytically studied the factors affecting the transverse mixing in natural streams. Webel and Schatzmann (1984) investigated effect of aspect ratio and roughness on the transverse mixing. Bruno et al. (1990) experimentally studied the effect of buoyancy on transverse mixing. Chau (2000) studied experimentally the effect of bed roughnesses and flow depths on transverse mixing. Boxall et al. (2003) studied the transverse mixing in sinuous natural open channels. Boxall and Guymer (2003) studied the transverse mixing in natural stream. Marion and Zaramella (2006) studied the effects of secondary currents and velocity gradients on the solute dispersion. Seo et al. (2006) studied the transverse mixing under slug test conditions by utilizing Stream Tube Routing method. Albers and Steffler (2007) analytically solved the three dimensional advection-dispersion equation using Vertically Averaged Moment (VAM) equations. Ahmad (2008) developed a finite volume model to study the steady state transverse mixing. Zheng et al. (2008) experimentally studied the transverse mixing phenomenon in the trapezoidal compound channel. Dow et al. (2009) conducted their experimentations on the North Saskatchewan River. Baek and Seo (2010) derived a new Stream Tube Routing method and analyzed its results matching properties with stream tube and moment based methods. Baek and Seo (2010) derived an equation to predict transverse mixing coefficient in curved channel under secondary currents. Zhang and Zhu (2011 b) proposed a modified Stream-tube method in order to calculate the transverse mixing coefficient in ice-covered rivers. Lee and Seo (2013) developed the theoretical equation to calculate the dispersion coefficient from observed dispersion tensor.

(b) Flow around Submerged Vanes

Submerged vanes have been used so far as river restoration structure and for managing the sediment. Odgaard and Kennedy (1983) performed physical model for the utilization of submerged vane as protector against erosion in bends. Odgaard and Spoljaric (1986) provided a design procedure to calculate transverse slope generated by vane induced transverse velocity component. Odgaard and Mosconi (1987) provided an experimental study on the submerged vane for utilizing it as bank protector for the bend in East Nishnabotna river in Iowa. Nakato et

al. (1990) utilized physical modeling in order to study the effect of submerged vane on the pump-intake shoaling in alluvial rivers. Odgaard and Wang (1991a) studied the flow pattern around the submerged vane by including various factors which can possibly affect the flow pattern and also developed a formula to calculate lift and drag coefficients. Wang and Odgaard (1993) critically analyzed the theory of tip vortex and utilized method of images for two vanes and for multiple vane arrays. Marelius and Sinha (1998) observed the flow pattern around the vane for vane angle $\theta > 30^o$ and also obtained the optimum angle of attack. Barkdoll et al. (1999) experimentally studied the effect of submerged vane on the entry of sediment in lateral diversion provided in the alluvial channels. Sinha and Marelius (2000) developed a numerical model using k-ε turbulence method in order to estimate flow pattern around submerged vane. Marelius (2001) studied experimentally the utilization of submerged vane in the coastal beach protection from high tides. Johnson et al. (2001) utilized these rock-vanes in order to control scour around vertical wall abutment. Flokstra (2002) developed a model based on the wing-theory so as to study the effect of vane on the mobility of mobile bed. Aware et al. (2005) studied the effect of vane arrangement on the scouring pattern around the bend in a river. Gupta et al. (2005) modeled the scouring pattern around submerged vane of rectangular shape and also optimized the angle of attack. Tan et al. (2005) studied the flow pattern around the vane and optimized the vane parameter so that vane can act as sediment manager. Gupta et al. (2006a) studied the effect of shapes and vorticity on vane parameters. Gupta et al. (2006b) studied the decaying of vortex generated from the submerged vane at downstream with and without collar present with submerged vane. By using rock vanes and optimizing their numbers, size, spacing, etc. Gupta et al. (2007) studied the effect of aspect ratio on the vortex generated by submerged vane and utilized moment of the momentum to analyze the strength of vortex. Ouyang et al. (2008) obtained an interaction model of vane by putting up the fact that vane interaction field associated with multiple vane array is different for different vane in the system in contradiction to the theory put forward by Wang and Odgaard (1991a). Allahyonesi et al. (2008) studied the effect of various longitudinal arrangements of submerged vanes on the sediment ingestion in lateral intake in alluvial channel. Ghorbani and Kells (2008) studied the effect of various sizes of submerged vanes on the scouring pattern around cylindrical pier. Ouyang (2009) optimized the shape and size of submerged vane by developing a numerical model which utilizes vortex panel method in order to manage the sediment deposition in alluvial channels. Gupta et al. (2010) studied the effect of collar on the effectiveness of preventing the scour hole around submerged vane and optimized its dimensions in scour hole

prevention. Han et al. (2011) experimentally studied the effect of submerged vanes on the flow characteristics of 90^o channel bend.

1.3 NEED FOR THE STUDY

Most of the cities are located on the banks of river and discharge their effluent in the river from either bank and also use it as source of water supply. If the water intake happens to be in the downstream of the effluent disposal and on the same bank, then it becomes essential to enhance the transverse mixing, so that, pollutants mix with more volume of water and less polluted water be available at the water intake. To increase the secondary current for the enhancement of the transverse mixing, it is desirable to have some structure, which could increase the secondary currents in that reach. Submerged vanes are suitable structure for this purpose. The present study is intended to study the effect of artificially induced secondary current on the transverse mixing, which has not been taken up so far.

1.4 OBJECTIVES

Following are the objectives of the present study:

(i) Development of numerical scheme for the solution of unsteady transverse mixing equation.

(ii) To study the secondary current induced by installation of series of submerged vanes on the channel beds. To optimize vane size, location, spacing and alignment for obtaining strong secondary current.

(iii) Measurement of concentration profile of tracer injected at either of banks of the channel in the presence of installed vanes and also without it for various flow conditions and vane configurations.

(iv) Determination of mixing coefficients using the measured concentration profiles. Also development of predictor for enhanced mixing coefficients incorporating the flow parameters, vane sizes and spacing.

(v) Final recommendations for use of submerged vanes for the enhancement of transverse mixing to be made.

1.5 STRUCTURE OF THE REPORT

The present study comprises of total eight chapters. Chapter 1 deals with the introduction of the subject of the matter, a brief literature review and objectives of the study. A detailed discussion regarding basic theory of pollutant transport and analytical and numerical solution of the governing equations are discussed in the Chapter 2. Chapter 2 also discusses the flow pattern around single vane and multiple vane rows experimentally and numerically. Chapter 3 deals with the numerical modeling of the transverse mixing equation for steady and transient state. Chapter 4 describes the experimental set up and procedure for collecting data through experimentations. Chapter 5 describes the flow pattern around submerged vanes and its utilization in describing its effect on transverse mixing process. Chapter 6 describes the analysis of data and calculation of transverse mixing coefficient in absence and presence of vanes while Chapter 7 concludes the outcome of the study.

Chapter 2

BASIC THEORY AND REVIEW OF LITERATURE

2.1 INTRODUCTION

Water resources which may be either groundwater, river or estuarine resources are always prone to pollution but due to greater visibility river pollution is discussed a lot (Orlob, 1983; Demuren and Rodi, 1986; Jobson, 1997; Pilechi et al., 2015; Young et al., 2000 a; Brusseau et al., 1997; Chaudhuri and Sekhar, 2005 & 2008; Eldho and Rao, 1997; Eldho et al., 1999; Kartha and Srivastava, 2008 a & b; Kumar et al., 2006; Sharma et al., 2012; Young et al., 2000 b, etc.). When any pollutant is spilled into the river, due to the dominance of vertical turbulence and least dimension of any river system, the pollutant gets mixed along the depth very quickly. The process of the pollutant getting mixed along the depth is termed as vertical mixing and mixing length is nearly 50-100 times of depth (Yotsoukura et al., 1970; Yotsoukura and Sayre, 1976). After getting mixed in the vertical direction, pollutant starts getting mixed in the transverse direction under the action of transverse turbulence and variation in vertical profiles of transverse velocity. This transverse spreading and mixing of pollutant under the action of transverse shear and turbulence is termed as transverse mixing (Ahmad, 2007). If the source of the pollutant is unsteady in nature, pollutant further travels downstream under the action of longitudinal gradients and this mixing of pollutant under the action of longitudinal gradients is termed as longitudinal mixing. As the vertical mixing is a very rapid process and is dominant near the source of pollutant spill whereas the longitudinal mixing is of important very far from the source so that it makes it unimportant to model for environmental concern. This chapter is a compendium regarding various processes involved of pollutant

mixing in river and then at last focusing on the process of transverse mixing and factors affecting it.

2.2 PHYSICAL PROCESSES OF POLLUTANT TRANSPORT

If a small quantity of any tracer like dye is injected into the river, the tracer cloud not only changes its shape but also increases in volume at the same time it is carried away downstream by the stream flow. The phenomenon of transport and dye tracer mixing involves various physical processes originating from various reasons in the transporting media and these important processes are classified as advection, diffusion and dispersion. These processes are discussed below briefly and their roles in tracer transport equation are discussed later in this chapter.

2.2.1 Molecular Diffusion

The spreading of tracer due to the motion of molecules of fluid is called as molecular diffusion. In laminar flow, the transport of tracer is mainly governed by the molecular diffusion in which motion of molecules is random and occurs from higher concentration to lower concentration. Fick's law of diffusion describes the transport of tracer due to molecular motion based diffusion by a gradient based law, which is as follows (Fischer et al., 1979; Elhadi et al., 1984; Rutherford, 1994; Ahmad, 2007):

$$J_m = -e_m \frac{\partial C}{\partial n} \tag{2.1}$$

Here, J_m = transport by molecular diffusion per unit area per unit time; n = direction normal to the unit area; and e_m = molecular diffusion coefficient.

2.2.2 Molecular diffusion equation

In order to derive the molecular diffusion equation, concept of mass conservation is used. Consider a control volume of sides Δx, Δy and Δz in x-, y- and z- directions, respectively, in Cartesian coordinate system as shown in Fig. 2.1. Let the mass flux across the surfaces x, y and z be as J_x, J_y and J_z, respectively and for surfaces $x+\Delta x$, $y+\Delta y$ and $z+\Delta z$ be $J_{x+\Delta x}$, $J_{y+\Delta y}$ and $J_{z+\Delta z}$, respectively, after time Δt. Thus, mass flux can be written as follows:

$$J_{x+\Delta x} = J_x + \frac{\partial J_x}{\partial x}\Bigg)_x \Delta x \tag{2.2a}$$

$$J_{y+\Delta y} = J_y + \frac{\partial J_y}{\partial y}\Bigg)_y \Delta y \tag{2.2b}$$

$$J_{z+\Delta z} = J_z + \frac{\partial J_z}{\partial z}\Bigg)_z \Delta z \tag{2.2c}$$

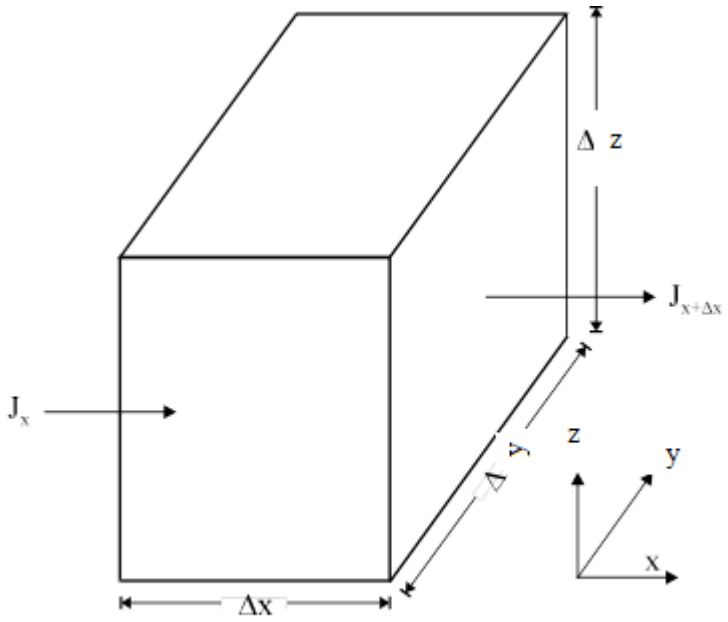

Fig. 2.1 Diffusive fluxes into and out of the control volume

Consider the mass accumulated in the control volume during the time, t is:

$$M_t = c_t \Delta x \Delta y \Delta z \tag{2.3}$$

Here, c_t = average concentration of tracer in a control volume.

Now, mass accumulated in control volume during time t+Δt is

$$M_{t+\Delta t} = \frac{\partial c}{\partial t}\Bigg)_t \Delta x \Delta y \Delta z \Delta t + M_t \tag{2.4}$$

Temporal rate of change of mass in control volume is simply given by

$$\frac{M_{t+\Delta t} - M_t}{\Delta t} = \frac{\partial c}{\partial t}\Bigg)_t \Delta x \Delta y \Delta z \tag{2.5}$$

Now, according to equation of mass conservation, rate of change of mass of tracer within the control volume is equal to the differences in the fluxes. Thus, mass balance equation of tracer can be written as

$$\frac{M_{t+\Delta t} - M_t}{\Delta t} = \left(J_x - J_{x+\Delta x}\right)\Delta y \Delta z + \left(J_y - J_{y+\Delta y}\right)\Delta x \Delta z + \left(J_z - J_{z+\Delta z}\right)\Delta x \Delta y \tag{2.6}$$

Now, substituting Eq. (2.2 a-c) and Eq. (2.5) in Eq. (2.6) yields

$$\frac{\partial c}{\partial t} = -\left[\frac{\partial J_x}{\partial x} + \frac{\partial J_y}{\partial y} + \frac{\partial J_z}{\partial z}\right] \tag{2.7}$$

Substituting Eq. (2.1) in Eq. (2.7) yields

$$\frac{\partial c}{\partial t} = e_m\left(\frac{\partial^2 c}{\partial x^2} + \frac{\partial^2 c}{\partial y^2} + \frac{\partial^2 c}{\partial z^2}\right) \tag{2.8}$$

It is worth to note that e_m is independent of x, y and z and Eq. (2.8) describes the nature of spreading of dye tracer under the action of molecular motion.

2.2.3 Advection

Advection can be defined as the process where tracer cloud moves bodily in the flowing stream under the action of imposed current. Advection helps in transporting any dissolved or suspended tracer away from the fixed source in the downstream, hence showing that it is an important phenomenon to be considered while modeling the transport of pollutant in the flowing media. In order to quantify the intensity of advection, term advective flux is defined as follows (Fischer et al., 1979; Orlob, 1983; Elhadi et al., 1984; Rutherford, 1994):

The amount of tracer/substance transported per unit time per unit area perpendicular to the current is termed as advective flux and is the product of velocity and transported concentration of tracer/substance. Mathematically, advective flux can be formulized as (Elhadi et al., 1984)

$$T_{ad} = uc \tag{2.9}$$

Here, T_{ad} = Advective transport per unit time per unit area; u = Velocity perpendicular to unit area; and, c = Concentration of substance/tracer transported.

2.2.4 Advection diffusion equation in laminar flow

In any laminar flow, the process of advection happens simultaneously with the molecular diffusion. Molecular diffusion mixes the tracer in the direction of concentration gradients whilst the advection helps the tracer to move forward in the direction of flow. It is also assumed that diffusion takes place in the flowing fluid same as if fluid is stationary. Thus the total rate of flux in the x-direction is given by the sum of advective and diffusive flux that is (Ahmad, 2007)

$$J_x = uc - e_m \frac{\partial c}{\partial x} \tag{2.10}$$

Substituting Eq. (2.10) in Eq. (2.7) for one dimension gives

$$\frac{\partial c}{\partial t} + \frac{\partial (uc)}{\partial x} = \frac{\partial}{\partial x}\left(e_m \frac{\partial c}{\partial x} \right) \tag{2.11}$$

Now expanding Eq. (2.11) for three dimensional:

$$\frac{\partial c}{\partial t} + u\frac{\partial c}{\partial x} + v\frac{\partial c}{\partial y} + w\frac{\partial c}{\partial z} = e_m\left(\frac{\partial^2 c}{\partial x^2} + \frac{\partial^2 c}{\partial y^2} + \frac{\partial^2 c}{\partial z^2} \right) \tag{2.12}$$

2.2.5 Turbulent diffusion

In any turbulence dominated flow, instantaneous velocity of a fluid particle can be broken into a temporally averaged steady component and a fluctuating component. The time-averaged component is responsible for the advective transport of the substance while the fluctuating component, which is responsible for the eddying motion in the flow, spreads and transports the tracer. This spreading and transport of tracer cloud due to the turbulence generated eddies is called as turbulent diffusion. The major difference between the turbulent diffusion and advective transport is that an advective transport is dominated by the flow and is unidirectional but the turbulent diffusion is eddy dominated process and transport of tracer could be in any direction as eddy motion is a random process. If u_i' is the fluctuating component of velocity in a certain i^{th} direction and c' is the fluctuating component of tracer concentration, then the transport of tracer is given by (Fischer et al., 1979; Elhadi et al., 1984; Rutherford, 1994)

$$T_t = \overline{u_i' c'} \tag{2.13}$$

Here, T_t = transport of substance by turbulent diffusion per unit time per unit area and the bar indicates the temporal averaging. Since the turbulent diffusion is also random like molecular diffusion and occurs from higher concentration to lower concentration, it can also be formulated similar to the molecular diffusion, in form of the gradient based on Fick's diffusion law as follows

$$T_t = -\varepsilon \frac{\partial c}{\partial n} \tag{2.14}$$

Here, ε = eddy diffusivity. Since similar equations could be written in other directions as in general the eddy diffusivities depends on local concentration gradients, hence, varies from location to location.

2.2.6 Advection diffusion equation in turbulent flow

Equation (2.12) can also be used to model tracer transport in turbulent flow. In turbulent flow, all the flow properties can be represented as sum of their ensemble mean and fluctuations. Hence, observed velocities and concentration can be represented as

$$u = \langle u \rangle + u' \tag{2.15a}$$

$$v = \langle v \rangle + v' \tag{2.15b}$$

$$w = \langle w \rangle + w' \tag{2.15c}$$

$$c = \langle c \rangle + c' \tag{2.15d}$$

Here, bracket denotes the ensemble mean of the quantity and prime denotes deviation from the ensemble mean. Hence, substituting Eqs. (2.15) in Eq. (2.12) yields

$$\begin{aligned} &\frac{\partial}{\partial t}\left(\langle c \rangle + c'\right) + \left(\langle u \rangle + u'\right)\frac{\partial}{\partial x}\left(\langle c \rangle + c'\right) + \left(\langle v \rangle + v'\right)\frac{\partial}{\partial y}\left(\langle c \rangle + c'\right) + \left(\langle w \rangle + w'\right)\frac{\partial}{\partial z}\left(\langle c \rangle + c'\right) \\ &= e_m\left(\frac{\partial^2}{\partial x^2}\left(\langle c \rangle + c'\right) + \frac{\partial^2}{\partial y^2}\left(\langle c \rangle + c'\right) + \frac{\partial^2}{\partial z^2}\left(\langle c \rangle + c'\right)\right) \end{aligned} \tag{2.16}$$

Since average of all fluctuating quantities like, u', v', w' and c' are zero. Hence, ensemble mean of quantities

$$\frac{\partial c'}{\partial t}, u'\frac{\partial \langle c \rangle}{\partial x}, v'\frac{\partial \langle c \rangle}{\partial y}, w'\frac{\partial \langle c \rangle}{\partial z}, \langle u \rangle \frac{\partial c'}{\partial x}, \langle v \rangle \frac{\partial c'}{\partial y}, \langle w \rangle \frac{\partial c'}{\partial z}, \frac{\partial^2 c'}{\partial x^2}, \frac{\partial^2 c'}{\partial y^2} \text{ and } \frac{\partial^2 c'}{\partial y^2} \quad (2.17)$$

are zero and these shall vanish from the Eq. (2.16). Also, equation of continuity for incompressible flow is given by

$$\frac{\partial u'}{\partial x} + \frac{\partial v'}{\partial y} + \frac{\partial w'}{\partial z} = 0 \quad (2.18)$$

Utilizing Eq. (2.17) and Eq. (2.18), Eq. (2.16) can be simplified as

$$\frac{\partial \langle c \rangle}{\partial t} + \langle u \rangle \frac{\partial \langle c \rangle}{\partial x} + \langle v \rangle \frac{\partial \langle c \rangle}{\partial y} + \langle w \rangle \frac{\partial \langle c \rangle}{\partial z} = e_m \left(\frac{\partial^2 \langle c \rangle}{\partial x^2} + \frac{\partial^2 \langle c \rangle}{\partial y^2} + \frac{\partial^2 \langle c \rangle}{\partial z^2} \right) - \left[\frac{\partial \left(\langle u'c' \rangle \right)}{\partial x} + \frac{\partial \left(\langle v'c' \rangle \right)}{\partial y} + \frac{\partial \left(\langle w'c' \rangle \right)}{\partial z} \right] \quad (2.19)$$

Comparing Eq. (2.19) with Eq. (2.12), it appears that first seven terms are identical except that point values of Eq. (2.12) have been replaced by the ensemble average in Eq. (2.19). Also, in Eq. (2.19), terms like, $-\left[\frac{\partial \left(\langle u'c' \rangle \right)}{\partial x} + \frac{\partial \left(\langle v'c' \rangle \right)}{\partial y} + \frac{\partial \left(\langle w'c' \rangle \right)}{\partial z} \right]$ appeared due to averaging of Eq. (2.12). It is true that average of fluctuations is zero but it is observed that sum of product of fluctuations is non-zero, as the turbulence quantities have correlation with each other. Thus, these additional terms are called as turbulent or eddy diffusion.

In channel flow, eddy or turbulent diffusion is more dominating phenomenon in spreading dye tracer than molecular diffusion. It does not curtail off the importance of the molecular diffusion and still remains the basic phenomenon which starts the spreading of dye later replaced by turbulent diffusion when turbulence of channel comes into play. Turbulent diffusion basically more rapidly tear apart the dye tracer and creates local concentration gradients which in turn enhances the molecular diffusion. Thus, one can say that due to the combined action of turbulent eddies and molecular diffusion, the tracer mixes more rapidly in turbulent flow than laminar flow.

According to ergodic hypothesis, "After the flow has attain a steady state, the value of ensemble mean is equal to temporal, spatial and volumetric average.' Thus, in Eq. (2.19), one can replace ensemble mean by temporal mean, as the whole analysis of turbulent flow is done by taking time-mean. Hence, Eq. (2.19) can be written as

$$\frac{\partial \bar{c}}{\partial t} + \bar{u}\frac{\partial \bar{c}}{\partial x} + \bar{v}\frac{\partial \bar{c}}{\partial y} + \bar{w}\frac{\partial \bar{c}}{\partial z} = e_m\left(\frac{\partial^2 \bar{c}}{\partial x^2} + \frac{\partial^2 \bar{c}}{\partial y^2} + \frac{\partial^2 \bar{c}}{\partial z^2}\right) - \left[\frac{\partial\left(\overline{u'c'}\right)}{\partial x} + \frac{\partial\left(\overline{v'c'}\right)}{\partial y} + \frac{\partial\left(\overline{w'c'}\right)}{\partial z}\right] \quad (2.20)$$

The overbar in Eq. (2.20) represents the time-averaged values. Since, Eq. (2.20) represents the transport of tracer in turbulent flow, but, solution of this equation is not possible unless the velocity and concentration fluctuation have a relationship with the average flow velocity and concentration.

G I Taylor in 1921, published a classical study, in which he showed that in homogeneous and stationary turbulent flow after a sufficient time has passed since the tracer is released in the flow, the variance of tracer cloud varies linearly with the time. Thus, according to him, Fick's law is applicable to the turbulent diffusion provided sufficient time has elapsed since tracer injection. Thus, by analogy with molecular diffusion, it can be written as:

$$\overline{u'c'} = -e_x \frac{\partial \bar{c}}{\partial x} \quad (2.21a)$$

$$\overline{v'c'} = -e_y \frac{\partial \bar{c}}{\partial y} \quad (2.21b)$$

$$\overline{w'c'} = -e_z \frac{\partial \bar{c}}{\partial z} \quad (2.21c)$$

Here, e_x, e_y and e_z are turbulent diffusion coefficients or eddy diffusivities in respective directions (Kalinske and Pien, 1944). There are considerable differences between eddy diffusivities and molecular diffusion coefficients. Firstly, molecular diffusion coefficient is of the order of 10^{-9} m^2/s whereas eddy diffusivities are of the order of 10^{-3} m^2/s. Secondly, molecular diffusion coefficient is independent of flow and directions and is a property of fluid whereas eddy diffusivities are varying with respect to direction of flow and flow geometry and is property of flow rather than fluid. Considering, e_x, e_y and e_z being constant and substituting Eq. (2.21 a-c) in Eq. (2.20) and removing overbars yields

$$\frac{\partial c}{\partial t} + u\frac{\partial c}{\partial x} + v\frac{\partial c}{\partial y} + w\frac{\partial c}{\partial z} = \left(e_m + e_x\right)\frac{\partial^2 c}{\partial x^2} + \left(e_m + e_y\right)\frac{\partial^2 c}{\partial y^2} + \left(e_m + e_z\right)\frac{\partial^2 c}{\partial z^2} \quad (2.22)$$

Hence, Eq. (2.22) represents the mass balance equation in turbulent flow and hence can be used in many practical problems where turbulence is dominant in the flow. Many investigators

like Ahmad et al. (1999), Ahmad and Kothyari (2001), Guan et al. (2002), etc. developed different models to solve the advection-diffusion equation.

2.3 DEPTH AVERAGING OF ADVECTION-DIFFUSION EQUATION

A general depth-averaged equation is derived here in this section by integrating Eq. (2.22) from bed z = b to water surface z = a, assuming flow to be steady. In order to integrate Eq. (2.22) Leibnitz's rule is used in extensive way, which states (Rutherford, 1994):

$$\int_{b(x,y)}^{a(x,y)} \frac{\partial}{\partial x} f(x,z)dy = \frac{\partial}{\partial x}\int_{b(x,y)}^{a(x,y)} f(x,z)dz - f(x,a)\frac{\partial a}{\partial x} + f(x,b)\frac{\partial b}{\partial x} \tag{2.23}$$

Hence, integrating Eq. (2.22) term by term and neglecting the e_m as it is very-very less than e_x, e_y and e_z, respectively. Thus, the integration leads to:

$$\begin{aligned}
&\int_b^a \frac{\partial c}{\partial t}dz + \frac{\partial}{\partial x}\int_b^a (uc)\mathrm{d}z - (uc)_a \frac{\partial a}{\partial x} + (uc)_b \frac{\partial b}{\partial x} + \frac{\partial}{\partial y}\int_b^a vc dz - \\
&(vc)_a \frac{\partial a}{\partial y} + (vc)_b \frac{\partial b}{\partial y} + (wc)_a - (wc)_b \\
&= \frac{\partial}{\partial x}\int_b^a e_x \frac{\partial c}{\partial x}dz - \left(e_x \frac{\partial c}{\partial x}\right)_a \frac{\partial a}{\partial x} + \left(e_x \frac{\partial c}{\partial x}\right)_b \frac{\partial b}{\partial x} + \\
&\frac{\partial}{\partial y}\int_b^a e_y \frac{\partial c}{\partial y}dz - \left(e_y \frac{\partial c}{\partial y}\right)_a \frac{\partial a}{\partial y} + \left(e_y \frac{\partial c}{\partial y}\right)_b \frac{\partial b}{\partial y} + \left(e_z \frac{\partial c}{\partial z}\right)_a - \left(e_z \frac{\partial c}{\partial z}\right)_b
\end{aligned} \tag{2.24}$$

Now, re-arranging the terms in Eq. (2.24) gives

$$\begin{aligned}
&\int_b^a \frac{\partial c}{\partial t}dz + \frac{\partial}{\partial x}\int_b^a uc\mathrm{d}z + \frac{\partial}{\partial y}\int_b^a vc dz = \frac{\partial}{\partial x}\int_b^a e_x \frac{\partial c}{\partial x}dz + \frac{\partial}{\partial y}\int_b^a e_y \frac{\partial c}{\partial y}dz + \\
&\left[c\left(u\frac{\partial a}{\partial x} + v\frac{\partial a}{\partial y} - w\right)\right]_a - \left[c\left(u\frac{\partial b}{\partial x} + v\frac{\partial b}{\partial y} - w\right)\right]_b - \left[\left(e_x \frac{\partial c}{\partial x}\frac{\partial a}{\partial x} + e_y \frac{\partial c}{\partial y}\frac{\partial a}{\partial y} - e_z \frac{\partial c}{\partial z}\right)\right]_a \\
&+ \left[\left(e_x \frac{\partial c}{\partial x}\frac{\partial b}{\partial x} + e_y \frac{\partial c}{\partial y}\frac{\partial b}{\partial y} - e_z \frac{\partial c}{\partial z}\right)\right]_b
\end{aligned} \tag{2.25}$$

Now, the concentration and water flux normal to the bed of river and water surface is zero. Hence, except first two terms on the right hand side of Eq. (2.25), all terms will vanish under the normal flux condition.

Now, integral over the depth can be written as

$$\frac{\partial}{\partial x}\int_{b}^{a} u c \mathrm{dz} = \frac{\partial}{\partial x}\left(\overline{huc}\right) \tag{2.26}$$

Here, overbar denotes the depth-averaged quantity. Implementing, Eq. (2.26) in Eq. (2.25), it yields

$$\frac{\partial\left(\overline{hc}\right)}{\partial t} + \frac{\partial}{\partial x}\left(\overline{huc}\right) + \frac{\partial}{\partial y}\left(\overline{hvc}\right) = \frac{\partial}{\partial x}\left(\overline{he_x \frac{\partial c}{\partial x}}\right) + \frac{\partial}{\partial y}\left(\overline{he_y \frac{\partial c}{\partial y}}\right) \tag{2.27}$$

Now, velocities and concentration can be expressed as summation of a depth averaged and a deviatioric part (Tennekes and Lumley, 1972; Pope, 2000):

$$u = U + u' \tag{2.28a}$$

$$v = V + v' \tag{2.28b}$$

$$c = C + c' \tag{2.28c}$$

Here,

$$U = \frac{1}{h}\int_{0}^{h} u dz \tag{2.29a}$$

$$V = \frac{1}{h}\int_{0}^{h} v dz \tag{2.29b}$$

$$C = \frac{1}{h}\int_{0}^{h} c dz \tag{2.29c}$$

Now, from definition, the deviatioric part when averaged yields zero. Thus, depth averaging of product of velocity and concentration yields

$$\overline{uc} = \overline{\left(U + u'\right)\left(C + c'\right)} = UC + \overline{u'c'} \tag{2.30}$$

As $\overline{u'} = \overline{c'} = 0$.

Assuming that e_x and e_y not vary along the depth, thus

$$\overline{e_x \frac{\partial c}{\partial x}} = e_x \frac{\partial C}{\partial x} \tag{2.31a}$$

$$\overline{e_y \frac{\partial c}{\partial y}} = e_y \frac{\partial C}{\partial y} \tag{2.31b}$$

Hence substituting Eqs. (2.30) and (2.31) in Eq. (2.27) yield

$$\frac{\partial(hC)}{\partial t}+\frac{\partial}{\partial x}(hUC)+\frac{\partial}{\partial y}(hVC)=\frac{\partial}{\partial x}\left(-h\overline{u'c'}+he_x\frac{\partial C}{\partial x}\right)+\frac{\partial}{\partial y}\left(-h\overline{v'c'}+he_y\frac{\partial C}{\partial y}\right) \quad (2.32)$$

In the Eq. (2.32), one can clearly identify that second and third term of left hand side represent advective fluxes in respective direction, whereas terms like $e_x\frac{\partial C}{\partial x}$ and $e_y\frac{\partial C}{\partial y}$ represent turbulent diffusion. Now, terms $-\overline{u'c'}$ and $-\overline{v'c'}$ which arose from depth averaging and non-uniformities of velocity profiles along vertical are called as dispersive terms and phenomenon occurring due to these non-uniformities is called as dispersion.

It was observed that after asymptotically large time, the longitudinal dispersive flux becomes proportional to the longitudinal gradient in the depth-averaged concentration (Beltaos and Day, 1976; Ahmad, 2009). Hence,

$$-\overline{u'c'}=E_x\frac{\partial C}{\partial x} \quad (2.33)$$

Here, E_x = longitudinal dispersion coefficient which accounts for the non-uniformities lies in the distribution of longitudinal velocity along vertical. By analogy

$$-\overline{v'c'}=E_y\frac{\partial C}{\partial y} \quad (2.34)$$

Here, E_y = transverse dispersion coefficient. Substituting Eq. (2.33) and (2.34) into Eq. (2.32) yields

$$\frac{\partial(hC)}{\partial t}+\frac{\partial}{\partial x}(hUC)+\frac{\partial}{\partial y}(hVC)=\frac{\partial}{\partial x}\left[h(E_x+e_x)\frac{\partial C}{\partial x}\right]+\frac{\partial}{\partial y}\left[h(E_y+e_y)\frac{\partial C}{\partial y}\right] \quad (2.35)$$

In Eq. (2.35), rate of transverse mixing is determined by transverse turbulent diffusion, which is assimilated in e_y, and swaying of transverse velocity from depth-averaged transverse velocity (quantified in E_y). Now, it is worth to note that since these two coefficients arise from two different processes but they are clubbed together in single coefficient, in order to represent the transverse mixing process which is responsible for spreading of the tracer in lateral direction. It was observed in real-time flow that value of dispersion coefficient is very-very greater than diffusion coefficient, thus, in Eq. (2.35), turbulent diffusion coefficients e_x and e_y are dropped. Thus, Eq. (2.35), may be written as

$$\frac{\partial(hC)}{\partial t}+\frac{\partial}{\partial x}(hUC)+\frac{\partial}{\partial y}(hVC)=\frac{\partial}{\partial x}\left(hE_x\frac{\partial C}{\partial x}\right)+\frac{\partial}{\partial y}\left(hE_y\frac{\partial C}{\partial y}\right) \qquad (2.36)$$

Equation (2.36) is used extensively in solving tracer transport problems in mid-field, where mixing is primarily in longitudinal and transverse directions (Ahmad, 2008).

2.4 TRANSVERSE MIXING PROCESS

In general flow systems, the width of rivers are very large compared to their depths and also in any flow system there is dominance of vertical turbulence in flow. Thus, mixing of solute in vertical direction is very rapid process and is predominant in the region near to the effluent source. After getting mixed into the vertical direction under the action of transverse turbulence and variation in vertical profiles of transverse velocity, pollutant starts to spread along the river width and mixes along the cross-section of the river. This transverse spreading and mixing of pollutant under the action of transverse shear and turbulence is termed as transverse mixing. The Eq. (2.36) is called as depth-averaged advection dispersion equation and is known to be the governing equation of the transverse mixing. If the tracer source is continuously supplying the tracer, i.e. steady tracer flow, the time differential of Eq. (2.36) shall be zero. For uniform flow "*h*" (depth of flow) shall be constant and can be taken outside the differential. Further, for one-dimensional flow, transverse velocity shall be taken zero. Under transverse mixing, the gradient of the concentration along the longitudinal direction is negligible compared to transverse concentration gradient thus first term of right hand side of Eq. (2.36) may be dropped. With above simplification, the transverse mixing equation in steady and uniform flow under steady tracer flow may be written as (Sayre, 1968; Chang, 1971; Lau and Krishnappan, 1977; Beltaos, 1980; Lau and Krishnappan, 1981; Demetrocopolous, 1994; Ahmad, 2008)

$$U\frac{\partial C}{\partial x}=E_y\frac{\partial^2 C}{\partial y^2} \qquad (2.37)$$

It is clearly understandable that mechanisms accounting for the lateral mixing of solutes are transverse turbulent diffusion and transverse dispersion. But major of the literature (Lau and Krishnappan, 1977; Lau, 1981; Lau and Krishnappan, 1981; Boxall and Guymer, 2003 a & b; Boxall et al., 2003; Albers and Steffler, 2007; etc.) reveals non-uniform distribution of transverse velocity in vertical direction, is a major phenomenon responsible for the lateral mixing of solutes.

2.5 ANALYTICAL MODELS FOR TRANSVERSE MIXING

It is evident that for pollutant transport modeling, modeling of transverse mixing is an important phenomenon. To model the transverse mixing process, solution of transverse mixing equation has to be obtained through

2.5.1 Constant coefficient method

2.5.2 Variable coefficient method

2.5.1 *Constant coefficient method*

Consider Eq. (2.36) for the source supplying the tracer at constant steady rate in one dimensional flow. Thus the temporal differential *i.e.* $\partial C/\partial t$ will become zero and hence Eq. (2.36) will get transformed in the following format

$$\frac{\partial(hUC)}{\partial x} = \underbrace{\frac{\partial}{\partial x}\left(hE_x \frac{\partial C}{\partial x}\right)}_{1} + \underbrace{\frac{\partial}{\partial y}\left(hE_y \frac{\partial C}{\partial y}\right)}_{2} \tag{2.38}$$

Now it is the known fact that longitudinal mixing usually does not interfere with the transverse mixing and generally after mixing it commences, hence the term (1) in Eq. (2.38) becomes zero, and Eq. (2.38) reduces to

$$\frac{\partial(hUC)}{\partial x} = \frac{\partial}{\partial y}\left(hE_y \frac{\partial C}{\partial y}\right) \tag{2.39}$$

Assuming that variation in depth, E_y is negligible and flow is uniform throughout the flow regime. Also assuming that channel is straight, thus, the flow depth, E_y and U are taken out of their respective brackets. Thus, the Eq. (2.39) reduces to Eq. (2.37). The Eq. (2.37) is called as governing equation of constant coefficient method. Discussed below are some of the analytical solution for different type of tracer sources, which are helpful in analyzing the transverse mixing process.

(i) Vertical line source

Assume a steady vertical line source at $x = 0$, $y = y_o$. Now at the both banks the transverse tracer flux is zero, thus it implies:

$$\frac{\partial C}{\partial y} = 0 \qquad \text{at } y = 0 \text{ and } y = B \qquad (2.40)$$

Thus for this vertical line source analytical solution for unbounded flow condition is given below:

$$C(x, y) = \frac{\hat{M}}{H\sqrt{4\pi E_y u x}} \exp\left[-\frac{u(y - y_o)^2}{4E_x x} \right] \qquad (2.41)$$

$\hat{M}$ = Mass inflow rate. Since Eq. (2.37) and Eq. (2.41) both are linear in nature, thus method of images can be applied to solve the problem in bounded flow conditions.

(ii) Vertical line source over a width (plane source)

For prismatic channels of arbitrary cross-sectional shape, Yotsukura and Cobb (1972) developed a method called as cumulative discharge model, which provides the analytical solution of transverse mixing equation where transverse velocity is zero. The transformed equation in x-q coordinate is given by

$$\frac{\partial C}{\partial x} = \frac{\partial}{\partial q}\left[h^2 U E_y \frac{\partial C}{\partial q} \right] \qquad (2.42)$$

Yotsukura and Cobb (1972), Yotsukura and Sayre (1976), Lau and Krishnappan (1977), etc. showed that for practical purpose the term h^2UE_y can be taken as constant and equals the average value across the cross-section with respect to q, that is

$$D_y = \overline{h^2 u E_y} \qquad (2.43)$$

This term D_y is known as diffusion factor. Thus Eq. (2.43) will reduce to the following format

$$\frac{\partial C}{\partial x} = D_y \frac{\partial^2 C}{\partial q^2} \tag{2.44}$$

Now the boundary conditions for Eq. (2.44) will be that there is no flux of pollutant across the flow boundaries and hence

$$\frac{\partial C}{\partial q} = 0 \qquad \text{at } q = 0 \text{ and } q = Q \tag{2.45}$$

Here, Q = stream discharge. Cumulative discharge method does take into account the channel curvature, effect of changes in depth and width, etc. Yotsukura and Cobb (1972) and Lipsett and Beltaos (1978) provided an analytical solution for Eq. (2.44) and assimilating the boundary conditions of Eq. (2.45) with it for a plane vertical source of length ($\omega_s = y_2 - y_1$) and it is as follows:

$$\frac{C}{C_\infty} = \frac{1}{2\omega_s}\left[\begin{array}{l} \frac{1}{2}\left\{erf\left(\frac{\eta_2+\eta}{\sqrt{2\xi}}\right)+erf\left(\frac{\eta_2-\eta}{\sqrt{2\xi}}\right)-erf\left(\frac{\eta_1+\eta}{\sqrt{2\xi}}\right)-erf\left(\frac{\eta_1-\eta}{\sqrt{2\xi}}\right)\right\}+ \\ \sum_{m=1}^{\infty}\left\{\begin{array}{l} erf\left(\frac{\eta_2+2m-\eta}{\sqrt{2\xi}}\right)+erf\left(\frac{\eta_2-2m-\eta}{\sqrt{2\xi}}\right)-erf\left(\frac{\eta_1+2m-\eta}{\sqrt{2\xi}}\right) \\ -erf\left(\frac{\eta_1-2m-\eta}{\sqrt{2\xi}}\right)+erf\left(\frac{\eta_2+2m+\eta}{\sqrt{2\xi}}\right)+erf\left(\frac{\eta_2-2m+\eta}{\sqrt{2\xi}}\right) \\ -erf\left(\frac{\eta_1+2m+\eta}{\sqrt{2\xi}}\right)-erf\left(\frac{\eta_1-2m+\eta}{\sqrt{2\xi}}\right) \end{array}\right\} \end{array}\right] \tag{2.46}$$

Here, $\eta = y/B$ (Here B = width of the stream); $\xi = {2D_y x}\big/{Q^2}$; C_∞ = fully cross-sectional mixed concentration of pollutants and *erf* denotes the error function.

(iii) Slug injection

For neutrally buoyant tracer released as a slug into any rectangular stream with constant longitudinal velocity, the concentration distribution is provided by the analytical solution developed by Shen (1978), which is as follows

$$C(x-ut,q,t) = \frac{1}{2Q\sqrt{\pi E_x t}}\sum_{m=0}^{\infty}\tau_m \cos\left(\frac{m\pi Q_a}{Q}\right)\exp\left[-\frac{(x-ut)^2}{4E_x t} - E_y\frac{m^2\pi^2 u^2 h^2 t}{Q}\right]\cos\left(\frac{m\pi q}{Q}\right) \tag{2.47}$$

Here, τ_m = 1, when m = 0 and τ_m = 2 when $m \neq 0$; Q_a = cumulative discharge at the location of the point source.

2.5.1.1. *Deficiencies of constant mixing coefficient method*

In spite, the fact that the constant transverse mixing coefficient model allows the mixing equation to be solved analytically and greatly enhances the problem solving. But, the thing which restricts the use of the constant mixing coefficient method is the complex bathymetry and velocity distributions. Since, the major assumption of the model is that, that the depth, velocity and transverse dispersion coefficient are constant along and across the channel but in the natural channels the depth and velocity are rather constant but vary across the width, hence the main assumption is invalidated from the real time observations. As the depth and velocity vary across the width it will definitely make the transverse dispersion coefficient to vary. Thus, from these problems arising from the invalid basic assumptions it is a requirement to shift towards a more realistic and heuristic approach to analyze the field problem of transverse mixing. Thus, it gave rise to a variable mixing coefficient approach, which will be discussed further.

(i) Non-uniform depth

In natural channel it is evident that major portion of core flow is a near rectangular channel but near to the bank the depth is somewhat shallower. Holley et al. (1972) conducted the experimental and numerical study on the rectangular and trapezoidal channels. Reach averaged velocity, depth of flow and transverse dispersion coefficients all were the same so that differences between the tracer concentrations can be predicted. The source was steady and continuous and was located at one bank of the channel. It was observed that tracer concentrations near bank were higher than the main core part in the case of trapezoidal channel. The reason given by the Holley et al. (1972) was that near the bank of trapezoidal channel the depth is small so that transverse flux is small. Due to this small transverse flux, the tracer gets accumulated near the bank. Hence, a greater tracer concentration was observed near the bank of trapezoidal channel. Ahmad (2008) also observed that near the bank of any natural river the tracer is more concentrated than the core region of flow. Hence, discrepancies like this lead to evaluation of variable mixing coefficient method and dumping of constant coefficient method. Pilechi et al. (2015) observed that in the bend water is higher at outer bend

while comparing with the water elevation at the inner bend. This difference in water elevation makes the thalweg stream-line to meander, which causes tracer plume to advect towards outer bend and inner bend alternatively. Pilechi et al. (2015) observed that due to generation of super-elevation, a localized field of positive pressure gradient was generated and this localized positive pressure gradient causes separation of flow from the outer bend. Pilechi et al. (2015) observed that advection due to meandering thalweg and dispersion caused by secondary currents enhanced transverse mixing coefficient and transverse mixing process.

(ii) Effect of variable dispersivity

Holley et al. (1972) were first to recognize the effect of variation of transverse dispersivity and was able to pose a problem of effect of variation in E_y on the rate of transverse mixing. Holley considered a trapezoidal channel and assumed following three distribution:

$$E_y = k_1 \bar{h} U_* = constant \tag{2.48}$$

$$E_y = k_2 h U \tag{2.49}$$

$$E_y = k_3 h u_* \tag{2.50}$$

Here, $\bar{h}$ = mean depth of flow; U* = cross-sectional averaged shear velocity. Coefficients k_1, k_2 and k_3 were chosen in such a way that mean value of E_y was same for every case considered in Eq. (2.48) to Eq. (2.50). It was observed that for steady source at the bank, bankside concentrations were higher for Eq. (2.49) and (2.50) than Eq. (2.48). The possible reason behind the variation in dispersivity is that near the bank, the value of depth and velocity is less and shear is more thus, Eq. (2.49) and Eq. (2.50) predicted lower values of E_y than Eq. (2.48), this clearly indicates that diffusivity is lower near bank than the core flow. Thus it clearly signifies the fact that variability in transverse dispersivity does affect the rate of transverse mixing. Ahmad (2008) also considered the effect of variability of the transverse mixing coefficient and obtained the similar observations to what Holley et al. (1972) have observed.

2.5.2 Stream tube model (*Variable coefficient method)*

One of the major flaw associated with the constant coefficient method is that it gives rise to the transverse mixing coefficients which are not realistic, e.g., Holley et al. (1972) observed the

negative value of lateral mixing coefficients in the area of high separation although they considered, the mixing coefficients to be constant throughout the flow field. Constant mixing model assumes flow field to govern by an average depth, velocity and cross-section but in real scenarios all aforesaid factors vary point to point and section to section.

Thus, Yotsukura and Cobb (1972) and Yotsukura and Sayre (1976) introduced a method called as "cumulative discharge method" which was based on orthogonal curvilinear system and is defined as

$$q(\alpha_o, \beta_o) = \int_{\beta_o=0}^{\beta_o} m_{\beta_o} h v_{\alpha_o} d\beta_o \tag{2.51}$$

Here, α_o and β_o = longitudinal and transverse coordinates in an orthogonal curvilinear system; α_o is parallel with the local depth-averaged longitudinal velocity and β_o is transverse across the flow; q = cumulative discharge; m_{β_o} = metric coefficient which accounts for channel curvature and lies between 0.8-1.2 for meandering channels and 1.0 for straight channels; v_{α_o} = depth averaged velocity. By convention $q = 0$ is taken for left bank and $q = Q$ for right bank.

Figure 2.2 shows a sketch of orthogonal curvilinear coordinate system. For an unsteady tracer source in steady flow, the tracer transport equation is as follows (Rutherford, 1994)

$$\frac{\partial C}{\partial t} + \frac{v_{\alpha_o}}{m_{\alpha_o}} \frac{\partial C}{\partial \alpha_o} = \frac{1}{h m_{\alpha_o} m_{\beta_o}} \frac{\partial}{\partial \alpha_o} \left(\frac{m_{\beta_o}}{m_{\alpha_o}} h E_{\alpha_o} \frac{\partial C}{\partial \alpha_o} \right) + \frac{v_{\alpha_o}}{m_{\alpha_o}} \frac{\partial}{\partial \alpha_o} \left(m_{\alpha_o} h^2 v_{\alpha_o} E_{\beta_o} \frac{\partial C}{\partial q} \right) \tag{2.52}$$

Here, E_α and E_β are the dispersion coefficients in α and β directions. Clearly from Fig. 2.2, due to the curvature, the $L_{AB} \neq L_{CD}$ and $L_{BD} \neq L_{AC}$, hence metric coefficient can be defined as

$$m_{\alpha_o} = \frac{L_{CD}}{L_{AB}} \tag{2.53a}$$

$$m_{\beta_o} = \frac{L_{BD}}{L_{AC}} \tag{2.53b}$$

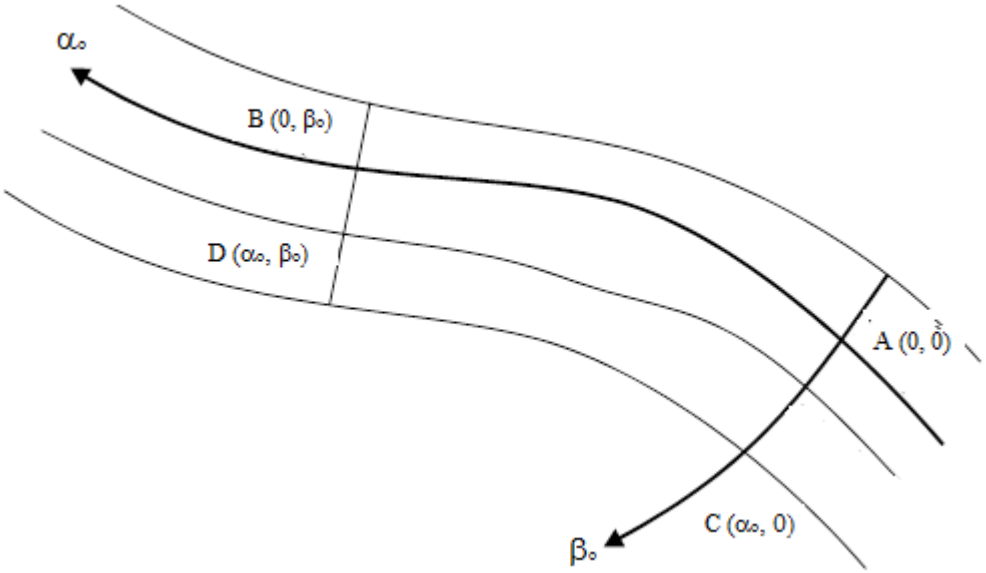

Fig. 2.2 Sketch showing an orthogonal curvilinear coordinate system

Yotsukura and Sayre (1976) assumed that source of pollution is a steady source, thus Eq. (2.56) will reduce to

$$\frac{\partial C}{\partial \alpha_o} = \frac{\partial}{\partial q}\left(m_{\alpha_o} h^2 v_{\alpha_o} E_{\beta_o} \frac{\partial C}{\partial q} \right) \tag{2.54}$$

Now, defining factor of diffusion as

$$D_y = m_{\alpha_o} h^2 v_{\alpha_o} E_{\beta_o} \tag{2.55}$$

Since, at the banks the longitudinal velocity and depth of flow is very low thus, the factor of diffusion varies across the channel. While using Eq. (2.54) and Eq. (2.55), the transverse velocity is not present in the equation explicitly but it did not mean that it has still not take into account the variation of water movements across the channel.

For convenience D_y can be written as

$$D_y = \psi h^2 U E_y \tag{2.56}$$

Here, ψ = a dimensionless shape factor which lies in the range of 1.0-3.6 (Beltaos, 1980) and is given by

$$\psi = \frac{1}{B}\int_{y=0}^{B}\left(\frac{h_z}{h}\right)^2 \frac{u}{U}dy \tag{2.57}$$

Now, several investigators like (Yotsukura and Cob, 1972; Sayre, 1979, etc.) assumed that variation of D_y can be taken to be uniform and constant over the flow field thus, taking Eq. (2.44) with the boundary conditions defined in Eq. (2.45) analytical solutions of Eq. (2.54) for unbounded flow with source place at $x = 0$ and $q = q_o$ is given by

$$C(x,q) = \frac{M}{\sqrt{4\pi D_y x}} \exp\left[-\frac{(q-q_o)^2}{4D_y x}\right] \tag{2.58}$$

By utilizing method of images, the effect of boundaries can be accommodated in the solution.

2.6 NUMERICAL SOLUTION OF TRANSVERSE MIXING EQUATION

Analytical solutions are not sufficiently accurate as they are evolved due to over-simplification of mass conservation equation. Thus, in order to provide more precise and generalized solution numerical methods are employed. Though, numerical methods required more effort and data to operate than the simple analytical solution but they provide much wide picture of process than doing preliminary calculations using simple analytical solutions. Though there are many numerical solutions available in literature, but a few are described below:

(i) Lau and Krishnappan (1981)

Lau and Krishnappan (1981) utilized the method developed by Stone and Brian (1963) to solve the advection-diffusion type equations of following format

$$\frac{\partial C}{\partial x} + V_k \frac{\partial C}{\partial \zeta} = D\frac{\partial^2 C}{\partial \zeta^2} \tag{2.59}$$

Here,

$$V_k = -\frac{1}{Q^2}\frac{\partial E_y}{\partial \zeta} \tag{2.60}$$

and $$D = \frac{1}{Q^2}E_y \tag{2.61}$$

Referring to the grid system shown in Fig. 2.3, Stone and Brian (1963) discretized the Eq. (2.59) and obtained the following finite difference analogue

$$\frac{1}{\Delta x}\left[g_s\left(C_{i+1,j} - C_{i,j}\right) + \frac{\theta_s}{2}\left(C_{i+1,j\ 1} - C_{i,j\ 1}\right) + m_s\left(C_{i+1,j+1} - C_{i,j+1}\right)\right]$$
$$+ \frac{V_{i,j}}{\Delta\zeta}\left[a\left(C_{i,j+1} - C_{i,j}\right) + \frac{\varepsilon_s}{2}\left(C_{i,j} - C_{i,j\ 1}\right) + b_s\left(C_{i+1,j+1} - C_{i,+1,j}\right) + d\left(C_{i+1,j} - C_{i,+1,j\ 1}\right)\right] \qquad (2.62)$$
$$= \frac{D_{i,j}}{2\left(\Delta\zeta\right)^2}\left[\left(C_{i,j+1} - 2C_{i,j} + C_{i,j\ 1}\right) + \left(C_{i+1,j+1} - 2C_{i+1,j} + C_{i+1,j\ 1}\right)\right]$$

In this scheme, Stone and Brian (1963) used weights or weighing coefficients, a, $\varepsilon_s/2$, b_s and d to approximate the derivative $\partial C/\partial\zeta$ and in order to approximate the derivative $\partial C/\partial x$, they used g_s, $\theta_s/2$ and m as weighing coefficients.

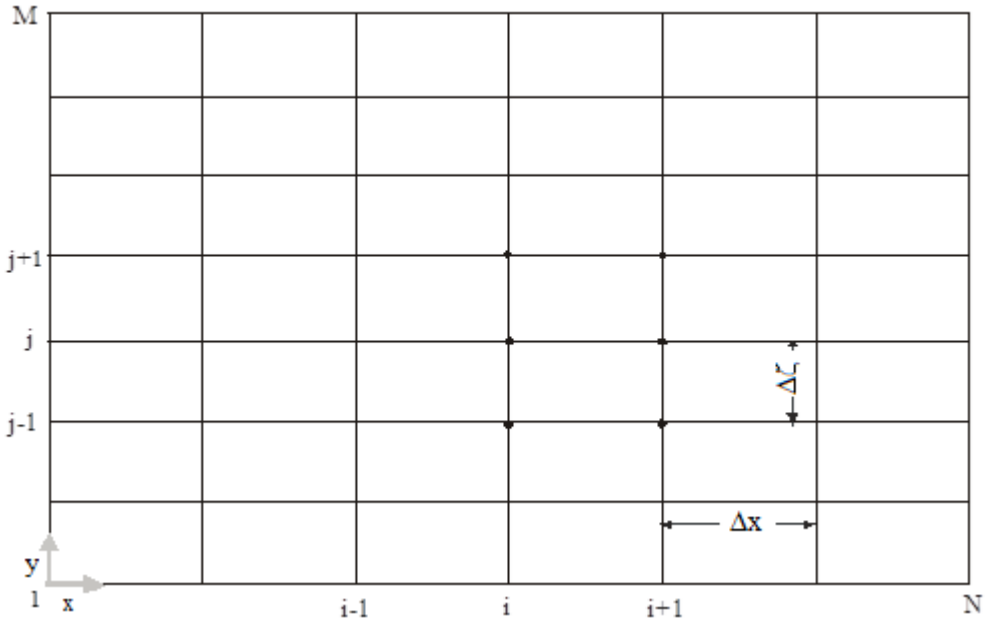

Fig.2.3 Grid system for Stone and Brian (1963) scheme (Lau and Krishnappan, 1981)

The following conditions on weighing coefficients are to be satisfied:

$$a + \frac{\varepsilon_s}{2} + b_s + d = 1 \qquad (2.63)$$

and $g_s + \frac{\theta_s}{2} + m = 1$ (2.64)

Lau and Krishnappan (1981) did not use any weighing factors for approximating the second derivative $\partial^2 C/\partial \zeta^2$. Crank-Nicolson scheme was utilized by Lau and Krishnappan (1981) in order to discretize Eq. (2.59). By optimizing the weighing coefficients so that they not only satisfy Eq. (2.63) and Eq. (2.64) though they give solutions which nearly matches the analytical solution, they obtained the following values of weighing coefficients:

$$g_s = \frac{2}{3}; \qquad \theta_s = m_s = \frac{1}{6}; \qquad a = b_s = d = \frac{\varepsilon_s}{2} = \frac{1}{4} \quad (2.65)$$

They suggested use of the aforesaid values of weighing coefficients when the values of *V* and *D* are not constant. If the concentration distribution at any station say *i* is known thus in order to obtain the value of concentration distribution at any unknown level say *i+1* has to be calculated for known boundary condition and zero flux conditions at side walls, Lau and Krishnappan (1981) proposed the following matrix notation for Eq. (2.62):

$$\begin{bmatrix} q_2 & -r_2 & & & & \\ -p_3 & q_3 & -r_3 & & & \\ & -p_4 & q_4 & -r_4 & & \\ & & \ddots & \ddots & \ddots & \\ & & & & -r_{M-1} & \\ & & & -p_M & -q_M & \end{bmatrix} \begin{bmatrix} C_{i+1,2} \\ C_{i+1,3} \\ C_{i+1,4} \\ \\ C_{i+1,M-1} \\ C_{i+1,M} \end{bmatrix} = \begin{bmatrix} S_2 \\ S_3 \\ S_4 \\ \\ S_{M-1} \\ S_M \end{bmatrix} \quad (2.66)$$

Here,

$$q_j = \frac{g_s}{\Delta x} + D_{i,j} \frac{1}{(\Delta\zeta)^2} + V_{i,j} \frac{1}{\Delta\zeta}(d - b_s), \ (j=2, 3... M);$$

$$p_j = -\frac{\theta_s}{2}\frac{1}{\Delta x} + D_{i,j} \frac{1}{2(\Delta\zeta)^2} + V_{i,j} \frac{1}{\Delta\zeta} d, \ (j=2, 3... M);$$

$$r_j = -\frac{m_s}{\Delta x} + D_{i,j} \frac{1}{2(\Delta\zeta)^2} - V_{i,j} \frac{1}{\Delta\zeta} b_s, \ (j=2, 3... M\text{-}1);$$

$$S_j = C_{i,j-1}\left[\frac{\theta_s}{2}\frac{1}{\Delta x} + D_{i,j}\frac{1}{2(\Delta\zeta)^2} + V_{i,j}\frac{\varepsilon_s}{2\Delta\zeta}\right] + C_{i,j}\left[\frac{g_s}{\Delta x} - D_{i,j}\frac{1}{(\Delta\zeta)^2} - V_{i,j}\frac{\varepsilon_s}{2\Delta\zeta}\right]$$
$$+ C_{i,j+1}\left[\frac{m}{\Delta x} + D_{i,j}\frac{1}{2(\Delta\zeta)^2} - V_{i,j}\frac{a}{\Delta\zeta}\right],$$

(j=2, 3... M); (2.67)

The set of the equations created during the solution were solved with the help of Gauss-Seidal method by Lau and Krishnappan (1981).

(ii) Luk et al. (1990)

Luk et al. (1990) developed a two dimensional model in order to solve the transient two-dimensional mixing equation in order to simulate transport of pollutant in natural river. They utilized the Stream-tube concept in order to derive their method called as MABOCOST (Mixing Analysis Based On Concept Of Stream Tube) by solving following equation in a curvilinear coordinate system (Fig. 2.4) as

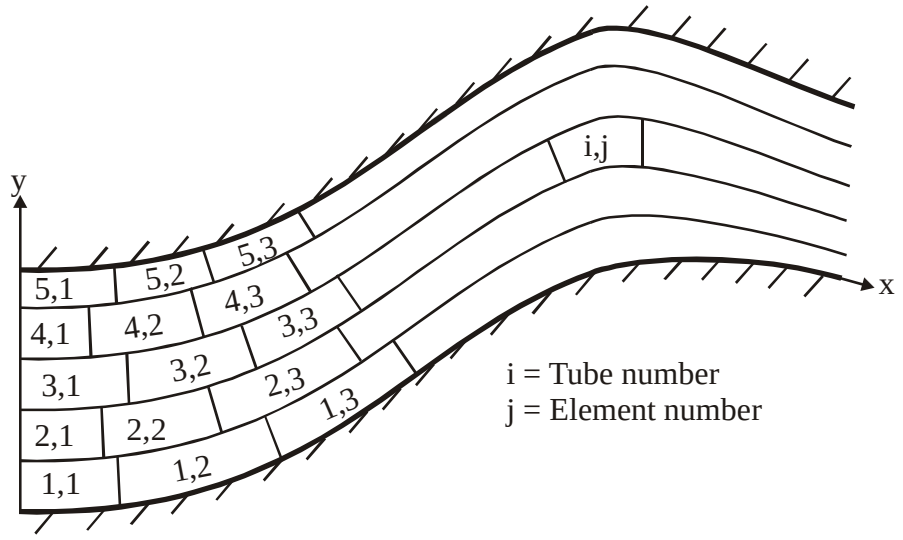

Fig. 2.4 Division of stream tubes into variable length elements (Luk et al., 1990)

$$\frac{\partial C}{\partial t} + \frac{U}{m_x}\frac{\partial C}{\partial x} = \frac{\partial}{\partial q}\left(\frac{h^2U^2E_y}{Q^2}\frac{\partial C}{\partial q}\right) + \alpha_d C + \beta_d \quad (2.68)$$

Here, α_d = decay constant of pollutant; β_d = any source or sink present in pollutant mixing zone. Luk et al. (1990) chose a simplest asymmetrical first order explicit scheme which is quite

stable, non-diffusive and non dispersive when courant number (C_r) is set as unity. Courant number is defined as follows

$$C_r = \frac{u\Delta t}{\Delta x} \tag{2.69}$$

Here, Δt and Δx = time step and longitudinal grid size of grid. Luk et al. (1990) analyzed that finite difference scheme they are using is stable only when Courant number is unity, hence replacing $C_r = 1$ in Eq. (2.69), they obtained the following equation in order to set the grid size and time step for finite difference grid that will be used in order to solve Eq. (2.68):

$$u\Delta t = \Delta x \tag{2.70}$$

From Eq. (2.70), Luk et al. (1990) obtained elements of various sizes as the Eq. (2.70) depends upon the local stream velocity hence for constant Δt or Δx the size of remaining variable in Eq. (2.70) will change which will cause change in grid-size. Luk et al. (1990) utilized split operator scheme to solve the Eq. (2.68). They first solved for the advection part of the Eq. (2.68) and they argued that since the grid was constructed on the basis that it takes unit time step for pollutant to advect from one element to another, hence they obtained following equation by advecting the pollutant to next element in temporal and spatial grid

$$C(i, j, t + \Delta t) = C(i, j-1, t) \tag{2.71}$$

Here, i = number of stream tubes; j = number of element in the stream tube. By following the step given by Eq. (2.71), Luk et al. (1990) allowed concentration of pollutant to get dispersed laterally to each adjacent element by utilizing following relationship

$$\begin{aligned} C(i, j, t + \Delta t) &= C(i, j, t) + \frac{\Delta t}{\theta_v} \sum_{p=1}^{m} \frac{\left(l\Delta x_l \overline{h\Delta y D_y \Delta C}\right)p}{\Delta q_l^2} \\ &+ \frac{(l\Delta x_l)_p \left|(h\Delta y)_p - h\Delta y\right| \Delta C_p}{\Delta q_l^2} + \sum_{p=1}^{k} \frac{\left(r\Delta x_r \overline{h\Delta y D_y \Delta C}\right)p}{\Delta q_r^2} \\ &+ \frac{(r\Delta x_r)_p \left|(h\Delta y)_p - h\Delta y\right| \Delta C_p}{\Delta q_r^2} \end{aligned} \tag{2.72}$$

Here, $D_y = \frac{h^2 U^2 E_y}{Q^2}$ = Diffusion factor; θ_v = volume of a mesh element; l, r = the fractions of overlapping area between an element and its adjacent element on the left and right sides, respectively; Δx = elemental length; Δy = elemental width; ΔC = the concentration excess; and Δn = the fraction of cumulative discharge between the centers of two elements. The subscript p represents the quantities for the *pth* adjacent element, and the subscripts l and r represent the quantity of the left and right adjacent elements, respectively. Overbars represent quantities averaged between an element and its adjacent elements. In order to simulate the decay of concentration of pollutant, Luk et al. (1990) considered the kinetics of chemical decay of pollutants to be of first order and applied the following step to simulate the observations

$$C(i, j, t + \Delta t) = C(i, j, t).\exp(\alpha_d \Delta t) \tag{2.73}$$

and finally Luk et al. (1990) added the if possible source or sink terms for the current time step to each individual element. These processes were repeated for all the time steps to obtain the concentration profiles at each time step for all elements. Luk et al. (1990) by performing various experiments observed that by interchanging the order of adding various processes that were being added in MABOCOST did not affected the quality of results in a considerable manner.

(iii) Demetracopoulos (1994)

Demetracopoulos (1994) utilized the stream tube model given by Fischer (1969) and modified by the Yotsokura et al. (1970), to give following equation for depth-averaged steady state conservative tracer transport equation

$$\frac{\partial C}{\partial x} = \frac{\partial}{\partial q}\left(m_x h^2 U E_y \frac{\partial C}{\partial q} \right) \tag{2.74}$$

Demetracopoulos (1994) stated that since the previous work done on the numerical solution of Eq. (2.44) incorporated adjustments of many such parameters which were not physically attributing to the mass transport process, thus he provided a non-linear interpolation scheme which accounted for the relative strengths of advection and diffusion terms in the tracer mass transport. By utilizing the work of Patankar (1980), Demetracopoulos (1994) transformed the

Eq. (2.74) into the following form

$$\frac{\partial C}{\partial x} = \frac{1}{Q^2}\frac{\partial}{\partial \chi}\left(D_y \frac{\partial C}{\partial \chi}\right) \tag{2.75}$$

Here, $\chi = q/Q$; $D_y = m_x h^2 U E_y$. By expanding Eq. (2.75), Demetracopoulos (1994) obtained the following equation

$$\frac{\partial C}{\partial x} + B_k \frac{\partial C}{\partial \chi} = D' \frac{\partial^2 C}{\partial \chi^2} \tag{2.76}$$

Here, $B_k = -\partial D'/\partial \chi$; $D' = D_y/Q^2$. Demetracopoulos (1994) observed that transverse directional mass transport was basically determined by an advective term and a diffusion term. In order to discretize, Demetracopoulos (1994) utilized the following one dimensional, steady state advection-diffusion equation

$$U \frac{\partial \phi}{\partial X} = e \frac{\partial^2 \phi}{\partial X^2} \tag{2.77}$$

Here, U = flow velocity; X = coordinate of flow field; ϕ = transportable property; e = diffusion constant. The analytical solution for Eq. (2.77) is as follows for domain; $0 \le X \le L$ and boundary conditions; $\phi = \phi_1$ for $X = 0$ and $\phi = \phi_2$ for $X = L$:

$$\frac{\phi - \phi_1}{\phi_2 - \phi_1} = \frac{\exp(\mathrm{Px/L}) - 1}{\exp(\mathrm{P}) - 1} \tag{2.78}$$

Here, P = Peclet Number = UL/e. By incorporating the exponential scheme to interpolate the advection and diffusion in transverse direction within computational cells, Demetracopoulos (1994) derived the following equation:

$$\left[-\frac{V_{i,j}}{\delta\eta}\left(1+\frac{1}{\exp(P_{i,j-1/2})-1}\right)-\frac{\exp(0.5P_{i,j-1/2})}{\exp(P_{i,j-1/2})-1}\left(\frac{D_{i,j}P_{1,j-1/2}}{\delta\eta^2}-\frac{V_{i,j}}{\delta\eta}\right)\right]C_{i,j-1}+\left[\frac{1}{\delta x}+\frac{V_{i,j}}{\delta\eta}\left(1+\frac{1}{\exp(P_{i,j+1/2})-1}+\frac{1}{\exp(P_{i,j-1/2})-1}\right)+\frac{\exp(0.5P_{i,j+1/2})}{\exp(P_{i,j+1/2})-1}\left(\frac{D_{i,j}P_{1,j+1/2}}{\delta\eta^2}-\frac{V_{i,j}}{\delta\eta}\right)-\frac{\exp(0.5P_{i,j-1/2})}{\exp(P_{i,j-1/2})-1}\left(\frac{D_{i,j}P_{1,j-1/2}}{\delta\eta^2}-\frac{V_{i,j}}{\delta\eta}\right)\right]C_{i,j}+\left[-\frac{V_{i,j}}{\delta\eta}\left(1+\frac{1}{\exp(P_{i,j+1/2})-1}\right)-\frac{\exp(0.5P_{i,j+1/2})}{\exp(P_{i,j+1/2})-1}\left(\frac{D_{i,j}P_{1,j+1/2}}{\delta\eta^2}-\frac{V_{i,j}}{\delta\eta}\right)\right]C_{i,j+1}=\frac{1}{\delta x}C_{i-1,j} \tag{2.79}$$

Demetracopoulos (1994) ensured that accomplishment of continuity of total flux must exist in the left hand and right hand side neighbor of control volume interfaces (i.e. j+1/2) so that solution of Eq. (2.79) can be obtained at grid points and Peclet number can be obtained at control volume.

(iv) Ahmad (2008)

Ahmad (2008) developed a finite volume model in order to study the transverse mixing in steady state streams. Ahmad (2008) integrated numerically the steady state transverse mixing equation described by Eq. (2.74) with m_x = 1. Ahmad (2008) transformed the Eq. (2.74) by taking cross-sectional average into the following format:

$$\frac{\partial C}{\partial x}=\overline{D_y}\frac{\partial^2 C}{\partial q^2} \tag{2.80}$$

Here,

$$\overline{D_y}=\overline{h^2 u e_y} \tag{2.81}$$

Since according to stream-tube model there should be no flux of pollutants across the flow, hence Ahmad (2008) provided following boundary conditions:

$$\frac{\partial C}{\partial x}=0 \text{ at } q=0 \text{ and } q=Q \tag{2.82}$$

In order to compare the variable e_y and constant e_y methods, Ahmad (2008) took the average value of $e_y/u_* h$ = 0.225 for constant mixing coefficient method. Ahmad (2008) solved the steady state transport equation numerically by incorporating the upwind scheme of finite difference, finally obtained following equation for a peculiar node *P (i,j)*:

$$a_s^j C_i^{j\ 1} + a_p^j C_i^j + a_n^j C_i^{j+1} = a_w^j C_{i\ 1}^j + b^j \quad (2.83)$$

Here,

a_s, a_n, a_p and a_w = coefficients of concentration; C_i^j = Concentration at node (i,j)

Also,

$$a_s^j = a_3^j \quad (2.84a)$$

$$a_p^j = \left(a_1^j + a_2^j + a_3^j\right) \quad (2.84b)$$

$$a_n^j = a_2^j \quad (2.84c)$$

$$a_w^j = a_1^j \quad (2.84d)$$

$$b^j = 0 \quad (2.84e)$$

$$a_1^j = \frac{h_j u_j \Delta y^2}{\Delta x} \quad (2.84f)$$

$$a_2^j = \left(\frac{h^j + h^{j+1}}{2}\right)\left(\frac{e_y^j + e_y^{j+1}}{2}\right) \quad (2.84g)$$

$$a_3^j = \left(\frac{h^j + h^{j-1}}{2}\right)\left(\frac{e_y^j + e_y^{j\text{-}1}}{2}\right) \quad (2.84h)$$

Ahmad (2008) observed that while solving the system of equation generated for different *i* and *j* from Eq. (2.83), a tri-diagonal matrix was formed. Thomas algorithm or tri-diagonal matrix algorithm (TDMA) was utilized by Ahmad (2008) to solve the tri-diagonal matrix iteratively and line by line until a converging value of concentration was obtained.

2.7 TRANSVERSE MIXING COEFFICIENT

It is a known fact that, in infinitely wide uniform channel, *i.e.* straight and rectangular channel, no secondary flow exists, hence there is no transverse velocity profile. Thus, it is not possible to establish an analogy of transverse mixing like vertical mixing with variation of eddy diffusivity and velocity profile along the depth. Hence, only by performing experimentations one is able to establish value of transverse mixing coefficient. Just like analogy with vertical mixing which commences due to vertical eddies generated due to bed friction, transverse mixing is also said to be due to transverse eddies. It is hence not proved yet that how the vertical eddies go under rotation to become transverse eddies. It can also be understood that

maximum scale of transverse eddies cannot go beyond channel width in wide channel but in shallow channel transverse eddies are restricted due to channel friction. Thus, it is the channel depth which governs the transverse mixing coefficient along with channel friction. Many investigators like Holley et al. (1972); Holley and Abraham (1973 a & b); Ward (1974); Engemann (1974); Beltaos (1975); Yotsoukura and Sayre (1976); Lau and Krishnappan (1977); Cotton and West (1980); Lau and Krishnappan (1981); Holley Jr. and Nerat (1983); Webel and Schatzmann (1984); Boxall and Guymer (2003); Boxall et al. (2003); Seo et al. (2006); Albers and Steffler (2007); Ahmad (2008); Zheng et al. (2008); Dow et al. (2009); Baek and Seo (2010) and Azamathulla and Ahmad (2012) tried to establish relation of transverse mixing coefficient with many parameters like flow velocity, bed roughness, with, depth, shear velocity, channel curvature, sinuosity, etc. Table 2.1, summarizes range of transverse mixing coefficient proposed by various investigators.

Table 2.1 Transverse mixing coefficient by various investigators

S.No.	Investigators	Range of transverse mixing coefficient (E_y/u_*h)	Remarks
1	Beltaos (1980)	0.22-0.42	for meandering channel
2	Holley Jr. and Nerat (1983)	0.5-2.5	river measurement
3	Webel and Schatzmann (1984)	0.175-0.177	smooth bed
		0.130-0.159	rough bed
4	Bruno et al. (1990)	0.21-1.89	buoyant tracer
5	Chau (2000)	0.14-0.21	smooth bed
		0.14-0.21	sandpaper
		0.13-0.19	steel mesh
		0.15-0.24	small stones
6	Seo et al. (2006)	0.23-1.21	for meandering river
7	Baek and Seo (2010)	0.21-0.91	Stream tube method

Secondary currents were observed to be the main factors to influence transverse mixing firstly studied by Fischer (1969). Altogether with secondary currents, aspect-ratio, bed friction, tracer buoyancy, etc. were also recorded in various literatures that affects spreading of tracer in lateral direction. Chang (1971) observed that maximum transverse mixing coefficient was obtained near the downstream portion of bend and minimum near the upstream portion of bend. While plotting the normalized transverse dispersion coefficient with aspect ratio (width-depth ratio), it was observed by Seo et al. (2006) that with the increase in the aspect ratio the normalized transverse mixing coefficient also increased as the strength of secondary currents was observed to increase with the increase in aspect ratio. Webel and Schatzmann (1984) observed that by non-dimensionalizing lateral mixing coefficient with flume velocity (E_y/Uh), it was observed that it increases by increasing bed friction while parameter E_y/u_*h was observed to decrease with increasing friction. It is not possible to establish a transverse analogy of vertical mixing for variation of velocity and eddy diffusivity along the depth due to absence of transverse velocity profile in a straight rectangular channel. Instead, one has to rely on experimental data for the estimation of transverse mixing coefficient.

There have been several experimental studies of transverse mixing in straight rectangular laboratory channels (Lau and Krishnappan, 1977; Okoye, 1970; Prych, 1970; Sayre and Chang, 1968; Sullivan, 1968; Miller and Richardson, 1974; Sayre and Chamberlin, 1964; Engelund, 1969; Nokes, 1986; Webel and Schatzmann, 1984; Elder, 1959; Engmann, 1974; Holley and Abraham, 1973; Kalinske and Pien, 1944). These provide estimates of the transverse mixing coefficient E_y provided the flow does not depart significantly from the plane shear flow. Analysis of data revealed that transverse mixing coefficient lies in the range (see Fig. 2.5)

$$0.10 < \frac{E_y}{hU_*} < 0.20 \qquad (2.85a)$$

It is likely that secondary currents were present in some of these experiments, which would increase the rate of transverse mixing in channels. An average value of E_y appears to be

$$E_y = 0.15hU_* \qquad (2.85b)$$

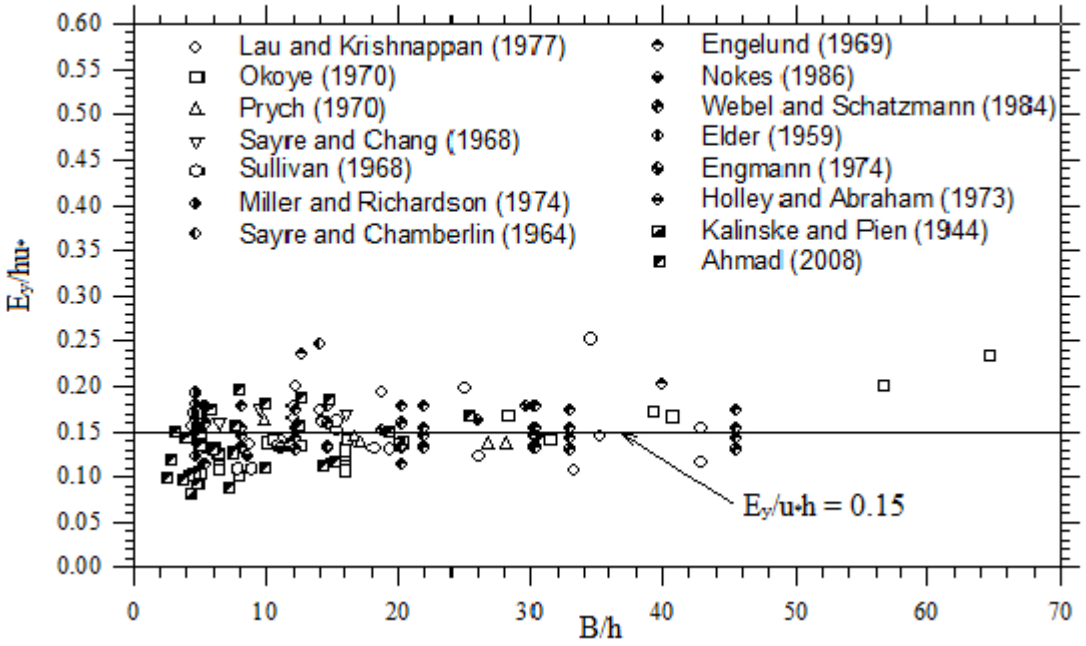

Fig. 2.5 Variation of E_y/hu_* with B/h (Ahmad, 2008).

2.8 TRANSVERSE MIXING LENGTH

It is essential to know up to what length in the longitudinal direction transverse mixing process will end and tracer will become well mixed across the channel cross-section. It is hereby accounted by transverse mixing distance or mixing length, denoted by L_y. From constant-coefficient method, it can easily be observed that as the tracer is advected away from source transverse concentration gradients decreases and vanishes asymptotically. Hence, in order to quantify the order of mixing, a ratio of minimum to maximum concentration, P_m, is defined across the channel. Transverse mixing distance is defined for certain value of P_m say 0.90, 0.95 or 0.98. For example for P_m = 0.98, mixing length is (Rutherford, 1994):

$$L_y = 0.536\frac{UB^2}{E_y} \qquad \text{for an outfall at either bank} \qquad (2.86a)$$

$$L_y = 0.134\frac{UB^2}{E_y} \qquad \text{for a source at mid-channel} \qquad (2.86b)$$

Another parameter of interest can be the crossing distance, which can be defined by the distance travelled along the longitudinal direction by tracer so that it can cross-over the

opposite bank. For the source at either of the channel bank with P_m = 0.98, crossing distance, L_c, is given by (Rutherford, 1994):

$$L_c = 0.054 \frac{UB^2}{E_y} \tag{2.87}$$

In the recent study, Pilechi et al. (2015) estimated mixing length distance of tracer to be 130 km from the outfall and recommended that in the river due to complex bathymetry and non-uniform cross-section, the estimated length was longer than what it was calculated from Eq. (2.86 a).

2.9 EFFECT OF ICE COVER ON THE TRANSVERS MIXING

Since in many countries, rivers are covered by ice and due to this ice, water which before winters was rich with oxygen and flora-fauna, becomes a target of oxygen deficiency and eutrophication in ice cover conditions. Thus, pollution of water happens, hence, it is essential to study effect of ice on mixing in river, with a bit diversification towards transverse mixing. Engmann and Kellerhals (1974) studied the effect of ice cover on transverse mixing and observed that due to the ice cover the lateral mixing coefficients were reduced by ~ 50% i.e. value of E_y/U_*h = 0.33 for open water conditions and E_y/U_*h = 0.17 for ice covered water condition. Engmann and Kellerhals (1974) intuitively depicted that due to the generation of ice cover on the water surface convection due to spiral motions and mixing due to turbulence were damped, hence reducing the mixing and mixing coefficients. Beltaos (1980) conducted experiments on four different river sites introducing tracer as a slug mass. Beltaos (1980) observed that transverse mixing coefficient was increased in the ice covered condition by a margin of 2.5 times which was opposite to the observations of Engmann and Kellerhals (1974). Lau (1985) measured the transverse mixing coefficients in four different reaches for open water and ice covered conditions and obtained that there was no considerable differences between transverse mixing coefficients measured in open water and ice covered conditions. Zhang and Zhu (2011) recently studied the effect of ice cover on transverse mixing in an unregulated river. They observed that E_y/U_*h was reduced by 21% for ice cover conditions than the open water conditions. They depicted that since in the winter river discharge decreases, the value of E_y/U_*h also decreased in considerable manner.

2.10 EFFECT OF BUOYANCY ON THE TRANSVERSE MIXING

Prych (1970) concluded that enhanced lateral spreading of buoyant tracer is due to the buoyancy generated secondary currents. He also concluded that standard deviation growth in longitudinal and lateral directions after a few distance downstream approaches the similar variation of standard deviations of concentration distribution in longitudinal and lateral directions as the neutrally buoyant tracer follows. Bruno et al. (1990) conducted experimentations in straight rectangular channel to establish effect of buoyancy on the process of transverse mixing. Bruno et al. (1990) plotted coefficient of variation (C_v) with $x' = xu_*/hU$, which represents the dimensionless downstream distance, for different values of buoyancy flux (B_o/hu_*^3). They observed that initially C_v was high, which infers that spreading in lateral direction was more due to buoyancy driven secondary currents but as the tracer moved downstream the buoyancy effects were reduced and value of C_v also reduced. After $x' = 13$ the value of C_v became constant and non-zero, which implied that it was the zone of complete transverse mixing and value of E_y was obtained to be same as of neutrally buoyant tracer. Bruno et al. (1990) observed that value of E_y/u_*h varied between 0.21-1.89 which is to the higher side of literature quoted value of 0.2-0.3 for neutrally buoyant tracer discharged in straight channel. For the limiting values of B_o/hu_*^3 they observed that the transverse mixing was higher in case of narrow outlets and heavier effluents than broader outlets and lighter effluents, respectively. Bruno et al. (1990) finally concluded that their experimental results show a good match with the observations of Prych (1970).

Thus, from the whole of the literature it can be concluded that transverse mixing is a process which is dominated by the strength of secondary currents. Fischer (1969) was first to study the effect of secondary currents on the transverse mixing and he observed that lateral mixing was more prominent under the action of secondary currents and he also observed that longitudinal movement of pollutant was ceased under the action of secondary currents. In the straight reaches of any river secondary currents are weak. As per the observations of Fischer (1969) secondary currents not only increase dilution of pollutants but also ceases their forward movement. Thus, in straight reaches an external device is to be used to enhance the transverse mixing of pollutants by generating strong secondary currents. In present study submerged vane was used as that secondary currents generating device and following sections will cover flow pattern around single submerged vane and multiple vane rows.

2.11 SUBMERGED VANES

Submerged vane is basically an aerofoil structure, which generates the excess turbulence in form of helical flow structure in the flow due to pressure difference between approaching flow side and downstream side of vane (Odgaard and Spoljaric, 1986; Odgaard and Mosconi, 1987; Odgaard and Wang, 1991; Wang and Odgaard, 1993). These vanes are in general placed at certain angle with respect to the flow directions which is usually in between, $10^o - 40^o$ (Fig. 2.6). Submerged vane differs from the traditional methods like groins, dikes, etc., which are usually placed normally to the flow and produce flow distribution by drag force and are not so much efficient in controlling the sediment transport. Submerged vanes utilize vorticity to minimize the drag and produce flow redistribution in the flow such that longitudinal flow is compelled to get diverted towards the transverse direction (Wang and Odgaard, 1993). Many investigators like Odgaard and Wang (1991a), Wang and Odgaard (1993), Marelius and Sinha (1998), Tan et al. (2005), Ouyang et al. (2008) have studied analytically and experimentally the flow structure of the submerged vanes.

2.12 FLOW PATTERN AROUND SINGLE SUBMERGED VANE

Odgaard and Spoljaric (1986) studied the flow pattern around single submerged vane and observed that flow downstream of submerged vane didnot affect the longitudinal velocity in considerable amount except in the near region of vane but effect of vortices were seen in transverse velocity profiles. They observed that near the vane the transverse velocity profile attained an S-shape profile but far from vane transverse velocity attained a linear variation. They also observed that helical motion sustained 30-40% cross section downstream of vane. Odgaard and Spoljaric (1986) also observed that there was no effective downwash and vane generated an effective vortex.

Odgaard and Wang (1991a) studied the flow pattern around the submerged vane. They described that submerged vane has got pressure gradient along two side where low pressure exists in the approaching side and high pressure at the downstream side, as shown in Fig. 2.6. These velocity components in low and high pressure sides give rise to the vortical motion in the form of a vortex sheet from the trailing edge of the vane. These vortices in vortex sheet rolls up to form a large vortex springing from a position near the top of a vane, known as tip vortex. This tip vortex when carried out downstream by the flow generates a set of helical

motion or secondary currents. They used the following formula to calculate the tangential velocity of tip vortex, which is a measure of its strength:

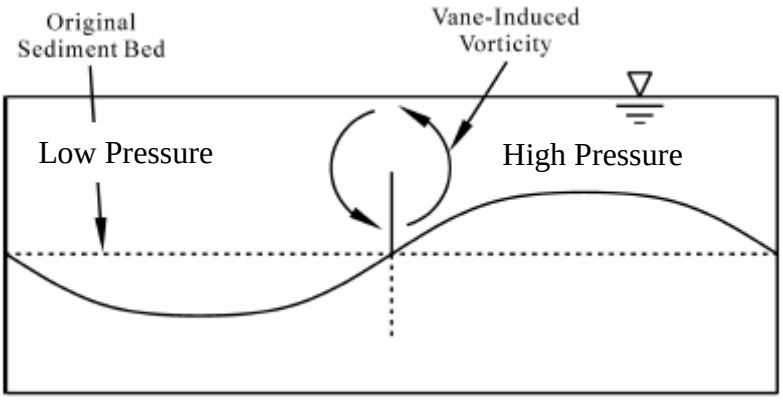

Fig. 2.6 Induced vorticity by vane due to pressure lag (Ouyang et al., 2008)

$$v_\theta = \frac{\Gamma}{2\pi r}\left[1 - \exp\left(-\frac{u_v r^2}{4\varepsilon s}\right)\right] \tag{2.88}$$

Here, v_θ = tangential velocity, Γ = circulation in horizontal direction at the origin, ε = eddy viscosity, s = downstream distance from mid of vane, u_v = velocity approaching vane and r = distance from core of the vortex. They used Eq. (2.88) for unbounded system having no boundary but Odgaard and Wang (1991a) modified the Eq. (2.88) by utilizing method of images to account for the effect of bed on the vortices. It was observed by Odgaard and Wang (1991a) that height of core is 0.8 times vane-height above average bed level. Odgaard and Wang (1991a) quoted that in order to evaluate the horizontal circulation, Γ; it must be related to the lift force exerted by vane on the flow (F_L). In order to hold the stagnation point at trailing edge, flow speeds up around the surface of vane and a bound vortex is formed. From Kutta-Juokowskii theorem Odgaard and Wang (1991 a) proved that horizontal circulation is proportional to the vertical circulation around the vane, which is associated with the shifting of rear stagnation point to the trailing edge of vane. Due to subsequent acceleration of fluid to overcome the blockage created by submerged vane, the trailing edge stagnation point which is just down of trailing edge move towards it. As the stagnation point reaches the trailing edge the tip vortex get de-attached from this edge, now in order to sustain this vortex must bound itself by forming close loops and which is in accordance with the Helmholtz's second theorem of vortices which suggests that detached vorticity either ends at the boundaries or if sustains in

the flow forms a closed loop. Odgaard and Wang (1991 a) calculated strength of bound vortex from Kutta-Juokowskii theorem. Due to bounded nature of bound vortex around vane, the maximum circulation that must be generated must be at this bounded state and must be equal to intensity of detached tip vortices. They evaluated the relation as, $F_L = \rho \Gamma UH$, here, ρ = fluid density and H = vane height. To calculate the distribution of velocity along the vertical, Odgaard and Wang (1991a) adopted a power law for velocity distribution, which is as follows:

$$u_z = \frac{m+1}{m}\left(\frac{z}{h}\right)^{1/m} U \tag{2.89}$$

Here, u_z = point velocity at height z above bed; h = depth of flow; U = Average velocity; m = resistance coefficient = $\kappa\sqrt{8/f}$; κ = von Karman constant ($\approx$ 0.4 for clear water); f = $8(u_*/U)^2$ = friction factor; u_* = $\sqrt{ghS}$ = shear velocity; S = bed slope; g = acceleration due to gravity (= 9.81 m/s^2). Odgaard and Wang (1991a) proposed the following formula to calculate the lift force F_L:

$$F_L = \frac{1}{2}\rho C_L U^2 \frac{(m+1)^2}{m(m+2)}\left(\frac{H}{h}\right)^{2/m} \tag{2.90}$$

Here, C_L = coefficient of lift. Odgaard and Wang (1991 a) assumed the distribution of vertical circulation as elliptical which infers that the value of circulation is maximum at the bed and zero at the top of the vane and they obtained the following formula for coefficient of lift (C_L):

$$C_L = \frac{2\pi\theta}{1+\frac{L}{H}} \tag{2.91}$$

Here, θ = angle at which vane is placed with respect to flow, L = length of vane. Odgaard and Wang (1991 a) obtained following equation for coefficient of drag, C_D:

$$C_D = \frac{1}{2\pi}\frac{L}{H}C_L^2 \tag{2.92}$$

They also suggested that optimum strength of secondary current will be produced when α lies between 15^o-30^o and L/h ratio lies in the range of 0.3-0.5.

Wang and Odgaard (1993) critically analyzed the theory of tip vortex and utilized method of images. They found that method of images gives the velocities which are having smaller magnitude than those obtained by experimental measurements. This could be due to discrepancy is non-accountability of the bound vortex which surrounds the vane into the generation of the transverse component of velocity. They observed that decay rate of depth averaged eddy viscosity obtained by the method quoted by Odgaard and Wang (1991 a) was lower than the measured value. This was due to not accounting the eddy viscosity generated by the vane. It was also observed by Wang and Odgaard (1993) that for small H/h ratio, vortex generated by vane tried to align itself at the mid-depth.

Marelius and Sinha (1998) observed the flow pattern around the vane for $\theta > 30^o$ and also obtained the optimum angle of attack. They defined optimal angle of attack as that peculiar angle of attack by placing or orienting the vane on that angle with respect to the flow that generates vortex of maximum strength. Marelius and Sinha (1998) chose moment of momentum (MOM) which is defined as tangential component of momentum multiplied with radial distance from a specified origin, to measure the strength of vortex so that angle of attack can be optimized. They recommended $\theta \approx 40^o$. Through experimentation, Marelius and Sinha (1998) observed presence of a horseshoe vortex on the pressure side, which is shown in Fig.2.7 and two suction side vortices formed in the wake of vane. Marelius and Sinha (1998) also observed two counter-rotating vortex legs at the edge of vane. They observed that the vortex leg leaving the leading edge decays quickly compare to that leaving from the trailing edge. Stagnation line is a line from which transverse components of velocity changes their direction.

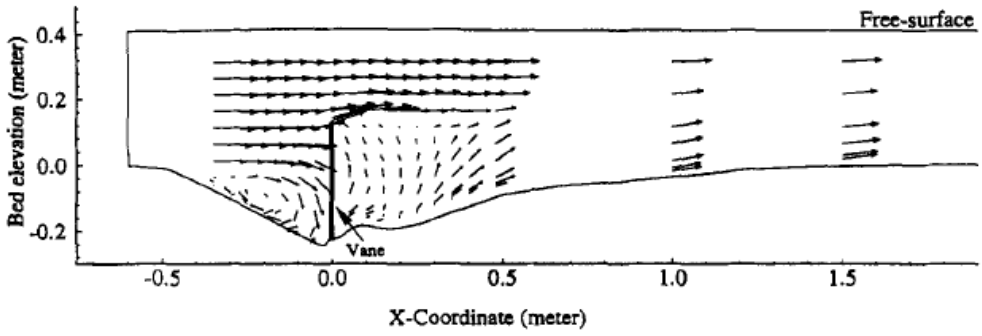

Fig.2.7 A view of horseshoe vortex near the vane (Marelius and Sinha, 1998)

Marelius and Sinha (1998) observed that stagnation line is close to leading edge to trailing edge. Large pressure area available for trailing edge vortex leg stabilizes it to withstand the viscous dampening whereas suction pressure and viscous dissipation works simultaneously on the leading edge vortex leg for its dissipation. They also provide reasoning for the occurrence of two suction side vortices as the destabilization effect of suction pressure. Under this effect the suction pressure acts as adverse pressure gradient for the sustenance of a large vortical structure and thus breaking it into two stabilized vortical structures. They observed that in the vicinity of the vane a system of counterclockwise suction and horseshoe vortices was formed which assists the transverse transport of sediment which is useful in river bank protection.

Tan et al. (2005) divided the flow structure around vane in four parts *viz.* left head zone, right head zone, immediate frontal zone and immediate lee zone, as shown in Fig.2.8. They defined flow over vane as that portion of approach flow which overtops the vane and travels downstream, for lower fluid they put criterion of blockage caused by vane to the moving fluid which compels fluid to plunge downwards towards channel bed. Tan et al. (2005) observed flow to be biased towards the centre of vane in the top flow due to the tendency of flow to diffuse laterally towards centre along the top of the vane (Fig. 2.8).

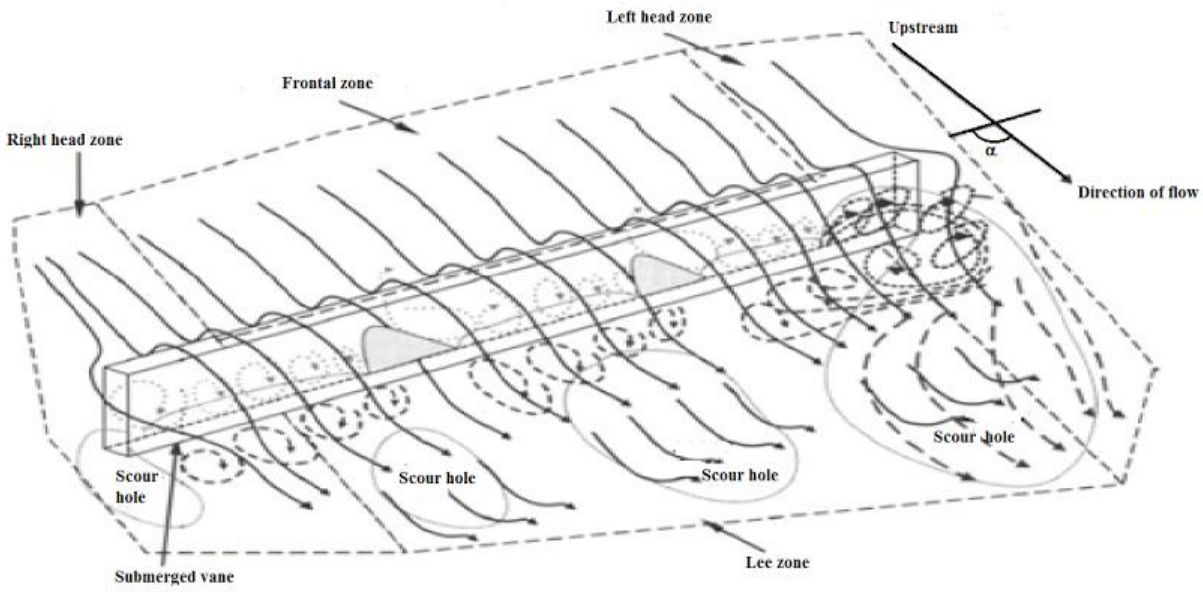

Fig. 2.8 Flow structures around the submerged vane (Tan et al., 2005)

Below vane they observed existence of horseshoe vortices. They also observed existence of large scaled helical cellular structures at the vane head which were highly unstable and were in continuous cycle of vortex initiation, development and its shedding. These cells formed in the immediate frontal zone and then either passed over or around the vane and thus, get attached in the lee zone with other cells to form a large helical structure. They also observed that upper fluid plunged over the vane towards the bed and increased the near bed velocity which enhanced the scouring rate of the channel bed to create a large scour hole in the lee zone of the vane. The down flow towards bed hinders the propagation of head zone helical structures. Hence, new counter-rotating helical cells were noticed to form which were much speedy and larger than pre-hindrance helical structures and rises up towards the downstream and get mixed with upper flow. A separation zone was observed near the immediate frontal zone. They observed that the lower fluid dived towards the bed and started moving back. Interactions of approaching flow and back-motion fluid generated this separation zone. Tan et al. (2005) observed that near the frontal zone, fluid was accelerated giving rise to a suction or low pressure zone whereas in the lee zone fluid is practically stagnant and hence have more pressure than frontal face. This pressure lag caused the motion of fluid towards the bed and in frontal face the currents moved upwards generating a new set of helical motion which moves downstream of vanes creating a series of scour hole separated by a ridge line. Tan et al. (2005) experimented with different angles of vane alignment, *viz.*, 15^o, 30^o, 45^o, 60^o and 90^o. They observed that 30^o is that angle at which optimum sediment diversion was obtained as effectiveness of vane as sediment diverter was optimum. They also experimented to achieve the optimum vane height so that effective sediment diversion is achieved. One-fifth of flow depth is that vane height which optimizes the vane diversion, below it causes the sediments to escape over it with flow and height above it blocks the flow so that sediment is accumulated in frontal zone and less effective diversion is achieved.

Gupta et al. (2007) studied the flow pattern around tapered vane. They observed that tapering the vane do effect the vortex properties around the submerged vane. They also suggested that moment of momentum (MOM) representative of lift force was observed to get influenced by tapering which in lieu affected the vortex characteristics. They observed that MOM is having a greater value for 33.7^o and minimum for tapering angle of 39.8^o and increases for tapering angle of 45^o. Similarly, loss of momentum was minimum for a tapering angle of 33.7^o and increased as tapering was increased due to extra lift induced by tapering effect known as vortex

lift. Gupta et al. (2007) also observed that non-dimensional moment of momentum (non-dimensionalized by loss in momentum multiplied by length over which this loss occurred) was maximum for tapering angle of 33.7^{o} and reduced considerably for tapering angle of 39.8^{o} and slightly increased for tapering angle 45^{o}.

Bhuyian et al. (2010) experimentally studied the flow structure around the bank attached vanes. They observed that during the flow in the bend, submerged vane direct the over-spilling flow towards the center while redirects the approaching flow to form the vortex sheet. By generating the vortex sheet of counterclockwise-rotating vortices it counteracted the bend generated clockwise rotating vortices. They also observed that, vanes aligned the near bed flow towards the center away from the outer bank hence protecting the outer bank of bend. Bhuyian et al. (2010) also observed that bend generated secondary currents are not only counteracted but sometimes they were also suppressed to maintain their position at mid-channel. Due to this a large scour was created on the channel bed and bend remained protected. Bhuyian et al. (2010) observed that vane when present in the flow system reduced the depth-averaged velocity what it was without structure by an extent of 60%. Bhuyian et al. (2010) observed that maximum turbulence intensity occurred near the mid channel and occurred deep near to the bed. It was also observed by Bhuyian et al. (2010) that flow was highly anisotropic without the vane present in the flow but as the vane was introduced anisotropy was observed to reduce in quick and considerable manner. For single vane, Bhuyian et al. (2010) observed that lateral distribution of mean turbulent kinetic energy was more uniform than when vane was not present in the flow indicating that vane generated currents nullified the bend generated secondary currents hence reducing the accumulation of turbulence on one side bend and distributing turbulence more uniformly across width.

Han et al. (2010) experimentally and through simulation studied the effect of submerged vanes on the flow through the bends. They observed that flow field was more uniformly distributed across the width of bend in comparison to the situation where no vanes were used, in which accelerated flow was concentrated on the outer bank and decelerated flow near the inner bank. A pair of vortices was observed by Han et al. (2010) which were generated by tip induced separation and helped in reducing bed shear stress in the bed which was responsible for the bed erosion. They also observed that field of vorticity was rather more stronger intense and less extended in comparison to the three vane rows where field was less intense and more spreaded

due to vane interaction. It was also observed by Han et al. (2010) that in the presence of vane, the bend-induced high turbulence and turbulent kinetic energy was reduced in considerable amount.

2.13 FLOW PATTERN AROUND MUTIPLE SUBMERGED VANE ROWS

Odgaard and Spoljaric (1986) observed that downstream of the vane arrays two counter-rotating vortices were present. They also observed that as the relative depth (H/h) was varied it also affected the helical structure downstream of the vane arrays. They observed that for range of H/h (i.e., ratio of vane height with depth of flow) between 0.2-0.5 an optimum strength of vortical structure was generated by vane arrays.

Odgaard and Wang (1991a) observed that more than one vane in array increase the vane flow field but reduce the effective circulations due to the interaction of their vortex field. The results obtained were observed to be somewhat less than that obtained from the simple superposition of the individual vorticity fields. They adjusted the values obtained by simple superposition by introducing a new parameter, known as vane interaction coefficient, λ, which was observed to be a function of transverse vane spacing (δ_n) and vane dimensions *i.e.* vane height (H) and vane length (L). They found that effective coherent structure can be generated with λ of the order of 0.9 by keeping the vane spacing within 2-3 times the vane height. Beyond this spacing, Odgaard and Wang (1991a) observed that each vane started acting as individual system and generated their individual vorticity field.

Wang and Odgaard (1993) supported the idea of Odgaard and Wang (1991a) of interaction between vorticity fields by providing the reason of generation of shear layer between area of vortices for two vane array. This shear layer reduces the effective circulation. They found that as the vane spacing was reduced, the intensity of effective circulation decreased and interaction was increased. They utilized the concept of interference of two finite wings placed parallel to each other and developed a model. The vortex induced from one of the wings induces a velocity component along the other wing known as down-wash velocity, which reduces the effective angle of the incidence. This reduction in effective angle of incidence leads to the reduction in effective circulation (Wang and Odgaard, 1993). Thus they also supported the introduction of interaction parameter, λ. They supported the observation of Odgaard and Wang (1991 a) who suggested the optimum spacing to be 2-3 times vane height, by obtaining

optimum coherence at vane spacing of 2 times vane height. For multiple vanes array, they obtained the following differential equations to obtain velocity in vane covered area, subscripted as v in Eq. (2.93a) and non-vane covered area subscripted as n in Eq. (2.93b):

$$\frac{d^2T_v}{d\eta^2} - c_1\frac{dT_v}{d\eta} - c_2T_v + c_3 = 0 \qquad (2.93a)$$

$$\frac{d^2T_n}{d\eta^2} - c_3T_n + c_3 = 0 \qquad (2.93b)$$

Here, $T = \left(\bar{u}/u_\infty\right)^2$; u_∞ = ambient or free velocity far from vane field; $\eta = y/B$; B = width of channel; y = transverse coordinate; $c_1 = (K_1/k)\,(B/h)\sqrt{8/f}$; $K_1 = c\left[1/(2\mathrm{m}+1) - 0.19\theta\right]$; c = $\exp(-\delta_s/H)\,\tan\theta$; δ_s = spacing between rows of vane; k = a coefficient varying between 0.1-0.6; $c_3 = (2/k)\,(B/h)^2\sqrt{f/8}$; $c_2 = c_3\left[1+\left(4C_DHL/f(\delta_s,\delta_n)\right)\right]$.

Barkdoll et al. (1999) studied the use of vane rows for effective diversion of discharge into the intake without intake getting clogged by sediments. They observed that, ratio of diverted discharge to main channel discharge (q_r) when was less than 0.43, a few sediment particles were observed to enter into the intake. As q_r was increased to 0.43, it was observed that dune became constant and sediment diverted in the intake after climbing up dune. Further increasing q_r to 0.83, it was observed that an unsteady vortex was generated at $q_r \approx 0.6$ which further enhanced entrainment and also a split in the flow generated which also induced more entrainment of sediment. As Barkdoll et al. (1999) further increased q_r to 1.25, they observed that unsteady vortex which was localized previously now converted into a sheet of rolling vortices which not only enhanced sediment entrainment further but also induced scouring in the downstream of diversion. Barkdoll et al. (1999) after putting three vane arrays observed that insertion of the submerged vane didn't effectively changed the flow features but what it has done was called as near bed flow contraction, in which the flow which was from near bed was diverted away from the intake by the vanes and the flow from near water surface discharges in to the intake diversion. Due to this inrush of near surface flow, the entrainment of sediment was minimized as per observation of Barkdoll et al. (1999). They also suggested that submerged vane can be effectively used for reducing sediment entrainment with skimming wall.

Johnson et al. (2001) applied rock vanes in the field to observe the effect of multiple vanes on the scouring pattern around abutment. Johnson et al. (2001) observed that rock vanes reduces the flow velocity by generating vortices from vane tip and deflects the flow towards center so that scouring did not occur around the abutment but occurred at the center of channel. Johnson et al. (2001) observed that when vanes were introduced in the flow of scour hole shifted more towards center and was diverted away by twenty centimeters from the place of scour hole which was generated in the absence of vane. They also observed that by using two vanes in the rows the scour was reduced by 95% while comparing with using single vane which reduced scouring by 80%. For optimum vane dimensions, Johnson et al. (2001) recommended use of multiple vanes rather than using single vane and recommended that the optimum angle of attack must be 30^o.

Flokstra (2002) modeled the flow pattern downstream of a submerged vane by dividing the flow field in two parts, *viz.* near field and far field. Near field is the flow field near to the vane where flow field was modelled according to the formulation provided by Odgaard and Wang (1991 a). Odgaard and Wang (1991 a) assumed that a separated vortex from submerged vane to be a potential tip vortex that was utilized by Flokstra (2002) to compute flow field near the submerged vane. In order to calculate drag and lift around the submerged vane, Flokstra used Eq. (2.90), (2.91) and (2.92) respectively. In the far field (flow field considerably away from the submerged vane), the generated vortex dissipates in the flow due to the viscous effects, Flokstra (2002) utilized the following equations to calculate the vorticity strength taking into account for the viscous effects on the circulations:

$$\Gamma(s) = \Gamma_o \phi_D(s) \tag{2.94a}$$

$$\phi_D(s) = 1 - e^{-\left(\lambda_d / s\right)},\ \lambda_d = \frac{3C_h H^2}{2\kappa h\sqrt{g}} \tag{2.94b}$$

Here, s = distance along the stream line; C_h = Chezy's coefficient.

Bhuyian et al. (2010) observed that velocity was more concentrated towards inner side of the bend for multiple vanes while comparing with the flow of the bend when only single vane was installed for bank protection. Also they observed that the magnitude of longitudinal velocity was not changed considerably. Bhuyian et al. (2010) also observed that the isovels which were

packed near the bed were distributed towards the water surface. The bed shear stress reduced considerably and hence, reduce chances of bed erosion. For multiple vanes, Bhuyian et al. (2010) observed that the depth-averaged velocity was reduced but not up to that mark which was reduced in the case of single vane due to the interference by the upstream vanes. It was also observed by Bhuyian et al. (2010) that in case of multiple vanes, the maximum value of non-dimensional longitudinal velocity shifted more towards mid-channel then in case of single vane. Bhuyian et al. (2010) observed that by applying multiple vanes, turbulent kinetic energy was distributed uniformly across the width in more uniform manner than single vane.

Azizi et al. (2012) studied the flow pattern around submerged vanes by tapering the leading edge for different angle of attack *viz.* $\theta = 0^o$, 30^o, 45^o and 60^o. Azizi et al. (2012) observed that at the leading edge, the intensity of secondary currents were decreased which in turn lead to decrement in the scour hole depth. They also observed that by increasing the Froude number, no significant increment in intensity of secondary currents was obtained. Azizi et al. (2012) also concluded that no significant effect was observed on vane efficiency when vane area was decreased by curtailing the vane material.

2.14 NUMERICAL MODELS DESCRIBING FLOW PATTERN AROUND SUBMERGED VANE ROWS

Sinha and Marelius (2000) modeled the flow past submerged vanes at high angle of attack by using standard K-ε model (Here, K = Turbulent kinetic energy and ε = rate of dissipation of turbulent kinetic energy). They transformed the standard K-ε model to the generalized non-orthogonal body fitted coordinates by using partial transformation approach. They discretized the governing continuity and standard K-ε equations on a non-staggered computational grid by using:

i. Second order accurate central finite-difference approximation for divergence operator used in the continuity equation, pressure gradient and viscous terms in momentum equations and source and viscous terms in the turbulence closure equations.

ii. Second order accurate upwind differencing scheme for the convective terms in the momentum and turbulence closure equations

Sinha and Marelius (2000) applied ADI (Alternate Directional Implicit scheme) scheme to solve the discretized mean flow equations. Sinha and Marelius (2000) applied uniform velocity profile at the inlet boundary. At the outlet, Sinha and Marelius (2000) imposed zero stream-wise diffusion of flow variable condition. Free surface of water was considered as fixed and was assumes to be a flat plane of symmetry by Sinha and Marelius (2000). Sinha and Marelius (2000) provided zero gradients for K, ε, stream-wise and transverse velocities in the direction perpendicular to the plane of symmetry. Profile of vane was calculated by a simplified blanking procedure of implicit operator by Sinha and Marelius (2000). Velocity deficit due to bed roughness, in simulations done by Sinha and Marelius (2000), was calculated by the formula proposed by Cebecci and Bradshaw (1977):

$$\Delta B = \left[B - 8.5 + \frac{1}{\kappa} \ln\left(k_s^+\right) \right] \sin\left\{0.4258\left(\ln\left(k_s^+\right) - 0.811\right)\right\} \tag{2.95}$$

Here, k_s^+ = non-dimensionalized roughness height (= $U_* k_s / \nu$)

Sinha and Marelius (2000) used d_{50} as k_s. Sinha and Marelius (2000) observed presence of a horseshoe vortex and two suction side vortices in the wake of a vane. Sinha and Marelius (2000) observed that horseshoe vortex which was formed due to the vertical pressure gradient, was located very close to upstream end of the vane and was having its rotation in clockwise direction. They observed that velocity deficit generated by vane in the flow persisted for a longer distance downstream of vane. In the wake region of the vane, Sinha and Marelius (2000) observed two counter-rotating legs, one on either side of the vane. They observed that vortex leaving the trailing edge was observed to be stronger than the leg of vortex leaving the leading edge. They observed that location of stagnation line (stagnation line represents the line after which transverse velocity changes direction) was more near to leading edge than trailing edge hence trailing edge was more exposed to larger pressure making vortex leg leaving trailing edge more stronger.

Ouyang et al. (2008) investigated the effect of vane interaction on the sediment management. In order to derive the model, Ouyang et al. (2008) assumed a row of N equal sized vanes of height H_i and length L mounted vertically with equal spacing on the sediment bed along the channel with angle θ to the flow. Ouyang et al. (2008) assumed that as the flow passes from the vane system, each individual vane induces a circulation generating a velocity field that

interferes with the development of induced circulation and reduced the effective circulation. Ouyang et al. (2008) assumed that effective angle of incidence is reduced by the transverse velocity components and the net circulation was given by:

$$\Gamma_i = \pi L U\left(\theta - \frac{v_i}{U}\right),\ i = 1, 2, 3,\ldots, \mathrm{N} \tag{2.96}$$

Here, v_i = transverse velocity components at vane i. Ouyang et al. (2008) applied wing theorem and represented vane system as system of vortices. Systems of vortices as assumed by Ouyang et al. (2008) were comprised of tip vortices separated from trailing edge and bound vortex embodying the vane. Ouyang et al. (2008) calculated the generated transverse velocity from the collaboration of induced vortices and formulated the following equation:

$$v_i = \sum_{j=1}^{N}\left(W_{ij} + B_{ij}\right),\ j = 1, 2, 3,\ldots, \mathrm{N} \tag{2.97}$$

Here, W_{ij} and B_{ij} were the transverse velocity components at vane i induced by vortex sheet and bound vortex of vane j, respectively. Ouyang et al. (2008) applied Biot-Savart law and assumed elliptic circulation distribution along the trailing edge of the vane, expressed W_{ij} as:

$$W_{ij} = \frac{\sigma_1^{ij}\Gamma_j}{4H_j} \tag{2.98}$$

Here,

$$\sigma_1^{ij} = \frac{1}{\pi}\int_{-1}^{1}\frac{\varsigma^2}{\left[\left(\frac{\delta_{ij}}{H}\right)^2 + \varsigma^2\right]\sqrt{1-\varsigma^2}}d\varsigma \tag{2.99}$$

Here, $d\varsigma = \frac{1}{H_j}dz$. Ouyang et al. (2008) utilized Milne-Thomson's (1966) 2D equal biplane model in order to calculate B_{ij} as follows:

$$B_{ij} = \sigma_2^{ij}\frac{\Gamma_j}{\pi L} \tag{2.100}$$

Here, $\sigma_2^{ij} = \dfrac{1}{1+4\left(\delta_{ij}/L\right)^2}$ (2.101)

Using Eq. (2.96), (2.97), (2.98) and (2.100), Ouyang et al. (2008) obtained the following matrix:

$$\begin{pmatrix} 1+\dfrac{\pi L}{4H_1} & \sigma_2^{12}+\sigma_1^{12}\dfrac{\pi L}{4H_2} & \cdots & \sigma_2^{1N}+\sigma_1^{1N}\dfrac{\pi L}{4H_N} \\ \sigma_2^{21}+\sigma_1^{21}\dfrac{\pi L}{4H_1} & 1+\dfrac{\pi L}{4H_2} & \cdots & \sigma_2^{2N}+\sigma_1^{2N}\dfrac{\pi L}{4H_N} \\ \vdots & \vdots & & \vdots \\ \sigma_2^{N1}+\sigma_1^{N1}\dfrac{\pi L}{4H_1} & \sigma_2^{N1}+\sigma_1^{N1}\dfrac{\pi L}{4H_1} & \cdots & 1+\dfrac{\pi L}{4H_N} \end{pmatrix} \begin{pmatrix} \Gamma_1 \\ \Gamma_2 \\ \vdots \\ \vdots \\ \vdots \\ \vdots \\ \Gamma_N \end{pmatrix} = \begin{pmatrix} \pi L U\theta \\ \pi L U\theta \\ \vdots \\ \vdots \\ \vdots \\ \vdots \\ \pi L U\theta \end{pmatrix} \quad (2.102)$$

Ouyang et al. (2008) utilized model derived by Odgaard and Mosconi (1987) to derive the following formula

$$\Gamma_0 = \frac{\pi L U\theta}{1+\pi L/4H} \quad (2.103)$$

Ouyang et al. (2008) defined an interaction parameter as

$$\lambda_i = \frac{\Gamma_i}{\left(\Gamma_o\right)_i};\ i = 1, 2, 3, \ldots, \mathrm{N} \quad (2.104)$$

From Eq. (2.102), (2.103) and (2.104), Ouyang et al. (2008) derived following equation:

$$\begin{pmatrix} 1+\dfrac{\pi L}{4H_1} & \sigma_2^{12}+\sigma_1^{12}\dfrac{\pi L}{4H_2} & \cdots & \sigma_2^{1N}+\sigma_1^{1N}\dfrac{\pi L}{4H_N} \\ \sigma_2^{21}+\sigma_1^{21}\dfrac{\pi L}{4H_2} & 1+\dfrac{\pi L}{4H_2} & \cdots & \sigma_2^{2N}+\sigma_1^{2N}\dfrac{\pi L}{4H_N} \\ \vdots & \vdots & & \vdots \\ \sigma_2^{N1}+\sigma_1^{N1}\dfrac{\pi L}{4H_1} & \sigma_2^{N2}+\sigma_1^{N2}\dfrac{\pi L}{4H_2} & \cdots & 1+\dfrac{\pi L}{4H_N} \end{pmatrix} \begin{pmatrix} \lambda_1 \\ \lambda_2 \\ \vdots \\ \vdots \\ \vdots \\ \vdots \\ \lambda_N \end{pmatrix} = \begin{pmatrix} 1+\dfrac{\pi L}{4H_1} \\ 1+\dfrac{\pi L}{4H_2} \\ \vdots \\ \vdots \\ 1+\dfrac{\pi L}{4H_N} \end{pmatrix} \quad (2.105)$$

Ouyang et al. (2008) utilized results of Wang (1991) to verify the model and observed that the results matched well with the derived model. Ouyang et al. (2008) observed that when the transverse distance between submerged vanes was reduced the magnitude of transverse velocities were reduced. Odgaard and Wang (1991 a) assumed that in multiple vane arrays, all the vanes generate equal intensity of vortices but Ouyang et al. (2008) observed that vorticity magnitude of inner vane was somewhat less than what it was generated from outer vanes. Ouyang et al. (2008) observed that when $\delta_n/L = 0.25$ functionality of inner vane was almost lost. Ouyang et al. (2008) measured the bed profile with and without inner vane and found that in both cases bed profiles were identical. For $H/L = 0.5$ and Ouyang et al. (2008) plotted interaction coefficients of inner and outer vanes as a function of δ_n/L. They observed that interaction coefficients decreased but inner vane's interaction coefficient reduced very rapidly and became 50% for $\delta_n/L \approx 0.6$. Hence, Ouyang et al. (2008) proposed that for effective working of vane system $\delta_n/L \geq 0.6$. They observed that for δ_n/L between 1-1.5, the interaction coefficients for all the vanes were less than 1 indicating a mutual interference between submerged vanes and when $\delta_n/L > 1.5$ interaction coefficients approached 1 indicating that each vane started acting as individual system thus stop generating coherent circulations. Ouyang et al. (2008) proposed that δ_n/L should be between 1-1.5 (where H/L was 0.5) which according to them satisfies the condition proposed by Odgaard and Wang (1991 a) that δ_n/H should be in between 2 to 3.

2.15 CONCLUDING REMARKS

This chapter presents brief discussion regarding transverse mixing process and flow pattern around submerged vanes. Transverse mixing process as discussed in present chapter is a two dimensional mixing phenomenon. Transverse mixing usually occurs in the mixing zone called as mid-field zone. Transverse mixing is analytically analyzed by depth averaged advection diffusion equation. Depending upon the variability and non-variability of transverse mixing coefficient, analytical methods of transverse mixing are categorized as constant coefficient method and variable coefficient method. Just like analytical methods many numerical methods are available that satisfactorily predict pollutant concentration profiles. It can be concluded from various reviewed literature that transverse mixing is a phenomenon generally dominated by secondary currents. Since secondary currents are the function of aspect ratio, bed roughness, buoyancy of tracer, etc., hence, transverse mixing also depends upon the aforesaid factors. It

was observed that transverse mixing coefficient increase with increase in secondary currents, buoyancy flux and sinuosity of bend. Dependency of transverse mixing coefficient on bed roughness, aspect ratio and ice cover are fields still need extensive research. In order to achieve an efficient dilution under transverse mixing conditions, secondary currents play an important role and these currents are weak in the straight reaches. No study have been conducted yet which use an external vortex generator which by generating transverse cellular currents can enhance the rate of transverse mixing as well as dilution rate of tracer plume. Submerged vanes are aero-foil placed at angle of 10^{o}-40^{o} with respect to flow direction. It was deduced from various investigations that submerged vanes generate a high turbulence field downstream. If multiple vanes were used then they interact with each other to generate a larger field of circulation then single vane but effective circulation will be rather less than the circulation generated by individual vane in same flow conditions. Thus, it can be concluded that by enhancing intensity of secondary currents, rate of transverse mixing can be increased. Thus, utility of submerged vanes in enhancing the rate of transverse mixing is a need of study and will be studied in further sections.

Chapter 3

NUMERICAL SOLUTION OF UNSTEADY TRANSVERSE MIXING EQUATION

3.1 INTRODUCTION

This section deals with numerical modeling of transient transverse mixing in streams. Finite volume technique is used to solve the governing equations in prismatic channels. The developed model takes care of variation of depth of flow, depth-averaged velocity and transverse mixing coefficient across the channel width. Transient transverse mixing model is demonstrated with the field data. The FV model proposed by Ahmad (2008) for the solution of steady transverse mixing equation is extended to determine the value of transverse mixing coefficient using concentration profiles at least two stations in the downstream of the injection site. Method of one-dimensional grid search is used for this purpose.

3.2 GOVERNING EQUATION

The process of transverse mixing of a conservative and neutrally buoyant substance in steady flow through a straight channel is modeled by the principle of conservation of mass of the substance and written as (Lau and Krishnappan, 1977; Shen, 1978)

$$\frac{\partial(hC)}{\partial t}+\frac{\partial}{\partial x}(uhC)=\frac{\partial}{\partial x}\left[hE_x\frac{\partial C}{\partial x}\right]+\frac{\partial}{\partial y}\left[hE_y\frac{\partial C}{\partial y}\right]-\alpha_d hC+\beta_d \tag{3.1}$$

where C = depth-averaged concentration; h = depth of flow; u = depth-averaged velocity in longitudinal direction; t = simulation time; x and y = longitudinal and transverse distances, respectively; E_x and E_y = depth-averaged mixing coefficients in the longitudinal and transverse

directions, respectively; α_d = decay constant for non-conservative pollutant; β_d = source or sink present in the mixing zone.

3.3 PROPOSED NUMERICAL FINITE VOLUME MODEL

3.3.1 Introduction to the finite volume method

Introduced into the field of computational fluid dynamics in the beginning of the seventies, the finite volume method has in recent years evolved as a powerful tool for solution of open channel flow problems. It discretizes the integral form of the equation, therefore, FV models do not fail at discontinuity in the concentration field. Zhao et al. (1994), Mingham and Causon (1999), Bradford and Sanders (2002), and Capart et al. (2003), used FV schemes to solve shallow water flow equations using approximate Reimann solvers. The computational results compared favorably with gauge records. Sanders et al. (2001) applied coupled flow and pollutant transport model based on FV scheme to predict the tidal transport of urban runoff in southern Califonia network of flood control channels that drain to near-shore bathing waters. They demonstrated that the FVM based scheme results in an accurate, stable, non-oscillating and computationally manageable model.

The finite volume method (FVM) uses the integral form of the conservation equations as its starting point. The solution domain is subdivided into a finite number of contiguous control volumes (CVs), and the conservation equations are applied to each CV. At the centroid of each CV lies a computational node at which the variable values are to be calculated. Interpolation is used to express variable values at the CV face in the terms of the nodal values. Surface and volume integrals are approximated using suitable quadrature formulae. As a result, one obtains an algebraic equation for each CV, in which a number of neighbour nodal values appear. The finite volume method accommodates different types of grid and is thus suitable for complex geometries. The grid defines only the control volume boundaries and need not be related to a coordinate system. Since a FVM is based on the integral form of the conservation equations, numerical schemes so formulated capture shocks accurately without numerical oscillations or excessive numerical dissipation. The finite volume approach is perhaps the simplest to understand and to program (Ferziger and Peric, 2002). All terms that need be approximated have physical meaning.

The present work explores the potential of the finite volume method for solution of the transverse mixing equation for various initial and boundary conditions particularly for those cases in which a mass flux condition is specified at the boundaries, i.e., discontinuity exists in the concentration field.

3.3.2 Finite volume model for transient transverse mixing

The integration of Eq. (3.1) over a control volume $d\Omega = \Delta x \Delta y.1$ (Here, *1* represents unit thickness of the grid) from time t to $t+\Delta t$ using Gauss's divergence theorem yields

$$\int_t^{t+\Delta t} \frac{\partial}{\partial t}\left(\int_\Omega (hC)d\Omega\right)dt + \int_t^{t+\Delta t}\int_{A_x} n_1.(huC\,\mathrm{i})dA_x dt = \tag{3.2}$$

$$\int_t^{t+\Delta t}\int_{A_x} n_1.\left(hE_x \frac{\partial C}{\partial x}\mathrm{i}\right)dA_x dt + \int_t^{t+\Delta t}\int_{A_z} n_2.\left(hE_y \frac{\partial C}{\partial z}\mathrm{j}\right)dA_y dt - \int_t^{t+\Delta t}\int_\Omega (\alpha_d hC)d\Omega dt + \int_t^{t+\Delta t}\int_\Omega \beta_d d\Omega dt$$

where n_1 = unit vector normal to the surface $A_x = 1 \times \Delta y$; n_2 = unit vector normal to the surface $A_y = 1 \times \Delta x$; i = unit vector in x-direction; and j = unit vector in y-direction.

The domain is divided into discrete control volumes as shown in Fig. 3.1. The index numbers i, and j show nodal points in the x- and y-directions, respectively. The control volume is positioned mid-way between the adjacent nodes. A general nodal point is identified by P and its neighbours as W, E, N, and S as per their location relative to P.

The two-dimensional grid is uniform and length of the each control volume is Δx in x-direction and Δy in y-direction. Each term of Eq. (3.2) is calculated for each control volume.

Assuming constant concentration all over the control volume Ω and equal to concentration at the centroid, the first term of Eq. (3.2) can be approximated as

$$\int_t^{t+\Delta t} \frac{\partial}{\partial t}\left(\int_\Omega (hC)d\Omega\right)dt \cong \left(C_P - C_P^0\right)\bar{h}_p \Delta x \Delta y \tag{3.3}$$

where $\bar{h}_p$ is the average depth of the control volume. Assuming, the variation of depth of flow with transverse direction as quadratic, the average depth $\bar{h}_p$ is given by

$$\bar{h}_p = \frac{1}{6}\left(h_n + 4h_p + h_s\right) \tag{3.4}$$

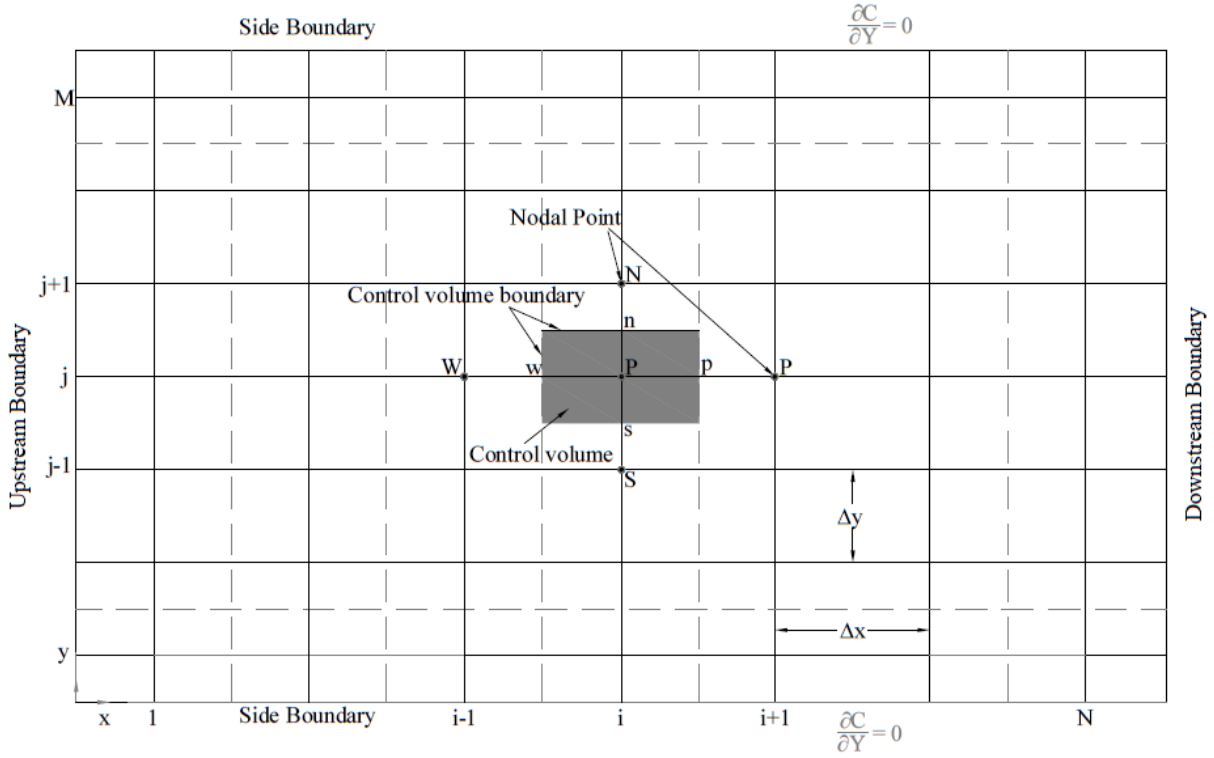

Fig. 3.1 A control volume around node P

Second term of Eq. (3.2) may be written as

$$\int_t^{t+\Delta t}\int_{A_x} n_1.(huC\mathrm{i})dA_x dt = \int_t^{t+\Delta t}\left[(huC\Delta y)_e - (huC\Delta y)_w\right]dt = h_e u_e \Delta z \int_t^{t+\Delta t} C_e dt - h_w u_w \Delta y \int_t^{t+\Delta t} C_w dt \tag{3.5}$$

Using weighted upwind scheme, one can obtain

$$C_e = \Psi C_P + (1-\Psi)C_E \tag{3.6a}$$

$$C_w = \Psi C_W + (1-\Psi)C_P \tag{3.6b}$$

where Ψ is a weighting factor introduced along the x-axis. The above scheme is upwind for $\Psi = 1$, and central difference for $\Psi = 0.5$.

Substitution of Eqs. (3.6a) and (3.6b) into Eq. (3.5) yields

$$\int_t^{t+\Delta t}\int_{A_x} n_1.(huC\mathrm{i})dA_x dt = h_e u_e \Delta y \int_t^{t+\Delta t}\left[\Psi C_P + (1-\Psi)C_E\right]dt - h_w u_w \Delta y \int_t^{t+\Delta t}\left[\Psi C_W + (1-\Psi)C_P\right]dt \tag{3.7}$$

Third term of Eq. (3.2) may be written as

$$\int_t^{t+\Delta t}\int_{A_x} n_1.\left(hE_x\frac{\partial C}{\partial x}\mathrm{i}\right)dA_x dt=\int_t^{t+\Delta t}\left[\left(hE_x\Delta y\frac{\partial C}{\partial x}\right)_e-\left(hE_x\Delta y\frac{\partial C}{\partial x}\right)_w\right]dt \tag{3.8}$$

Approximating fluxes on east and west faces as

$$\left(hE_x\Delta y\frac{\partial C}{\partial x}\right)_e=h_eE_{xe}\Delta y\frac{(C_E-C_P)}{\Delta x} \tag{3.9a}$$

$$\left(hE_x\Delta y\frac{\partial C}{\partial z}\right)_w=h_wE_{xw}\Delta y\frac{(C_P-C_W)}{\Delta x} \tag{3.9b}$$

Substitution of Eqs. (3.9a) and (3.9b) into Eq. (3.8) yields

$$\int_t^{t+\Delta t}\int_{A_x} n_1.\left(hE_x\frac{\partial C}{\partial x}\mathrm{i}\right)dA_x dt=h_eE_{xe}\frac{\Delta y}{\Delta x}\int_t^{t+\Delta t}(C_E-C_P)dt-h_wE_{xw}\frac{\Delta y}{\Delta x}\int_t^{t+\Delta t}(C_P-C_W)dt \tag{3.10}$$

Like-wise fourth term of Eq.(3.2) may be written as

$$\int_t^{t+\Delta t}\int_{A_z} n_2.\left(hE_y\frac{\partial C}{\partial y}\mathrm{j}\right)dA_y dt=h_nE_{yn}\frac{\Delta x}{\Delta y}\int_t^{t+\Delta t}(C_N-C_P)dt-h_sE_{ys}\frac{\Delta x}{\Delta y}\int_t^{t+\Delta t}(C_P-C_S)dt \tag{3.11}$$

Decay term of Eq. (3.2) may be written as

$$\int_t^{t+\Delta t}\int_\Omega(\alpha_d hC)d\Omega dt=\alpha_d\bar{h}_P\Delta x\Delta y\int_t^{t+\Delta t}C_P dt \tag{3.12}$$

Assuming that no source or sink is present in the mixing zone, thus, β_d is omitted from Eq. 3.2. Substitution of Eqs. (3.3), (3.7), (3.10), (3.11) and (3.12) into Eq. (3.2) yields

$$\begin{aligned}(C_P-C_P^0)\bar{h}_p\Delta x\Delta y+h_eu_e\Delta y\int_t^{t+\Delta t}[\Psi C_P+(1-\Psi)C_E]dt-h_wu_w\Delta y\int_t^{t+\Delta t}[\Psi C_W+(1-\Psi)C_P]dt=\\ h_eE_{xe}\frac{\Delta y}{\Delta x}\int_t^{t+\Delta t}(C_E-C_P)dt-h_wE_{xw}\frac{\Delta y}{\Delta x}\int_t^{t+\Delta t}(C_P-C_W)dt+\\ h_nE_{yn}\frac{\Delta x}{\Delta y}\int_t^{t+\Delta t}(C_N-C_P)dt-h_sE_{ys}\frac{\Delta x}{\Delta y}\int_t^{t+\Delta t}(C_P-C_S)dt-\alpha_d\bar{h}_P\Delta x\Delta y\int_t^{t+\Delta t}C_P dt\end{aligned} \tag{3.13}$$

Consider that the channel is prismatic and h, u and E_x vary only in z-direction, i.e.,

$$h_P=h_e=h_w;\quad u_P=u_e=u_w;\quad \text{and}\quad E_{xP}=E_{xe}=E_{xw} \tag{3.14}$$

$$\text{Let}\quad h_n=\frac{h_N+h_P}{2};\quad h_s=\frac{h_S+h_P}{2};\quad E_{yn}=\frac{E_{yN}+E_{yP}}{2};\ \text{and}\ E_{ys}=\frac{E_{yS}+E_{yP}}{2} \tag{3.15}$$

Substitution of the above values in Eq. (3.13) yields

$$a_{1P}\left(C_P - C_P^0\right) + a_{2P}\int_t^{t+\Delta t}\left[\Psi C_P + (1-\Psi)C_E\right]dt - a_{3P}\int_t^{t+\Delta t}\left[\Psi C_W + (1-\Psi)C_P\right]dt =$$
$$a_{4P}\int_t^{t+\Delta t}\left(C_E - C_P\right)dt - a_{5P}\int_t^{t+\Delta t}\left(C_P - C_W\right)dt + \qquad (3.16)$$
$$a_{6P}\int_t^{t+\Delta t}\left(C_N - C_P\right)dt - a_{7P}\int_t^{t+\Delta t}\left(C_P - C_S\right)dt - a_{8P}\int_t^{t+\Delta t}C_P\,dt$$

Where $a_{1P} = \bar{h}_p \Delta x \Delta y;\ \ a_{2P} = h_P u_P \Delta y;\ \ a_{3P} = a_{2P};\ \ a_{4P} = h_P E_{xP}\dfrac{\Delta y}{\Delta x};$ (3.17)

$$a_{5P} = a_{4P};\ \ a_{6P} = h_n E_{y_n}\frac{\Delta x}{\Delta y};\ a_{7P} = h_s E_{y_s}\frac{\Delta x}{\Delta y};\ \text{and}\ a_{8P} = \alpha_d \bar{h}_P \Delta x \Delta y$$

Subscript P indicates values of parameters correspond to node P.

Introducing temporal weighing factor α_t, integration of concentration at a nodal point over a time step Δt may be obtained as:

$$\int_t^{t+\Delta t} C\,dt = \left[\alpha_t C + (1-\alpha_t)\in\right]\Delta t \qquad (3.18)$$

where $\in$ is concentration at previous time t.

Computation of time integral at each nodal points of Eq. (3.16) using Eq. (3.18) yields the following equation in terms of index numbers i and j:

$$a_s^j C_i^{j-1} + a_p^j C_i^j + a_n^j C_i^{j+1} = a_e^j C_{i+1}^j + a_w^j C_{i-1}^j + B_i^j \quad ; \qquad i = 2 \to N-1 \text{ and } j = 2 \to M-1 \qquad (3.19)$$

where $a_s^j = \alpha_t\, a_7^j;\quad a_p^j = -\left(\dfrac{a_1^j}{\Delta t} + \alpha_t\, a_9^j\right);\quad a_n^j = \alpha_t\, a_6^j;\quad a_e^j = \alpha_t\, a_{10}^j;\quad a_w^j = -\alpha_t\, a_{11}^j;$ (3.20)

$$B_i^j = b_s^j \in_i^{j-1} + b_p^j \in_i^j + b_n^j \in_i^{j+1} + b_e^j \in_{i+1}^j + b_w^j \in_{i-1}^j \qquad (3.21)$$

in which $\overline{h^j} = \dfrac{1}{6}\left[\dfrac{\left(h^{j+1} + h^j\right)}{2} + \dfrac{\left(h^{j-1} + h^j\right)}{2} + 4h^j\right];\quad a_1^j = \overline{h^j}\Delta x \Delta y\,;\quad a_2^j = a_3^j = h^j u^j \Delta y\ ;$

$$a_4^j = a_5^j = h^j E_x^j \frac{\Delta y}{\Delta x};\quad a_6^j = \frac{\left(h^{j+1} + h^j\right)}{2}\frac{\left(E_y^{j+1} + E_y^{j+1}\right)}{2}\frac{\Delta x}{\Delta y};\quad a_7^j = \frac{\left(h^{j-1} + h^j\right)}{2}\frac{\left(E_y^{j-1} + E_y^{j+1}\right)}{2}\frac{\Delta x}{\Delta y};$$

$$a_8^j = \alpha_d \overline{h^j} \Delta x \Delta y;\ a_9^j = \Psi a_2^j - (1-\Psi) a_3^j + a_4^j + a_5^j + a_6^j + a_7^j + a_8^j;\ a_{10}^j = (1-\Psi) a_2^j - a_4^j$$

$$a_{11}^j = \Psi a_3^j + a_5^j; \qquad b_s^j = -(1-\alpha_t) a_7^j; \qquad b_p^j = -\left(\frac{a_1^j}{\Delta t} - (1-\alpha_t) a_9^j \right); \qquad b_n^j = -(1-\alpha_t) a_6^j;$$

$$b_e^j = (1-\alpha_t) b_{10}^j; \quad \text{and} \quad b_w^j = -(1-\alpha_t) a_{11}^j \tag{3.22}$$

Transverse concentration gradient, i.e., $\frac{\partial C}{\partial y}$ at the side boundaries are equal to zero. Thus in Eq. (3.19) for j = 1, $\frac{\partial C}{\partial y}\big|_s = 0$ as a result of which $a_s^j = 0$ and for $j = M$, $\frac{\partial C}{\partial y}\big|_n = 0$ as a result of which $a_n^j = 0$ for i=2, N-1. The discretized equations for nodal points i = 1 and N are to be written separately.

(a) Discretised equation for upstream boundary

Discretised equation at upstream boundary is obtained by solving Eq. (3.2) for control volume shown in Fig. 3.2a.

Following the same procedure as adopted for solving Eq. (3.2) for the interior control volumes, the different terms of Eq. (3.2) are solved herein with the following changes to account for the upstream boundary:

(a) In the second term, $C_w = C_A$, i.e., upstream boundary conditions; and

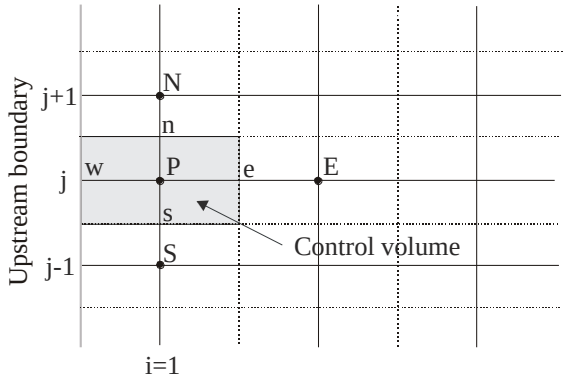

Fig. 3.2a Control volume around node P at upstream boundary

(b) In the third term, assuming quadratic variation of concentration along x-axis, the concentration gradient at face w for i=1 is written as

$$\left.\frac{\partial C}{\partial x}\right)_w = \frac{1}{3\Delta x}\left(9C_P - 8C_A - C_E\right) \tag{3.23}$$

Different coefficients of Eq. (3.19) for i=1 are as follows:

$$\mathrm{B_i^j} = b_s^j \in_{\mathrm{i}}^{j-1} + b_p^j \in_i^j + b_n^j \in_i^{j+1} + b_e^j \in_{i+1}^j + b_w^j \in_{i-1}^j + B_u \tag{3.24}$$

$$a_9^j = \Psi a_2^j + a_4^j + 3a_5^j + a_6^j + a_7^j + a_8^j; \quad a_{10}^j = (1-\Psi)a_2^j - a_4^j - a_5^j/3; \quad \mathrm{a_{11}^j} = 0;$$

and $$B_u = -\left(a_3^j + \frac{8a_5^j}{3}\right)\left[\alpha_t C_A + (1-\alpha_t)\in_A\right] \tag{3.25}$$

Other coefficients remain same as given in Eqs. (3.20) and (3.22).

(b) Discretised equation for downstream boundary

Discretised equation at downstream boundary is also obtained by solving Eq. (3.2) for control volume shown in Fig. 3.2b.

Following the same procedure as adopted for solving Eq. (3.2) for the interior control volumes, the different terms of Eq. (3.2) are solved herein with the following changes to account for the downstream boundary:

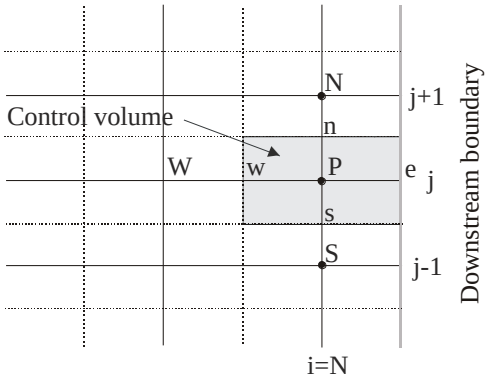

Fig. 3.2b Control volume around node P at downstream boundary

(a) In the second term, $C_e = C_B$, i.e., downstream boundary conditions; and

(b) In the third term, assuming quadratic variation of concentration along x-axis, the concentration gradient at face e for i=N is written as:

$$\left.\frac{\partial C}{\partial x}\right)_e = \frac{1}{3\Delta x}\left(C_W - 9C_P + 8C_B\right) \tag{3.26}$$

Different coefficients of Eq. (3.19) for i=N are as follows:

$$\mathrm{B_i^j} = b_s^j \in_{\mathrm{i}}^{j-1} + b_p^j \in_i^j + b_n^j \in_i^{j+1} + b_e^j \in_{i+1}^j + b_w^j \in_{i-1}^j + B_d \tag{3.27}$$

$$a_9^j = -(1-\Psi)a_3^j + 3a_4^j + a_5^j + a_6^j + a_7^j + a_8^j; \qquad \mathrm{a_{10}^j} = 0; \qquad a_{11}^j = \Psi a_3^j + a_5^j + a_4^j/3;$$

$$\text{and } B_d = -\left(-a_2^j + \frac{8a_4^j}{3}\right)\left[\alpha_t C_B + (1-\alpha_t)\in_B\right] \tag{3.28}$$

Other coefficients remain same as given in Eqs. (3.20) and (3.22).

(c) Solution of system of equations

The system of algebraic equations given by Eq. (3.19) is tri-diagonal in form. Thomas algorithm or the tri-diagonal matrix algorithm (TDMA) can be used to solve such a system of equations for known fluxes at upstream and downstream boundaries (Versteeg and Malalasekera, 1995). The TDMA is applied iteratively, in a line-by-line fashion, to solve Eq. (3.19). Computation is started with i=1. The tri-diagonal form of system of equations for i=1 may be written as

$$\begin{vmatrix} a_p^1 & a_n^1 & 0 & 0 & 0 & 0 & 0 & 0 \\ a_s^2 & a_p^2 & a_n^2 & 0 & 0 & 0 & 0 & 0 \\ 0 & a_s^3 & a_p^3 & a_n^3 & 0 & 0 & 0 & 0 \\ 0 & 0 & - & - & - & 0 & 0 & 0 \\ 0 & 0 & 0 & a_s^j & a_p^j & a_n^j & 0 & 0 \\ 0 & 0 & 0 & 0 & - & - & - & 0 \\ 0 & 0 & 0 & 0 & 0 & a_s^{M-1} & a_p^{M-1} & a_n^{M-1} \\ 0 & 0 & 0 & 0 & 0 & 0 & a_s^M & a_p^M \end{vmatrix} \times \begin{vmatrix} C_1^1 \\ C_1^2 \\ C_1^3 \\ - \\ C_1^j. \\ - \\ C_1^{M-1} \\ C_1^M \end{vmatrix} = \begin{vmatrix} a_e^1 C_2^1 + B_1^1 \\ a_e^2 C_2^2 + B_1^2 \\ a_e^3 C_2^3 + B_1^3 \\ - \\ a_e^j C_2^j + B_1^j \\ - \\ a_e^{M-1} C_2^{M-1} + B_1^{M-1} \\ a_e^M C_2^M + B_1^M \end{vmatrix} \tag{3.29}$$

The above equation cannot be solved for $\mathrm{C_1^j}$ as concentration at nodes for i=2 are not known (see Fig. 3.3). Thus some initial value of concentration (e.g. zero) at nodes for i=2 are assumed and the above equation is solved for $\mathrm{C_1^j}$. Subsequently, the calculation is made for i = 2, N. In

the second iteration, calculation is again started with i=1 and subsequently done for i=2, N. Such iterations are repeated several times until a convergent solution is obtained.

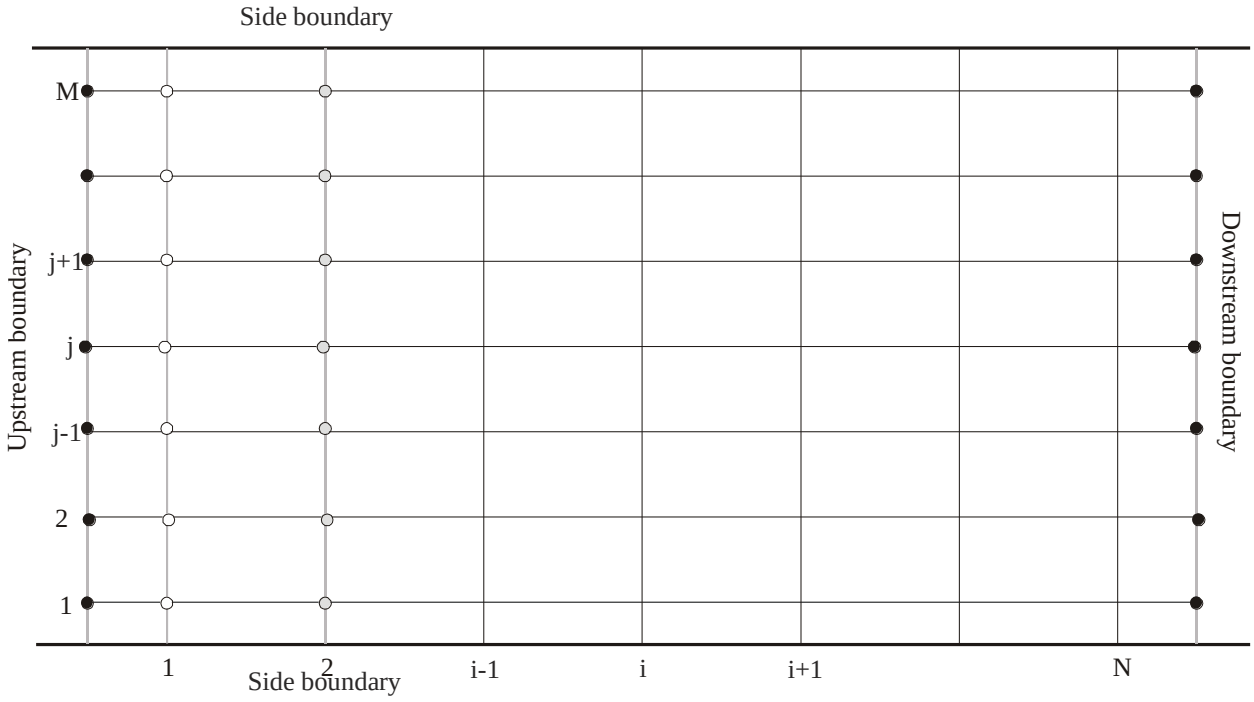

Fig. 3.3 2D-Tridiagonal matrix algorithm

3.4 VALIDATION OF MODEL FOR STEADY TRANSVERSE MIXING

The proposed model is validated by comparing the computed results with the Yotsukura and Cobb's analytical solution of Eq. (3.1) for continuous injections of pollutants spread over a width. For injection near the bank, the following input parameters from a field experiment in the Grand river are used (Lau and Krishnappan, 1981): width of the stream, B = 59.2 m; depth of flow, h = 0.506m; velocity, U = 0.353 m/s; transverse mixing coefficient, E_y = 0.009 m^2/s; cross-sectional mixed concentration, C_∞ = 3.99 ppb; and width of source, ω = 5.92 m. Concentration profiles are calculated using Yotsukura and Cobb's analytical solution at distances x = 213, 463, 713, 963, 1213, and 1463 m downstream of the injection site of the pollutant. The proposed FV model is also used to calculate concentration profiles at the above distances taking Δx = 1.0 m and Δy = 0.10 m. Concentration at the upstream is calculated by equating the mass of the pollutant leaving the downstream boundary to the mass of the pollutant entering into the upstream boundary, which comes out to be 39.9 ppb. The computed

concentration profiles using the analytical model and the proposed FV model agree closely as seen in Fig. 3.4.

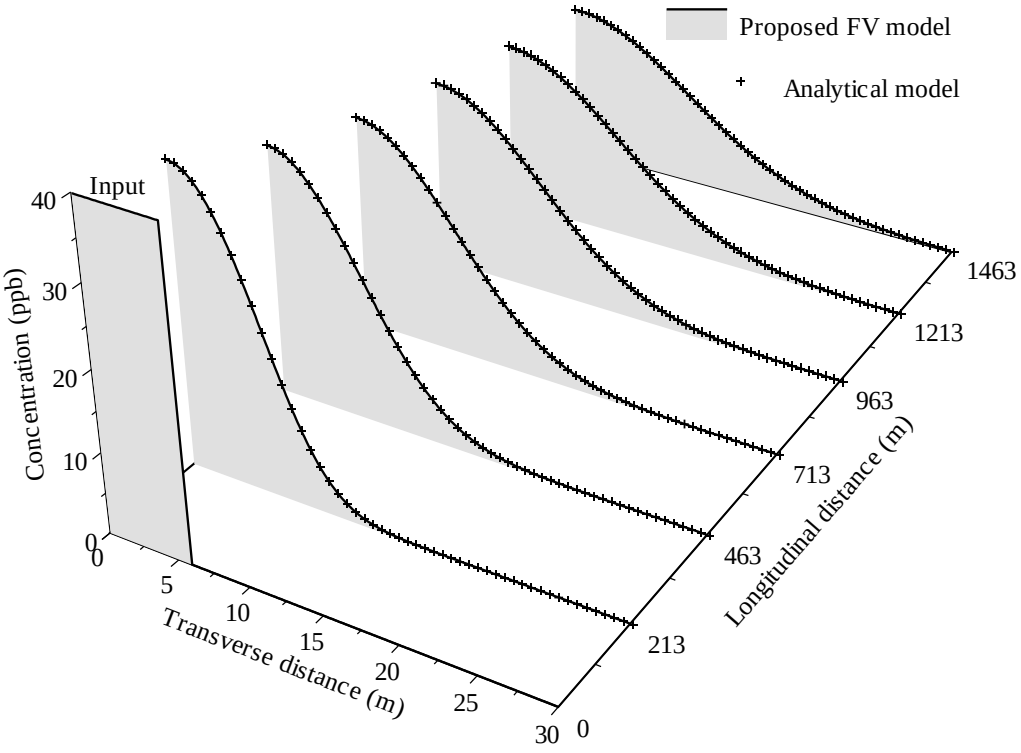

Fig. 3.4 Comparison of concentration profiles computed using the proposed FV model and the analytical model for injection of pollutant near the bank (Ahmad, 2008)

3.5 MODEL DEMONSTRATION FOR TRANSIENT TRANSVERSE MIXING

The proposed model is demonstrated for transient transverse mixing in stream for finite duration injection of the pollutant. For this purpose, a typical cross-section of Lesser slave river is considered as shown in Fig. 3.5 (Beltaos and Day, 1976). The river channel is assumed to be prismatic. Contours of velocity and variation of depth-averaged velocity across the width are also shown in Fig. 3.5. Input data are B = 57 m; Bed slope, S = 0.0001; and ω = 11.4 m. Transverse mixing is estimated by $E_y = 0.225\bar{h}\sqrt{g\bar{h}S}$. Injection of dye of concentration 100 ppm is made continuously in the middle of the stream for 10 s. Concentration profiles are computed using the proposed model taking Δx = 1.0 m and Δy = 1.0 m at time 200s, 500s and 800s. These profiles are shown in Fig. 3.6.

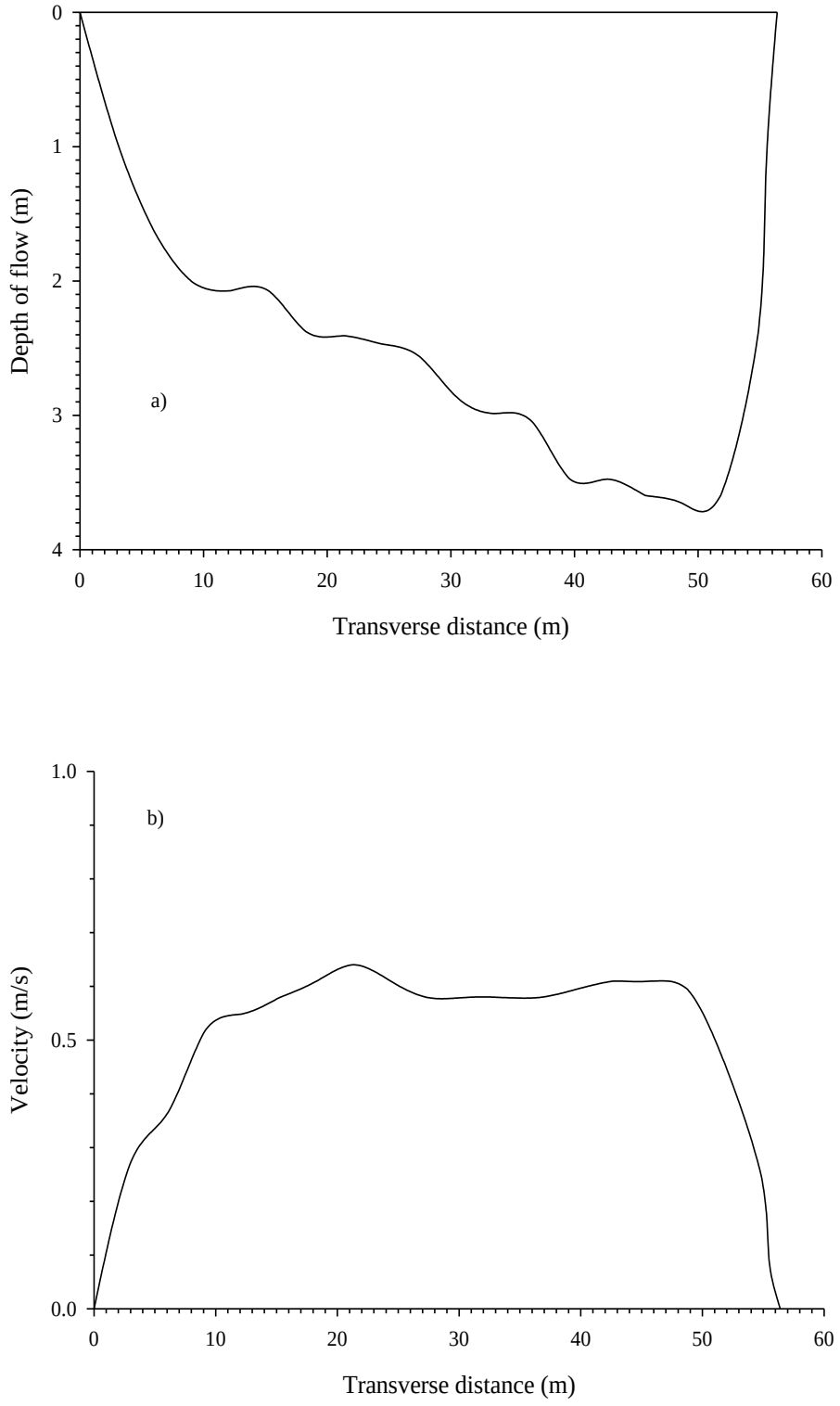

Fig 3.5. A schematic representation of a) Cross section of Lesser Slave River; b) Velocity distribution across the transect (After Beltaos and Day, 1976).

As the cloud of dye moves in downstream, it spread out in space domain and as a result peak concentration decreases. No oscillations have been noticed at the discontinuity of the concentration field.

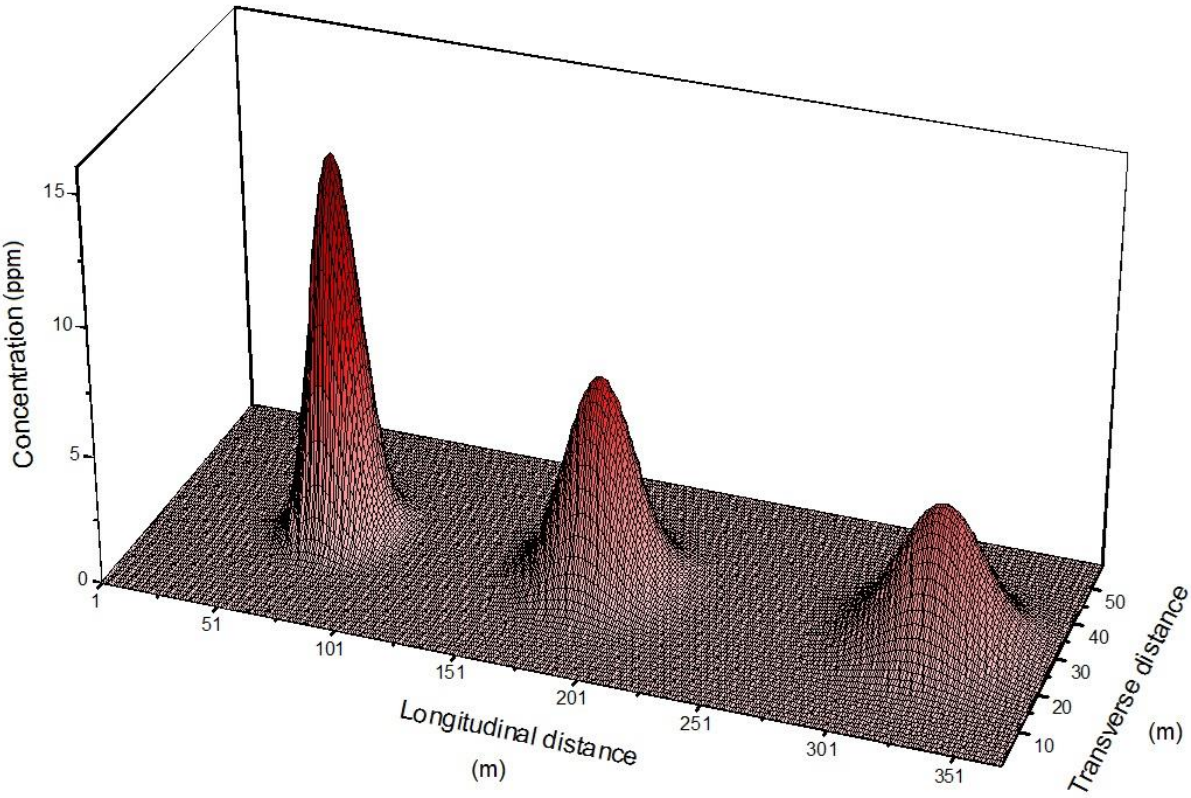

Fig. 3.6 Concentration profiles at time 200 s, 500 s, and 800 s

3.6 DETERMINATION OF E_Y USING THE CONCENTRATION PROFILES

The FV model proposed by Ahmad (2008) for the solution of steady transverse mixing equation is extended to determine the value of E_y by using concentration profiles at least two stations in the downstream of the injection site. Method of one-dimensional grid search is used for this purpose.

The one dimensional grid search method is based on the Bisection procedure, which is used to find roots of one- dimensional functions. Also one can find the optimum value of E_y, which is such that it produces maximum agreement between the predicted and the observed concentration profiles at the stations. The agreement between predicted and observed

concentration profiles has been judged in the present study in terms of the error (ERS), which is defined as

$$\text{ERS} = \left(1 - \frac{\text{Peak computed concentration}}{\text{Peak observed concentration}}\right) \times 100\% \qquad (3.30)$$

The measured concentration profile at the first station is used as input and concentration profile at the other downstream stations are predicted by the proposed scheme. Using some trial value of E_y the error at each station is calculated by Eq. (3.30) and the average value of error (ERS) is obtained. The value of E_y producing minimum value of ERS is considered as the optimum one.

A global optimum value of mixing coefficient exists due to parabolic nature of steady transverse mixing equation (see Fig. 3.7). The initial approximate value of E_y is taken equal to $0.13hU_*$. Let the initial E_y correspond to point ① (see Fig. 3.7). An incremental value, ΔE_y of mixing coefficient equal to one tenth of the initial E_y is taken and error is calculated at the points ② and ③. The point corresponding to minimum error is searched. Let in this case, the point be ②. Now error is calculated at the next point ④ and again minimum error is searched; let that point be again ②. This means that the optimum value of E_y lies somewhere in the bracketing triplet (①,② and ④). Now the grid is bisected and ERS(5) and ERS(6) are calculated. If ERS(2) < (ERS(5) and ERS(6)) then the grid is again bisected and same process is followed, until one reaches up to the desired accuracy. But if ERS(6) or ERS(5) is minimum then the same process is continued in the required direction.

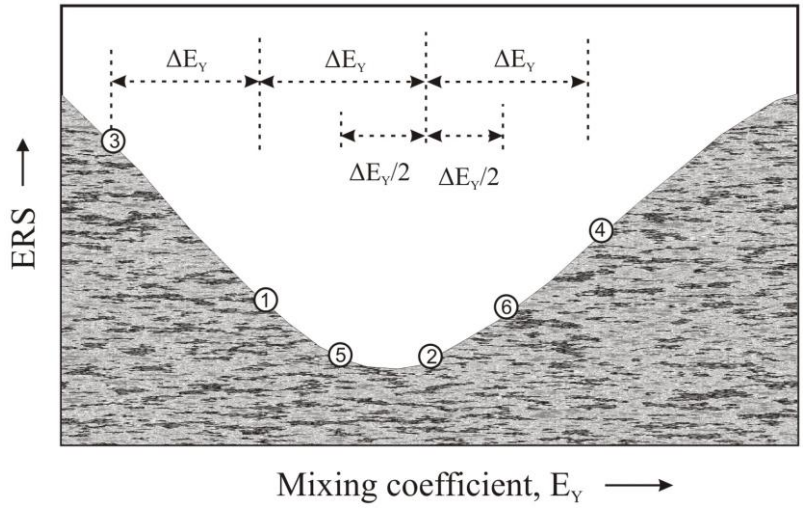

Fig. 3.7 One-directional grid search method (after Ahmad et al. 1999)

3.7 CONCLUDING REMARKS

The governing equation for transient transverse mixing in a prismatic channel is solved by finite volume method using upwind and central difference schemes. The model takes care of variation of transverse mixing coefficient across the width. Satisfactory agreement is found between concentration profiles computed using the proposed finite volume model and the analytical model for constant mixing coefficient and continuous pollutant injection. No oscillations have been noticed at the discontinuity of the concentration field. The proposed model is demonstration for transient transverse mixing using data of Lesser Slave River. It is found that as the cloud of dye moves in the downstream, it spread out in space domain and as a result peak concentration decreases. The FV model proposed by Ahmad (2008) for the solution of steady transverse mixing equation is extended to determine the value of E_y using concentration profiles at least two stations in the downstream of the injection site. Method of one-dimensional grid search is used for this purpose.

Chapter

4

EXPERIMENTAL WORKS

4.1 INTRODUCTION

The experiments were performed at Hydraulic Laboratory of Civil Engineering Department, Indian Institute of Technology Roorkee. In the present study, the experiment was aimed at to study the enhancement in transverse mixing of the tracer in the presence of submerge vanes. The concentration profiles of the tracer downstream of its injection in the channel without submerged vanes and with submerged vanes for their different configuration were measured. This section deals with the experimental set-up, its procedure and data collection.

4.2 EXPERIMENTAL SET UP

4.2.1 Setup

The experiments were performed in a recirculating concrete flume of width 1.0 m, depth 0.30 m and length 19 m. The bed slope of the flume was 0.000632. The flume was marked at every one meter length from its upstream. The water was supplied to the flume through an overhead tank, in which the level of water was kept constant to have a constant discharge for a particular opening of the valve-fitted in the delivery pipe of the tank. An orifice meter was also fitted in the delivery pipe for the discharge measurement. Flow from the flume was taken into a sump through a channel fitted with a sharp-crested weir for the discharge measurement. Water was again lifted using a pump to the overhead tank.

Two rows of grid walls, flow straighteners and wooden wave suppressor were provided upstream of the channel to stabilize the flow. A tail gate was provided at the end of the flume

to maintain the uniform flow. The railing of the flume was made parallel to the bed prior to conductance of the experiment. The flume layout is shown in Fig. 4.1 and a photograph showing the flume is shown in Fig. 4.2.

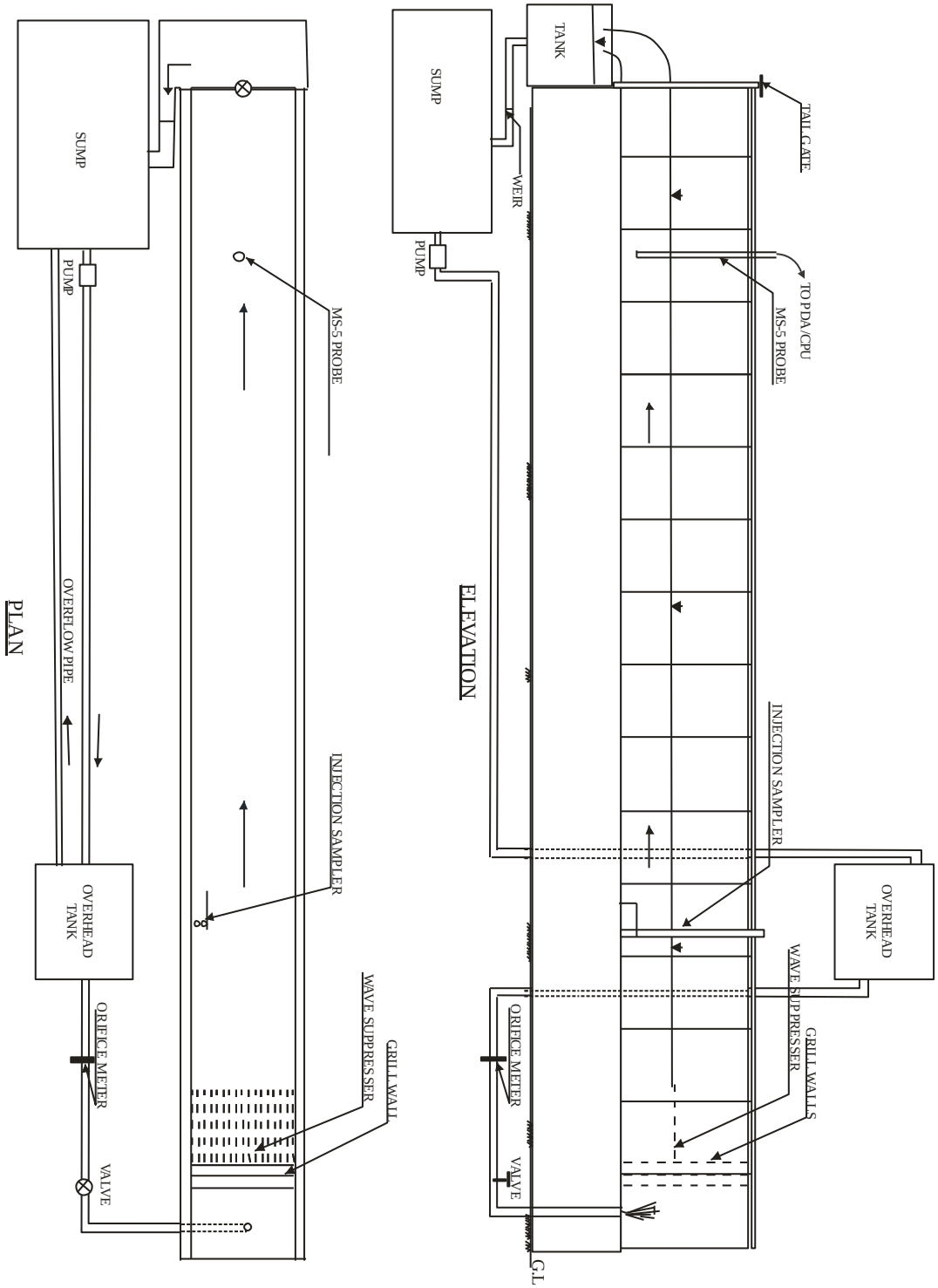

Fig. 4.1 Layout of the Flume

Fig. 4.2 Photograph showing the Flume

(a) Tracer Injecting System

The Rhodamine WT was used as tracer due to its high detectability and conservative in nature. The tracer injecting system consisted of two overhead tanks-one over the other (see Figs. 4.3 and 4.4). The tracer of known concentration was poured in both the tanks. Tracer from lower tank was continuously pumped to the upper tank and overflow of the upper tank was ensured to maintain a constant head of tracer in the upper tank all the time. The tracer was supplied to the tracer injection sampler through a 6 mm polythene pipe from the upper tank.

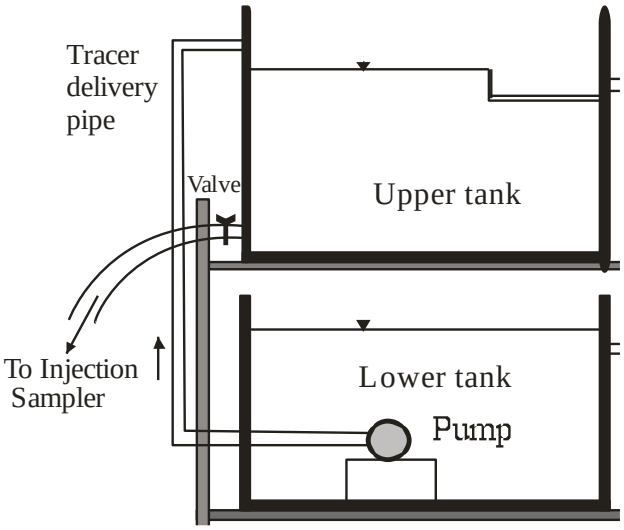

Fig. 4.3 Tracer Injection System

Fig. 4.4 Photograph showing Tracer Injection System

Injection sampler, used in the present experimental work, consisted of four tubes of 2 mm diameter placed at 35 mm spacing as shown in Fig. 4.5 (Only two vertical tubes are shown in Fig. 4.5). The tubes had a number of vertical holes at the interval of 20 mm and connected to a

manifold. Polythene pipe from the injection system fed the tracer to the manifold. The tracer was injected in a channel of 100 mm width formed by placing a plate in the main channel at a distance of 100 mm from its left wall. The injection of tracer thus represents the plane source of a width 100 mm. The Rhodamine WT dye concentration was measured across the width of the channel - downstream of injection point using Hydro lab MS-5 probe as shown in Figs. 4.6. Fig. 4.7 shows a sample of online monitoring of concentration using Hydro lab MS-5 interfaced with computer.

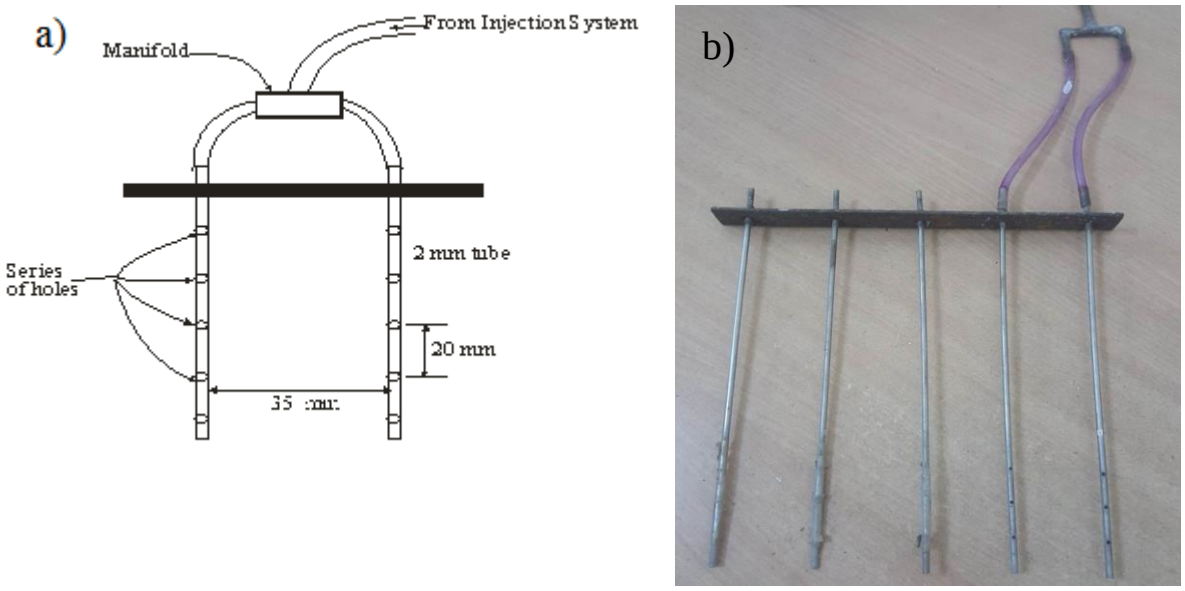

Fig. 4.5 Tracer Injection Sampler a) Line sketch of tracer injector; b) A photograph of tracer injector

Fig. 4.6 Photograph showing MS-5 Probe

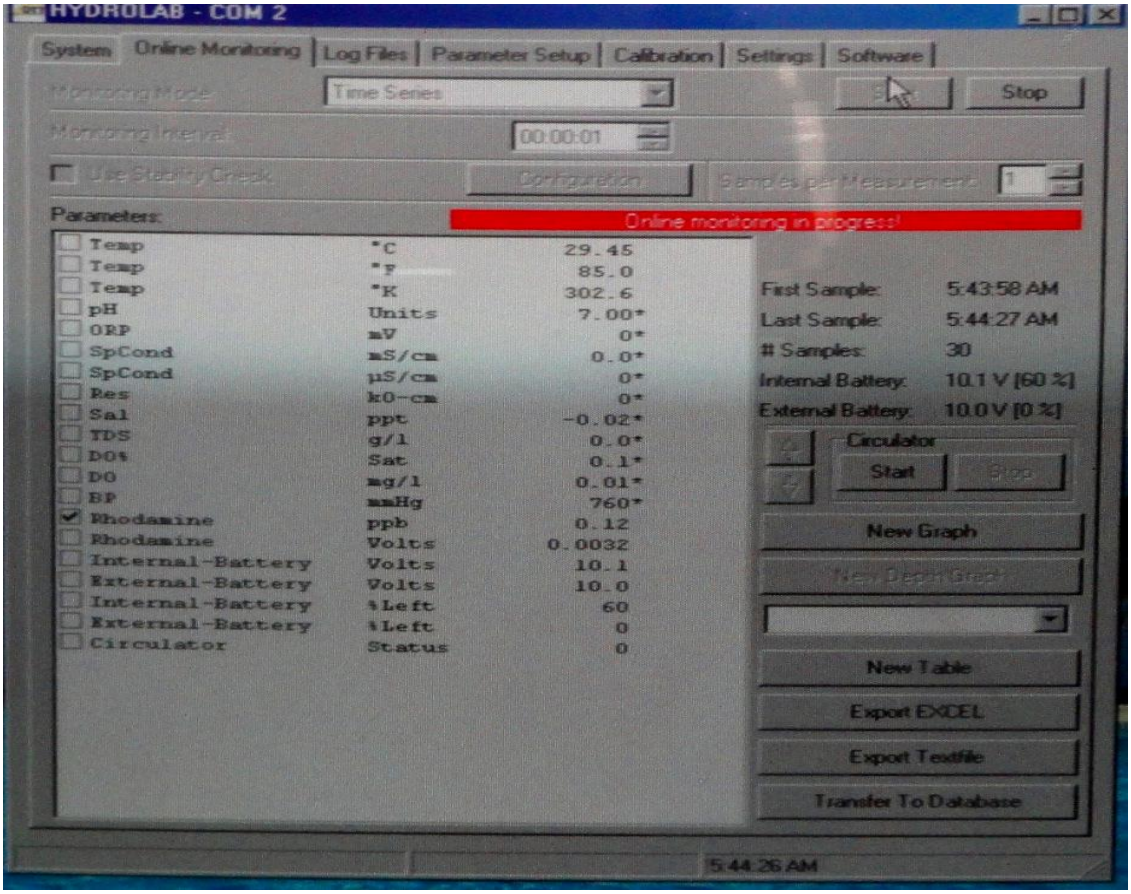

Fig. 4.7 Hydrolab MS-5 interfaced with computer for online monitoring of concentration

(b) Hydro Lab MS-5

The state of the art equipment Hydro Lab MS-5 was also used for an on-site measurement of concentration of Rhodamine WT. Hydro Lab MS-5 is a simple yet high tech multi probe sonde, which supports several probes that are built around a set of reliable sensors and electronic components. Some basic parameters like temperature, pH, conductivity, salinity, Total Dissolved Solids (TDS), Dissolve Oxygen (DO), concentration of Rhodamine WT and depth can be measured with the help of this instrument. The sensor is an in-situ optical fluorometer that determines Rhodamine concentration in a given water sample. The sample is irradiated using green (550 nm) light. The Rhodamine WT sensor absorbs the green light energy and fluoresces or emits red (590–715 nm) light. The sensor directly measures the amount of red light emitted by the Rhodamine in the water sample. The multiprobe can either display the Rhodamine signal as a scaled voltage from 0–5 V or as a concentration from 0–1000 ppb.

(c) Prandtl-Pitot tube

In order to measure the transverse velocity profile, Pitot tube was used. Working of Pitot tube is very simple, when approaching flow strikes the nozzle or face of Pitot tube, it converts the velocity head into the pressure head. The converted pressure head gives rise to head difference, Δh. The local velocity can be calculated using:

$$U = \sqrt{2g\Delta h} \tag{4.1}$$

In experimentations, Pitot tube was placed initially near to wall, so that, velocity near to wall can be measured. After that, Pitot tube was traversed across the channel width at an interval of 0.1 m and velocity was calculated by measuring head difference at the mid-depth of the flow. Since, Pitot-tube was unable to take velocity on the wall, hence, velocity was taken at y = 0.98 m which was near to wall. Velocity profiles in transverse direction were measured for depths of flow, z = 0.1241 m, 0.1025 m and 0.09 m.

(d) Micro Acoustic Doppler Velocimeter (Micro ADV)

Micro ADV is basically an acoustic instrument used to measure three dimensional velocity field in the flow. Micro ADV has basically three receivers and one transmitter (Fig. 4.8). Transmitter transmits the acoustic waves into the flow having particular frequency and phase. As the fluid media is mobile, due to which transmitted acoustic waves suffers due to Doppler Effect. According to Doppler Effect, "Velocity of moving source or receiver is proportional to rate of change of phase shift." and is calculated by

$$U_i = \frac{V_s}{4\pi f_r}\frac{d\varphi_i}{dt} \tag{4.2}$$

Here, U_i = velocity in i^{th} direction; V_s = velocity of sound in media; f_r = frequency of waves transmitted; φ_i = phase in i^{th} direction and t = time coordinate.

Doppler shifted acoustic waves are received by receivers which send the received waves to the calculation unit of ADV. In calculation unit, a pre-calibrated transformation matrix was used to multiply the obtained velocity component to generate more precise velocity components.

Fig. 4.8 Mini ADV capturing velocity of flow

(e) Design of Vanes

The vanes to be installed in the channel were designed as per the methodology proposed by Odgaard and Wang (1991a). At the design stage, the depth of the flow *h*, bed slope of the channel S, mean velocity of flow U, and median size of sediment d_o are known. If the vane system is to be designed for a river bend, the radius of the bend R_a is also known. However, for the installation of vane in straight channel like in the case of water intake and present case, radius of the bend will be equal to infinity. Assuming the channel to be wide, calculate $\sqrt{8/f} = U/\sqrt{(gSh)}$ and then the channel's resistance parameter, $m = \kappa\sqrt{8/f}$. Here, κ = von Karman's universal constant = 0.41 and *f* = friction factor = $8(u_*/U)^2$. Also calculate the sediment Froude number from the median diameter of the sediment (not applicable in the present case). Odgaard and Wang (1991a) and Odgaard and Kenedy (1983) recommended that the height of vane H should be equal to 0.2-0.5 times the depth of flow. Choose some value of

T_o/h (T_o = submergence of flow over the vane) out of 0.5, 0.7 and 1.0. Calculate the length of vane L keeping the aspect ratio H/L= 0.3. Take δ_n (transverse spacing between vanes in a row) = 3H and δ_s (longitudinal spacing between two vane rows) = 15H or 30H. It is to be noted that a number of alternate designs are possible for a specific problem.

In the present study, data for design of vanes are depth, bed slope and channel velocity. Depths of the flow were 0.09 m, 0.1025 m and 0.1241 m, which were utilized to design the dimensions of vane. The bed slope in all experimentation was constant and equals to 6.32×10^{-4}. The average velocities of flow were 0.448 m/s, 0.388 m/s and 0.267 m/s for depths of flow = 0.1241 m, 0.1025 m and 0.09 m, respectively. Since three sets of vanes were designed according to the recommendations of Odgaard and Wang (1991a) which are as follows

(i) Depth of flow = 0.1241 m; Length of submerged vanes = 0.12 m; Height of submerged vanes = 0.06 m; Thickness of submerged vanes = 2 mm; lateral spacing = 0.125 m; longitudinal spacing = 1 m.

(ii) Depth of flow = 0.1025 m; Length of Submerged vanes = 0.1 m; Height of submerged vanes = 0.04 m; Thickness of submerged vanes = 2 mm, lateral spacing = 0.1 m; longitudinal spacing = 1 m.

(iii) Depth of flow = 0.09 m; Length of Submerged vanes = 0.05 m; Height of submerged vanes = 0.02 m; Thickness of submerged vanes = 2 mm, lateral spacing = 0.05 m; longitudinal spacing = 1 m.

Calculations for one set of vanes are given below:

Depth of flow = 0.1241 m

Height of vane = 0.2- 0.5 times of depth of flow = 0.02482 m – 0.06205 m, let us take height of vane 0.06 m.
Length of vane = 2-3 times height of vane = 0.12 – 0.18 m, let us take length of vane = 0.12 m.

Take $T_o/h = 0.5$ (say)

Lateral spacing of vanes δ_n = 2-3 times height of vane = 0.12 – 0.18 m, let us take lateral spacing of vane = 0.125 m

Longitudinal spacing of vane δ_s = 10-30 times height of vane = 0.60 – 1.80 m, let us take longitudinal spacing of vane = 1 m.

Table 4.1 gives the designed dimensions of vane with respect to the depth of flow.

Table 4.1 Designed dimensions of submerged vanes

Depth of flow (m)	Dimensions of submerged vanes				
	H (m)	L (m)	δ_n (m)	δ_s (m)	θ (degrees)
0.09	0.02	0.05	0.05	1	30
0.1025	0.04	0.1	0.1	1	30
0.1241	0.06	0.12	0.125	1	30

Four arrays of designed vanes are shown in Fig. 4.9.

Fig. 4.9 Four arrays of installed vanes

4.2.2 Procedure

After establishing the flow in the channel, the tracer was injected continuously at x = 0 from the tracer injection system. The tracer concentration was measured using MS-5 probe at

longitudinal distances x = 5 and 15 m downstream of the injection section and at transverse distances y = 0.02 m, 0.1 m, 0.2 m, 0.3 m, 0.4 m, 0.5 m, 0.6 m, 0.7 m, 0.8 m, 0.9 m and 0.95 m. After measuring the concentration profile along transects, a check for mass conservation was applied to the measured concentration. In order to apply the check, transverse profile of longitudinal velocity was measured and an average velocity was calculated. Depth of flow was measured along each transects. On measuring the concentration from left bank across transect, the mass rate is calculated in each elemental portion of divided transect by multiplying concentration with average velocity, average depth and width of element.

After obtaining the mass rate, which is also termed as area of concentration curve, for all transects an average value of area was calculated and all pre-calculated mass rate were normalized with average rate to yield recovery factor (R.F.). The range of R.F. in the experimentation was between 0.95-1.05 for each section. After obtaining the R.F., it is multiplied with the measured concentrations to obtain the mass conserved concentrations. Three sizes of vanes were used in the experimentations which were 0.02 m × 0.05 m, 0.04 m × 0.1 m and 0.06 m × 0.12 m, whose lateral spacing was 0.05 m, 0.1 m and 0.125 m, respectively (Fig. 4.10.). Three flow conditions were maintained in order to perform experimentations for depth of flow which were 0.09 m, 0.1025 m and 0.1241 m. For every vane size five runs were done *viz*. 4 vane rows, three vane rows, 2 vane rows and no vane row. Three different vane sizes were used in the study for three different depths of flow. The calculation gives a total of 45 runs for present study. Fig. 4.11 shows a typical concentration profile across the transverse direction.

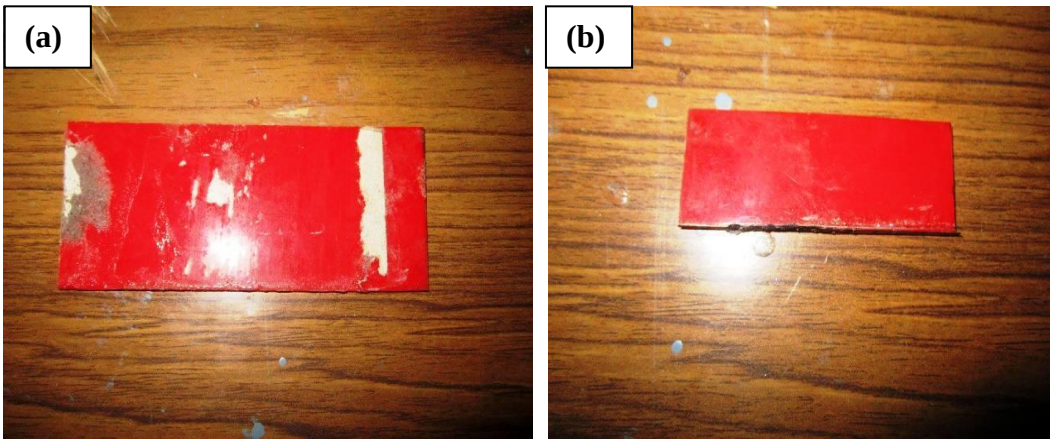

Fig. 4.10 Submerged vanes of size (a) 0.04 m ×0.1 m and (b) 0.02 m × 0.05 m.

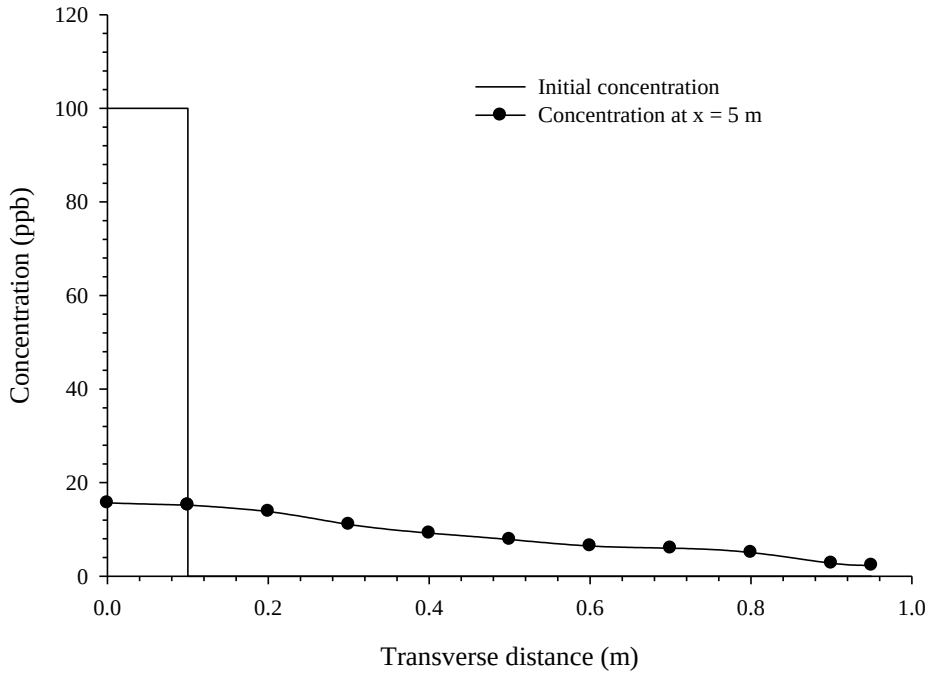

Fig. 4.11 Variation of concentration across the transverse direction (Depth of flow = 0.1241 m, Height of vane = 0.06 m, Length of vane = 0.12 m, Discharge = 0.056 m^3/s).

4.3 NORMALIZATION OF CONCENTRATION PROFILES

Since concentration profiles were measured in different flow depths and discharges, thus, have some scale effects in their measurements. In order to remove these scale effects, these concentration profiles were normalized so that they can be compared over one scale. In order to normalize the concentration profile, let us suppose that initial concentration of dye be Co and rate of dye discharging be Qo. Also, assume that concentration of profile at point of measurement be C and discharge of flow be Q. Now from principle of mass conservation:

$$C_o Q_o = CQ \tag{4.3}$$

Now, discharge of flow,

$$Q = BUh \tag{4.4}$$

where B = width of channel; U = flow velocity; h = depth of flow.

Also,

$$Q_o = bUh \tag{4.5}$$

where b = width of section of injection.

Thus, implanting Eq. (4.4) and (4.5) into Eq. (4.3) and simplifying it, value of initial concentration was obtained as:

$$C_o = \frac{CB}{b} \tag{4.6}$$

Before introducing the submerged vanes to the flow, blank concentration was measured which represented the equilibrium concentration of Rhodamine WT dye present in the flow in spite of experimental release of dye. After measuring the transverse mixing in plane shear flow, four rows of submerged vanes were introduced and aforesaid procedure of concentration measurement was repeated. Now, one vane row was removed and repetition of process was performed until all vanes were removed.

4.4 MEASUREMENT OF FLOW PATTERN AROUND SUBMERGED VANE

Submerged vane utilize the flow velocity to generate vorticity field. Vorticity field as per investigators like Wang and Odgaard (1993), Tan et al. (2005), Ouyang et al. (2008), etc. are consist of high level of turbulence. In order to measure the intensity of vorticity field, 3D flow has to be measured accurately, so that flow downstream of vane could be understood for its utilization in pollutant management. Hence, by using micro ADV, velocity flow field was measured downstream of the vane rows. Four rows of submerged vanes were attached to the bed so as to perform experimentations of flow pattern around submerged vanes. Vanes used in experimentations were *viz.* 0.06 m × 0.12 m whose lateral spacing respectively was 0.125 m. Initially, four vane rows of above mentioned vane sizes were installed and flow was made to attain a uniform depth of 0.1241 m, initially. The depth, z = 0.1241 m was the depth corresponding to full discharge condition. Three transects were chosen at the downstream of last installed vane rows, which were respectively at x = 3H, 8H and 20H from last vane row (Here, H = Height of submerged vane). On each sections three points were marked on which vertical distribution of velocity was measured by using micro-ADV and these three points were

y = 0.45 m, 0.5 m and 0.55 m, respectively, away from left bank of channel. Seven points were marked over on each of the aforesaid three points in order to measure velocity on each of those seven points. After measuring the velocity on each of the vertical for all the three transects, now one row of submerged vane was removed and again velocity distribution was taken on each vertical of the transects. Similar procedure was repeated for two, one and without vane rows case. After measuring the vertical distribution of velocity on each of transect, now again four rows of submerged vane of afore-mentioned size *i.e.* 0.06 m high and 0.12 m long vane, were installed. Depth of flow was now allowed take a uniform level of 0.1025 m and again the above described process was repeated. Again the vane rows were decreased from four to three and process of measurement was repeated. Similar process was repeated for two, one and without vane rows cases. Now again after reinstalling the four vane rows and establishing depth of flow to the level of 0.09 m and repeat the above described procedure for four, three, two, one and with vane cases for each transect and each vertical.

4.5 RANGE OF DATA

Range of data collected in the present study is given in Table 4.2.

Table 4.2 Range of data collected in present study

S. No.	Parameters	Range
1	Slope	6.32×10^{-4}
2	Discharge	0.024-0.056 m^3/s
3	Flow velocity	0.27-0.45 m/s
4	Depth of flow	0.09-0.1241 m
5	Width of flume	1.0 m
6	Hydraulic radius	0.076-0.099 m
7	Height of vanes	0.02-0.06 m
8	Length of vanes	0.05-0.12 m

9	Angle of attack	30^o
10	Number of vane rows	4
11	Number of vanes per row	7-19
12	Longitudinal distance of vane rows	1 m
13	Lateral distance between vanes	0.05-0.125 m
14	Distance of first vane from wall	0.25-0.75 m

4.6 CONCLUDING REMARKS

Experimentations were conducted to measure concentration profile across the channel downstream of tracer injection section in the flow with and without submerged vanes. The tracer was injected in the flow from a vertical plane source generating two dimensional mixing in the flow *i.e.* longitudinal and transverse directions. Various vane configurations whose size varied from 0.02 m × 0.05 m to 0.06 m × 0.12 m were utilized in experimentations. Despite being measured in different flow conditions and for various vane configurations, concentration profiles are normalized to bring these concentration profiles to scale where they can be compared. Velocity profiles were measured for various vane configurations *viz.* four, three, two, one and without vanes, in their downstream at three transects situated at 3H, 8H and 20H from last vane row installed. The size of vane kept for velocity measurement was 0.06 m × 0.12 m.

Chapter 5

FLOW PATTERN AROUND SUBMERGED VANES

5.1 INTRODUCTION

Submerged vane is basically an aerofoil structure, which generates the excess turbulence in the form of helical flow structure in the flow due to pressure difference between approaching flow side and downstream side of the vane (Odgaard and Spoljaric, 1986; Odgaard and Mosconi, 1987; Odgaard and Wang, 1991; Wang and Odgaard, 1993). These vanes are in general placed at a certain angle with respect to the flow direction which is usually 10^o to 40^o. Submerged vanes are used for sediment management in the river system. It differs from the traditional methods like groins, dikes, etc., which are usually placed normally to the flow and produce flow distribution by drag force and are not so much efficient in controlling the sediment transport. Submerged vanes utilize vorticity to minimize the drag and produce flow redistribution in the flow such that longitudinal flow is compelled to get diverted towards the transverse direction (Wang and Odgaard, 1993). Many investigators like Odgaard and Wang (1991a), Wang and Odgaard (1993), Marelius and Sinha (1998), Tan et al. (2005), Ouyang et al. (2008) have studied analytically and experimentally the flow structure of the submerged vane. In this chapter, an attempt was made to develop a numerical model to predict flow pattern and turbulence characteristics around and downstream of a single submerged vane and a series of vane rows containing multiple vanes in a vane row. In this attempt, ANSYS-CFX software was used which used methods of Computational Fluid Dynamics (CFD) to simulate

flow by using standard *K*-ω model. Experimental results of various turbulence characteristics are also included at the end of the chapter to provide the picture of how turbulence structure of flow changes when rows of submerged vanes are introduced in the flow.

5.2 REVIEW OF CFD MODELS

5.2.1 Mean Flow equations

The mean flow equations describing the motion of fluid are given by continuity and momentum equations. Continuity equation is based on the law of conservation of mass which states that mass of a fluid in a given volume of observation (control volume) is conserved. Momentum equations were independently developed by Navier and Stokes by utilizing Newton's second law of motion and hence are known as Navier-Stokes equation. While Reynolds averaging of Navier-Stokes (N-S) equation, generation of various correlations of fluctuating turbulent quantities makes use of the N-S equation very complicated as relation of these correlation with mean flow characteristics is unknown. Hence, by evaluating the relationship between these correlations and mean flow quantities with the help of semi-empirical equations or by generating partial differential equations for various transport quantities like turbulent intensities, kinetic energy, etc., the problem of "closure" of Reynolds averaged Navier-Stokes (RANS) equation is evaluated. This problem of "closure" gave rise to the generation and evaluation of turbulence model (Pope, 2000; Rodi, 1980). The mean flow equations are

Continuity Equation

$$\frac{\partial \rho}{\partial t} + \nabla.(\rho u) = 0 \tag{5.1}$$

Momentum equations (Navier-Stokes equation)

$$\frac{Du}{Dt} = -\frac{1}{\rho}\nabla p + \nu \nabla^2 u \tag{5.2}$$

Here, $\frac{D}{Dt} = \frac{\partial}{\partial t} + u\frac{\partial}{\partial x} + v\frac{\partial}{\partial y} + w\frac{\partial}{\partial z}$ = Material Derivative

p = pressure in the fluid.

5.2.2 Turbulence Models

Turbulence is a highly irregular and a coherent phenomenon (Tennekes and Lumley, 1972; Nezu and Nakagawa, 1993). It is a known fact that turbulence varies with the time and space and acts randomly, i.e., the value it will be having in preceding time is not necessarily will be same in subsequent time. Hence, it is quite difficult to measure the turbulence quantities due to their random nature in the field. While deriving Reynolds Averaged Navier-Stokes (RANS) equation quantities including cross turbulence quantities product were evolved during Reynolds averaging process which were also difficult to measure. Thus, in order to relate these quantities with the flow characteristics, turbulence models were derived starting with Prandtl's mixing length theory in 1936 to Average stress method or ASM model. In the present study standard *K*-ω model was applied for simulation of flow. The reason behind not using popular standard *K*-ε model in the present study was its incapability to capture the flow in separation region and hence over-predicting the flow, whilst *K*-ω was successfully established to be efficient in capturing separation regions (Versteeg and Malalsekera, 2007). Thus, here pro's and con's of *K*-ω models are discussed with different types of *K*-ω model.

a) K-ω turbulence model

The turbulent kinetic energy, *K*, and turbulent frequency, *ω*, are required to calculate the value of eddy viscosity, *ξ*, obtained by employing the standard *K-ω* (Wilcox, 1988) turbulence closure model. The equation of transport of *K* and *ω* are given as follows (where repeated indices indicate summation):

$$\frac{\partial K}{\partial t} + u_i \frac{\partial K}{\partial x_i} = \frac{\partial}{\partial x_i}\left[\frac{\left(\mu + \frac{\rho\xi}{K}\right)}{\rho}\frac{\partial K}{\partial x_i}\right] + \frac{P_k}{\rho} - \beta^* k\omega \qquad (5.3\text{ a})$$

$$\frac{\partial \omega}{\partial t} + u_i \frac{\partial \omega}{\partial x_i} = \frac{\partial}{\partial x_i}\left[\upsilon + \frac{\xi}{\sigma_\omega}\frac{\partial \omega}{\partial x_i}\right] + \gamma_1\left[2S_{ij}.S_{ij} - \frac{2}{3}\omega\frac{\partial u_i}{\partial x_j}\delta_{ij}\right] - \beta_1\omega^2 \qquad (5.3\text{ b})$$

Here,

u_i = component of velocity in the i^{th} direction where i = 1, 2, 3, etc.

x_i or x_j = coordinate of variable x into the i^{th} or j^{th} direction.

μ = dynamic viscosity of fluid.

v = kinematic viscosity of fluid.

S_{ij} = Strain tensor = $\frac{1}{2}\left[\frac{\partial u_i}{\partial x_j} + \frac{\partial u_j}{\partial x_i}\right]$

P_k = Production of kinetic energy = $2\rho\xi S_{ij}.S_{ij} - \frac{2}{3}\rho K\frac{\partial u_i}{\partial x_j}\delta_{ij}$.

σ_k = Coefficients in *K-ω* turbulence scheme associated with transport of turbulent kinetic energy.

σ_ω = Coefficient in Wilcox's *K-ω* turbulence scheme associated with transport of turbulent frequency

γ_1 = Coefficient in Wilcox's *K-ω* turbulence scheme associated with production of turbulent frequency

β_1 = Coefficient in Wilcox's *K-ω* turbulence scheme associated with dissipation of turbulent frequency

β^* = Coefficient in Wilcox's *K-ω* turbulence scheme associated with dissipation of turbulent kinetic energy

It was observed in the experimentations that where there has adverse pressure gradients leading to the separation of flow and into the stagnation zone, the K-ε model over-predicts the turbulence characteristics of the flow field. The reason behind this flaw is that K-ε model was developed on the assumption that there exists a dynamic equilibrium between production of turbulence and dissipation of turbulence under the action of fluid viscosity, but in the aforesaid zones due to high shear strains on the fluid flow and excessive separations causes violation of the assumption of equilibrium, hence overprediction of the turbulence quantities. Wilcox

(1988; 1993 a, b; 1994), Menter (1992 a,b; 1994; 1997) and Menter et al. (2003) developed a model by stating that ξ is not a universal variable to define the length scale of eddies as it is overpredicted in the zone of high shear strain, recirculations and redevelopment of flow. Hence, Wilcox (1988) defined a parameter turbulence frequency, ω, as the transportable parameter to define the length scale of eddies. Hence, the brief description of the K-ω model is given as follows:

b) Wilcox K-ω model

Wilcox (1988; 1993 a, b; 1994) proposed that ε is not the possible length scale determining variable for different eddy scales present in the flow but he postulated that turbulence frequency, $\xi = K/\omega$, to be the better to determine the possible length scales. By utilizing ω as second variable Wilcox developed following formula for length scale:

$$L_t = \sqrt{K}/\omega \tag{5.4}$$

Thus after having developed equation for the length scale, Wilcox developed following relation to evaluate eddy viscosity, (ξ):

$$\xi = K/\omega \tag{5.5}$$

In order to compute the Reynolds stress, Wilcox utilized the Boussinesq's equation, given by:

$$\tau_{ij} = -\rho\overline{u_i' u_j'} = \rho\varepsilon\left[\frac{\partial u_i}{\partial x_j} + \frac{\partial u_j}{\partial x_i}\right] - \frac{2}{3}\rho K\delta_{ij} \tag{5.6}$$

Here,

$\tau_{ij} = -\rho\overline{u_i' u_j'}$ = Reynolds stress

ρ = Density of fluid

δ_{ij} = Kronecker delta $\begin{cases}\delta_{ij} = 0 \text{ if } i \neq j \\ \delta_{ij} = 1 \text{ if } i = j\end{cases}$

The equation of transport of K and ω developed by Wilcox is given by Eq. (5.3b) and coefficients involved in the Eq. (5.3 b) are given by Table 5.1. Initially K-ω model was used to model the whole flow domain as no damping function is needed to analyze the near wall flow or low Reynolds number flow. In order to analyze the near wall flow, value of K is set to zero at the wall and henceforth $\omega \rightarrow \infty$ in the near wall region, thus in order to supply the large values of ω near the wall, Wilcox, evaluated the following hyperbolically varying expression for calculation of ω near the wall:

$$\omega_P = \frac{6\nu}{\beta_1 y_P^2} \tag{5.7}$$

Here, y_P = point from the wall within the limits $30 < y_P^+ < 500$, where assumptions of log-law and dynamic energy equilibrium are satisfied.

Table 5.1 Coefficients in Wilcox K-ω transport equation

σ_k	σ_ω	γ_1	β_1	β^*
2	2	0.553	0.075	0.09

Advantages: -

(i) Wilcox *K-ω* model gives a good approximation of near wall flow, recirculating flows, wakes, etc.

(ii) The flow is more easily computed and refined.

Disadvantages: -

(i) As $\omega \rightarrow 0$, ε use to become indeterminate as can be seen in Eq. (5.5).

(ii) Results of the present model was observed to be highly depends on the assumed free stream value of ω.

c) Menter SST K-ω model

Menter (1992) found that K-ε model was unsatisfactory for boundary layers with adverse pressure gradient. Thus he was led to use a hybrid model having following features:

(i) Attachment of the K-ε model with K-ω model in the near wall region.

(ii) Utilization of standard K-ε equation in the fully turbulent region away from the wall.

Reynolds stress computations and turbulent kinetic energy transport equation were same as in the Wilcox's K-ω model. For, ε, Menter (1992) developed following transport equation:

$$\frac{\partial \omega}{\partial t} + u_i \frac{\partial \omega}{\partial x_i} = \frac{\partial}{\partial x_i}\left[\upsilon + \frac{\xi}{\sigma_{\omega,1}} \frac{\partial \omega}{\partial x_i} \right] + \gamma_2 \left[2S_{ij}.S_{ij} - \frac{2}{3}\omega \frac{\partial u_i}{\partial x_j}\delta_{ij} \right] - \beta_2 \omega^2 + \frac{2}{\sigma_{\omega,2}\omega} \frac{\partial K}{\partial x_i} \frac{\partial \omega}{\partial x_i} \quad (5.8)$$

$\sigma_{\omega,1}$ = Coefficient in Menter's *K-ω* turbulence scheme associated with transport of turbulent frequency

$\sigma_{\omega,2}$ = Coefficient in Menter's *K-ω* turbulence scheme associated with transport of turbulent frequency by cross-diffusion

γ_2 = Coefficient in Menter's *K-ω* turbulence scheme associated with production of turbulent frequency

β_2 = Coefficient in Menter's *K-ω* turbulence scheme associated with dissipation of turbulent frequency

The last extra term in Eq. (5.8) arises from the transformation done by Menter (1992), i.e., he replaced $\xi = K\omega$ rather using $\xi = K/\omega$ and is also termed as cross diffusion term. Table 5.2., describes the various coefficients used in SST *K*-ω transport equation. Menter et al. (2003) provided the following improvement in their model to make it CFD friendly:

Table 5.2 Coefficients in Menter SST *K*-ω transport equation

σ_k	$\sigma_{\omega,1}$	$\sigma_{\omega,2}$	γ_2	β_2	β^*
1	2	1.17	0.44	0.083	0.09

(i) **Blending functions:** Numerical instabilities were seem when ε was calculated from K-ε model far from the wall and transformed K-ε model near the wall. Thus, to achieve smooth transition between the two models, blending functions were introduced as:

$$C' = F_C C_1 + (1 - F_C) C_2 \tag{5.9}$$

Here,

C_1 = value of eddy viscosity from the original K-ε model

C_2 = value of eddy viscosity from the transformed K-ε model

$F_C = F_C (L_t/y, R_{ey})$

$L_t = \sqrt{K}/\omega$

$R_{ey} = \omega y^2/\nu$

The function F_C is chosen in such a way that:

a) It is zero at the wall.
b) Tends to be unity at far field.
c) Produces smooth transition around a distance halfway between the wall and edge of the boundary layer.

(ii) **Limiters:** The eddy viscosity is limited to give improved performances in advance pressure gradients and wake regions while turbulent kinetic energy (TKE) is limited to prevent the building up of turbulence in the stagnation regions. The limiters provided by Menter et al. (2003) are as follows:

$$\xi = \frac{a_1' K}{\max\left(a_1' \omega, S' F_C \right)} \tag{5.10}$$

Here,

$S' = \sqrt{2 S_{ij} . S_{ij}}$

a_1' = a constant

F_C = blending function

$$P_k = \min\left(10\beta^* \rho k\omega, 2\rho\varepsilon S_{ij}.S_{ij} - \frac{2}{3}\rho K \frac{\partial u_i}{\partial x_j}\delta_{ij}\right)$$

Advantages:

(i) Present model is computationally easier than other turbulence models.

Disadvantages:

(i) Present K-ω model was observed to fail to introduce subtle interactions between turbulent stresses and mean flow.

5.3 DEVELOPMENT OF CFD MODEL

Geometry to be created in ANSYS-CFX is a rectangular channel, 1.0 m wide, 0.1241 m deep and 19 m long. Study was conducted for three vane sizes 0.02 m × 0.05 m, 0.04 m × 0.1 m and 0.06 m × 0.12 m. Only single vane size of length = 0.12 m; height = 0.06 m; and thickness = 0.002 m was utilized in order to study the flow pattern as well as magnitude of vorticity. This vane was placed at mid-width of the channel i.e. 0.5 m from either of the banks and was placed 6.53 m downstream from the inlet of the channel. The developed CFD model is described below:

a) Creation of geometry

Computation Fluid Dynamics (CFD) is an emerging tool to analyze the flow pattern around a structure and to deduce that how that structure is going to affect the flow pattern. Utilization of CFD has been done in many research areas like to study flow pattern around a cylinder, to deduce the critical submergence of intake, to study the flow pattern in porous media, etc. Only a single study have been found in literature to study flow pattern around submerged vane which was done by Sinha and Marelius (2000) by using K-ε model of turbulence closure. The main drawback of that model was that there were differences in computed results and observed results. In the present CFD modeling, various turbulence closure methods were applied to simulate the flow pattern around submerged vanes and it was found that k-ω model of turbulence closure replicated the flow pattern around submerged vane in real aspect. It is evident from literature that where other closure methods fail to account for adverse pressure gradient generated wake and recirculatory flows, K-ω model simulate these types of flows in a satisfactory manner. Submerged vane model was prepared and meshed using the ICEM CFD (Here, ICEM stands for Integrated Computer Engineering and Manufacturing and CFD stands

for Computational Fluid Dynamics) software in this study. In order to create the model of submerged vane, a channel volume was created of dimension 10 m long, 1 m wide and depth of the volume was kept according to the depth of flow *viz.* 0.1241 m as shown in Fig. 5.1.

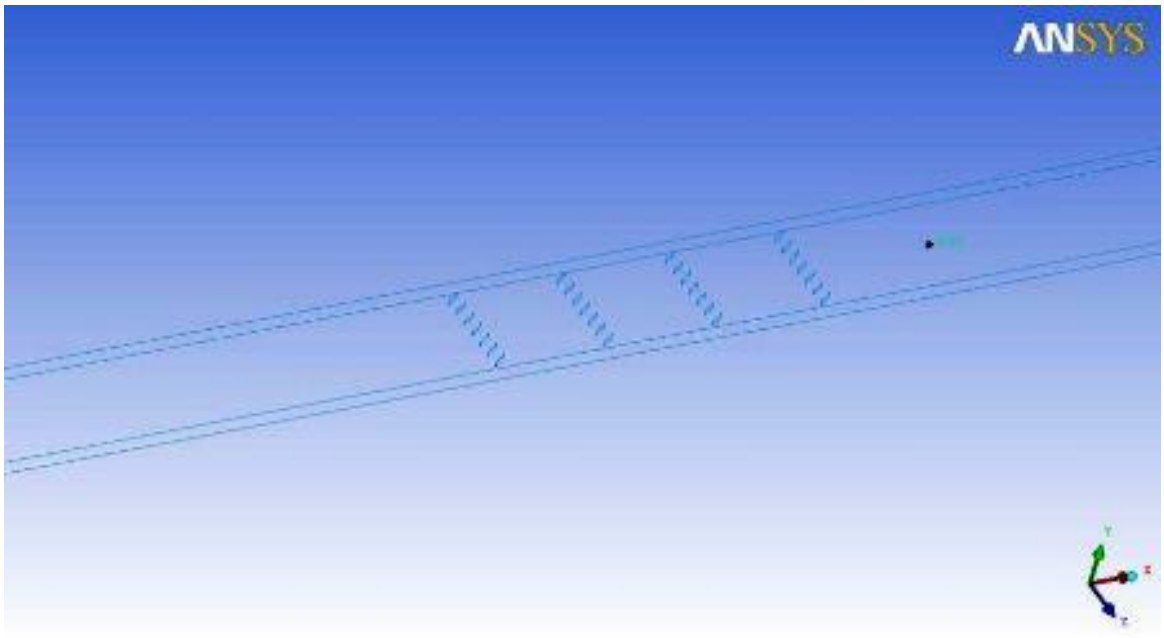

Fig. 5.1 Model of submerged vanes generated by ICEM-CFD

The vanes were placed at the distance of 3.5 m from the inlet section and in a row of 7 vanes each being separated by a lateral distance of 0.125 m. First vane of row was having a lateral distance of 0.08 m from the left wall of flume. A sum of 4 vane rows were utilized in order to measure the flow pattern around submerged vane. After creating the geometry of the vane containing vane, the geometry was meshed by utilizing appropriate meshing in order to visualize the flow structure around the vane.

b) Meshing and mesh profile of geometry

After creation of geometry, 3D blocking is initialized. A suitable blocking is created around the vane rows so as to completely cover the vane domain. All the rows were being covered up by blocks created by edge splitting. Each created vertices is associated to a point as shown in Fig. 5.2. After being done the point-vertices association, blocks around the vanes were assigned as the SOLID blocks. Main feature associated with the solid-blocking is that whenever the volume was meshed, the block remained monolithic without any mesh elements, so during

simulation, flow will not pass through the block but will pass around the vane block. After assigning the vane block as solid block, size of mesh element was given which here was 8 mm. After giving size of mesh element update mesh was clicked which assigned total number of mesh elements as 7 million. A pre-mesh was created, while creating the pre-mesh the option of solid was unchecked in the software, otherwise it lead to formation of multi-edged mesh elements. Since, a more precise flow pattern has to be observed around the vane rows, a non-uniform mesh has to be used. Thus, a non-uniform mesh was created by clicking right mouse button around pre-mesh option. After creation of non-uniform mesh in blocks around submerged vanes, mesh quality was checked which came out as 0.83. In order to have a good mesh, mesh quality should be greater than 0.3 (ICEM CFD Manual, 2011). After the complete meshing of the geometry now all the sides are classified according to their boundary conditions.

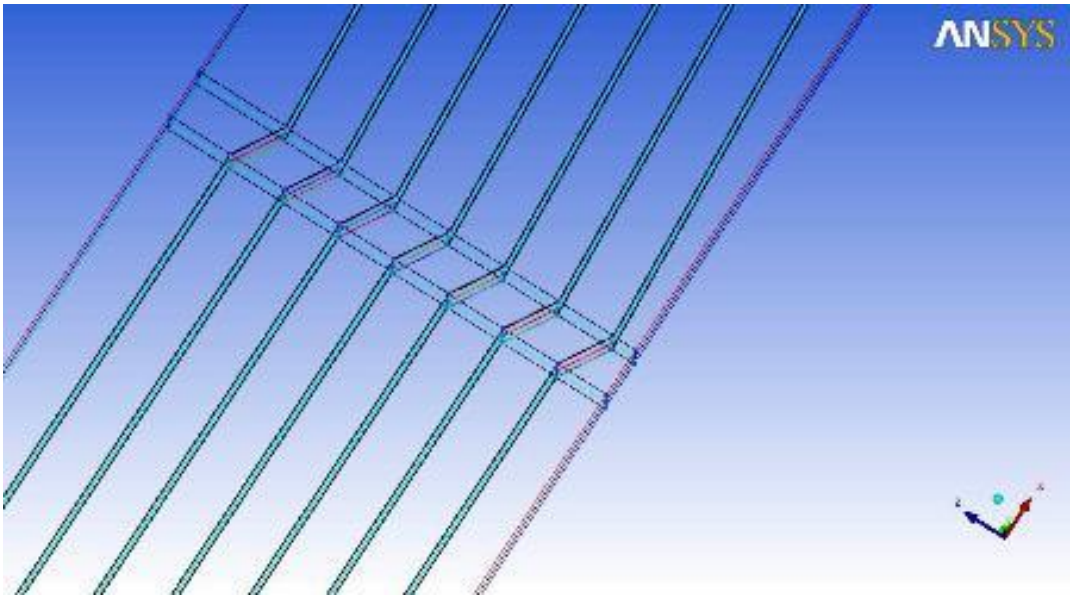

Fig. 5.2 Blocking of submerged vanes generated by ICEM-CFD

c) Assignment of boundary types to faces of geometry

After the meshing of volume, the faces of volume geometry are assigned boundary types according to the task. Inlet and outlet boundary conditions of the faces are decided according to the direction of flow. Rest of the faces except water level are assigned as simple walls, through which transverse flow is not possible and by default no-slip condition is assigned to walls.

Now in order to represent the water surface of flow "symmetry" boundary type is applied, which signifies that no flow go across the boundary and it is equivalent to the wall.

A default fluid is assigned to the fluid media flowing through the volume. Saving the file in form of ".cfx5" file, now geometry is exported to the ANSYS-CFX software for its analysis. In Fig. 5.3, a meshed model of vane is shown in which before the vane block region mesh is of uniform and was having size 8 mm. Size of vane changed logarithmically from coarse size (8 mm), starting outside of the block region of vane, to finer size into the block region. The finer mesh size into the block region of vane is important as it can resolve the flow in more proficient manner near the vane and hence, flow pattern around the vane could be visualized in more accurate manner.

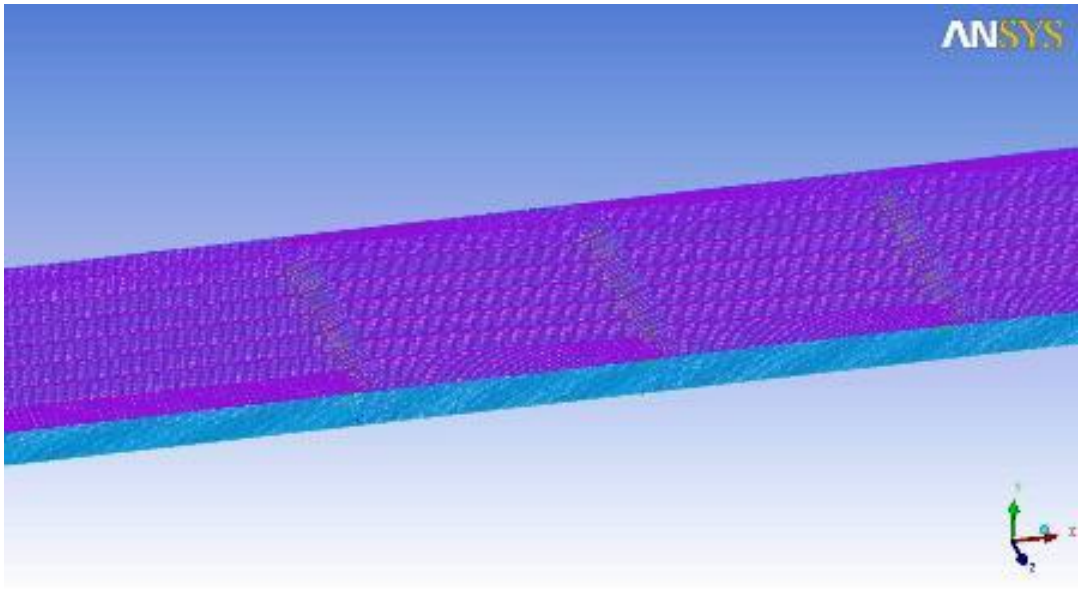

Fig. 5.3 Meshing of submerged vanes generated by ICEM-CFD

(i) Inlet boundary condition

In the inlet boundary conditions, a uniform flow boundary condition is assumed. It is also assumed that there is no transverse and vertical component of velocity, only longitudinal component of velocity exists. An average velocity of 0.41 m/s is given as initial velocity from inlet boundary. In the ANSYS-CFX, water is chosen as flowing media from inlet boundary. For the operating pressure conditions, the hydrostatic pressure distribution was chosen as one

of the input parameter. After assigning of inlet boundary condition, next outlet boundary conditions was to be assigned.

(ii) Outlet boundary condition

At the exit plane, all the variables are obtained by assuming zero streamwise diffusion or motion. Resulting velocity field is corrected to ensure that continuity of model is maintained. By ensuring the correction for the continuity, an ensured convergence was obtained and model produced robust and validated results.

(iii) Solid boundaries

Solid boundaries were entitled to "WALL" boundary conditions, which acclaims that there must be no across flow through it or normal gradient to the wall is always zero - this condition is known as "no-slip" condition. In boundary conditions assigned to solid boundaries, all were classified as smooth boundaries. Next step was to model the water surface.

(iv) Water surface

Water surface was modeled by assuming it to be a hard sloping lid across which there is no flow possible. In order to compute the velocity, it was assumed that water is flowing with the same inlet velocity along the water surface. Also in order to measure the water surface elevations and to check the uniformity of flow, water surface elevations were taken at three different sections. It was observed that flow was completely uniform and flow only varied at the maximum of 0.2 mm within the three sections, hence practically flow can be termed to a uniform flow.

5.4 FLOW PATTERN AROUND A SUBMERGED VANE

5.4.1 Validation of Model

CFD is an easy tool to compute and demonstrate how flow is behaving in complex situation without performing experimentation in reality. Since, at many a time the CFD tool generates and captures the flow pattern in efficient way but is not capable to regenerate the magnitude of flow field in accurate manner. Thus, it is essential to validate the developed model so as to investigate the flow pattern and various flow quantities which are difficult to measure

experimentally. In order to validate the present model, experimental study conducted by Wang and Odgaard (1993) was considered. Wang and Odgaard (1993) conducted experimentations for single vane and multiple vane arrays. Bed of the channel was fully covered with the sand of size 4 mm. Vane was cut from a metal sheet of the thickness 0.75 mm and the length of vane was 0.152 m and height was 0.076 m. Depth of flow maintained by Wang and Odgaard (1993) during this experimentation was 0.152 m and average velocity of flow was 0.24 m/s. In CFD model, since Wang and Odgaard (1993) did not mentioned the length of channel, hence, an arbitrary length of 10 m was assigned as length of model. After creating the model with dimensions described by Wang and Odgaard (1993) in their study, suitable boundary conditions were applied to each boundary of model. At the inlet of channel a uniform flow of velocity 0.24 m/s was introduced and flow velocity was computed at x = 8H and 20H, where H is the vane height. These were the longitudinal sections at which Wang and Odgaard (1993) experimentally measured the longitudinal velocity along the vertical. Results of simulation were compared with experimental results obtained by Wang and Odgaard (1993) and can be seen in Fig. 5.4 a & b.

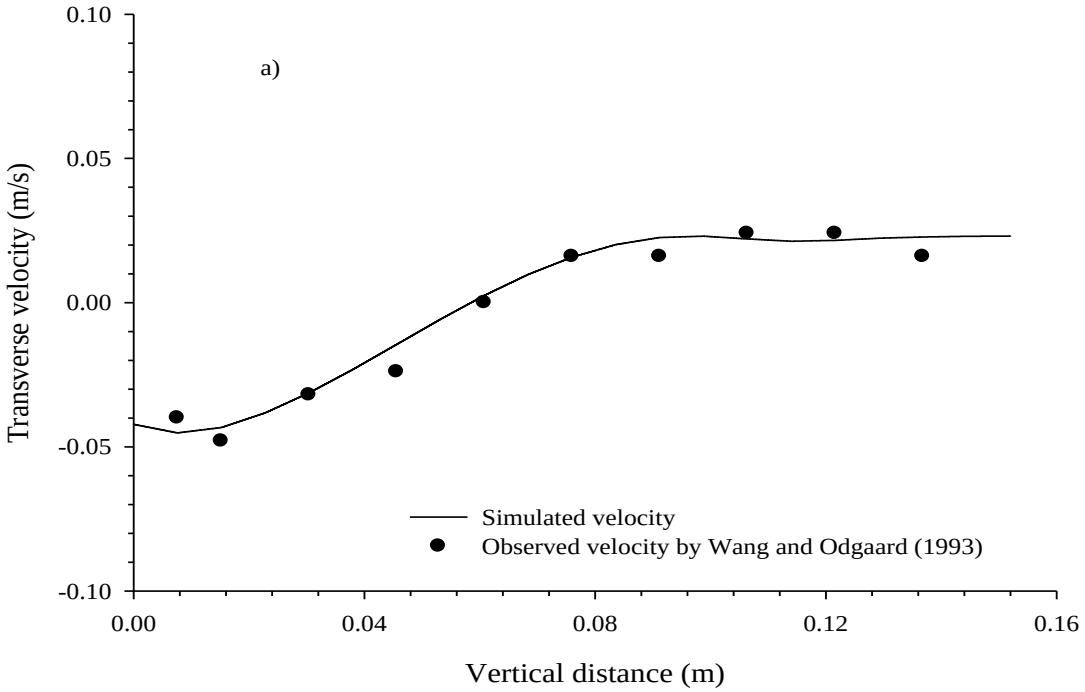

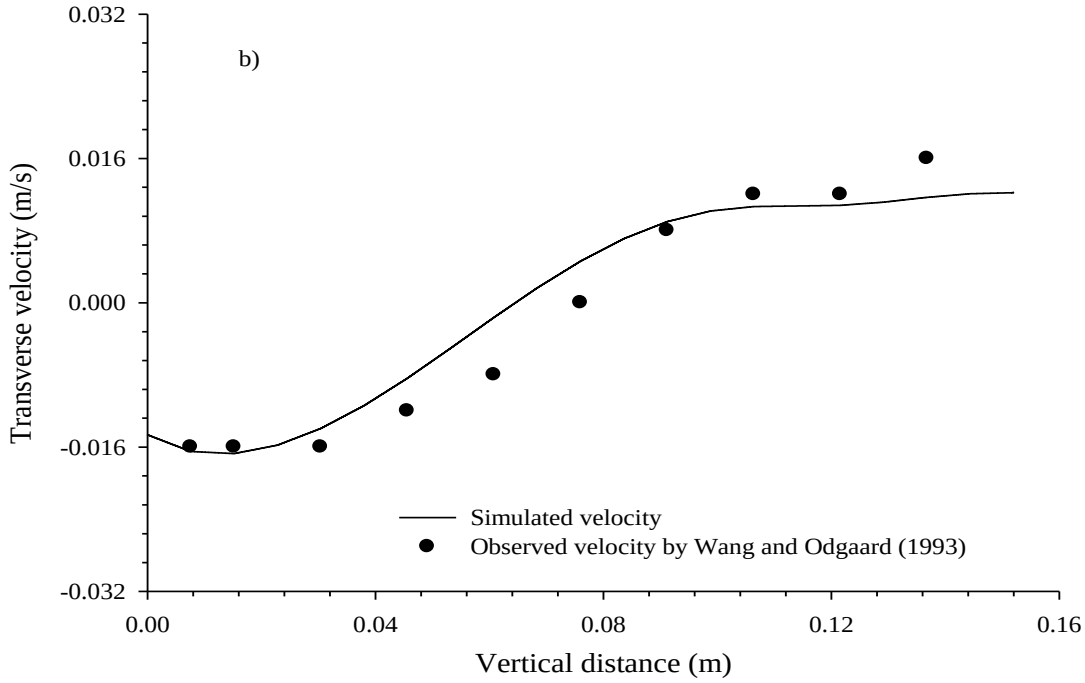

Fig. 5.4 Validation of single vane model for a) x = 8H and b) x = 20H

It can be clearly seen from Figs. 5.4 a & b that velocities simulated from CFD using standard *K*-ω model were very much in accordance with what it was measured by Wang and Odgaard (1993). Sometimes changing size of mesh may change the results. Thus, a grid dependency test was performed, which can be seen in Fig. 5.5. It can be observed from Fig. 5.5 that changing the size of mesh did not produced any comparative differences in the results. Thus, model can be said as a mesh independent model. Thus, model can be used to study the turbulence characteristics around submerged vanes so that submerged vane can be utilized to enhance the rate of transverse mixing for pollutant.

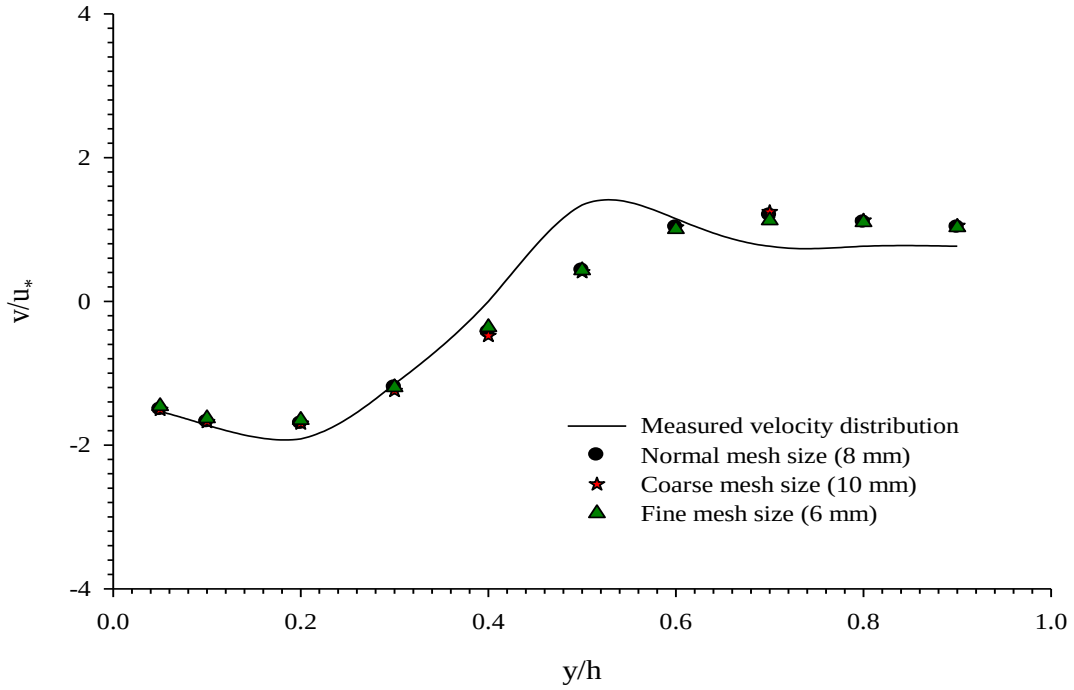

Fig 5.5 Grid dependency test

5.4.2 Optimization of vane parameters

a) Angle of attack

Angle of attack of submerged vane is an important parameter in generation of circulations in flow. Odgaard and his associates (Odgaard and Kennedy, 1983; Odgaard and Spoljaric, 1986; Odgaard and Mosconi, 1987; Odgaard and Wang, 1991 a, etc.) suggested that the angle of attack of vane should be between 15^o-30^o for maximum generation of circulations. Marelius and Sinha (1998) showed that in order to generate optimum strength of vortical currents from the submerged vane, the angle of attack must be 40^o. While, Johnson et al. (2001) during their experimentations with rock vanes as controller of vertical wall abutment scour, observed that vane angle of 30^o serves as optimum angle which can reduce the scouring in effective manner. Voisin and Townsend (2002) observed that by keeping angle of attack of 2^o with respect to flow optimum secondary currents may be generated to counteract bend generated currents. Tan et al. (2005) also suggested that by putting angle of attack as 30^o the maximum diversion of sediment was obtained. Bhuyian et al. (2010) also suggested angle of attack to be 30^o for maximum secondary current generation. Gupta et al. (2010) also proposed angle of submerged

vane to be 40^o with collar so that scour around pier can be reduced. In the present study flow simulation was carried out for different flow conditions, various sizes and angle of attack of the vanes. Vorticity at a distance of two times vane height was computed. As an illustration for vane having height = 0.06 m and length = 0.12 m, for depth of flow = 0.1241 m with four angles of attack, *i.e.* 15^o, 30^o, 45^o and 60^o is shown in Fig. 5.6. It was observed that for 28.7^o maximum value of vorticity was obtained and was in accordance with the various previous investigations. Thus, it can be suggested that for an angle of attack of 28.7^o, optimal strength of vorticity is generated and can be utilized for various purposes having its effect in far reaches in downstream.

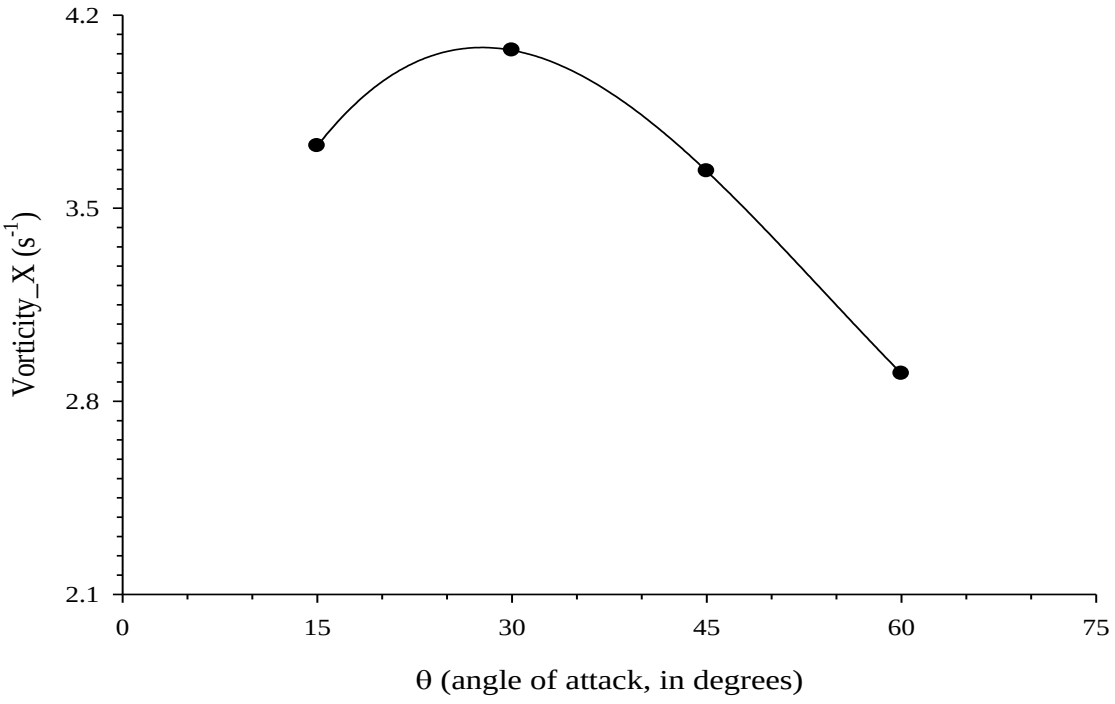

Fig. 5.6 Variation of vorticity with angle of attack (Vorticity_X stands for vorticity in x-direction).

b) Height of the vane

Vane height is again an important parameter which is associated with the generation of vortices. Odgaard and Kennedy (1983), Odgaard and Spoljaric (1986) and Odgaard and Mosconi (1987) suggested to keep the height of vane in between 0.2-0.5 times the depth of flow. Odgaard and Wang (1991 a) also suggested height of vane to be between 0.2-0.4 times of

flow depth in order to generate optimum secondary currents. Voisin and Townsend (2002) proposed that for vane height 0.35 times depth of flow, vane generates sufficiently strong currents to preserve the bend walls. Tan et al. (2005) observed that when vane height was 1/8th-1/3rd of depth of flow, flow deviates maximum sediment towards bank. Flokstra (2006) suggested that vane height should be less than 0.4 times depth of flow. Ouyang (2009) suggested that when vane height is 0.58-0.70 times water depth, it generates efficient vortical flow. Variation of vorticity with vane height as shown in Fig. 5.7 as an illustration for vane of size 0.06 m high, 0.12 m long for depth of flow 0.1241 m, three vane heights 0.18h, 0.4h and 0.64h (Here, h = depth of flow). It was observed that for vane height equal to 0.4 times depth of the flow, the maximum vorticity generates, which is with the accordance of the previous studies conducted and was very much near to the optimum height proposed by Voisin and Townsend (2002).

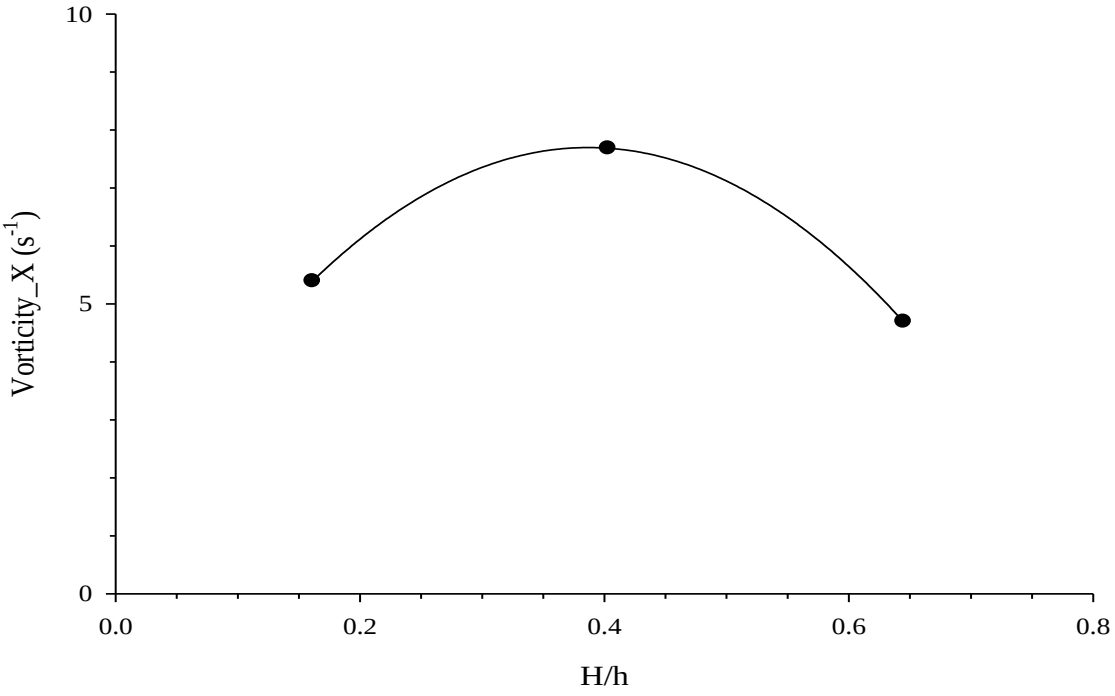

Fig.5.7 Variation of vorticity with vane height.

c) Length of vane

Length of a vane is associated with the amount of drag and lift produced around the hydro-foil, more will be the length more will be the contact-drag which in turn will give rise to more lift.

For a constant free stream velocity and density of fluid, that's the condition which prevails here, in accordance with the Kutta-Juokowskii theorem, lift generated is proportional to the strength of circulation generated by airfoil/ hydrofoil and vice-versa (Bertin and Smith, 1979). Odgaard and Spoljaric (1986) observed that keeping length of vane from 2.5 to 3 times vane height will generate optimum amount of circulation to counteract process of bed erosion. Voisin and Townsend (2002) proposed that optimum length for the vane should be 0.33 times the width of channel. Flokstra (2006) in his study observed that model of his works well if length of submerged vane varies from 4-8 times vane height. Ouyang et al. (2008) in their study observed that by changing height or length of submerged vane no effective change in bed profile was met. Ouyang (2009) observed that increase in length will decrease the efficiency of vane and hence proposed length of vane to be 0.5 times depth of flow. It can be observed that a very little study has been conducted on the length of submerged vane. Variation of vorticity with vane length can be seen in Fig. 5.8. Three vane length H, 2H and 5H (Here, H = 0.06 m) were utilized for the optimization of length. It can be seen from Fig. 5.8., that the length of vane is proportional to the vorticity.

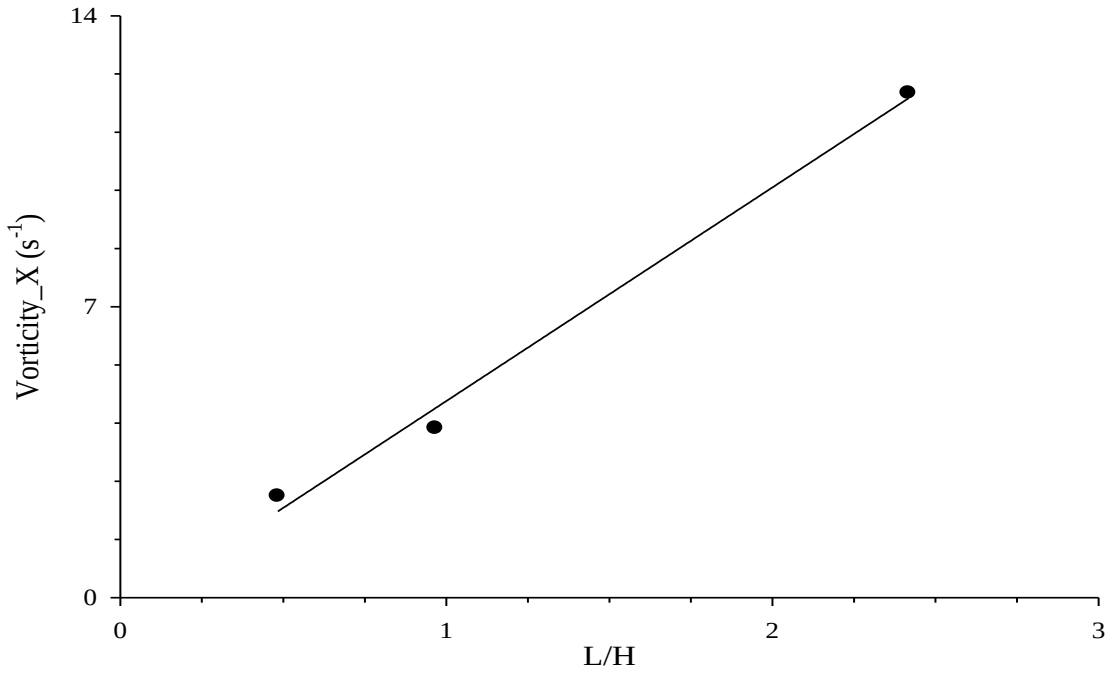

Fig. 5.8 Variation of vorticity with vane length.

For large length, more area was available for fluid to have more drag around the vane. More drag around vane gave rise to more lift and stronger vortices will be generated from vortex bounding the vane and hence an increase in vorticity was observed which was in accordance with Kutta-Juokowskii theorem (Bertin and Smith, 1979).

5.4.3 Flow Pattern around a Submerged Vane

As discussed, CFD can be utilized in order to investigate the flow pattern around submerged vanes, thus, an investigation of flow pattern around vane was done. In this study a brief investigation was carried out to study the behavior of vorticity, turbulent kinetic energy and turbulent dissipation rate at the sections x = 3H, 8H and 20H downstream of a submerged vane. Thus, from investigations, the following conclusions can be drawn to evaluate the single vane's performance in mixing of the pollutant.

a) Vorticity downstream of a vane

Submerged vanes are best known to generate high amount of vorticity downstream of it as referred by various investigators like Odgaard and Wang (1991), Wang and Odgaard (1993), Marelius and Sinha (1998), Sinha and Marelius (2000). The vorticity generated by vanes have been used by investigators to stop bank erosion, deepening channel, diverting sediment, etc. Fig 5.9, is an illustrious representation of flow pattern downstream of a submerged vane having size 0.06 m high, 0.12 m long for depth of flow 0.1241 m. It can be observed from Fig. 5.9, two counter-rotating vortices were formed in the low pressure side. The reason behind existence of two counter-rotating vortices is dismantling of a large vortical structure due to the suction existing at low pressure side in two counter-rotating vortices. Similar observations were mentioned by Sinha and Marelius (1998) and Tan et al. (2005). A plunging flow was observed being spill over the vane to generate more turbulence which was in accordance with observations of Tan et al. (2005).

Fig. 5.10, shows the enlarged view of the flow pattern around submerged vane and two-counter-rotating vortices in suction side of submerged vane. A vortex sheet is generated by the vane in downstream which is clearly seen from Fig. 5.9 and 5.10, having its rotation in transverse direction. These rotations can be very much helpful in order to induce high amount

of transverse mixing of pollutants as it is noted in literature that secondary currents do affect the intensity of mixing by enhancing the transverse dispersion rate (Lau and Krishnappan,

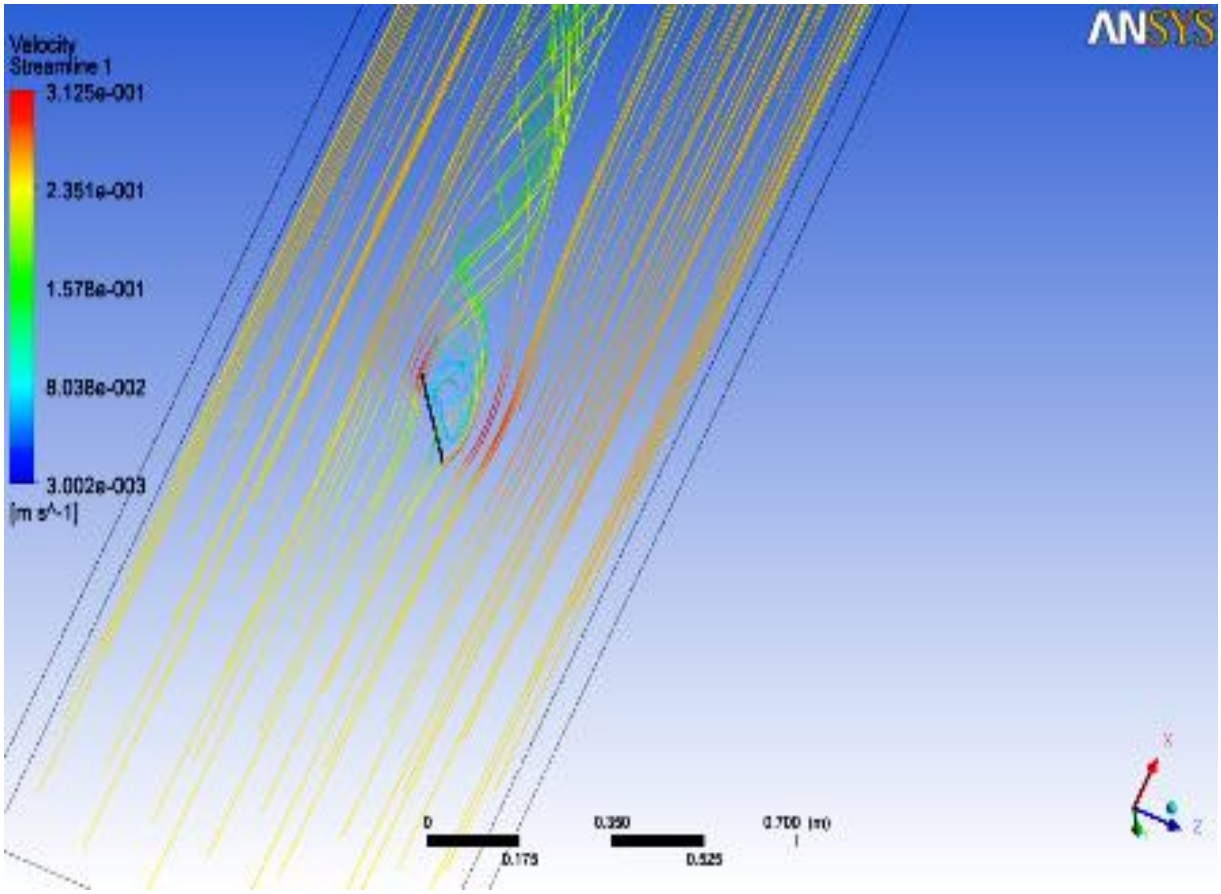

Fig.5.9 Flow pattern downstream of a vane.

1979; Bruno et al., 1990; Boxall and Guymer, 2003; Boxall et al., 2003). In contradiction to the assumption of Odgaard and Wang (1991a) and Wang and Odgaard (1993) who suggested that vortices generated by submerged vane are potential or Rankine or tip vortices, the vortices generated by the vane were rather horse-shoe vortices, which were observed by Sinha and Marelius (1998) and Tan et al. (2005) in their respective studies.

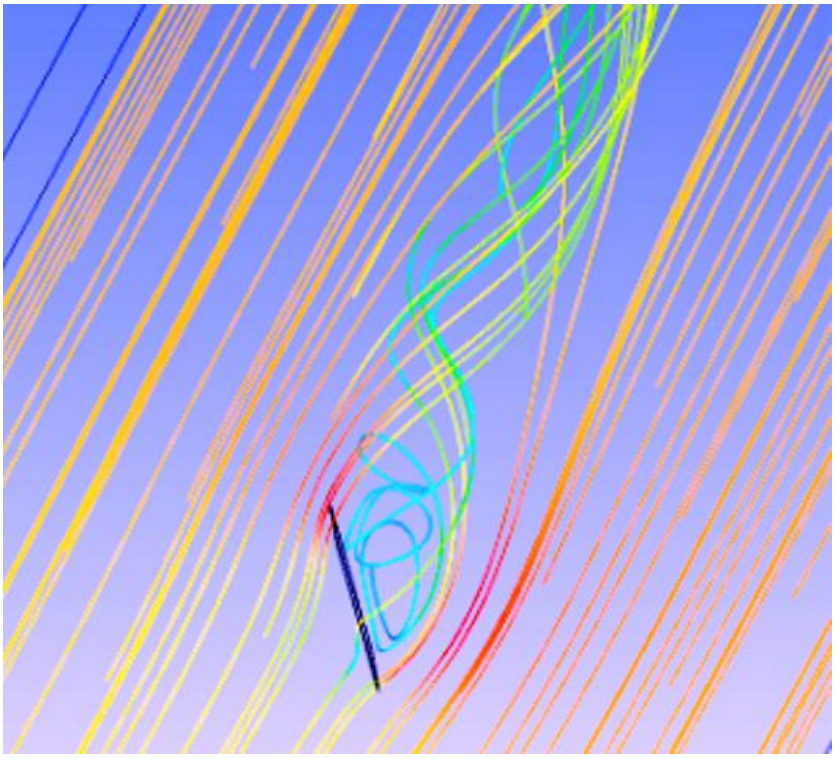

Fig.5.10 Enlarged view of flow pattern downstream of a submerged vane.

Fig. 5.11, shows the variation of the vorticity downstream of submerged vane, illustration is shown for vane having size 0.06 m high, 0.12 m long for depth of flow 0.1241 m. It can be seen in Fig. 5.11 that vorticity rises to maximum at the trailing edge, which is situated at 1.12 m from the inlet. Odgaard and Wang (1991 a) and Wang and Odgaard (1993) reported in their respective study that trailing edge was solely responsible for generation of vortices at the downstream of the vane, present results agrees with their observation. After attaining a maxima vorticity decreased in the further downstream under the action of viscosity. Marelius and Sinha (1998) by using moment of momentum or angular momentum as an indicator of vorticity observed similar pattern.

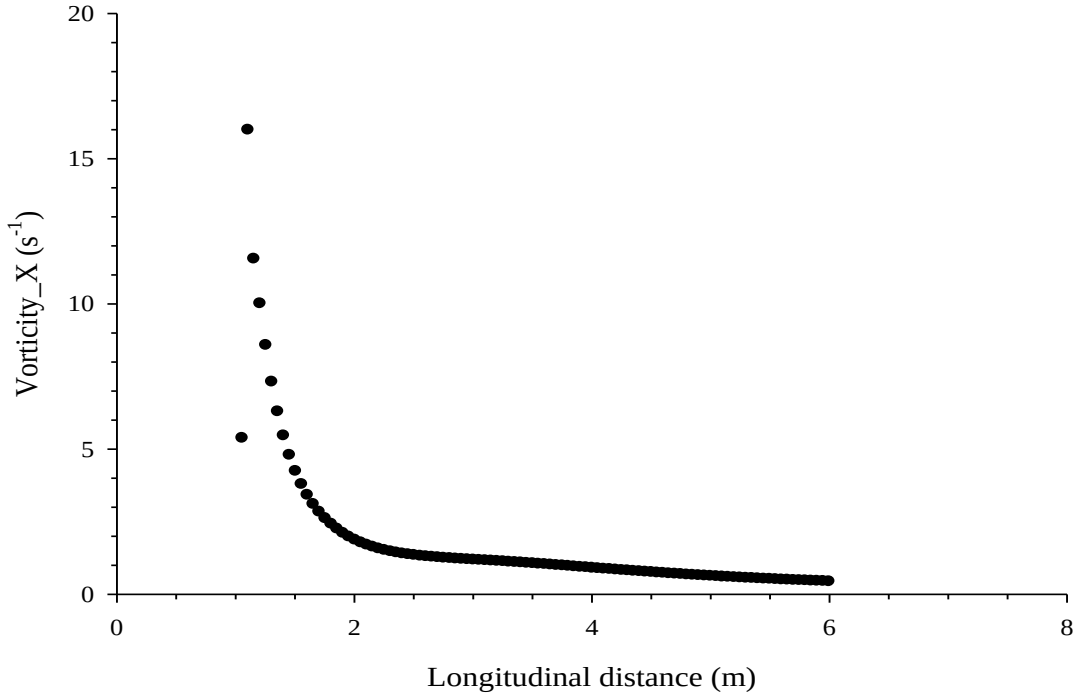

Fig.5.11 Spatial variation of vorticity downstream of a vane.

b) Turbulent kinetic energy

Turbulent kinetic energy is basically a measure of amount of turbulence generated in flow. Since, submerged vane is acting as an obstruction to the flow, hence, will generate large amount of turbulent kinetic energy. Fig. 5.12, illustrates the variation of turbulent kinetic energy for vane having size 0.06 m high, 0.12 m long for depth of flow 0.1241 m. It can be observed from Fig.5.12, that at upstream of the submerged vane, turbulence was zero and as the leading edge was approached by the flow a sudden leap in the turbulent kinetic energy was observed. On close inspection of Fig. 5.12, it can be deduced that although leading edge was responsible for leap in the turbulent kinetic energy but maxima of this variation was observed to reach at trailing edge which again reinstates the fact that flow turbulence downstream of vane is rather affected by trailing edge than the leading edge. Similar observation was observed by Sinha and Marelius (1998) in their experimental study. As the flow, recedes away further downstream from trailing edge there is exponential drop in the turbulent kinetic energy due to the action of viscosity. Fig.5.12 also suggests that with respect to the upstream value of

turbulent kinetic energy, level of downstream kinetic energy is high of the order of 0.0003 m^2/s^2.

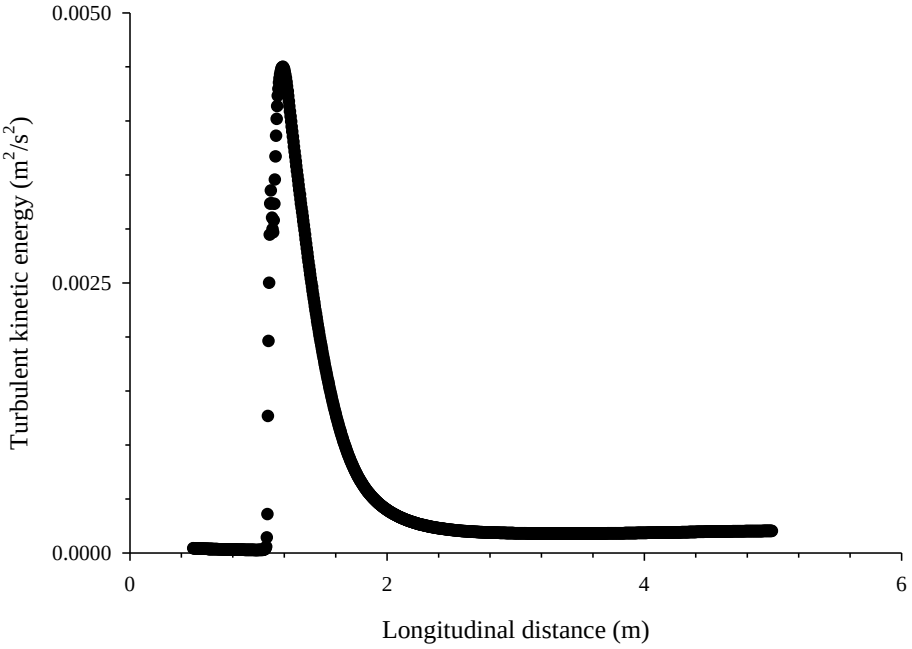

Fig.5.12 Spatial variation of turbulent kinetic energy with single vane

5.5 FLOW PATTERN AROUND MULTIPLE ROWS OF SUBMERGED VANES

5.5.1 Validation of the model

a) Validation of the model with measured longitudinal velocity

After creation of meshed volume, simple volume geometry of channel without vane was created and meshed. The meshed geometry was then validated to check whether given model follows the law of continuity or not. For validation a flow with velocity of 0.35 m/s was passed through the inlet section of the model. Fig. 5.13 a & b illustrates variation of velocity in vertical direction for four vane rows in which each vane having size 0.06 m high, 0.12 m long for depth of flow 0.1241 m. Velocity profiles at three different sections were compared with the measured profiles and it was found that it matches with the measured velocity profile as shown in Figs. 5.13 a & b.

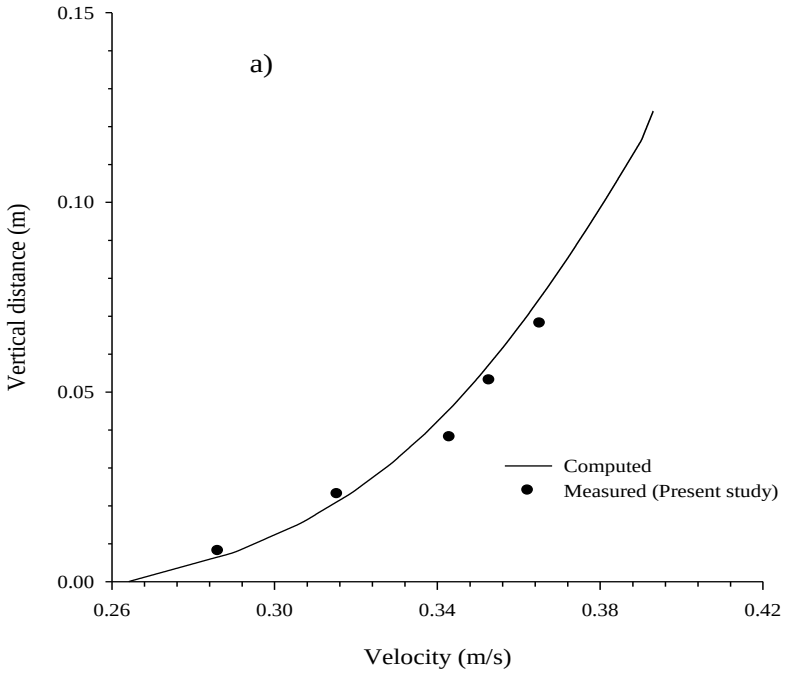

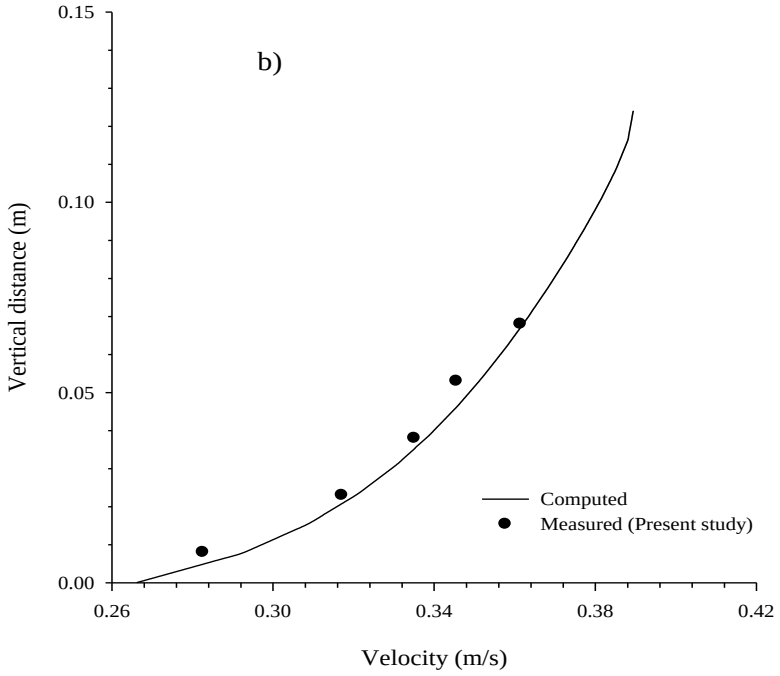

Fig.5.13 Validation of continuity of model for a) x = 3H and b) x = 20H where, H = vane height.

b) Validation of model with transverse velocity

In order to validate the model that whether the flow pattern was in similarity with what it was discussed in literature, analysis was performed by comparing the observations from experimentations with the simulated velocity profile. A channel volume was created of dimension 19 m long, 1 m wide and 0.1241 m deep. Submerged vanes utilized were having dimensions as 0.12 m long, 0.06 m high and 0.002 m thick and were aligned with the direction of flow with angle of attack of 30^o. Vane arrays were having a lateral spacing of 0.125 m. Flow simulation were done for different vane configurations but in Fig. 5.14. a & b transverse velocity profile of four and three vane rows were used to validate the model at a longitudinal distance of x = 3H in both the simulations. In order to validate the model a plot was plotted in which transverse velocity simulated from model was compared with the observations of present experimentations. It can be seen from Figs. 5.14 a & b that simulated velocity profile is comparable to the observed data to some scattering of data also present in it which may be due to non-accounting the vortices generated by leading edge, it only accounted the vortices separated from trailing edge.

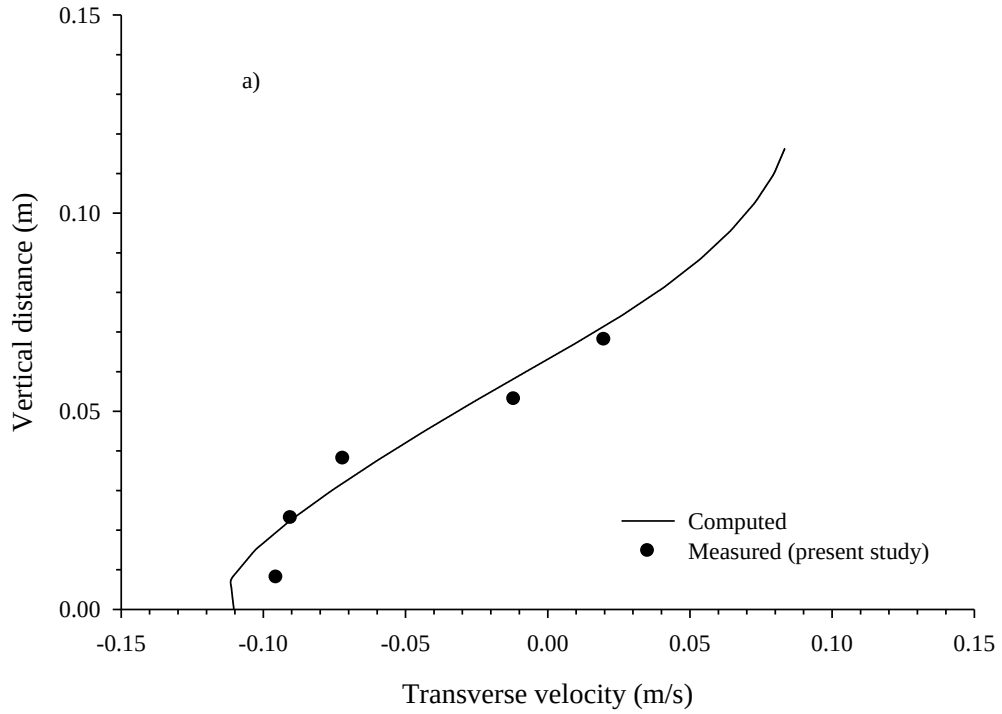

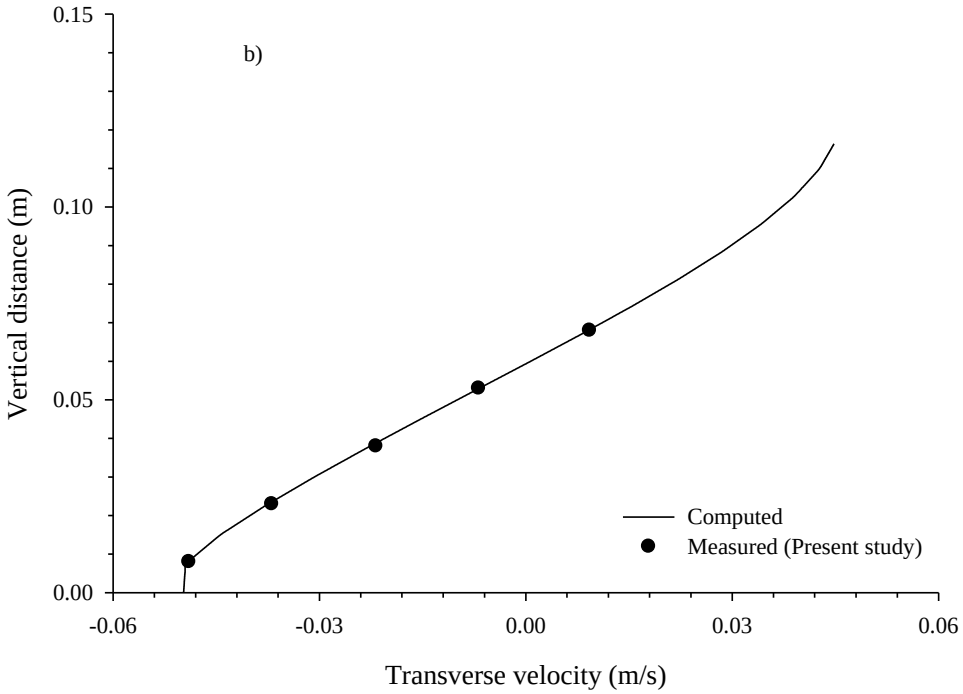

Fig. 5.14 Validation of model with transverse velocity a) three vane rows; b) four vane rows.

5.5.2 Optimization of vane parameters in multiple vanes array system

a) Lateral spacing of the vane array

Lateral spacing of the vanes in an array is an essential component in generating a coherent structure downstream of the vanes. According to Odgaard and Wang (1991 a), each submerged vane acts as an individual vortex generator and generates a sheet of vortices in downstream. According to Odgaard and Wang (1991 a) , if the vanes are placed very near to each other, each vortices will interact with each other and would reduce the effective circulation and effectiveness of vane will reduced. If the vane are spaced very far, each vane will generate individual vortices which will be dissipated very easily and again vanes will be ineffective, that is what Odgaard and Wang (1991 a) observed. Thus, they optimized the spacing between vanes as 2-3 times vane height in which vanes will interact effectively and will generate a coherent structure downstream of array, which in turn will help vane to work effectively. Wang and Odgaard (1993) supported the observation of Odgaard and Wang (1991 a) and justified that in the presence of down-wash component over vane, the effectiveness of vane will be less if they

are very closely placed. The vanes will not be able to interact to generate a coherent structure, if vanes are placed far in transverse direction. Hence, Wang and Odgaard (1993) also suggested that 2-3 times vane height is an optimum spacing in order vane generates an optimized circulation in downstream. Voisin and Townsend (2002) proposed that optimum transverse spacing between two vanes is 0.24 times the channel width. Flosktra (2006) agreed with the observation of Odgaard and Wang (1991 a) that presence of vane in the neighborhood interferes with the generated circulation and hence strongly objected the keeping of second vane near to another.

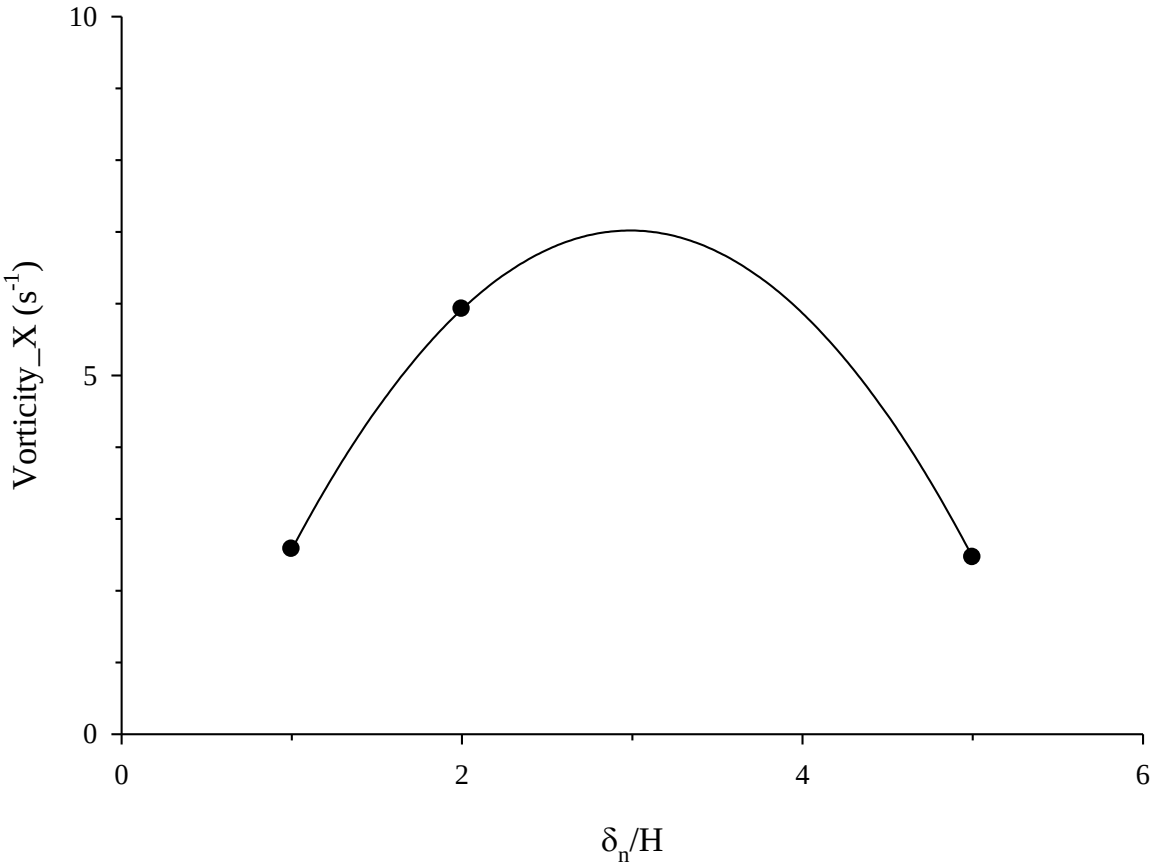

Fig. 5.15 Variation of vorticity with transverse spacing between vanes

Fig. 5.15 shows the variation of vorticity with the transverse spacing between vanes for single vane rows in which each vane having size 0.06 m high, 0.12 m long for depth of flow 0.1241 m. It can be seen from the Fig. 5.14 that vorticity was maximum for δ_n = 3H, which matches with the observation of Odgaard and Wang (1991 a). Hence, it is suggested that by keeping vanes at a distance of 3 times vane height an optimum strength of circulation can be obtained.

b) Longitudinal spacing of the vane arrays

In the literature, in the multiple vane arrays arrangement much emphasis was given to the lateral spacing of vanes, a few studies have been conducted to show the effect of longitudinal spacing. Odgaard and Wang (1991 a) observed that by changing longitudinal spacing of vane arrays from 15H to 30H, the induced bed level change from submerged vanes was reduced up to 20%. Voisin and Townsend (2002) proposed that by putting vanes at a distance of 0.7 times bed width of the channel, vanes will interact effectively. Allahyonesi et al. (2008) proposed that keeping vane arrays at a distance of 4H an effective diversion of sediment in the away direction from intake was obtained. Thus, it can be seen that there is no mutual agreement between investigators that on what distance vane arrays should be placed so that an effective circulation can be obtained. In the present study, flow simulation has been carried out to optimize longitudinal vane spacing.

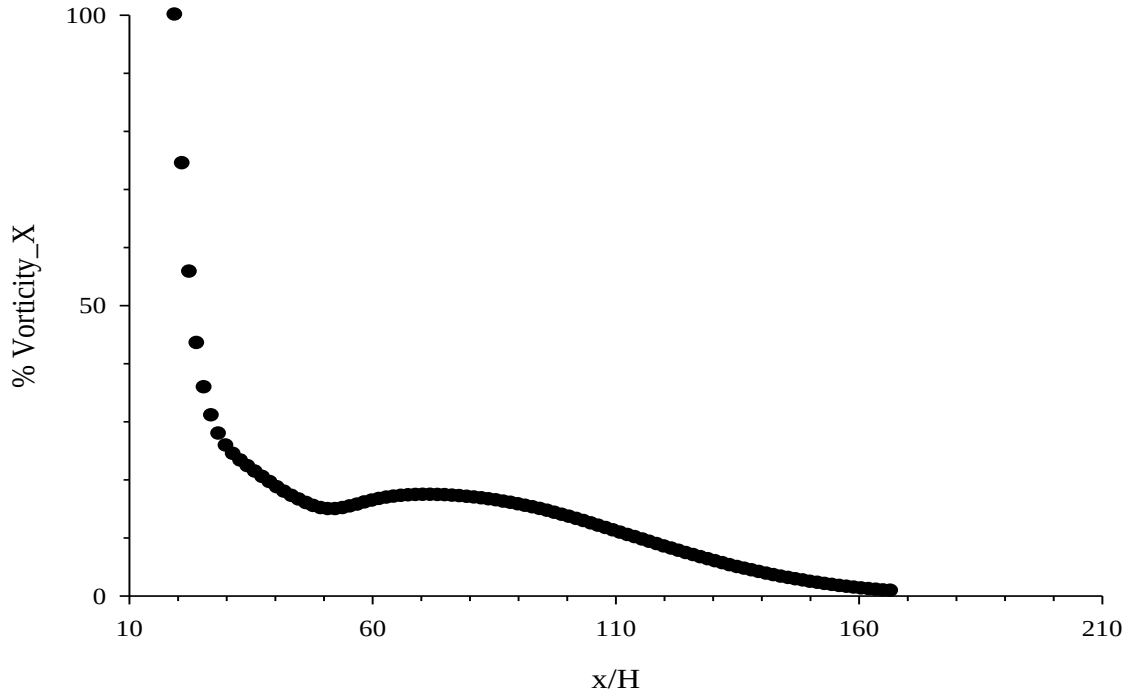

Fig. 5.16 Variation of percentage vorticity with longitudinal distance.

A non-dimensionalized vorticity is plotted with the non-dimensionalized longitudinal spacing (Fig. 5.16). Here, vorticity is non-dimensionalized with respect to peak value and "x" is non-dimensionalized distance with respect to the vane height. Now for instance if somebody has to

obtain vorticity at some distance where the vorticity will be the 50% of the original vorticity. Hence, for this from the ordinate read the % vorticity and corresponding to this, from abscissa, read corresponding value of x/H. Thus, knowing the value of H (Height of vane), an optimum value of x can be obtained from Fig. 5.16 where next row of vane can be installed to generate vorticity having 50% strength than the vorticity generated by first row of vane.

5.5.3 Flow pattern around multiple vane array system

In case of multiple vane array system, it was observed that near to the submerged vanes a large vortical field exists as can be seen in the Fig. 5.17 a, b & c. Fig. 5.17 a, b & c illustrates flow downstream of multiple vane arrays and each vane having size 0.06 m high, 0.12 m long for depth of flow 0.1241 m was arranged in four vane arrays. Near to the vane arrays at x = 3H, due to proximity to the vane arrays, the intensity of vortices were higher and each submerged vane generated its individual vortex as can be seen in Fig. 5.17 a. After moving further downstream, as is shown in Fig. 5.17 b, all the vortices which were generated at individual level at x = 3H, now coalesce with each other to form a larger vortical field having lower vorticity than what it was measured at x = 3H. From Fig. 5.17 c, one can clearly deduce that, that at x = 20H, now all the vortices have merged into each other to form a vortical field having a single larger vortex but magnitude of the vortex reduced by 5 times from the value of vorticity it was having at x = 3H. The reason behind gradual decrease of the intensity of vortices is the action of viscosity on the flow turbulence. At x = 3H, the section is near to the vane rows where production of turbulence is much larger than the viscous effects, thus, each vane is able to generate its own vortex as shown in Fig. 5.17 a. As the vortices travels downstream, viscosity starts overcoming them and in order to maintain their realm, each of the vortices start converging in each other to sustain turbulence in flow as can be seen in Fig. 5.17 b. When viscosity overcomes the most of the vortical field, the intensity of vortex then start decreasing until it is finished completely by flow viscosity as the Fig. 5.17 c suggests.

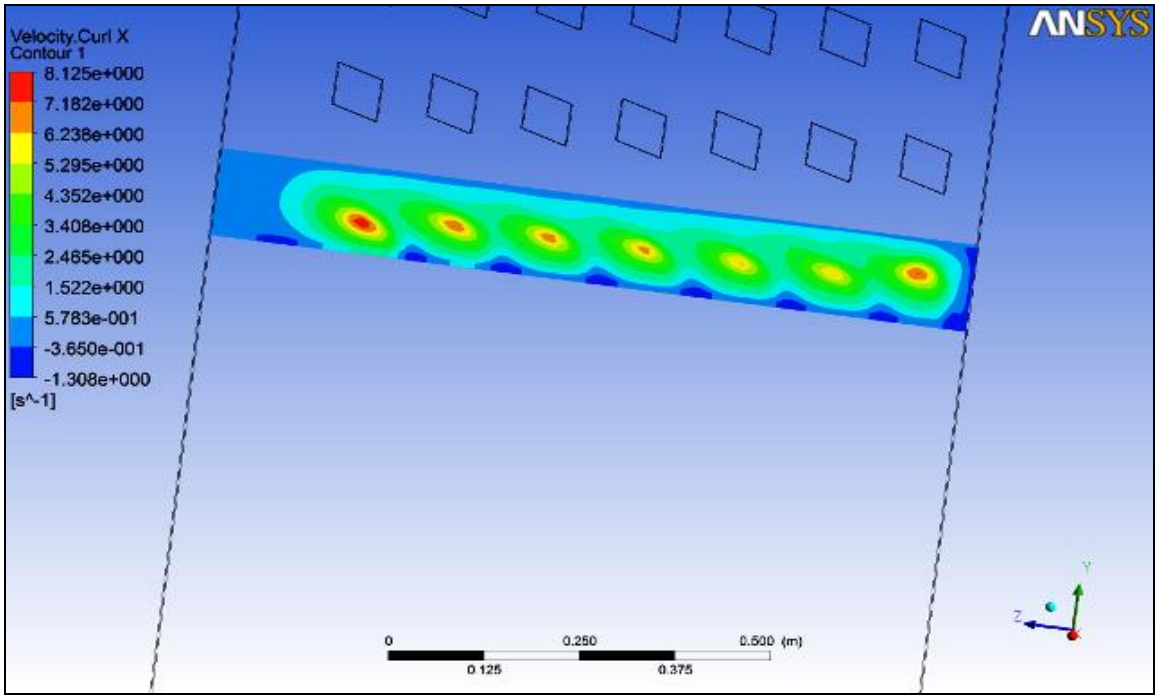

Fig. 5.17 a Variation of vorticity along the longitudinal distance for x = 3H

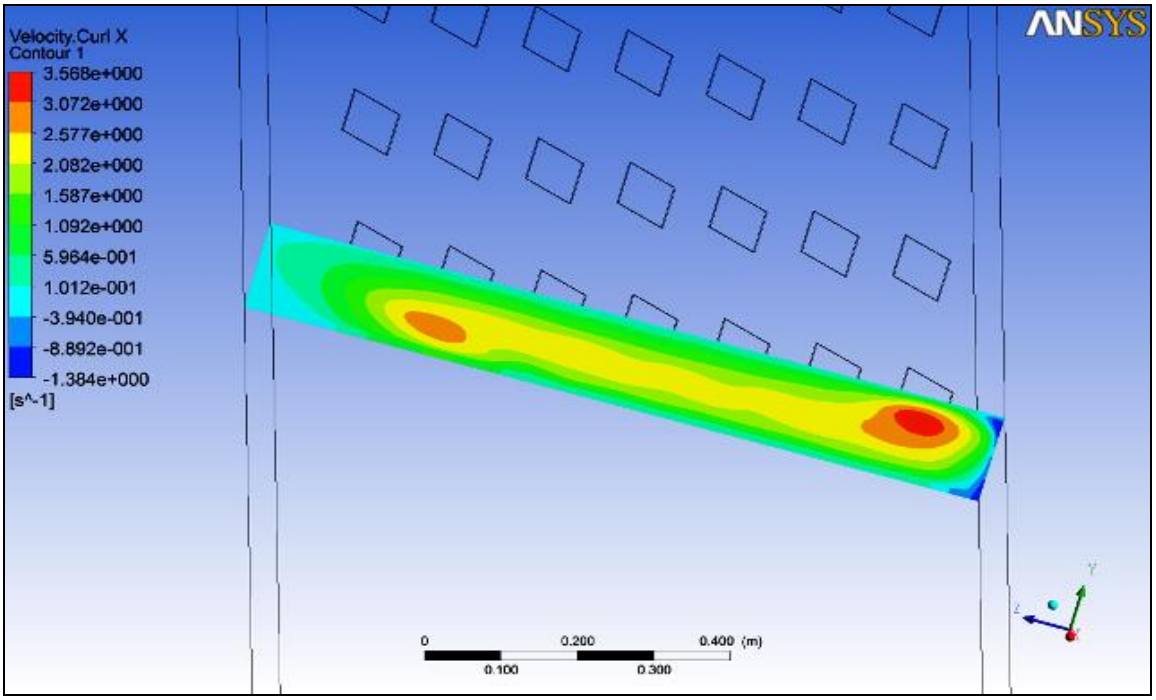

Fig. 5.17 b Variation of vorticity along the longitudinal distance for x = 8H.

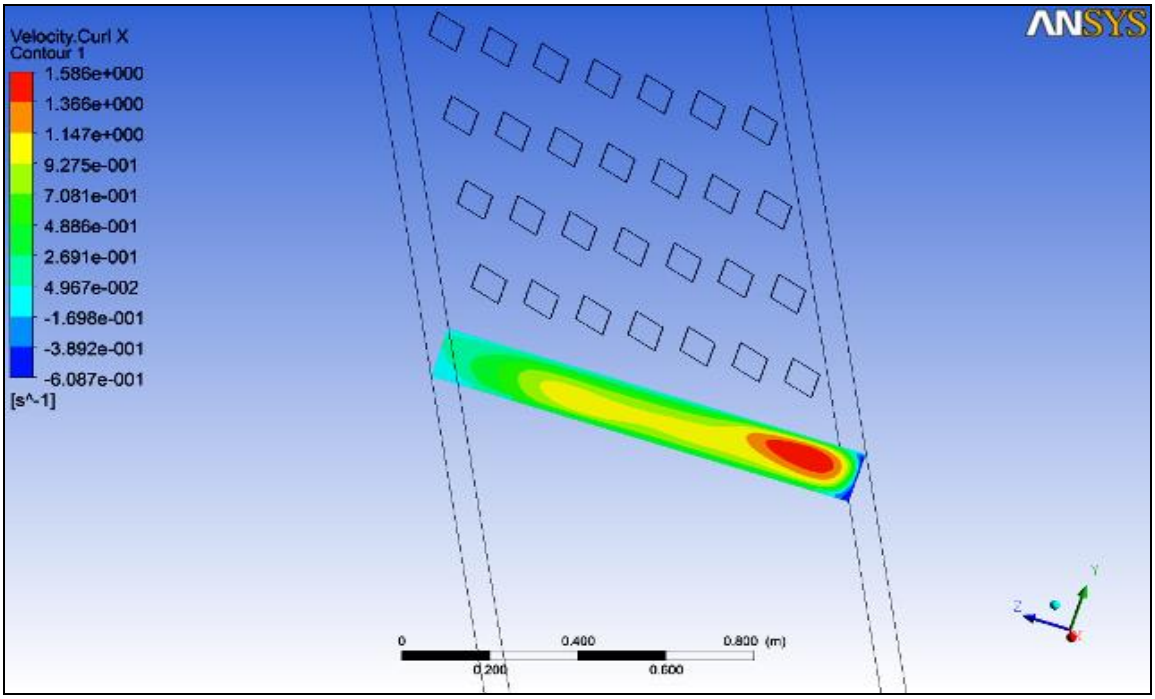

Fig. 5.17 c Variation of vorticity along the longitudinal distance for x = 20H.

5.6 TURBULENCE CHARACTERISICS OF FLOW DOWNSTREAM OF VANE ARRAYS

Turbulence characteristics of flow downstream of vane arrays were calculated using the measured instantaneous velocity at three lateral distances i.e., y = 0.45 m, 0.5 m, and 0.55m; three longitudinal distance x = 3H, 8H and 20H for no vane, one, two, three and four arrays of vanes.

In the present experimentation, submerged vane of height 0.06 m and of length 0.12 m was used. Depth of flow used in the experimentations was 0.1241 m. Lateral distance between each vane in a row was 0.125 m and initially four rows were placed longitudinally at an interval of 1m. Each of the vane was placed at 30^{o} with respect to the direction of flow.

The variation of turbulence parameter u', v', w', u'w', total kinetic energy TKE, and average velocity along vertical are shown in Figs. 5.18 to 5.20 for no vane and Figs. 5.21 to 5.23 for four arrays of vanes as illustration. In Figs. 5.18 a) to 5.23 a) show the variation of longitudinal turbulent intensity (u′) on the three verticals situated at transverse distances *viz.* y = 0.45 m, 0.5 m and 0.55 m and for the three longitudinal section *viz.* x = 3H, 8H and 20H, for no vane and 4 vane rows condition. For no vane condition, it was observed that for all the three verticals at all

three longitudinal sections, the longitudinal turbulent intensity nearly superimpose each other as shown in Figs 5.18 a) to 5.20 a). This superimposition of longitudinal turbulent intensity variation concludes that turbulence in the flow is homogeneous (Nezu and Nakagawa, 1993). The longitudinal turbulent intensity was observed to decrease with the increase in depth of flow, when measured from the bed of the channel which was in accordance with the observation of many investigators like Blinco and Partheniades (1970), Nezu and Rodi (1986), Nezu and Nakagawa (1993), etc. As can be seen from the Figs. 5.21 a) to 5.23 a), for the case of four vane rows the most attenuated longitudinal turbulent intensity profile was observed at x = 3H in all the three verticals. Going away from the submerged vane rows, the disturbance in the longitudinal turbulent intensity profile starts diminishing as the viscosity dissipates the separated vortices to make the variation of longitudinal turbulent intensity more uniform. At, x = 20H, it was observed that turbulent intensity profiles at all three verticals became nearly constant and were nearly superimposing each other indicating the homogenization of flow turbulence.

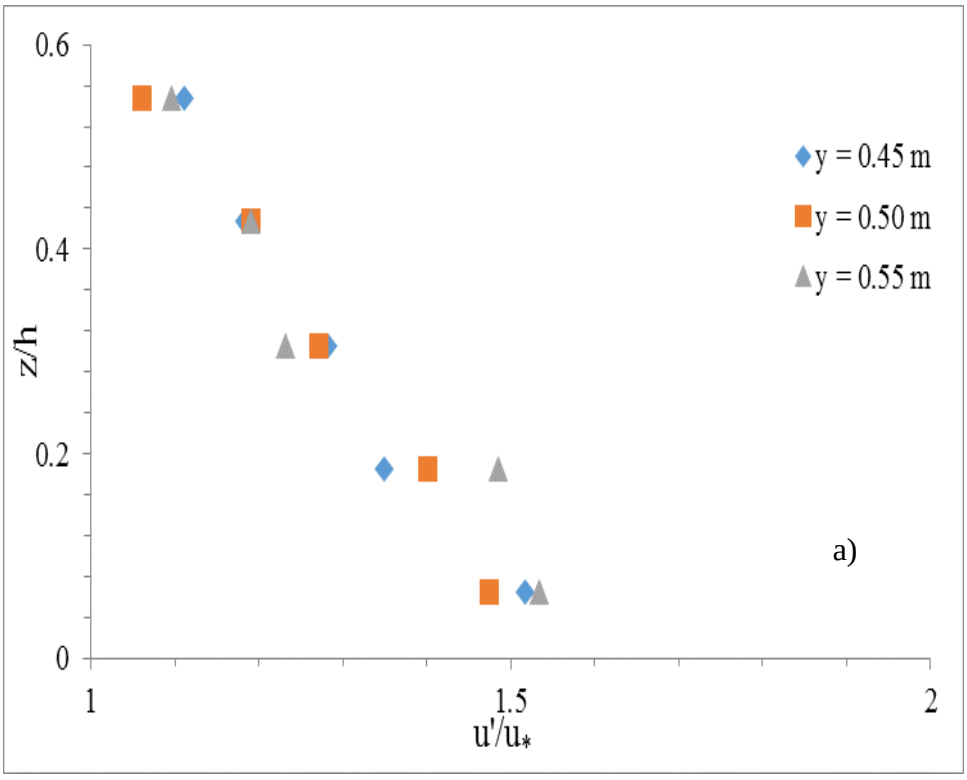

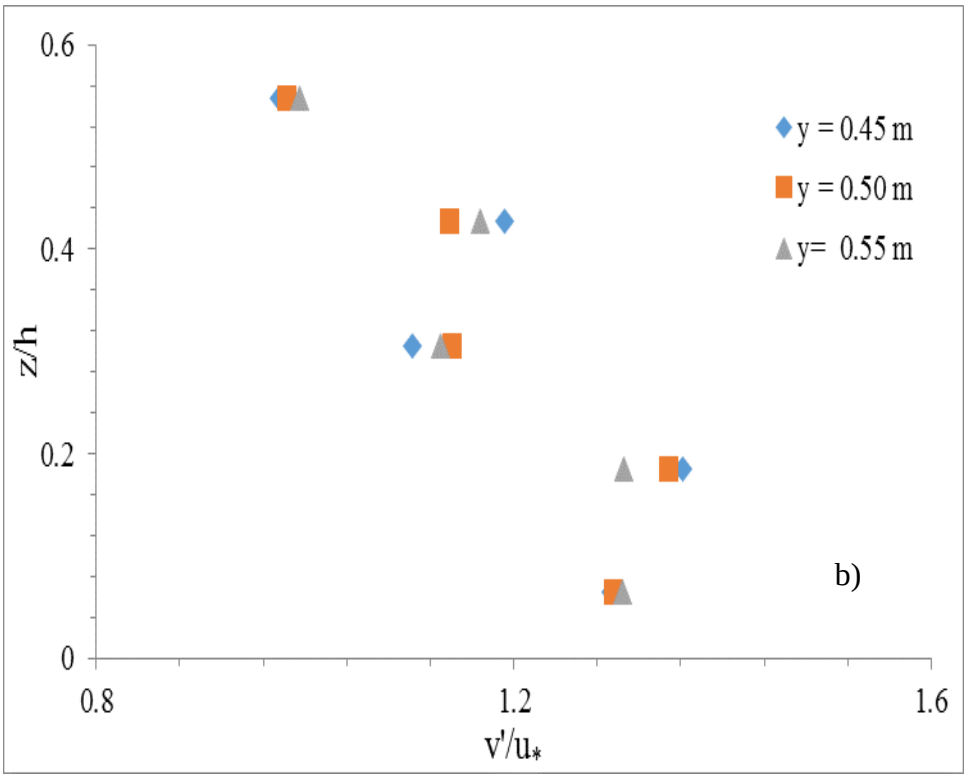

Fig. 5.18 a-b Variation of various turbulence quantities at x = 3H for no vane.

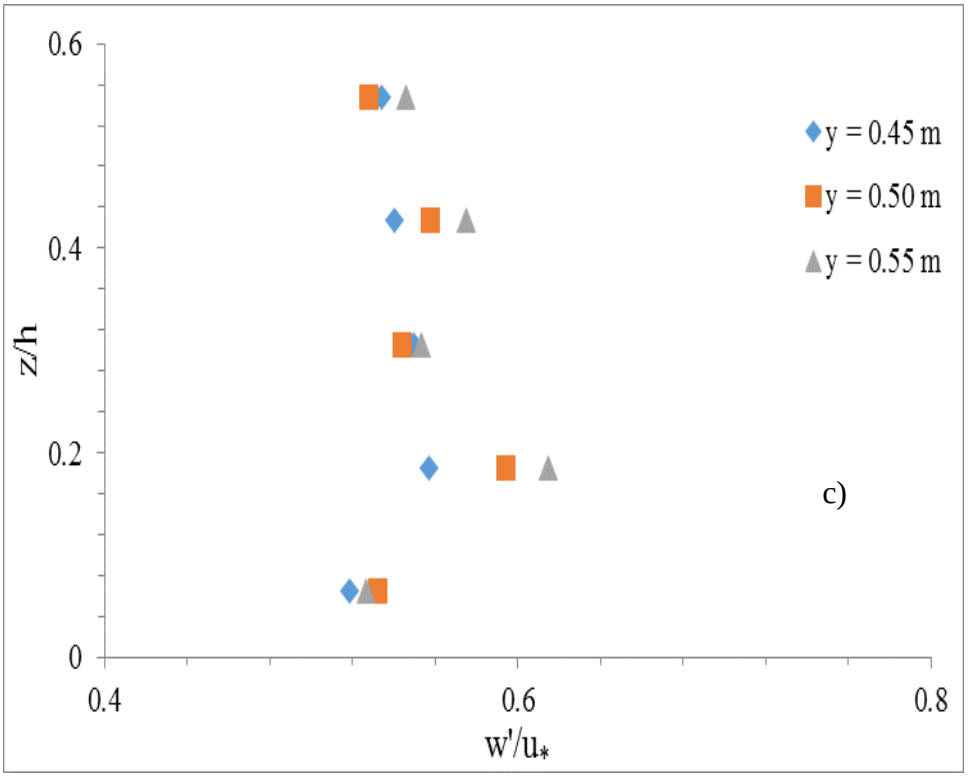

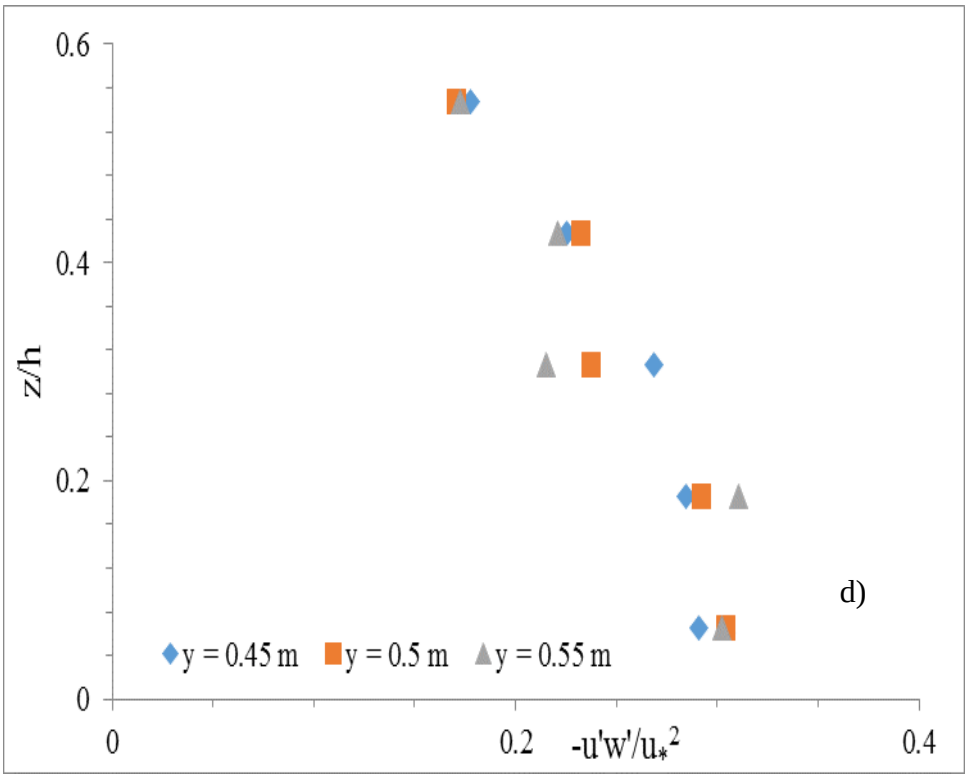

Fig. 5.18 c-d Variation of various turbulence quantities at x = 3H for no vane.

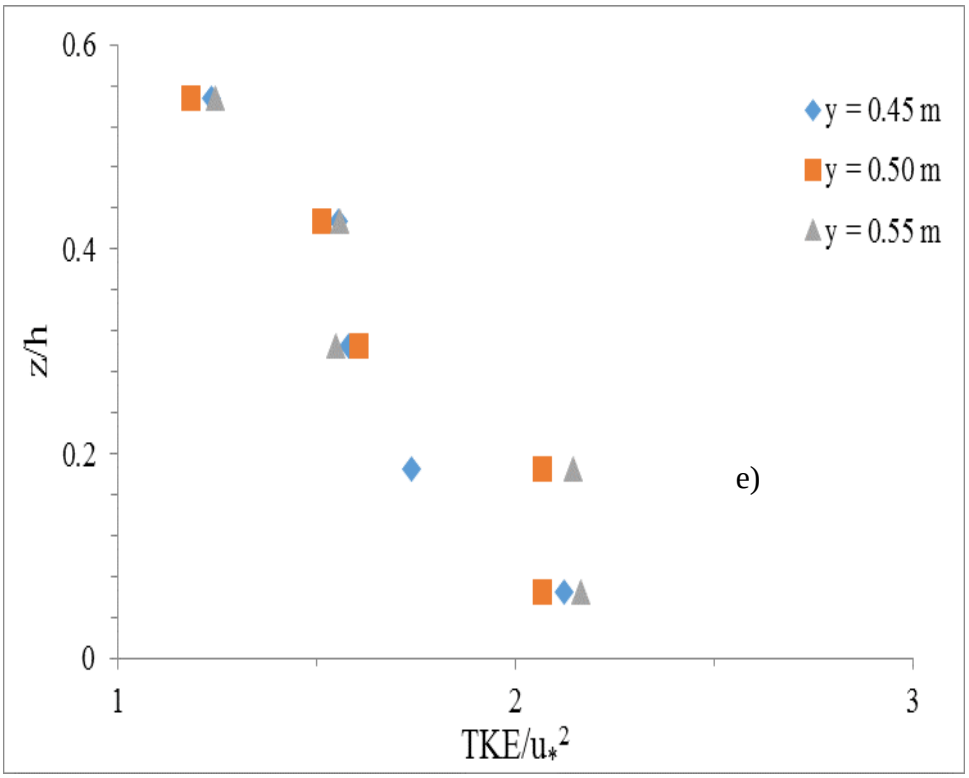

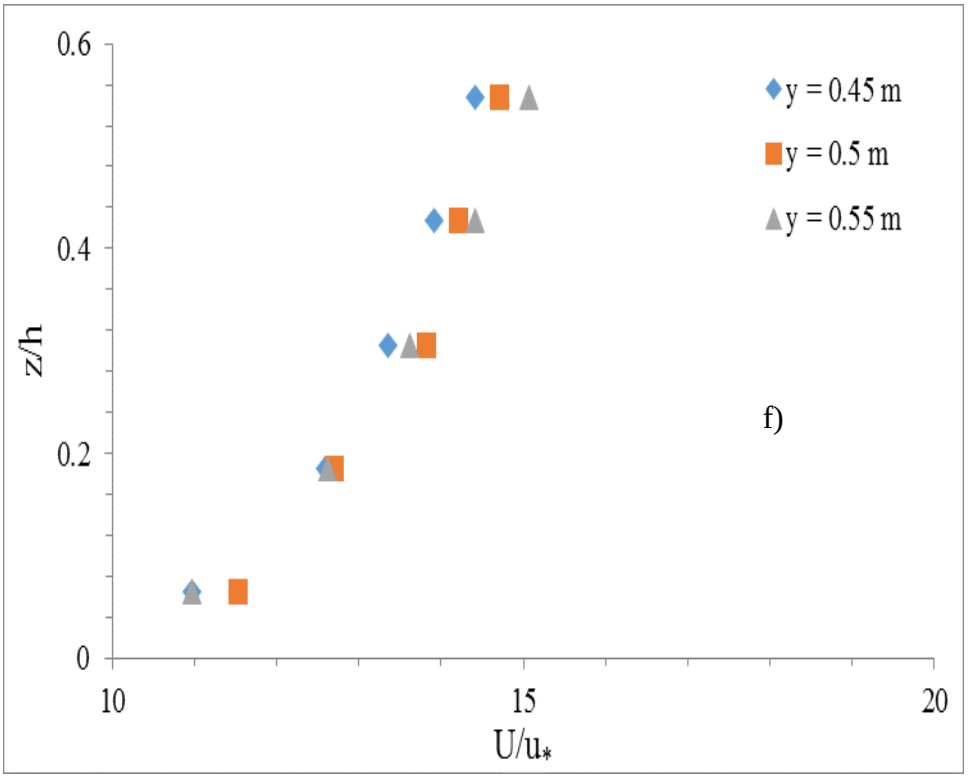

Fig. 5.18 e-f Variation of various turbulence quantities and velocity profile at x = 3H for no vane.

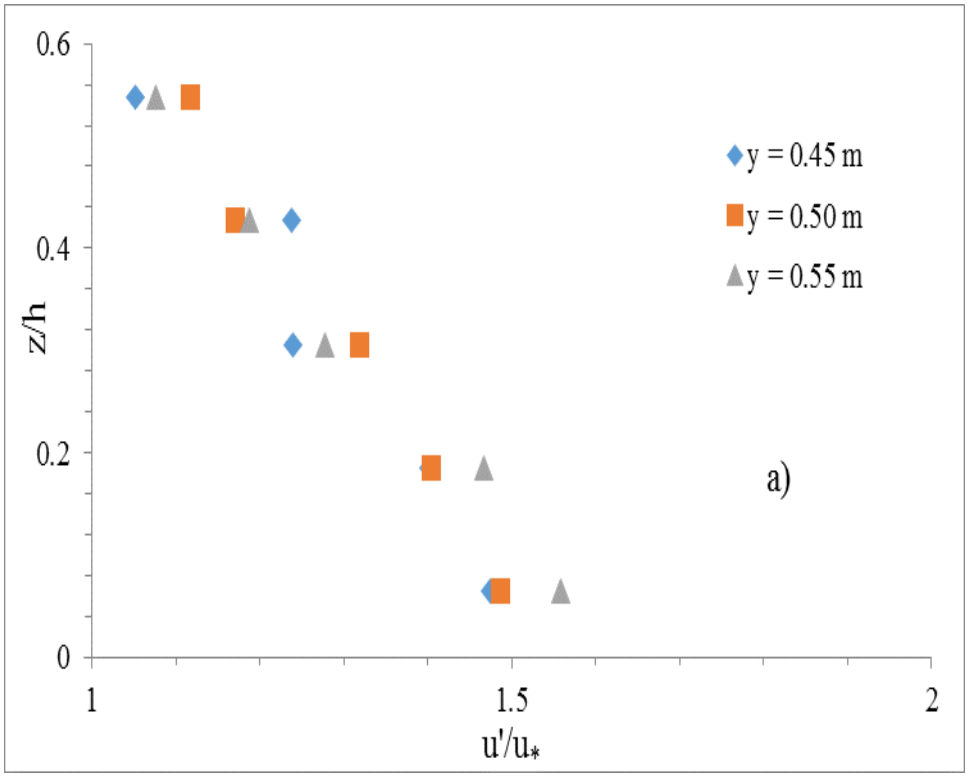

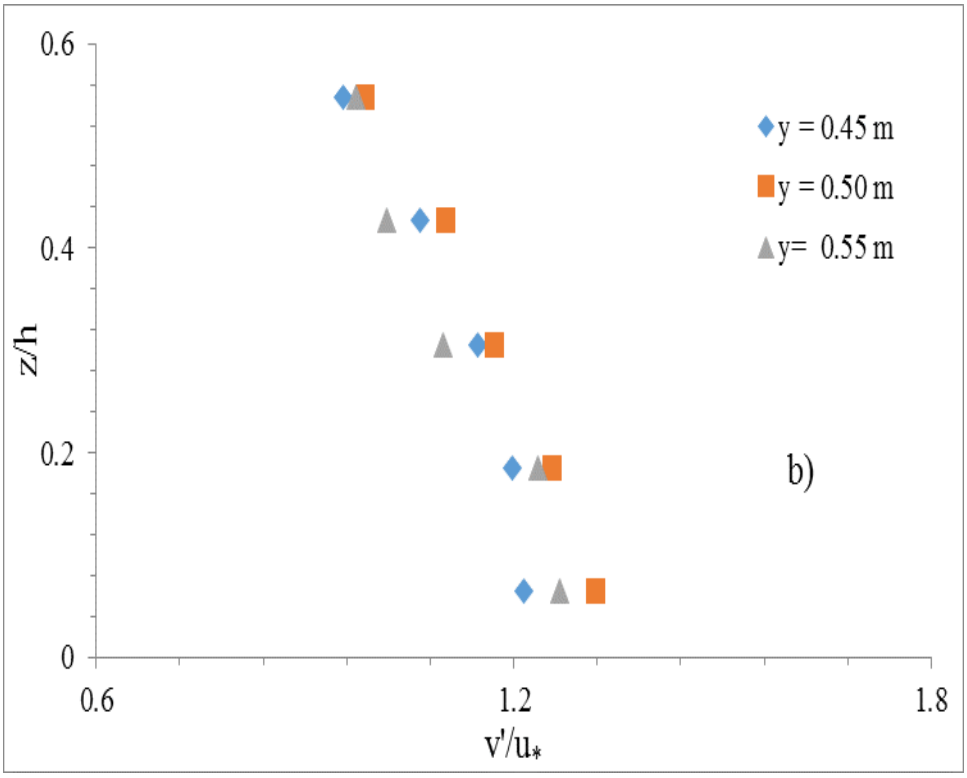

Fig. 5.19 a-b Variation of various turbulence quantities at x = 8H for no vane

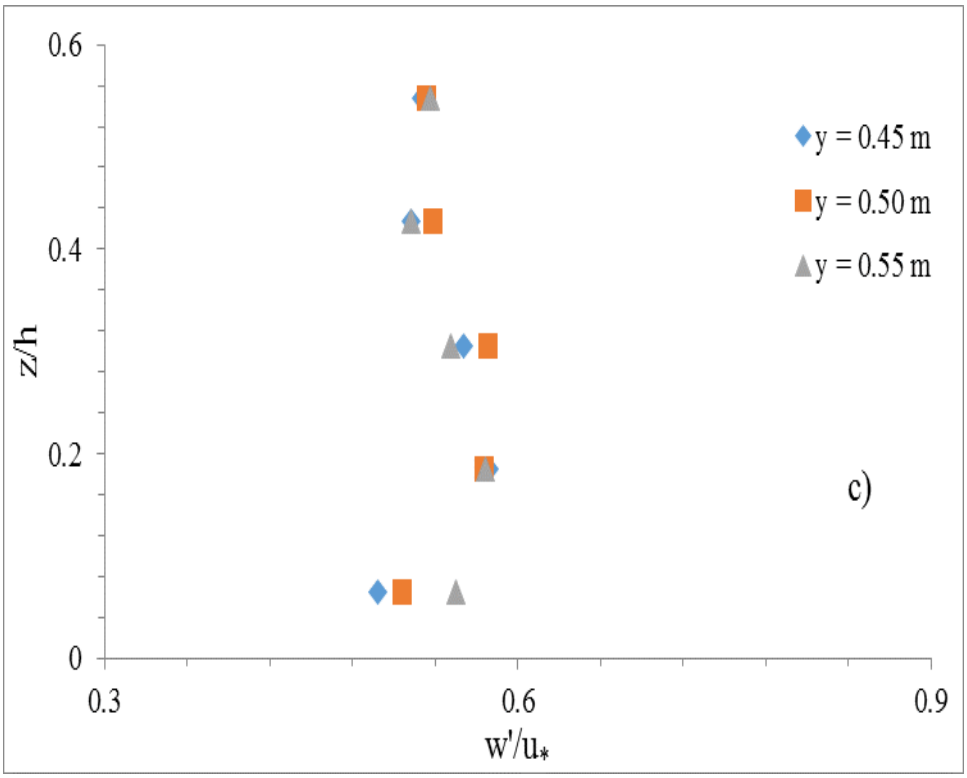

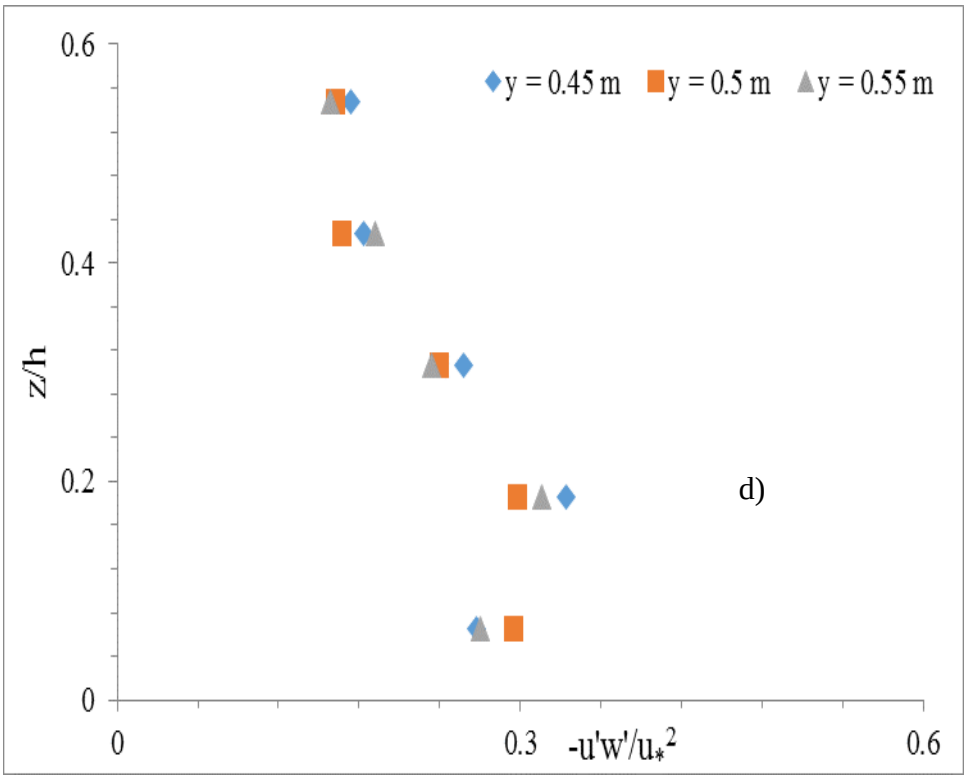

Fig. 5.19 c-d Variation of various turbulence quantities at x = 8H for no vane

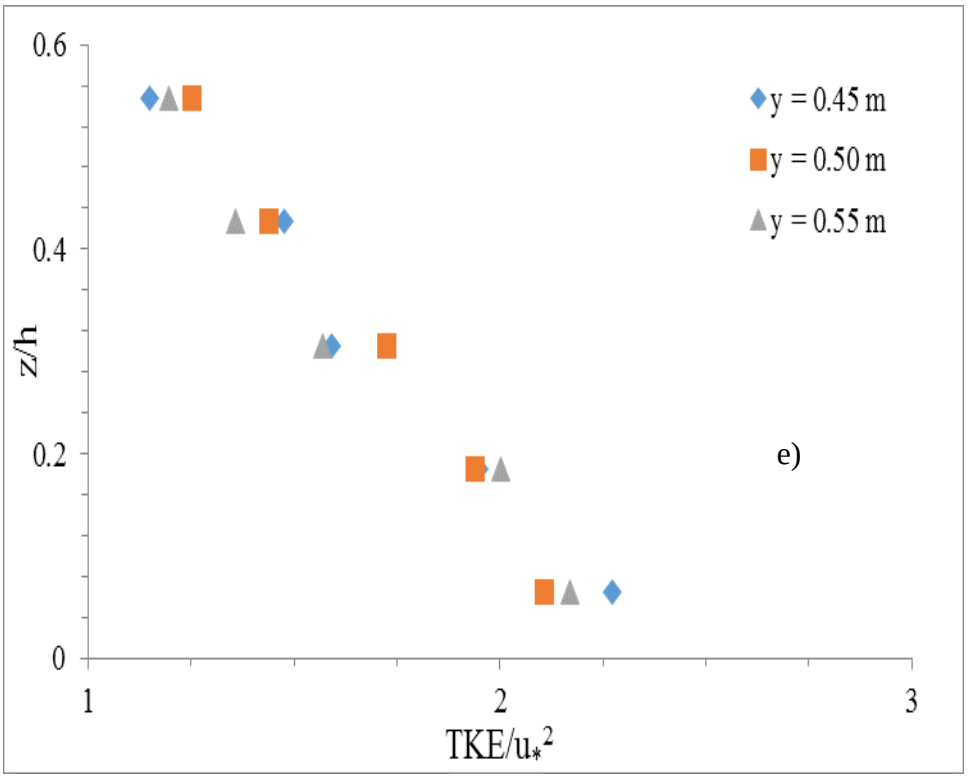

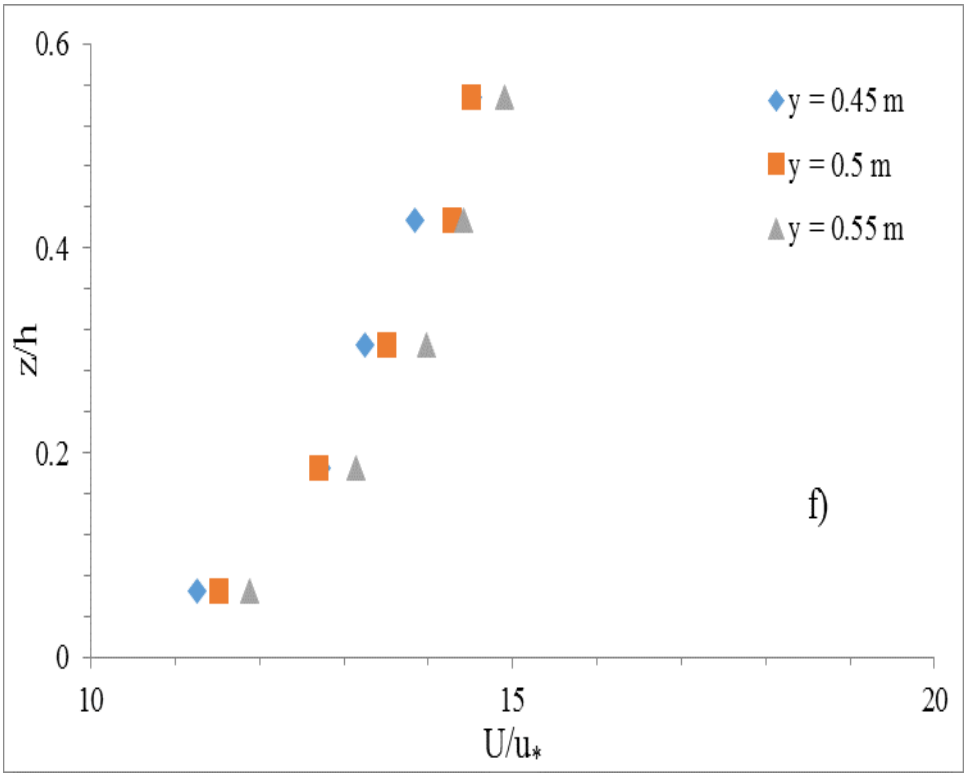

Fig. 5.19 e-f Variation of various turbulence quantities and velocity profile at x = 8H for no vane

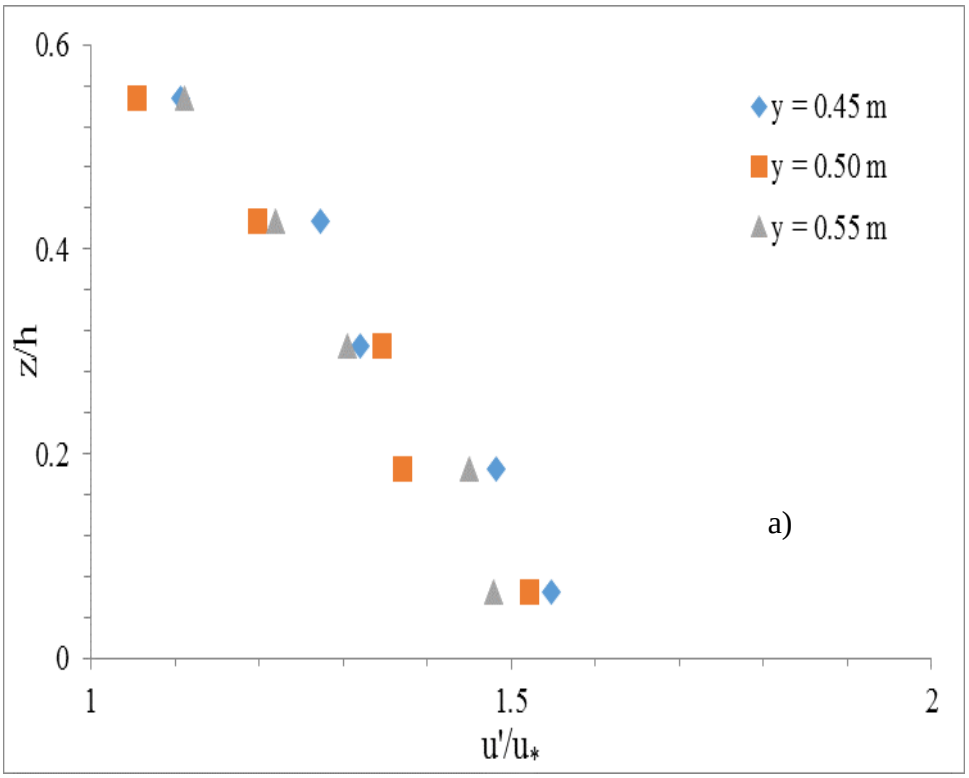

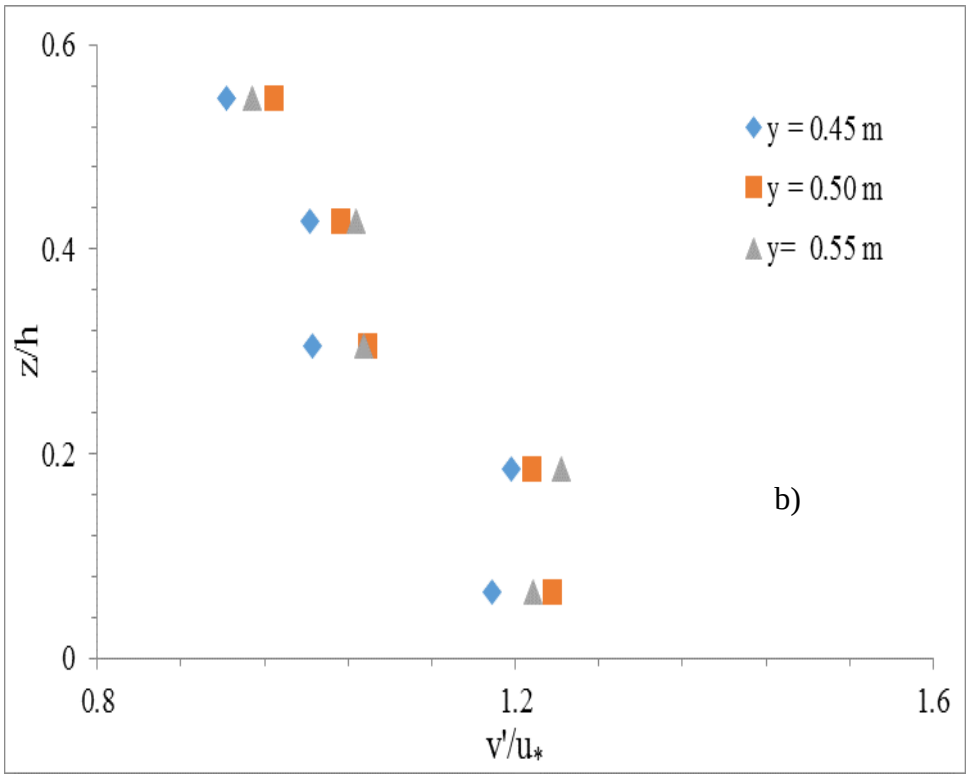

Fig. 5.20 a-b Variation of various turbulence quantities at x = 20H for no vane

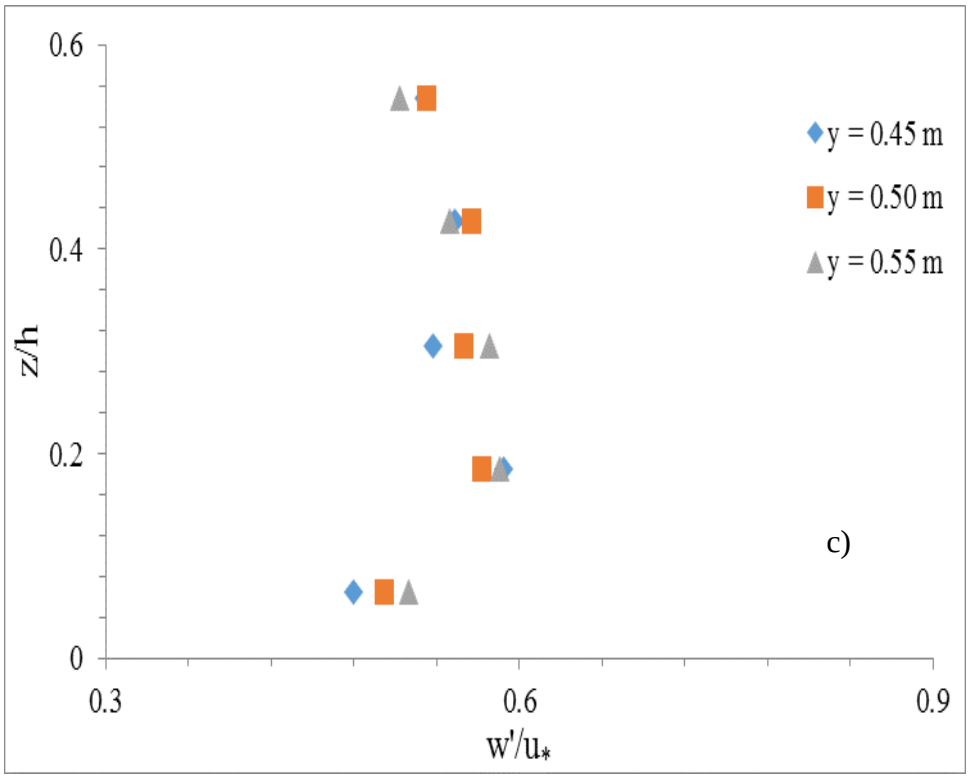

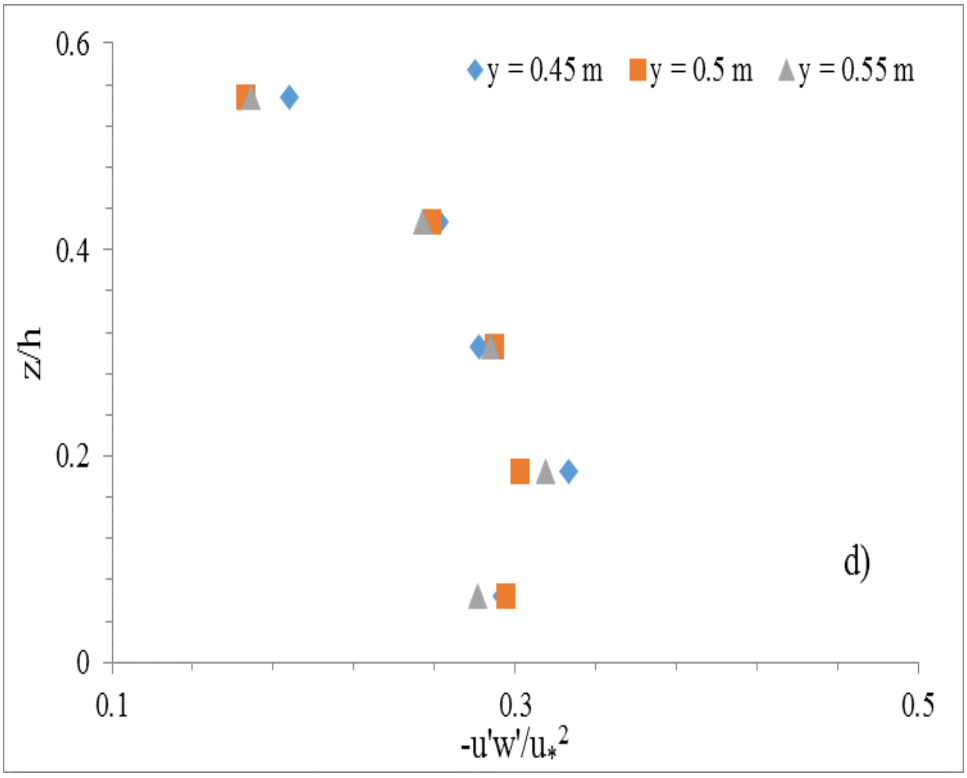

Fig. 5.20 c-d Variation of various turbulence quantities at x = 20H for no vane

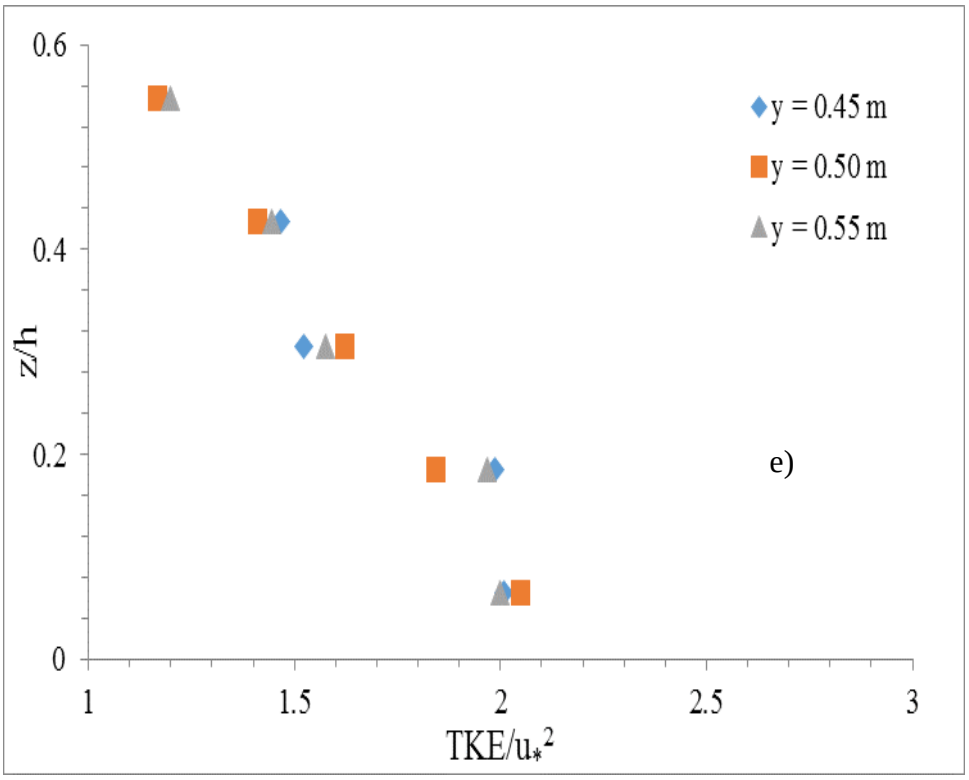

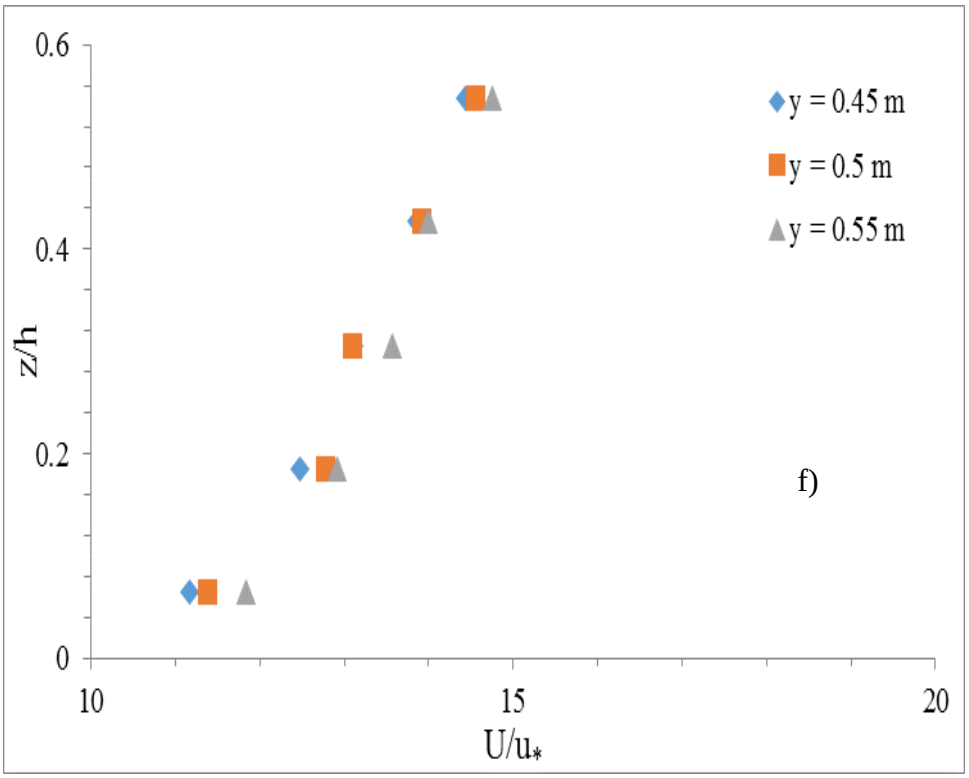

Fig. 5.20 e-f Variation of various turbulence quantities and velocity profile at x = 20H for no vane

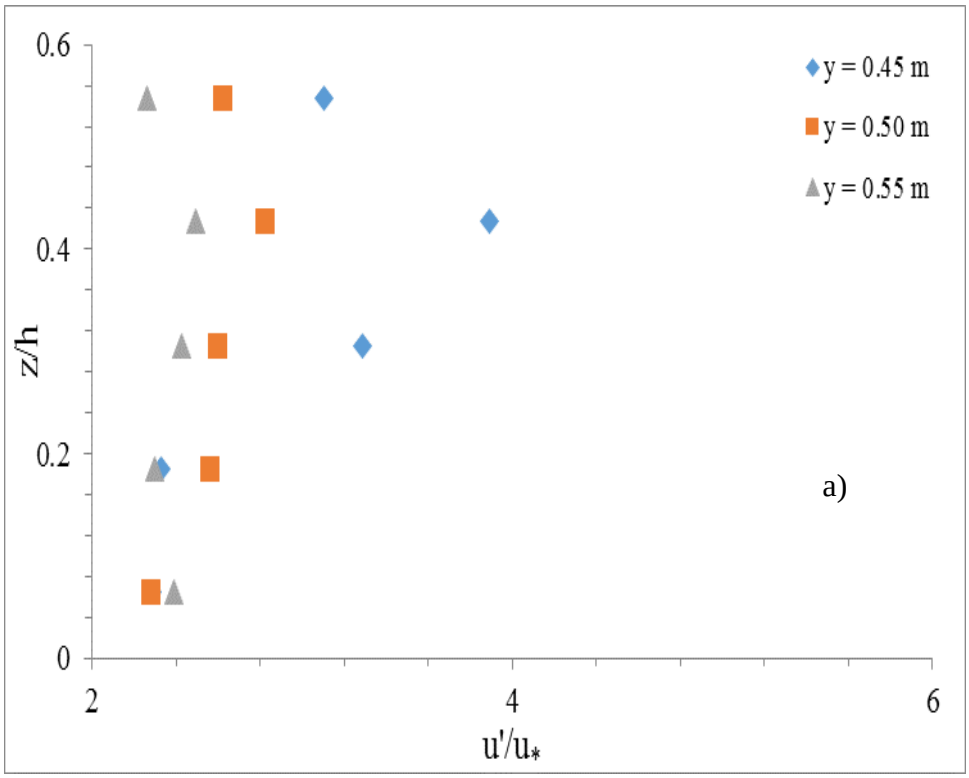

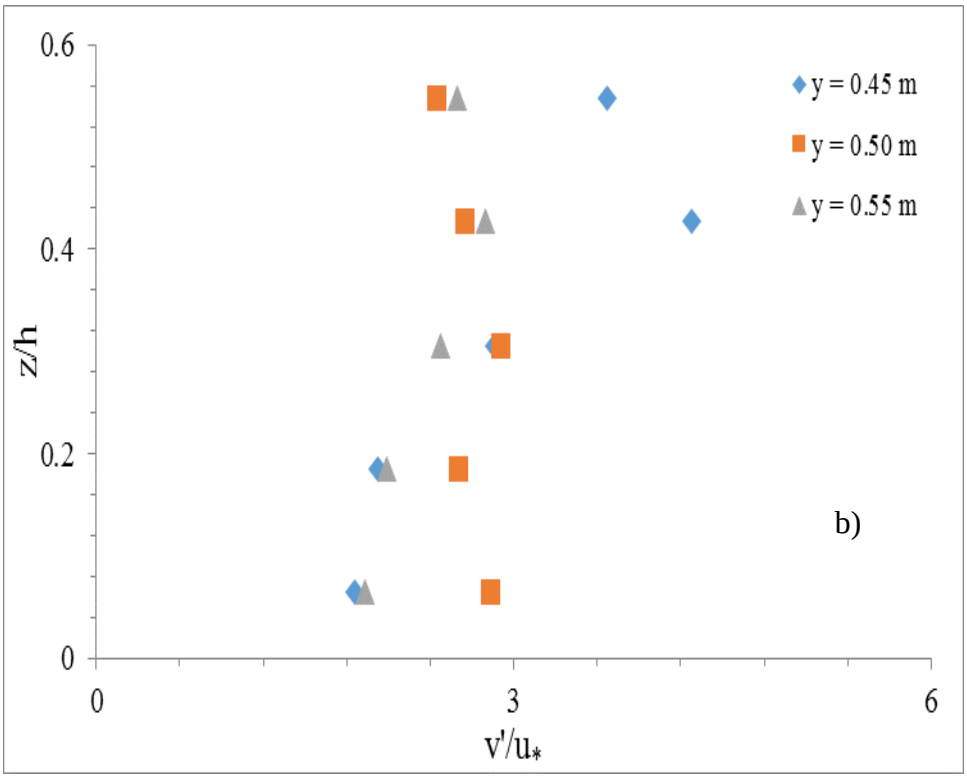

Fig. 5.21 a-b Variation of various turbulence quantities at x = 3H for four arrays of vanes

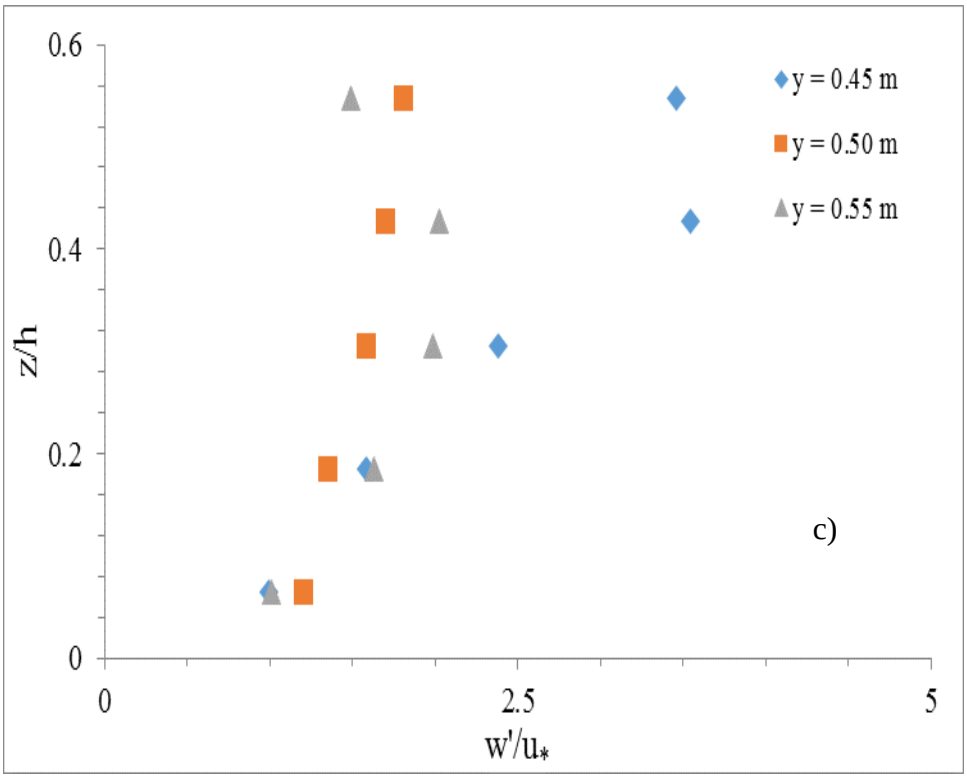

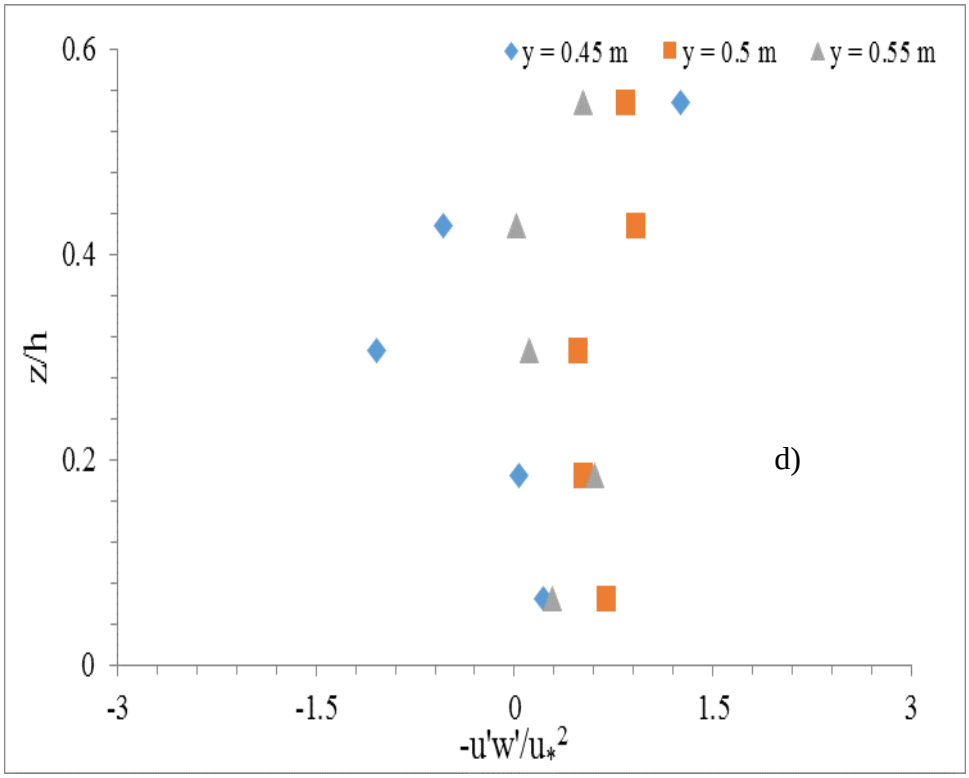

Fig. 5.21 c-d Variation of various turbulence quantities at x = 3H for four arrays of vanes

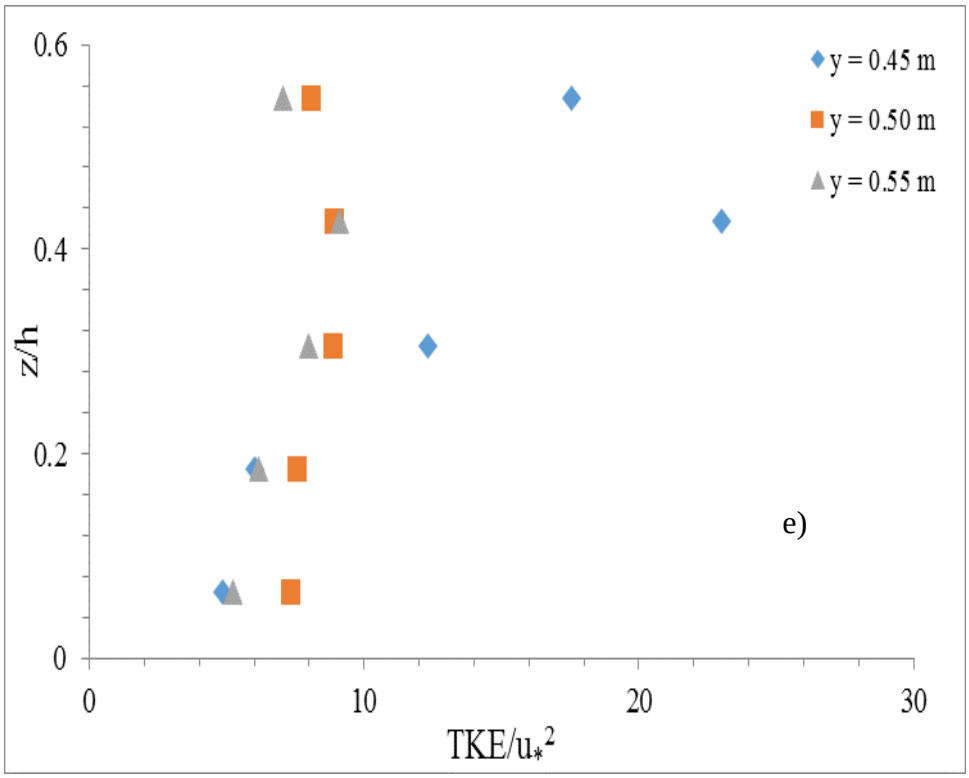

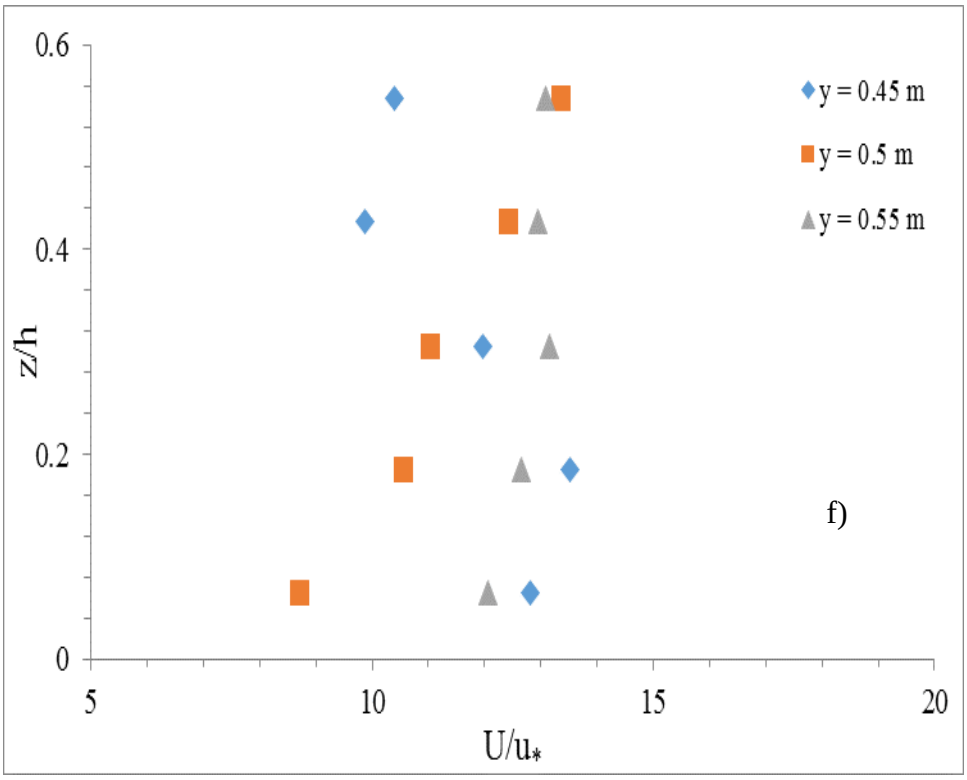

Fig. 5.21 e-f Variation of various turbulence quantities and velocity profile at x = 3H for four arrays of vanes

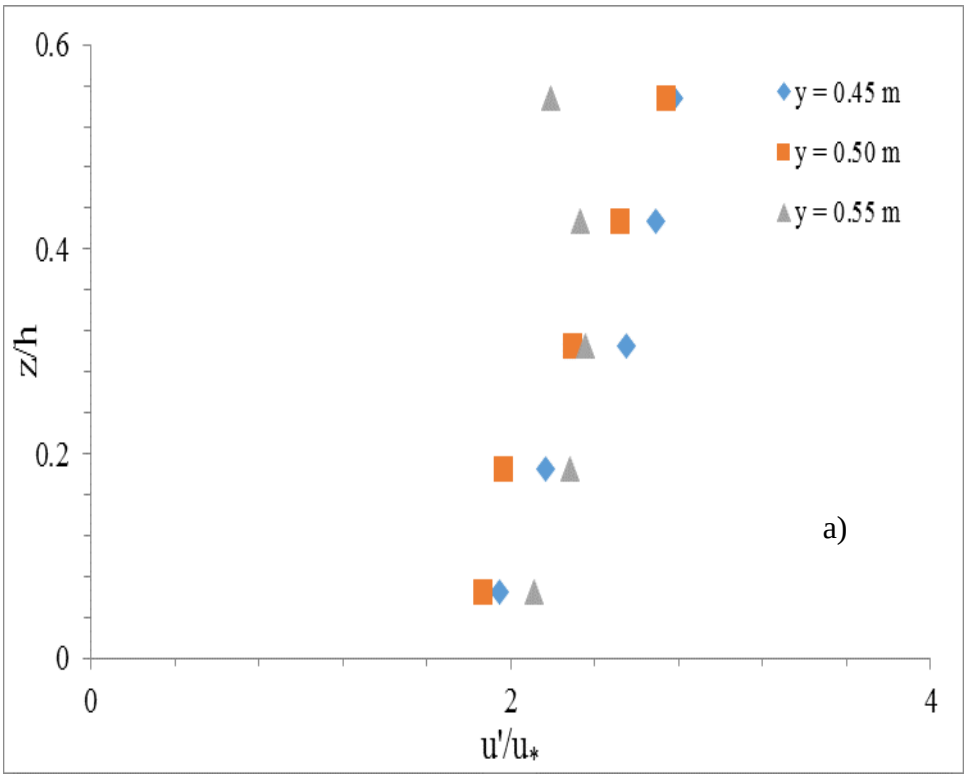

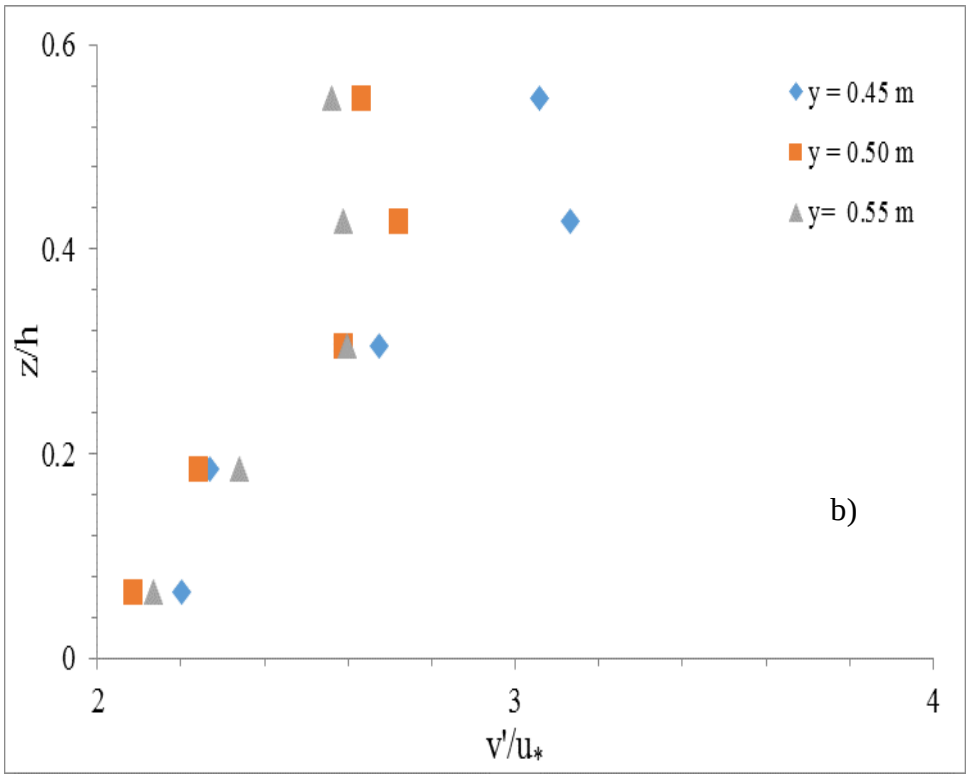

Fig. 5.22 a-b Variation of various turbulence quantities at x = 8H for four arrays of vanes

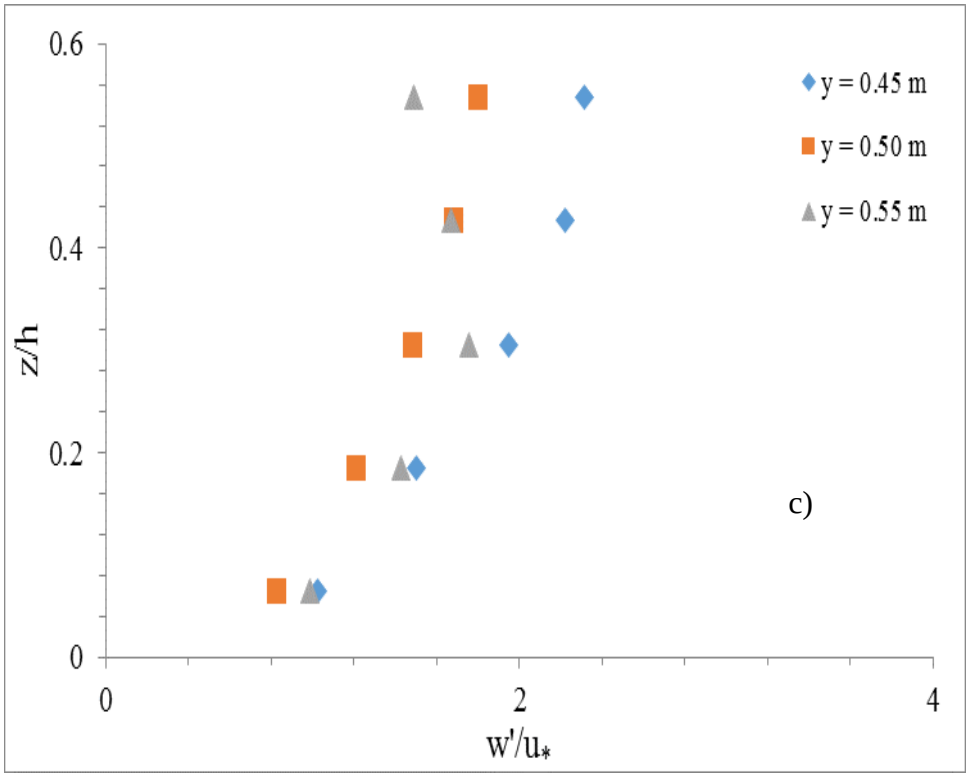

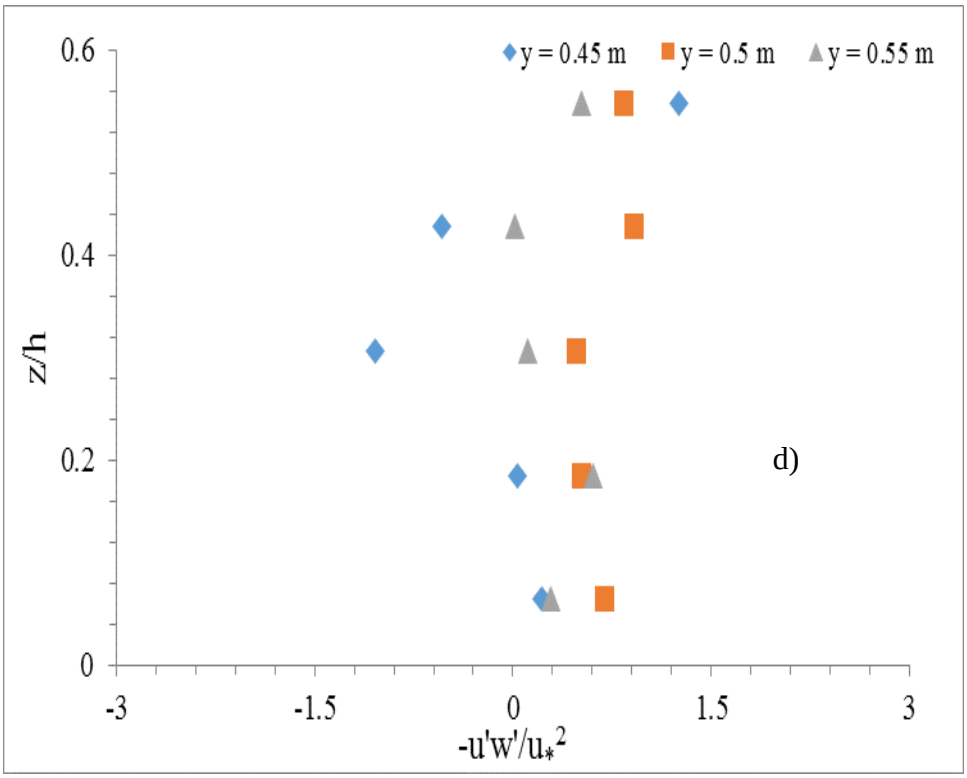

Fig. 5.22 c-d Variation of various turbulence quantities at x = 8H for four arrays of vanes

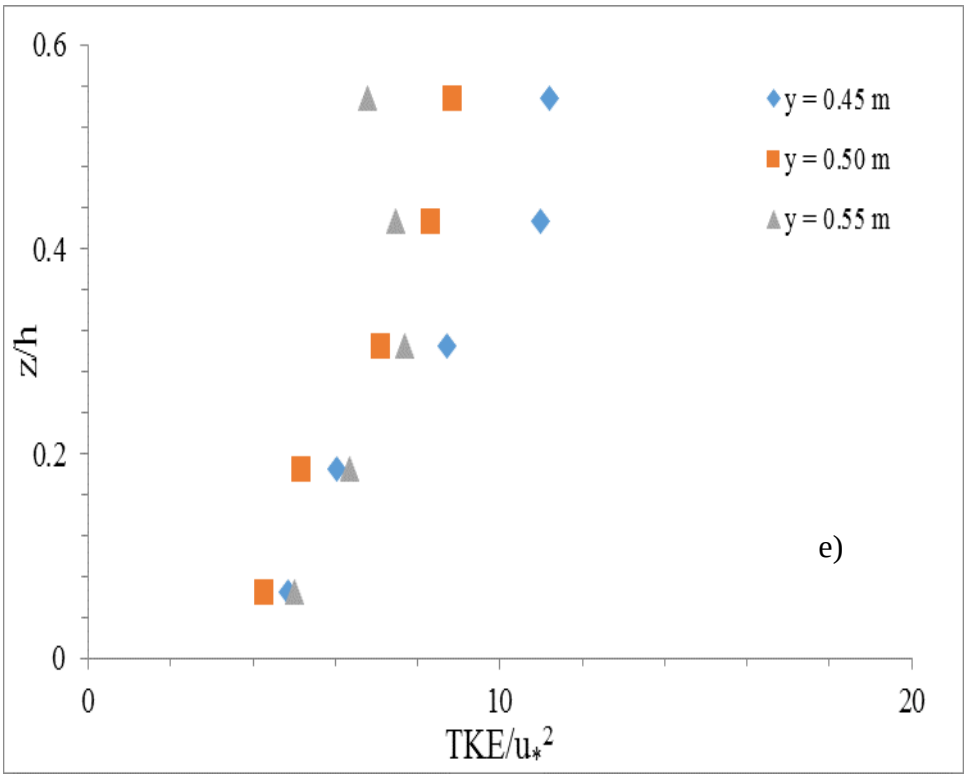

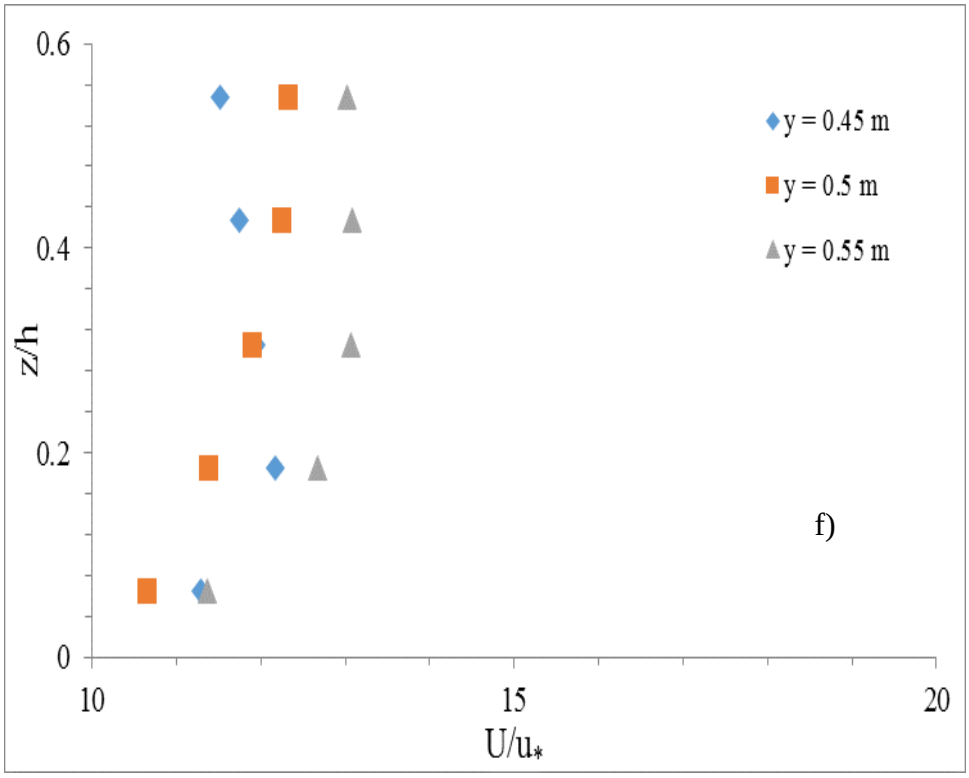

Fig. 5.22 e-f Variation of various turbulence quantities and velocity profile at x = 8H for four arrays of vanes

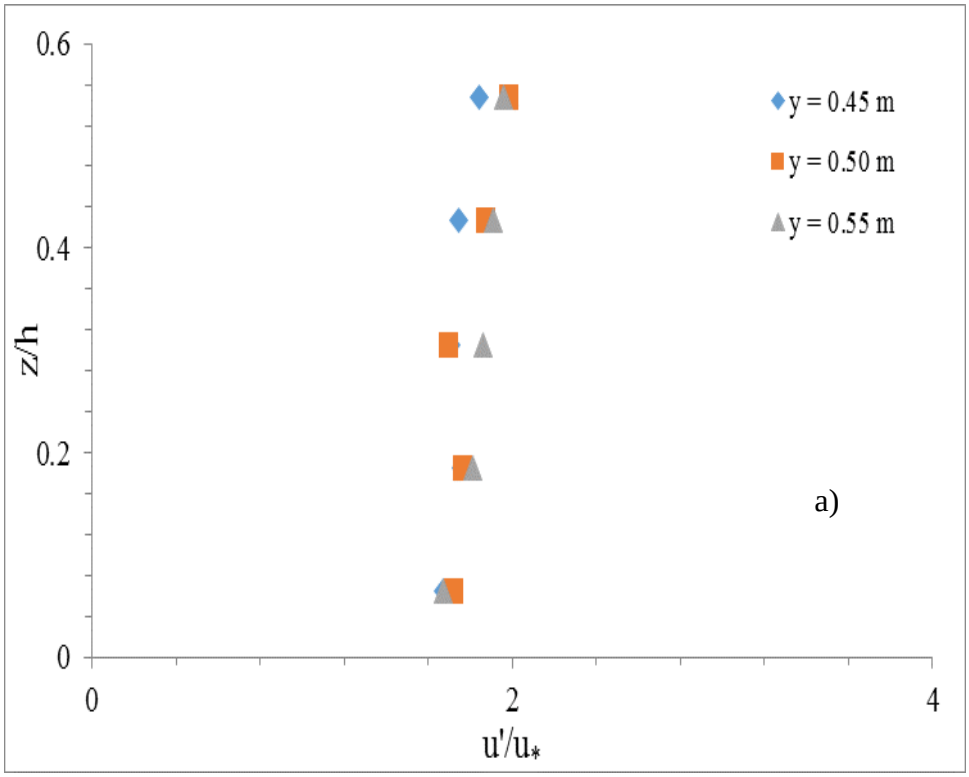

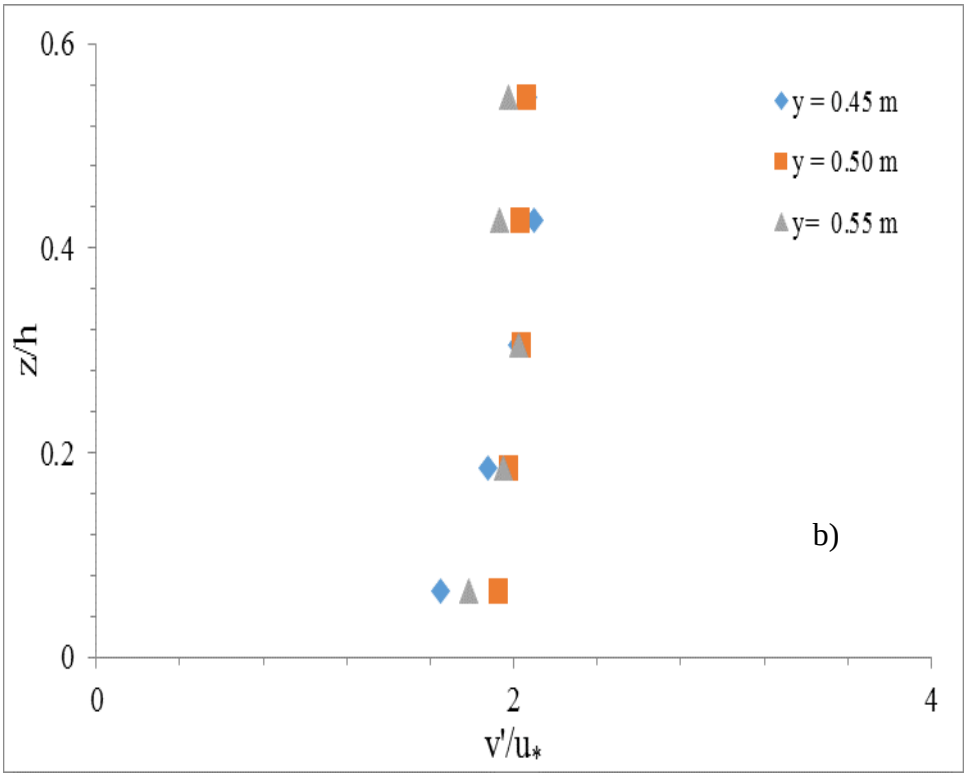

Fig. 5.23 a-b Variation of various turbulence quantities at x = 20H for four arrays of vanes

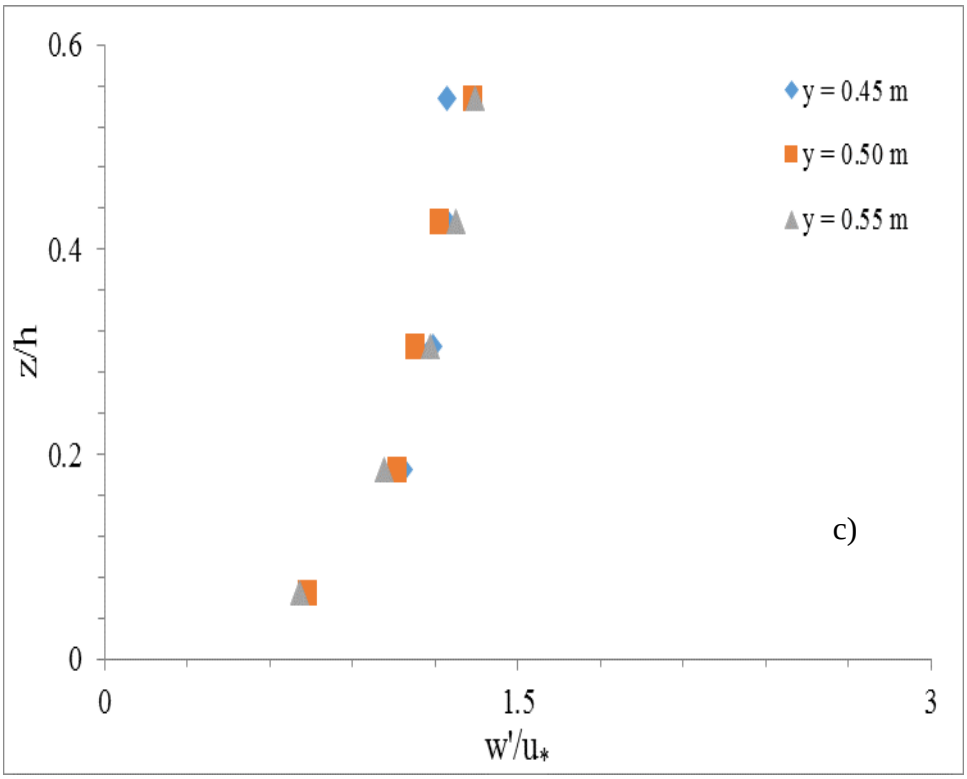

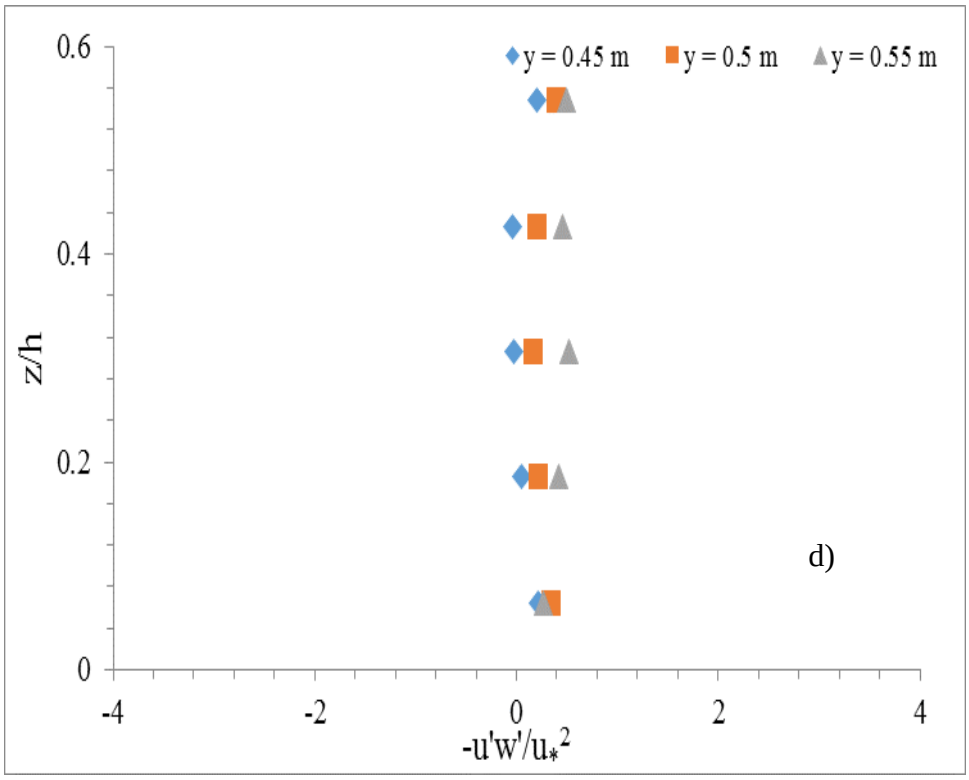

Fig. 5.23 c-d Variation of various turbulence quantities at x = 20H for four arrays of vanes

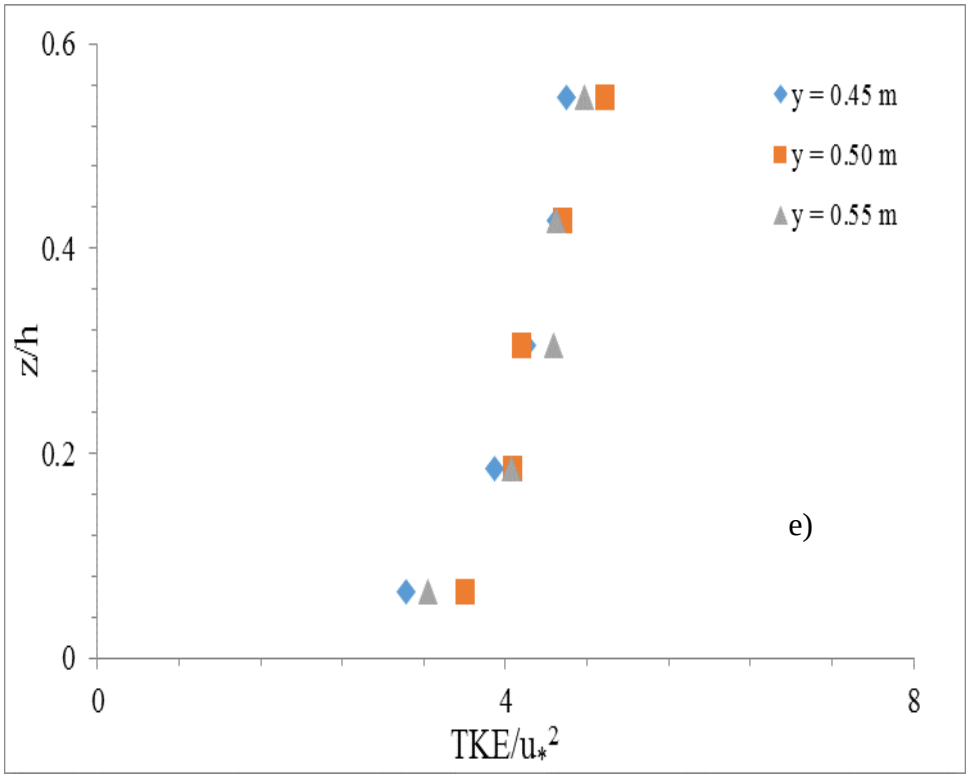

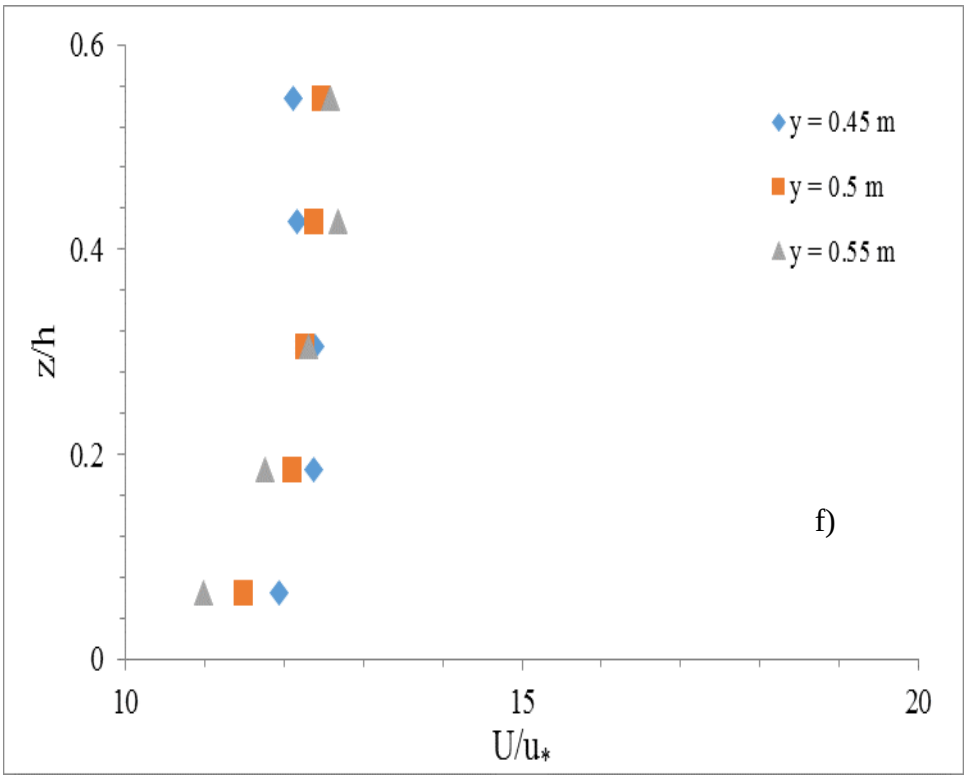

Fig. 5.23 e-f Variation of various turbulence quantities and velocity profile at x = 20H for four arrays of vanes

5.7 CONCLUDING REMARKS

This chapter dealt with the numerical modeling of the flow pattern around the single vane and multiple vane rows. Dimensions and spacing of the vanes have also been optimized for maximum vorticity in the flow downstream of vanes. While optimizing the angle of attack of submerged vane, it was observed that for 30^{o} angle of attack, maximum amount of vane circulation were generated. It was also observed that for vane height equal to 0.4 times depth of flow generates maximum circulations, which was in accordance with the value suggested by Odgaard and his associates. In case of length of vane, it was observed that as the length of vane was increased the strength of vorticity was also observed to be increased. The reason behind this phenomenon was the enhancement of strength of bound vortex which circumscribes the vane and is responsible for starting vortices in the flow. It was observed that in the case of single submerged vane that flow not only separates around the edges but also flow over the submerged vane plunges to downstream to generate more turbulence. It was also concluded

from turbulent kinetic energy that trailing edge has more importance in vortex generation through separation than the leading edge, as the turbulent kinetic energy suffered a drastic increase at the trailing edge and as flow leaves the trailing edge, turbulent kinetic energy suffers a drastic decrease. It was also observed that equilibrium value of turbulent kinetic energy at downstream of vane is more than what it was before flow was altered by vane. In case of multiple vane rows, it was observed that by keeping lateral spacing at 3 times height of vane which was in accordance with the observations of Wang and Odgaard (1993). Longitudinal spacing of vane array have also been optimized to generate maximum circulation in which after placing one vane row in the flow another row is placed at a longitudinal distance depending upon what % vorticity is needed downstream of the installed vane row. In case of multiple vanes, it was observed that at the distance very near to vane row, each vane row generates a circulation of its own. In the further downstream, vortices coalesce with each other to form a larger field of circulation but effective magnitude of circulation was observed to be less than the magnitude of circulation if it was generated by each vane in individual manner. Moving further downstream, it was observed that under the action of viscosity, circulation field was dissipated and less disturbed flow field was obtained. It was observed from the experimental observations of flow around vane rows that as vane was introduced in the flow the homogeneity of turbulence in flow was disturbed. It was also observed that more were the rows of vanes in the flow more heterogeneous was the flow turbulence. It was observed that vortices were originating from vane at a height of 0.83H (Here, H = vane height), which was very near to observation of Odgaard and Wang (1991 a), who suggested the height of point of origin of vortices on the vane to be 0.81H.

Chapter 6

ENHACING TRANSVERSE MIXING USING SUBMERGED VANES

6.1 INTRODUCTION

In this chapter, the collected data are analyzed to develop relationship for transverse mixing coefficient for no vane and arrays of vane conditions. Effects of arrays of vanes on transverse mixing process are also being discussed here.

Second section of the present chapter discusses the effect of the submerged vane rows on the transverse velocity. In third section of the present chapter effect of submerged vane rows on concentration profile was discussed by varying vane configurations. In fourth section of this chapter, effects of the submerged vane rows on the transverse mixing coefficient by varying vane configurations. In this section a predictor was proposed which can give transverse mixing coefficient in the presence of submerged vane rows. In the final and fifth section of present chapter, validation of the proposed predictor was done.

6.2 EFFECT OF VANE ARRAYS ON TRANSVERSE VELOCITY

Variation of transverse velocity along depth for zero one, two, three and four array of vanes is shown in Fig. 6.1 for a) y = 0.45 m; b) y = 0.5 m and c) y = 0.55 m & x = 8H. These figures reveal that as array of vanes increases the transverse velocity increases which signify that transverse mixing shall be higher for higher number of arrays of vanes.

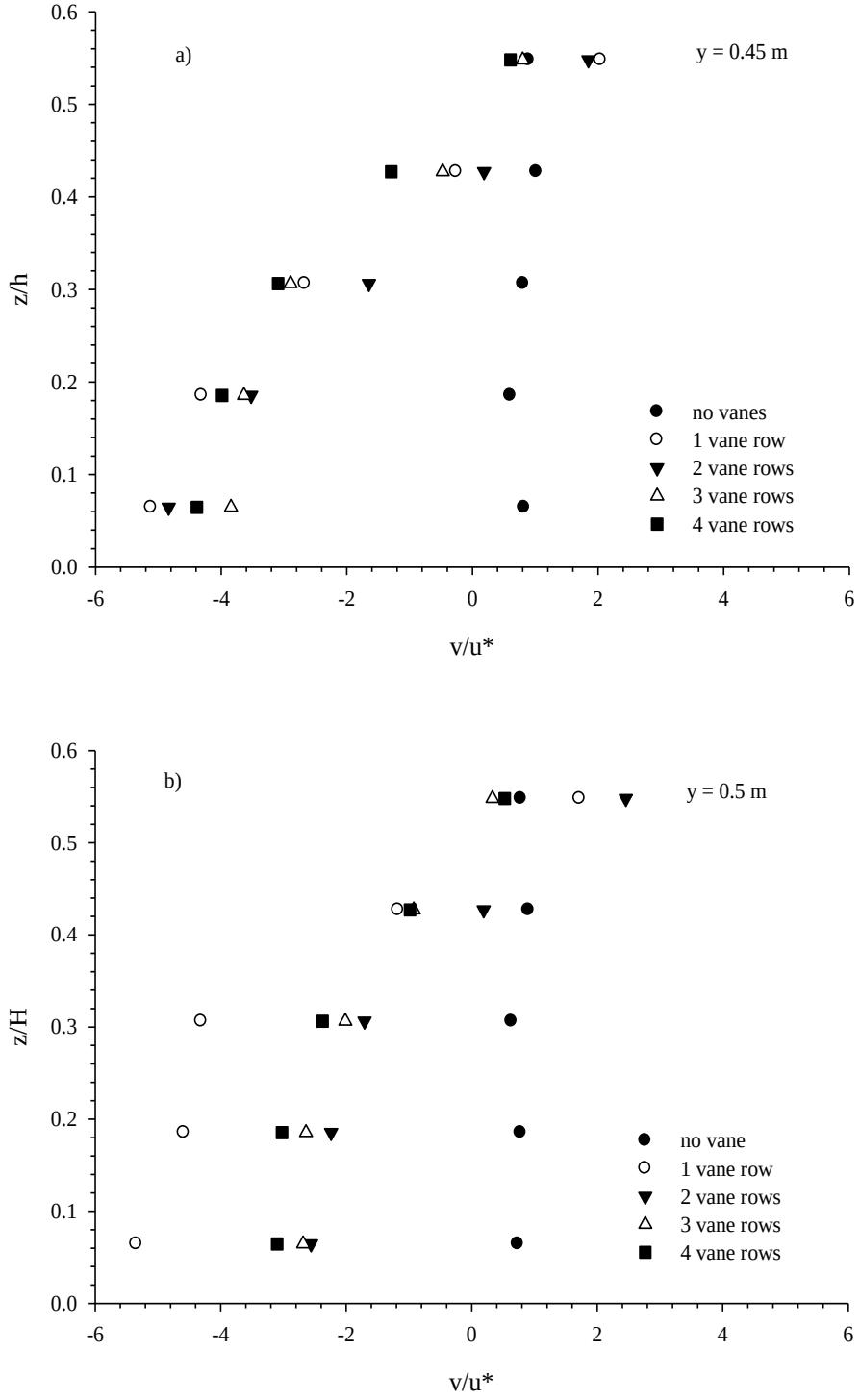

Fig. 6.1 a)–b) Variation of transverse velocity with and without vane rows for a) y = 0.45 m; b) y = 0.5 m for x = 8H.

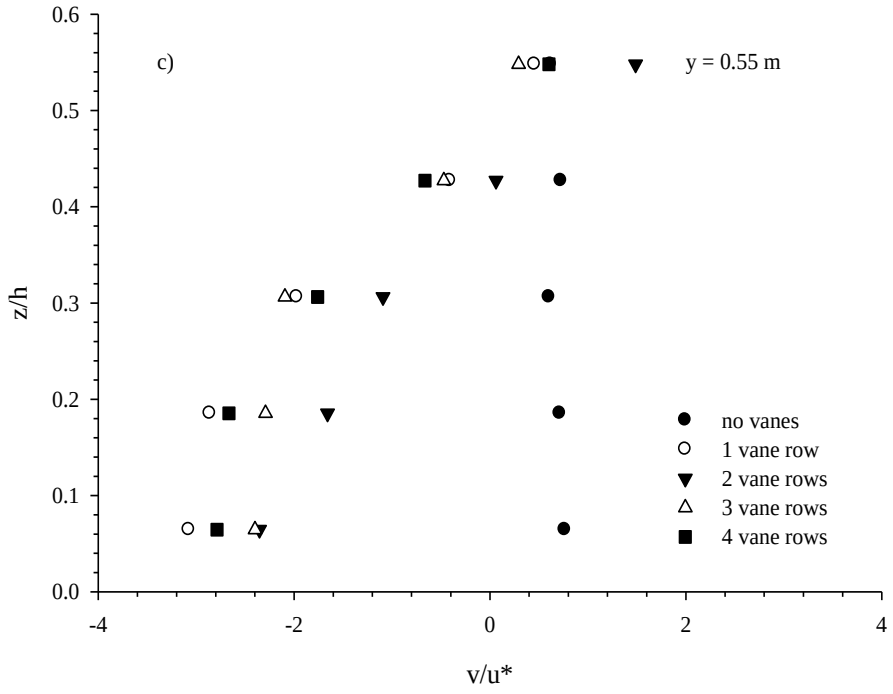

Fig. 6.1 c) Variation of transverse velocity with and without vane rows for c) y = 0.55 m for x = 8H.

6.3 EFFECT OF SUBMERGED VANES ON THE CONCENTRATION PROFILES

It is evident from the literature and observations by various investigators (Odgaard and Kennedy, 1983; Odgaard and Mosconi, 1987; Odgaard and Wang, 1991 a & b; Wang and Odgaard, 1993; Marelius and Sinha, 1998) that submerged vanes generate the secondary currents in the form of transverse circulations.

Figs. 6.2 to 6.7 show variation of tracer concentration across the width of the channel at distance x = 5 m and 15 m for depth of flow = 0.09 m, 0.1025 m and 0.1241 m, vane height = 0.02 m, 0.04 m, and 0.06 m and vane rows = 0, 1, 2, 3, and 4. It is evident from the Figs. 6.8-6.13 that in the case of 4 vane rows generation of circulation field was large and was extended to a greater distance; hence the mixing was highest in the case of 4 vane rows. As the number of vanes were reduced from 4 to three the magnitude of the circulations reduced and so reduced the extent of circulation field. Hence, the mixing was reduced and profile tends to become peaky at left wall. Further, reducing the number of rows from three to two it was

observed that concentration distribution started to skew further and degree of uniformity along the concentration distribution curve was reduced as circulation strength further reduced.

Again decreasing number of rows from two to one it was observed that concentration distribution curve almost attained the Gaussian profile with a single skewed peak and uniform distribution of dye tracer was now moreover diminished as strength of circulations was further reduced. Under no vane case, tracer dye has maximum concentration near the left bank. Also most of the dye was mixed around the half of the channel width. Thus it reinstates the fact that presence of submerged vane enhances the transverse distribution of dye.

Figures 6.8 to 6.13 clearly reinstate the fact that as the number of vane rows increases, the extent of transverse dispersion increases. It shows that across any transect as the number of rows of vane was increased the dye is uniformly mixed across the channel cross sections. As the numbers of rows of vanes were reduced the uniformity of mixing reduced and concentration became more and more skewed towards left bank from where dye was discharged, this implies that transverse dispersion has reduced to great extent.

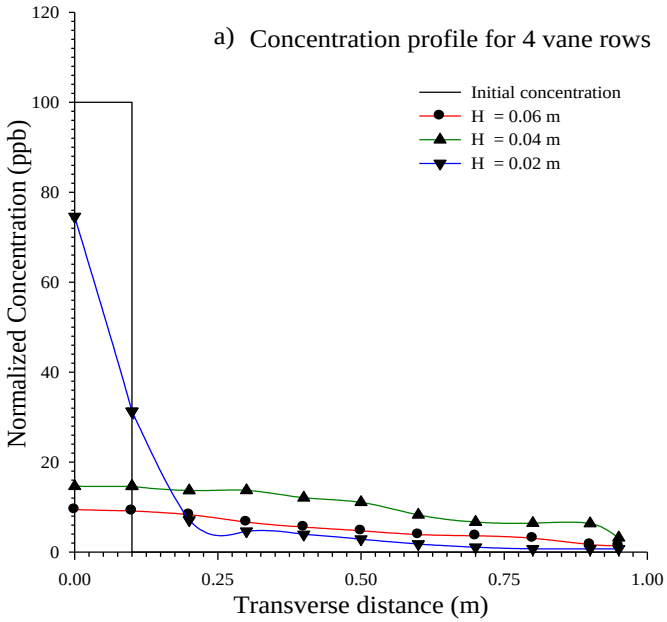

Fig. 6.2 a Concentration distribution of dye across transects for 4 vane rows for h = 0.1241 m and x = 5m

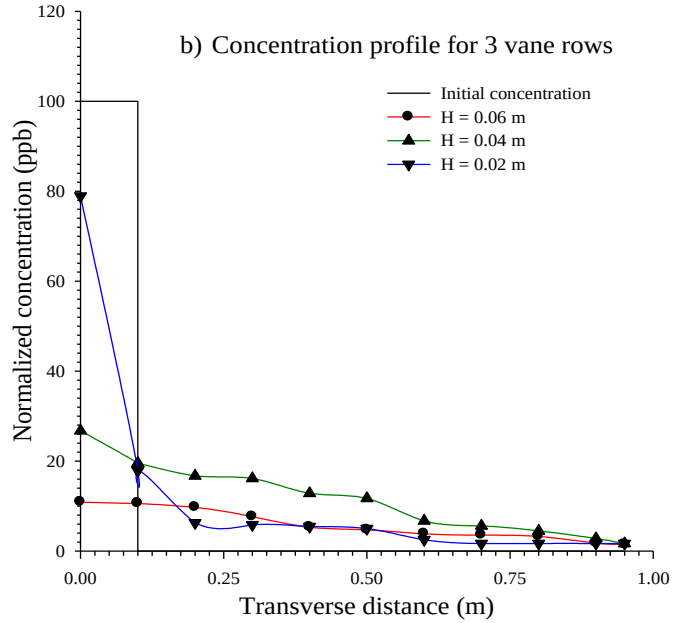

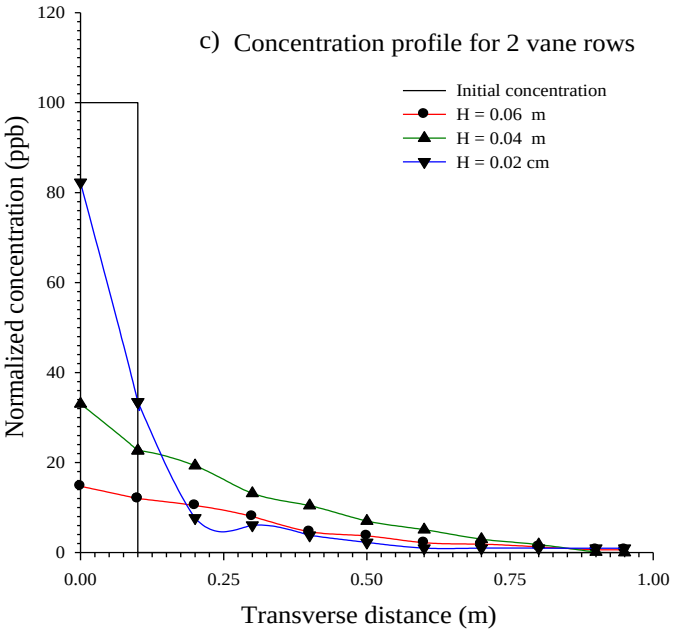

Fig. 6.2 b-c Concentration distribution of dye across transects for b) 3 vane rows; c) 2 vane rows for h = 0.1241 m and x = 5m.

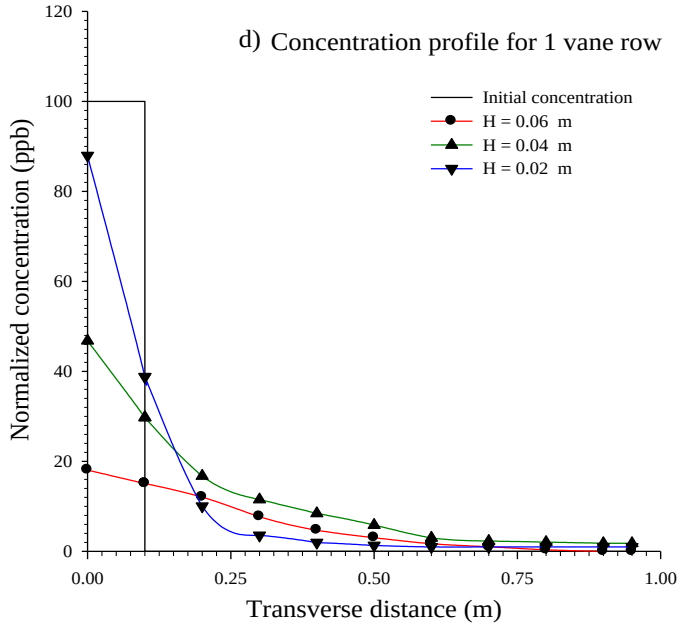

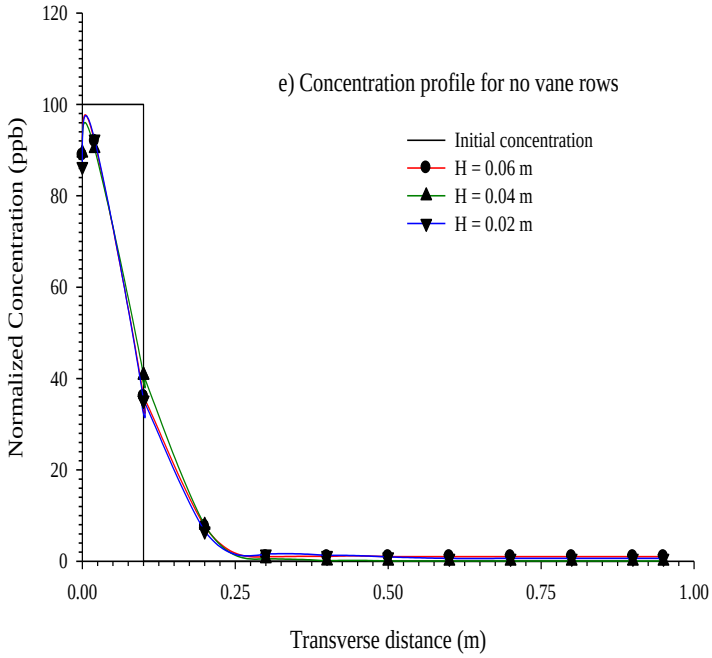

Fig. 6.2 d, e Concentration distribution of dye across transects for d) 1 vane row; e) for no vane row for h = 0.1241 m and x = 5m.

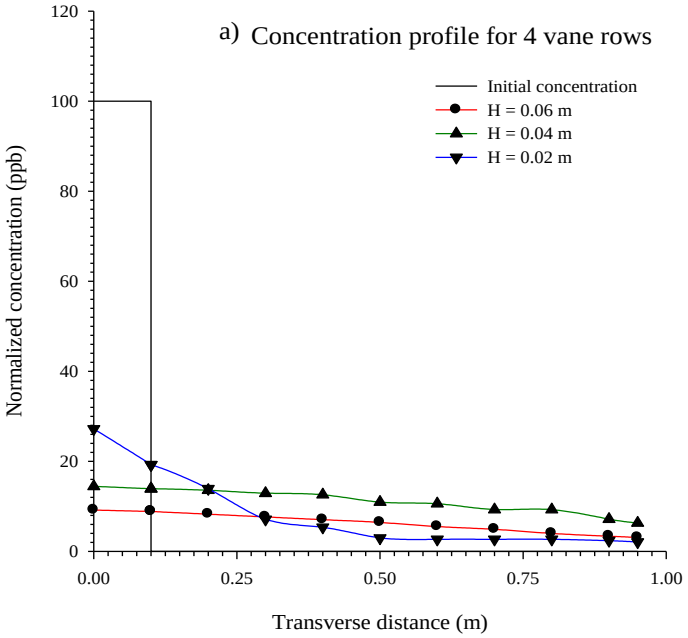

Fig. 6.3 a Concentration distribution of dye across the transects for 4 vane rows for h = 0.1241 m and x = 15m

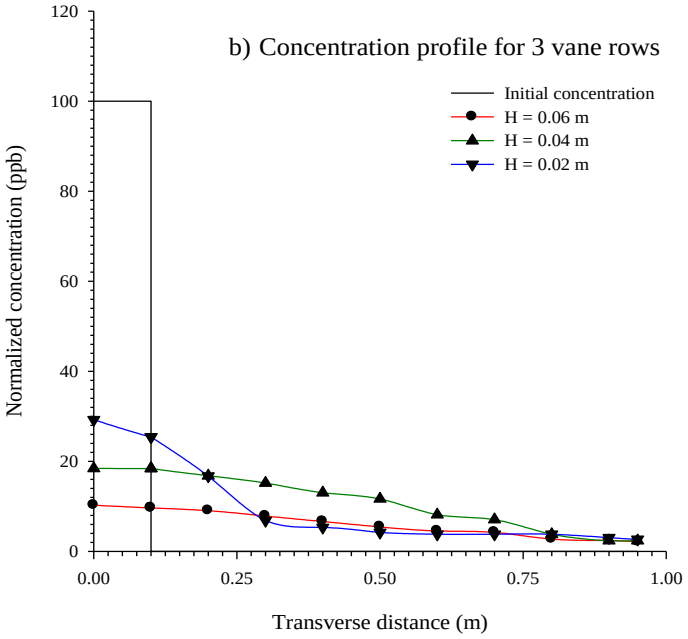

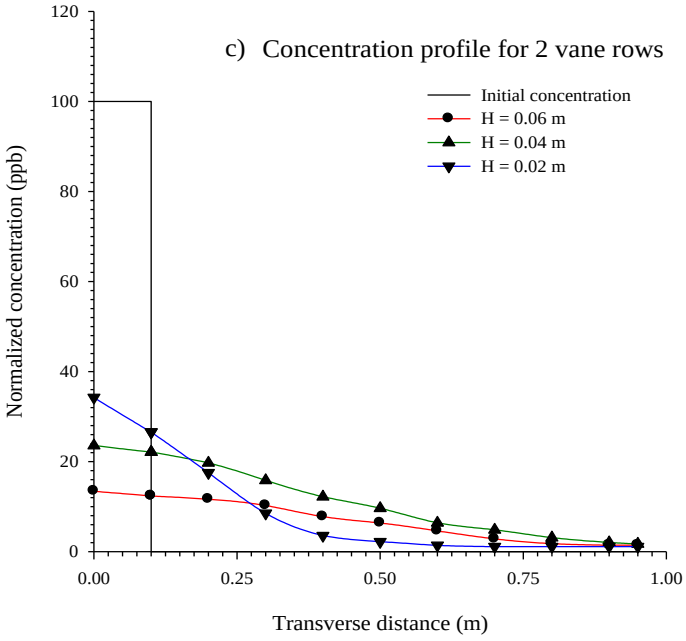

Fig. 6.3 b-c Concentration distribution of dye across the transects for b) 3 vane rows; c) 2 vane rows for h = 0.1241 m and x = 15m

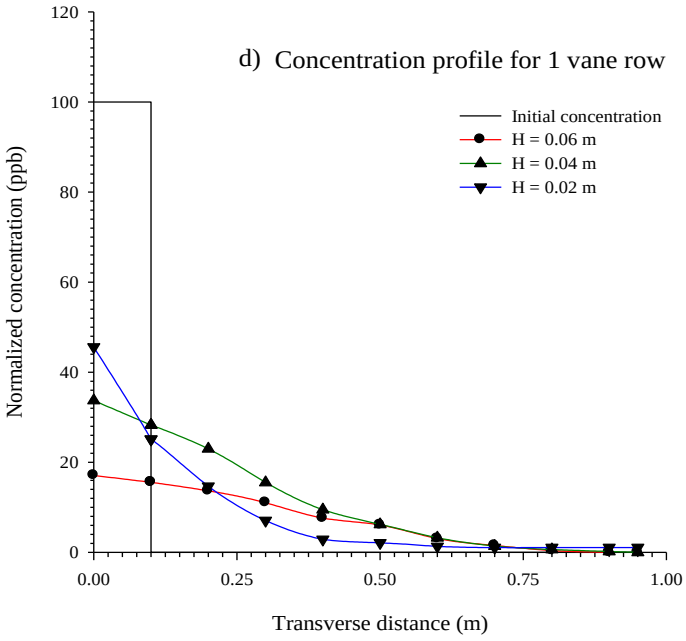

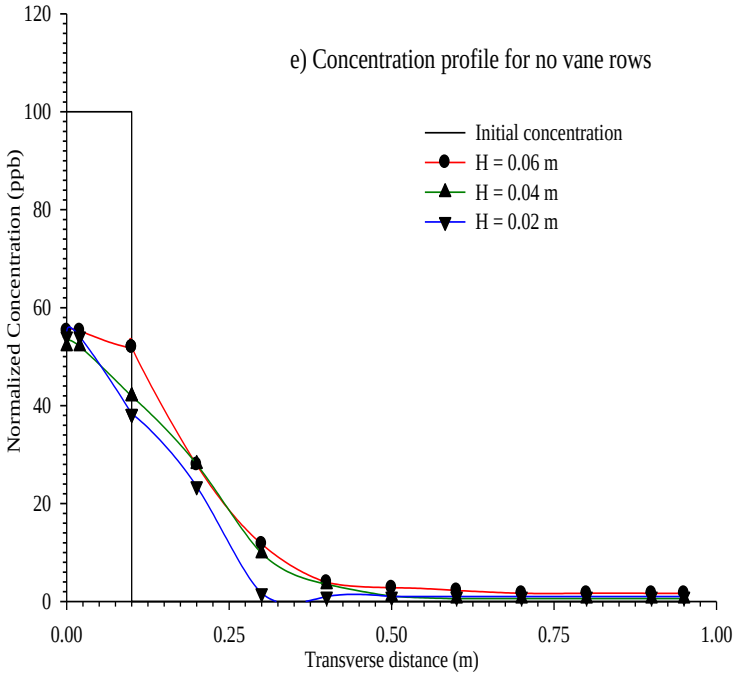

Fig. 6.3 d, e Concentration distribution of dye across the transect for d) 1 vane row; e) no vane row for h = 0.1241 m and x = 15m.

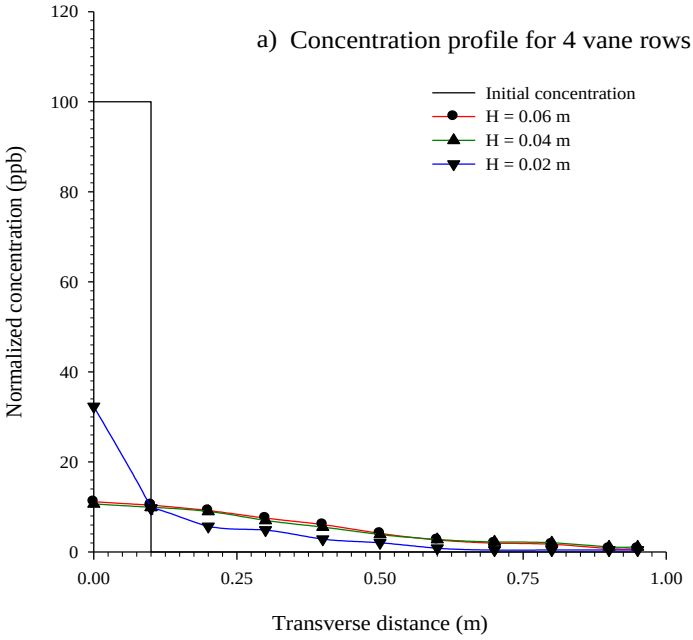

Fig. 6.4 a Concentration distribution of dye across the transects for 4 vane rows for h = 0.1025 m and x = 5m

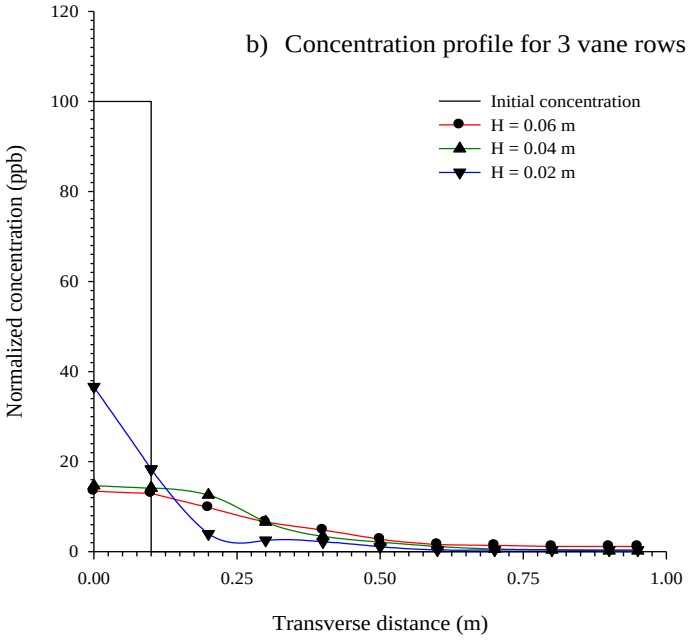

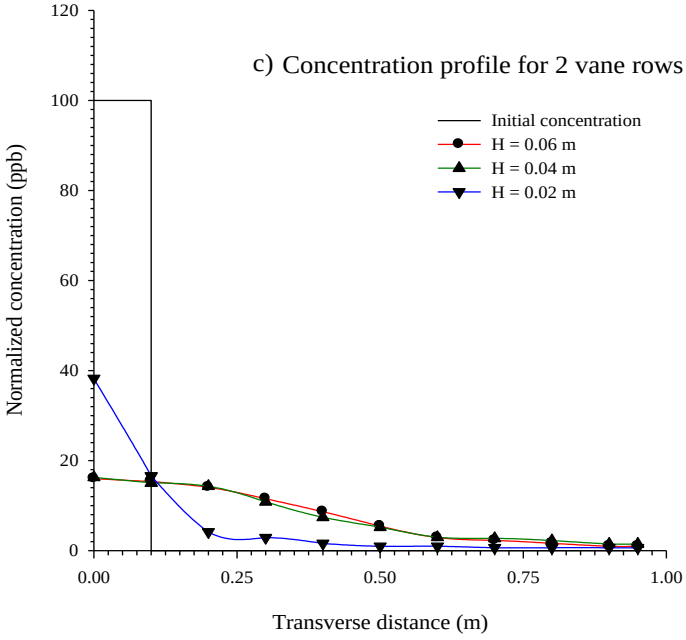

Fig. 6.4 b-c Concentration distribution of dye across the transects for b) 3 vane rows; c) 2 vane rows for h = 0.1025 m and x = 5m

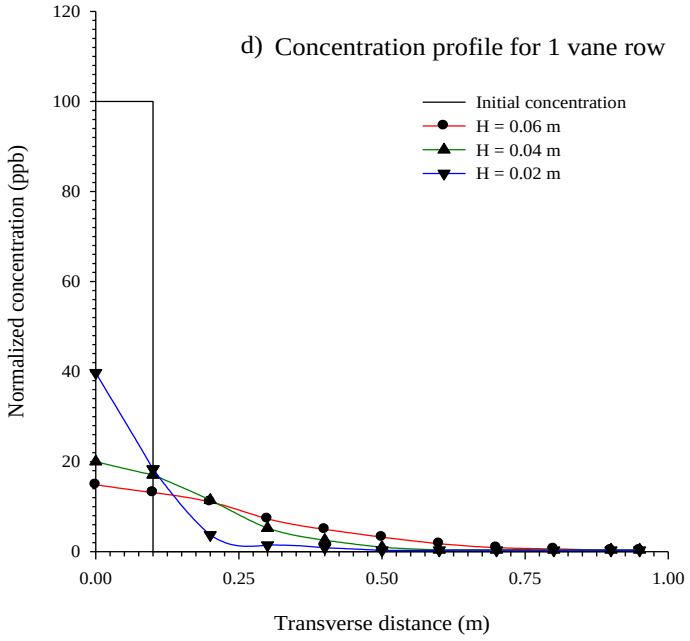

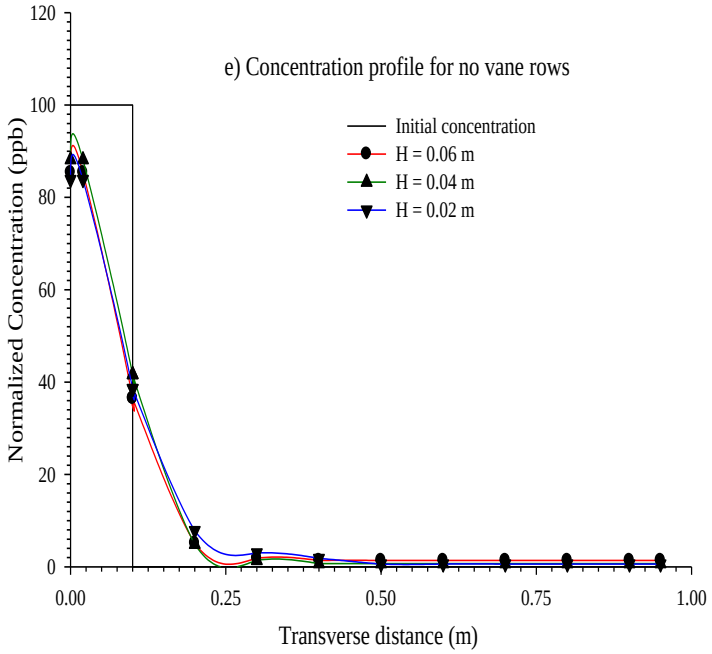

Fig. 6.4 d, e Concentration distribution of dye across the transect for d) 1 vane row; e) no vane row for h = 0.1025 m and x = 5m.

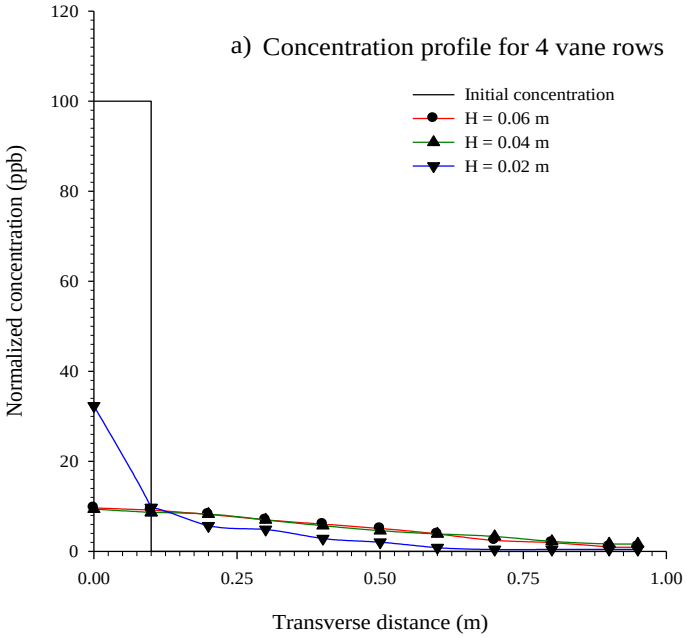

Fig. 6.5 a Concentration distribution of dye across the transects for 4 vane rows for h = 0.1025 m and x = 15m

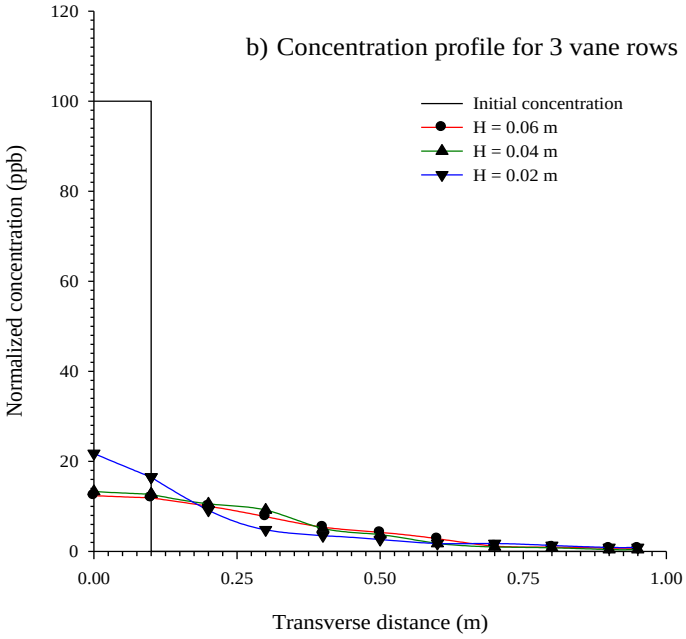

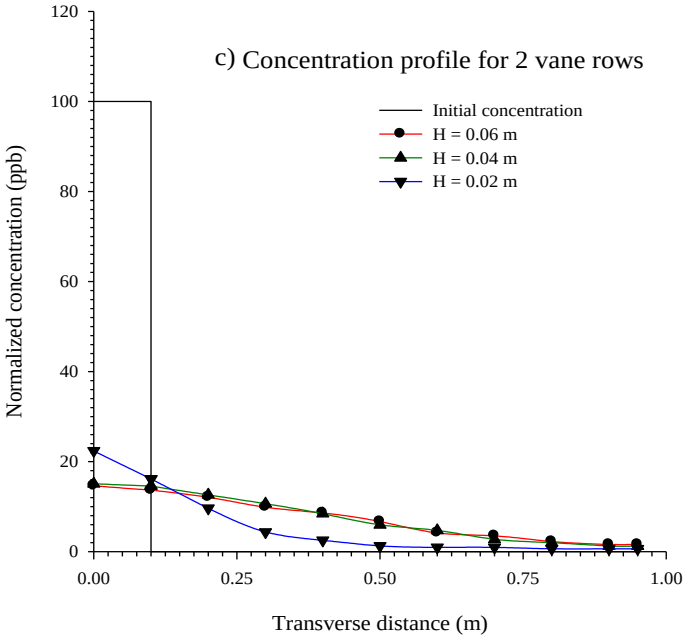

Fig. 6.5 b-c Concentration distribution of dye across the transects for b) 3 vane rows; c) 2 vane rows for h = 0.1025 m and x = 15m

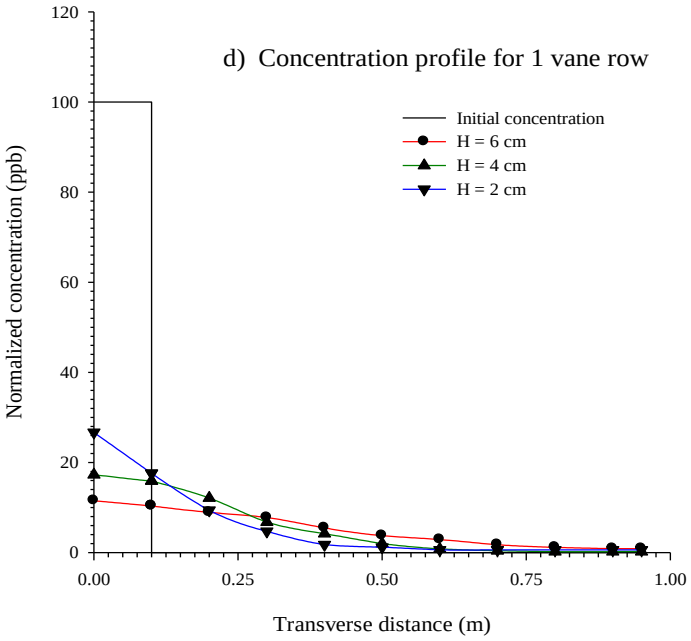

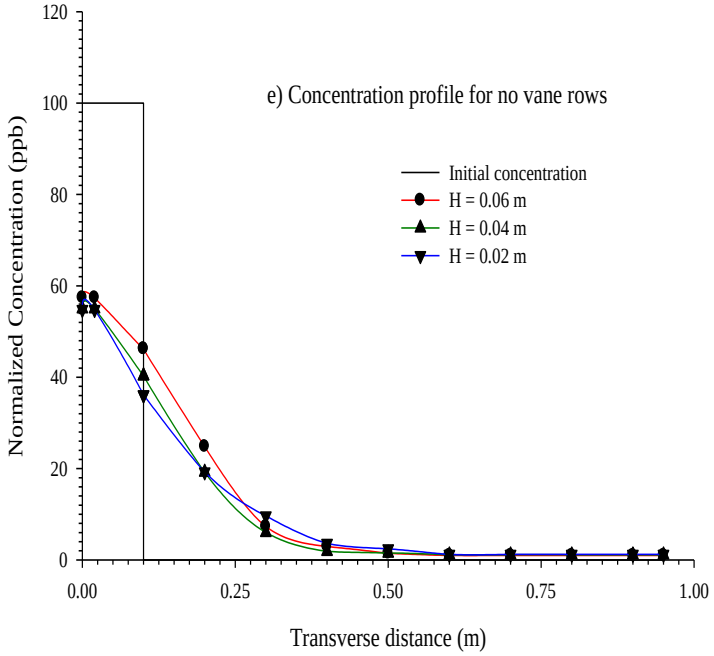

Fig. 6.5 d, e Concentration distribution of dye across the transects for d) 1 vane row; e) no vane row for h = 0.1025 m and x = 15m

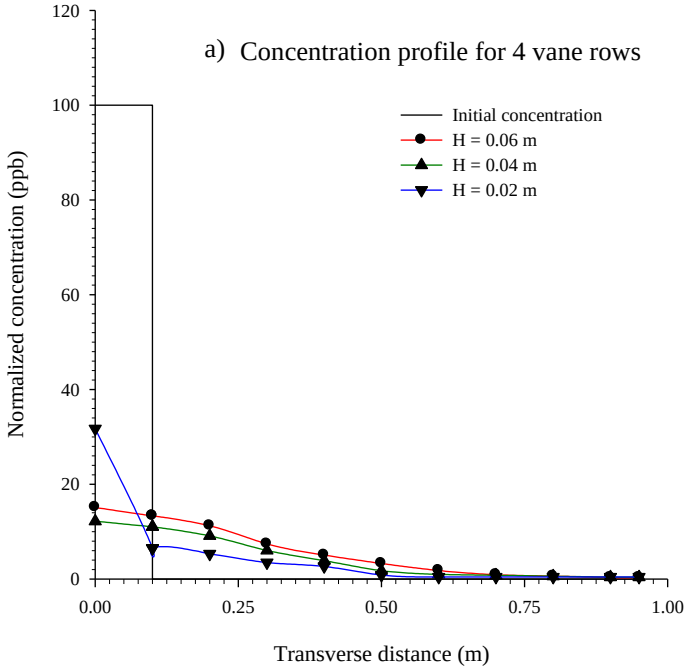

Fig. 6.6 a Concentration distribution of dye across the transects for 4 vane rows for h = 0.09 m and x = 5m

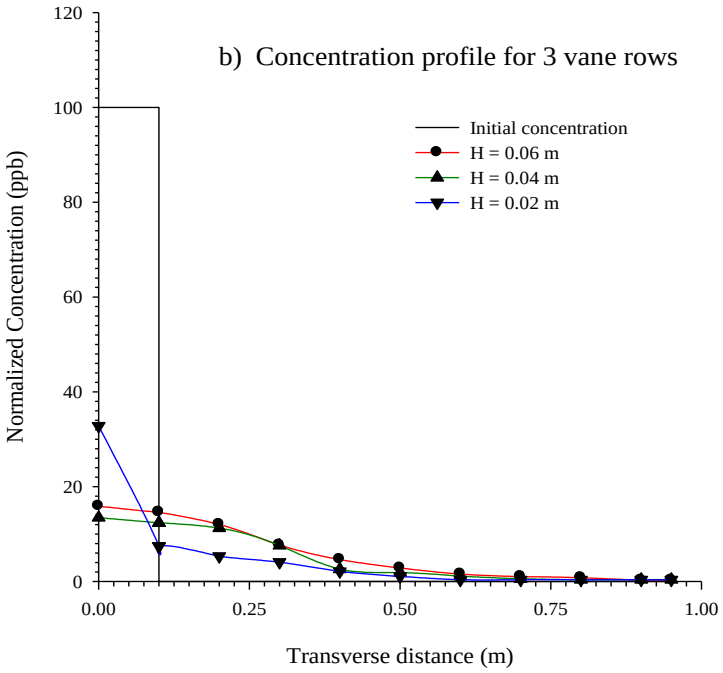

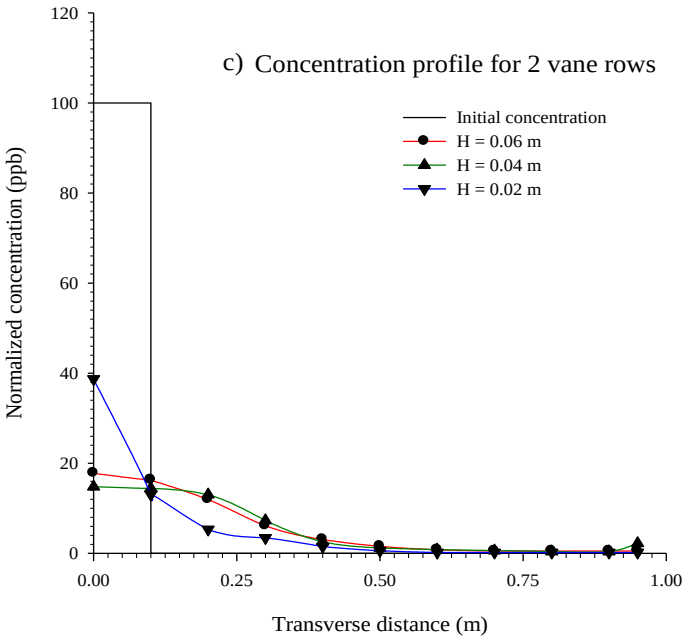

Fig. 6.6 b-c Concentration distribution of dye across the transects for b) 3 vane rows; c) 2 vane rows for h = 0.09 m and x = 5m

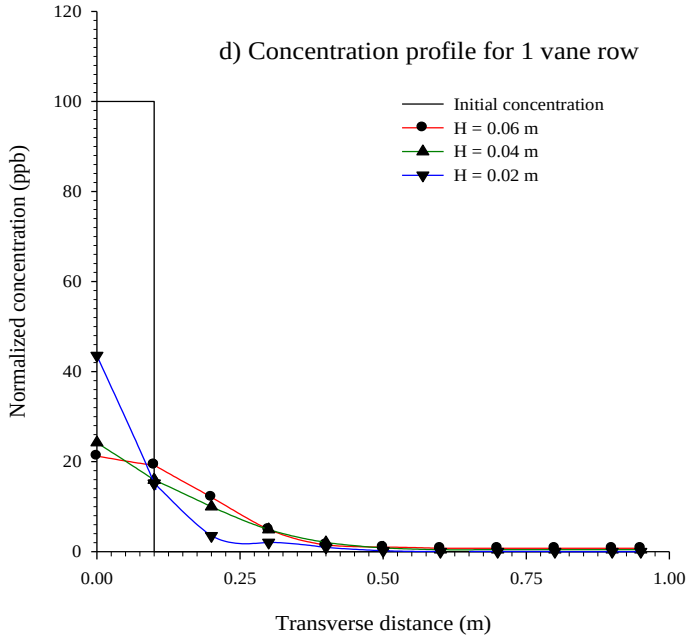

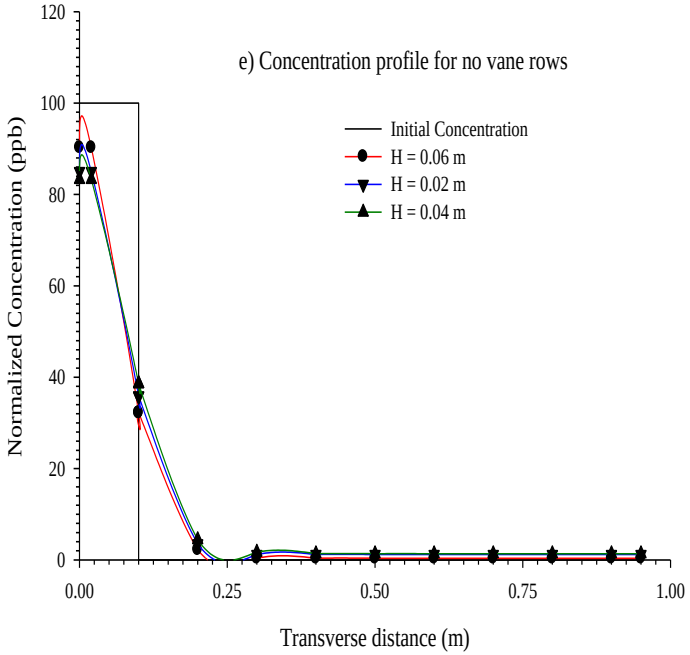

Fig. 6.6 d, e Concentration distribution of dye across the transects for d) 1 vane row; e) for no vane rows for h = 0.09 m and x = 5m.

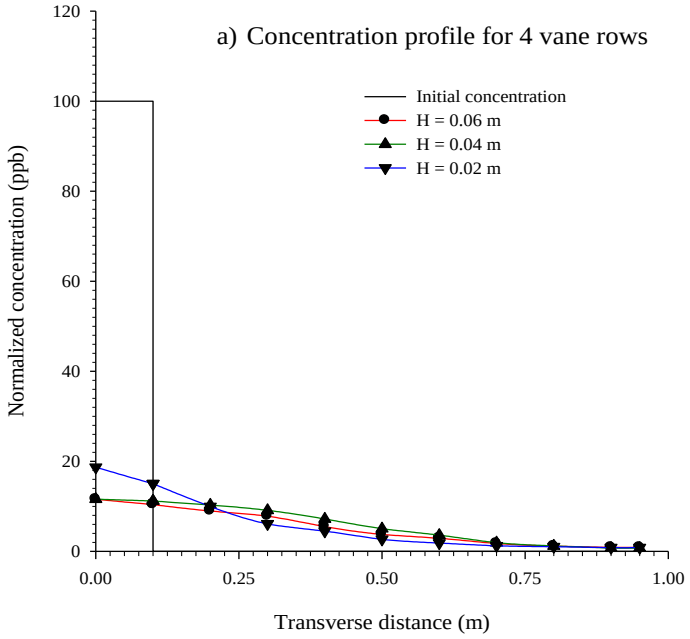

Fig. 6.7 a Concentration distribution of dye across the transects for 4 vane rows for h = 0.09 m and x = 15m

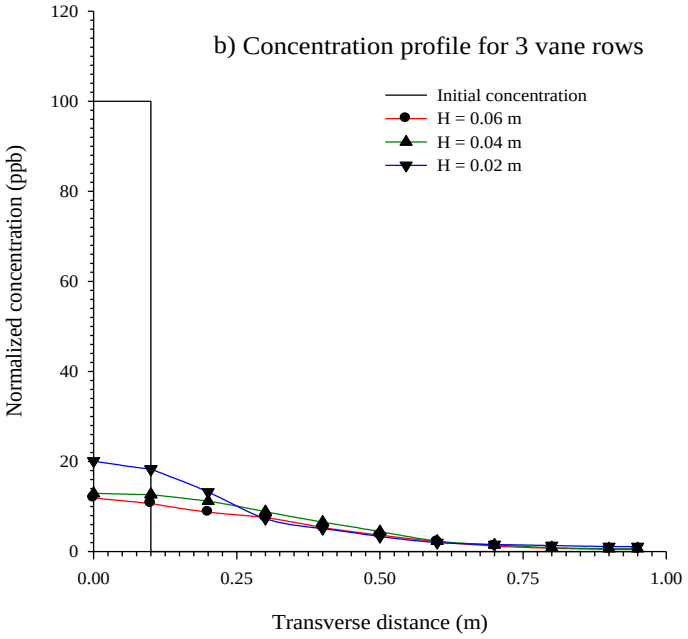

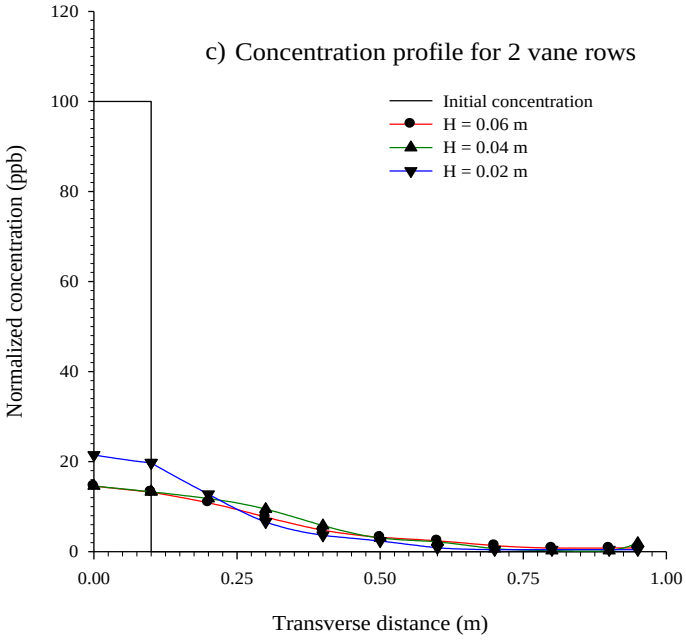

Fig. 6.7 b-c Concentration distribution of dye across the transects for b) 3 vane rows; c) 2 vane rows for h = 0.09 m and x = 15m

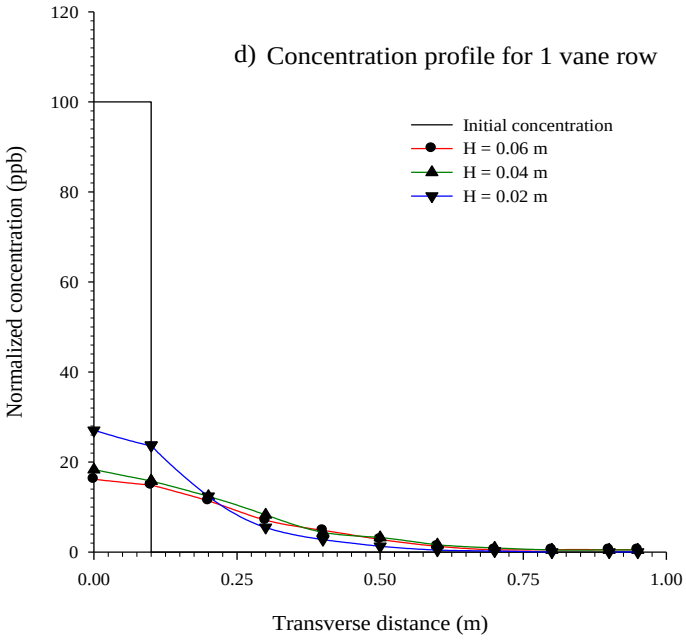

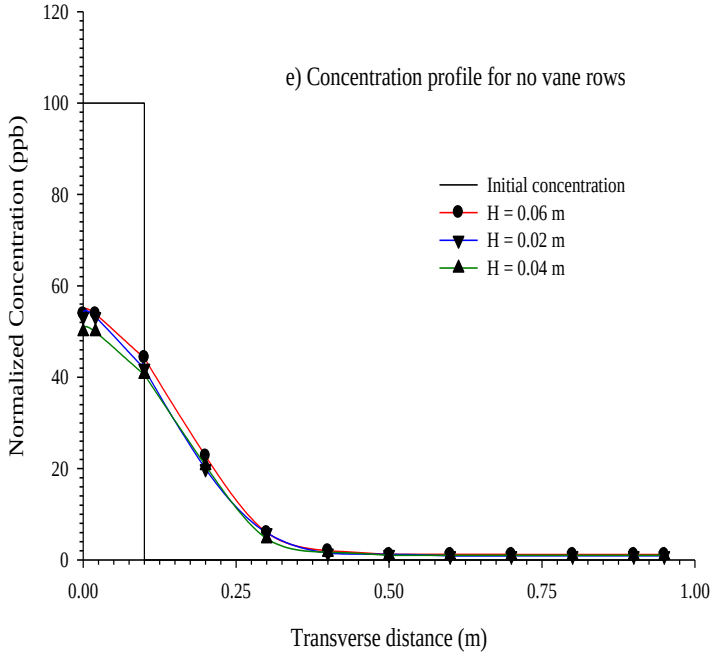

Fig. 6.7 d, e Concentration distribution of dye across the transects for d) 1 vane row; e) for no vane rows for h = 0.09 m and x = 15m.

6.4 EFFECT OF SUBMERGED VANES ON TRANSVERSE MIXING COEFFICIENT

Figures 6.8 a-c shows variation of ratio of transverse mixing coefficients with vane (E_{yv}) and without vane (E_y) with ratio of height of vane and depth of flow. From these figures, it can be seen that as the vane size increases there is a drastic increase in the transverse mixing coefficient. This is due to the fact that a high magnitude of transverse circulations is generated in the flow as vane size increases.

Further, the transverse mixing coefficient for higher arrays/rows of vanes is high. For example for depth of flow of 0.1241 m, the transverse mixing coefficient for four, three, two and one array of vanes of vane size 0.06 m $\times$ 0.12 m, are 23, 17, 13, and 7.5 times, respectively higher than the transverse mixing coefficients with no vane condition (Fig. 6.14a). However such order of increase in the transverse mixing coefficient with vane for lower depth of flow is low. Flow with H/h of the order of 0.25 is not significant for enhancement in the transverse mixing.

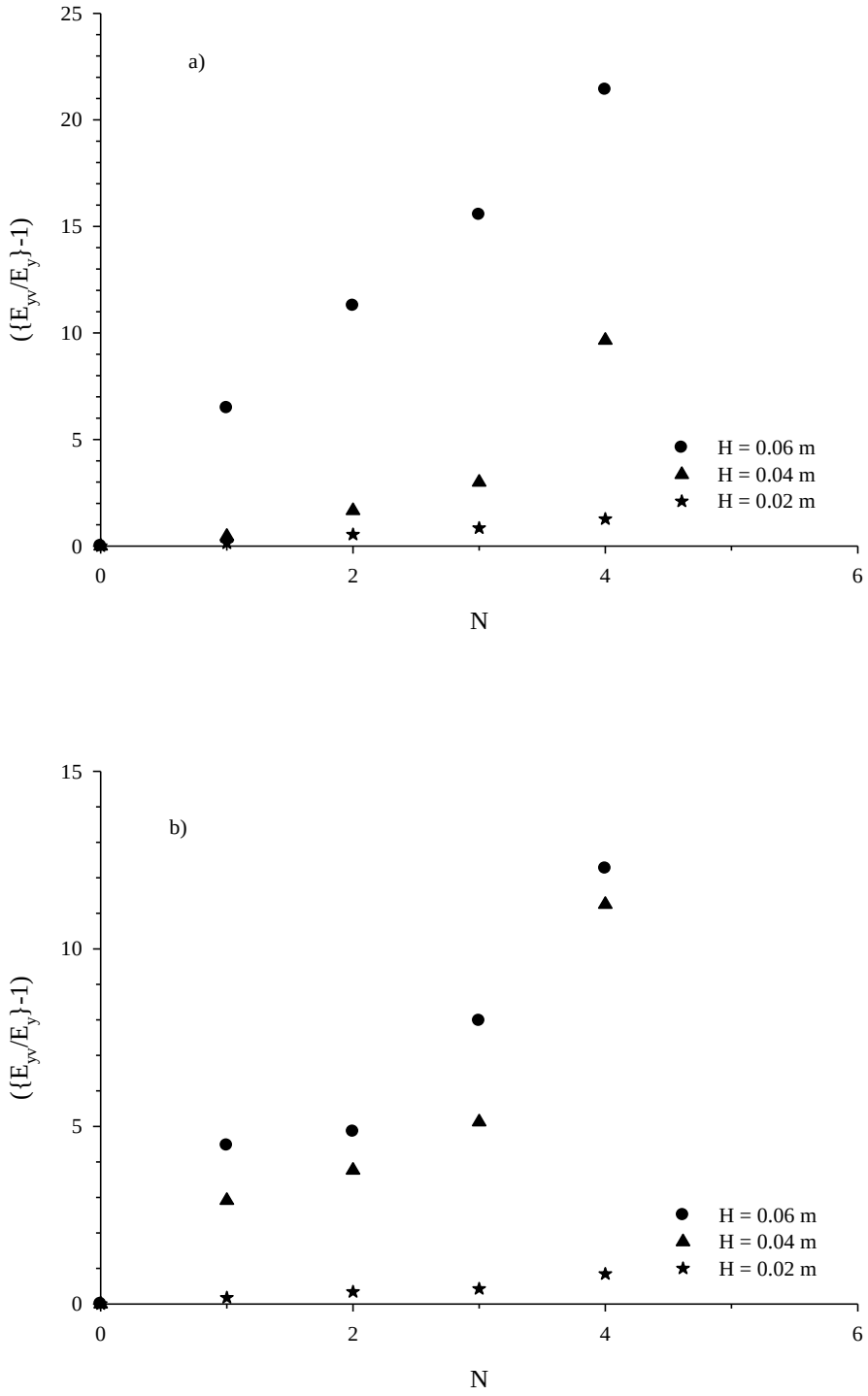

Fig. 6.8 a-b Variation of transverse mixing coefficient with number of vane rows for depth of flow a) 0.1241 m; b) 0.1025 m.

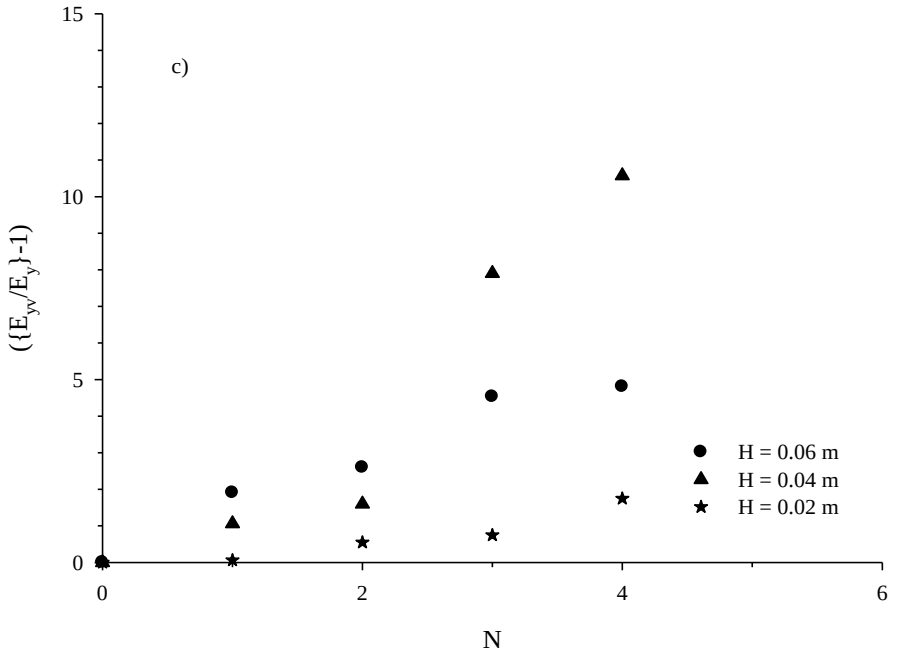

Fig. 6.8 c Variation of transverse mixing coefficient with number of vane rows for depth of flow = 0.09 m.

Using the collected data, the following relationship is proposed to inherit the effect of the submerged vanes on the transverse mixing coefficient:

$$\frac{E_{yv}}{E_y} - 1 = 7.6404(\mathrm{H/h})^{2.2043}(N)^{1.3313} \qquad (R^2 = 0.75) \qquad (6.1)$$

Here, E_{yv} = Transverse mixing coefficient with vanes; E_y = Transverse mixing coefficient for plane shear flow condition; H = height of vane; h = depth of flow and N = number of vane rows. Results clearly indicate that as the value of H/h increases, transverse mixing increases as the height of vane is a measure of size of circulation that will induce in the flow. Also, the numbers of vane rows are in direct proportion with the extent of transverse mixing process as can be seen from Eq. (6.1). Fig. 6.9 shows the degree of agreement between the predicted values of E_{yv}/E_y-1 and observed values of E_{yv}/E_y-1. It can be observed that a good degree of agreement was observed between predicted and observed values.

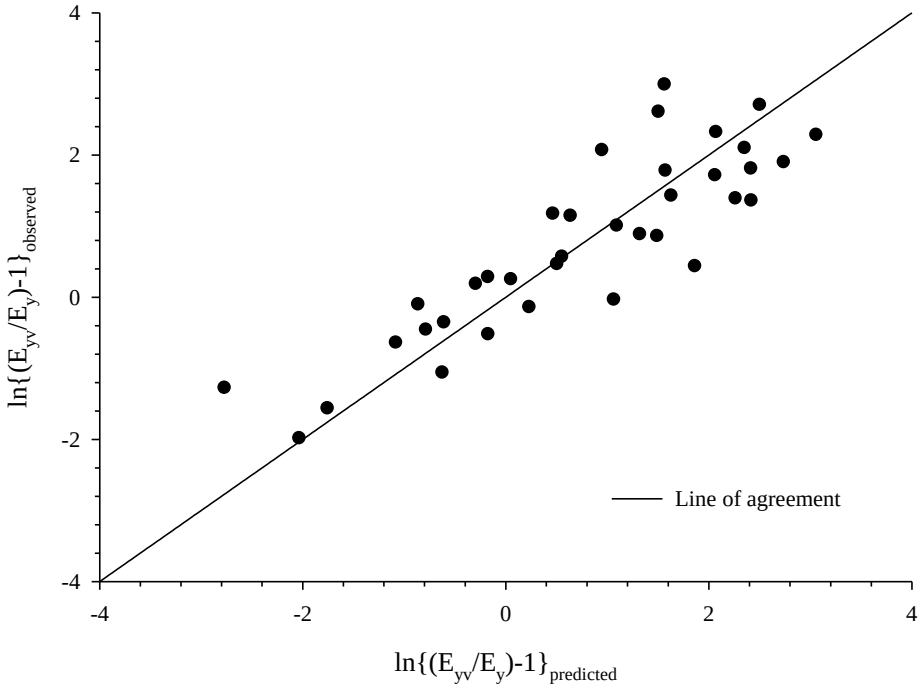

Fig. 6.9 Degree of agreement between predicted *ln*{($E_{yv}/E_{y)}$-1} and observed *ln*{($E_{yv}/E_{y)}$-1}.

6.5 VALIDATION OF TRANSVERSE MIXING COEFFICIENT PREDICTOR

In order to validate the use of predictor, concentration profiles were plotted for two longitudinal distance *viz.* 5m and 15 m from the point of injection in the presence and absence of vanes in which concentration profiles were predicted using value of transverse mixing coefficient calculated by Eq. (6.1) and using scheme developed by Ahmad (2008).

It can be observed from Figs. 6.10-6.13 that predictor not only predicted the profiles in proficient way but also reinstated the fact that in the presence of vanes, transverse mixing rate enhances. The predicted variation of concentration profiles can be compared with the profiles measured experimentally and it can easily be deduced that predicted concentration profiles have similar variation with the experimentally measured concentration profiles. Hence, it can be said that Eq. (6.1) can be used to predict the transverse mixing coefficient for determination of concentration profiles in the presence of vanes.

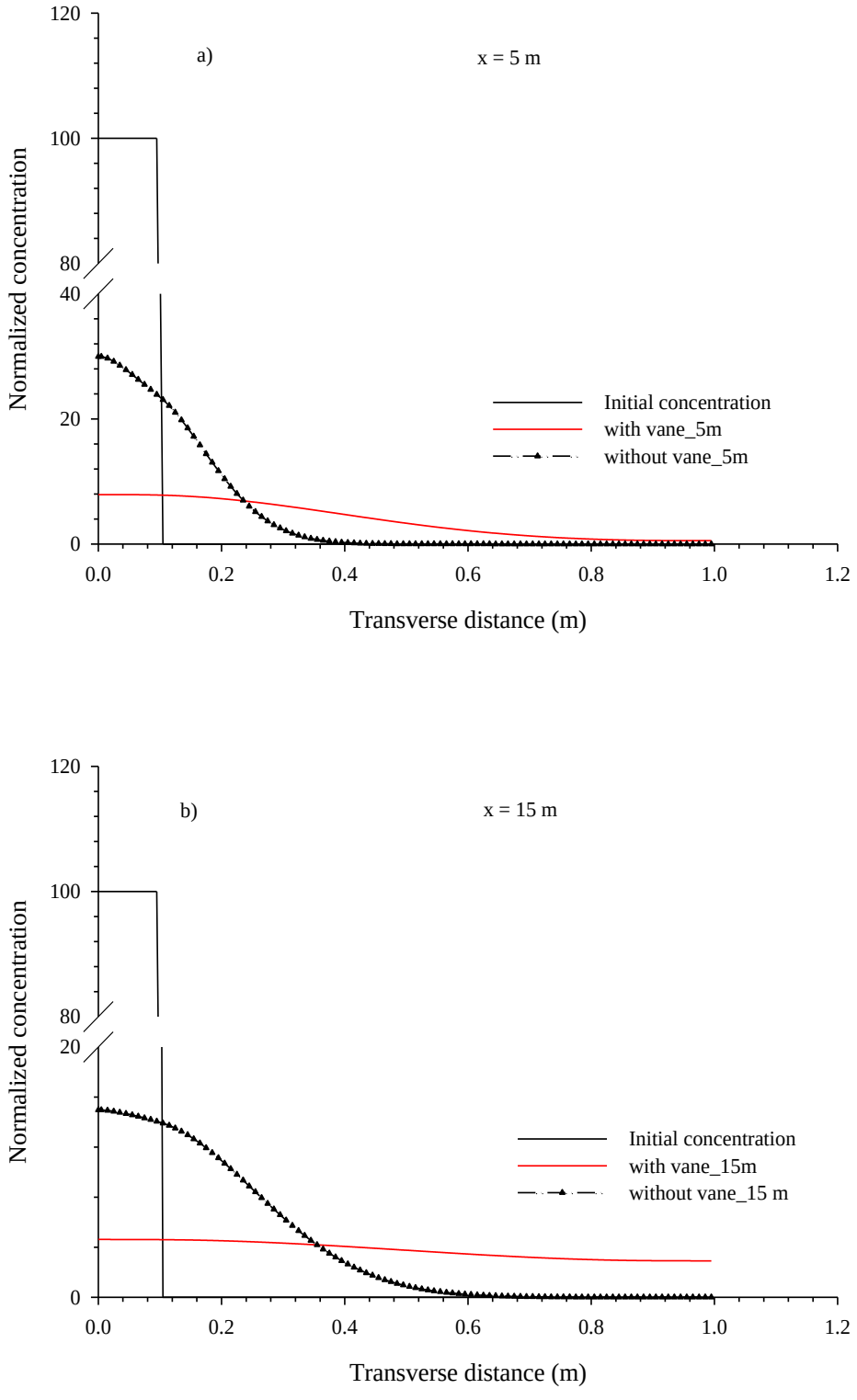

Fig. 6.10 Validation of concentration profiles with vanes and without vanes from predicted E_y for a) x = 5m and b) x = 15 m for depth of flow = 0.1241 m and height of vane = 0.06 m.

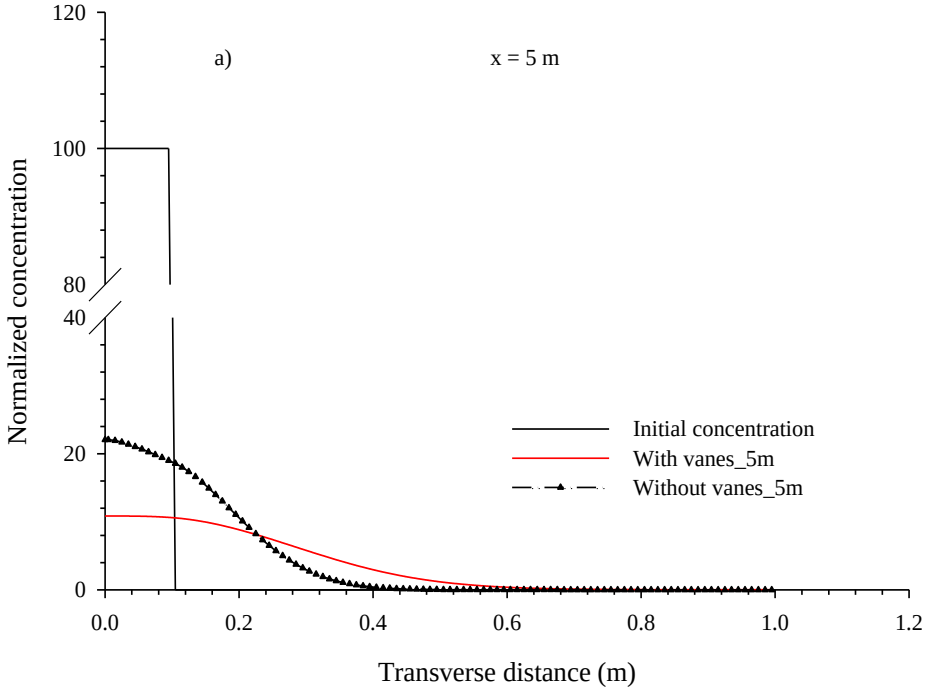

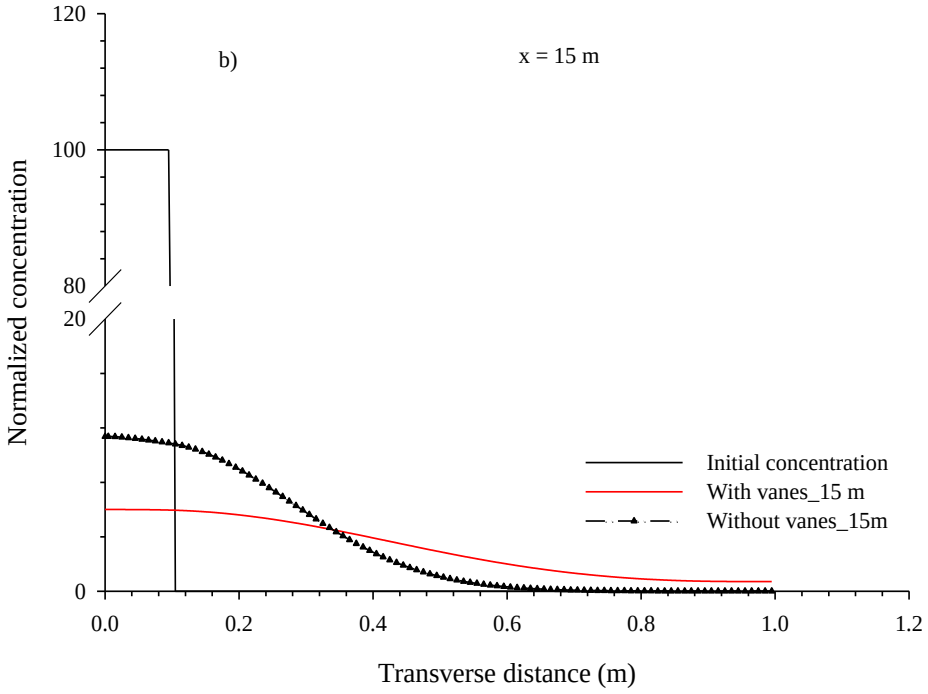

Fig. 6.11 Validation of concentration profiles with vanes and without vanes from predicted E_y for a) x = 5m and b) x = 15 m for depth of flow = 0.1025 m and height of vane = 0.04 m.

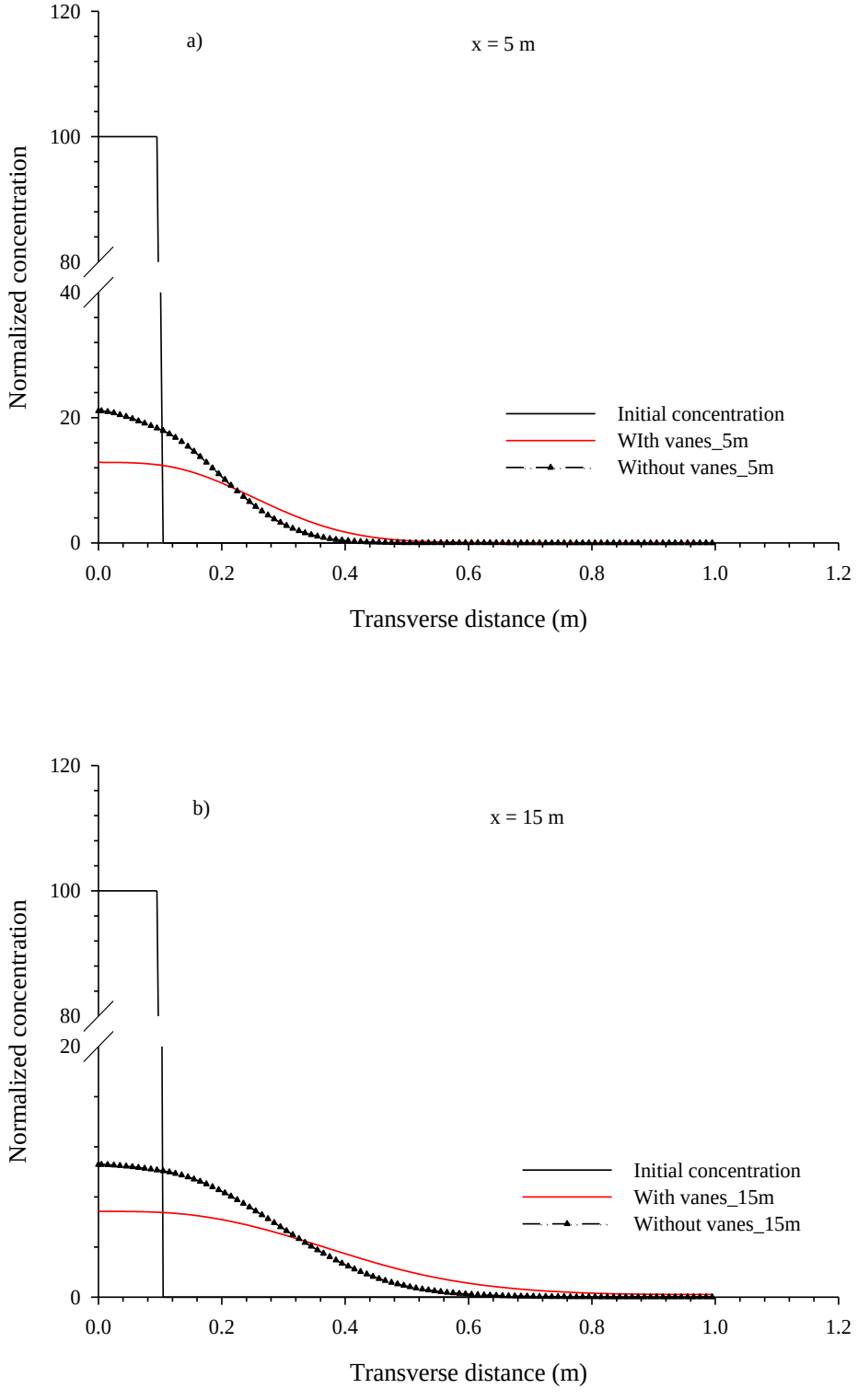

Fig. 6.12 Validation of concentration profiles with vanes and without vanes from predicted E_y for a) x = 5m and b) x = 15 m for depth of flow = 0.09 m and height of vane = 0.02 m.

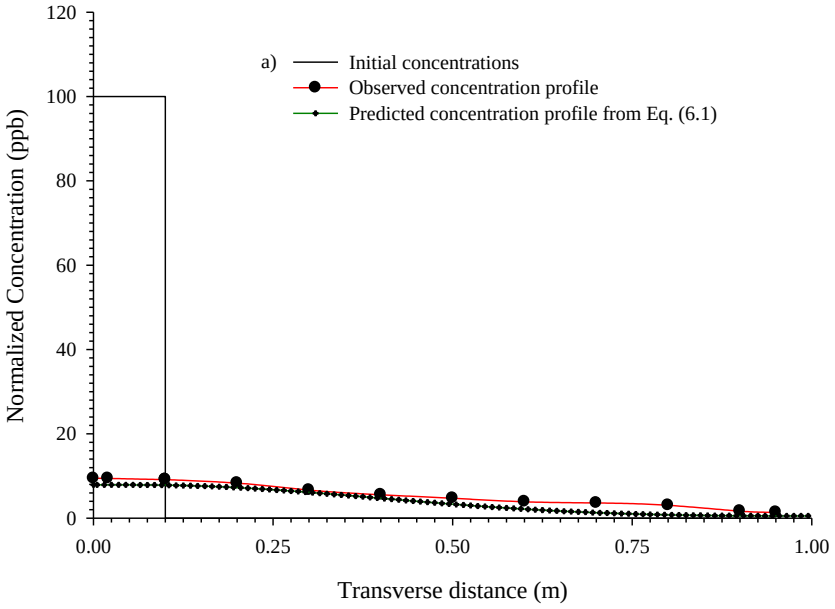
a)
Initial concentrations
Observed concentration profile
Predicted concentration profile from Eq. (6.1)
Normalized Concentration (ppb)
120
100
80
60
40
20
0
0.00
0.25
0.50
0.75
1.00
Transverse distance (m)

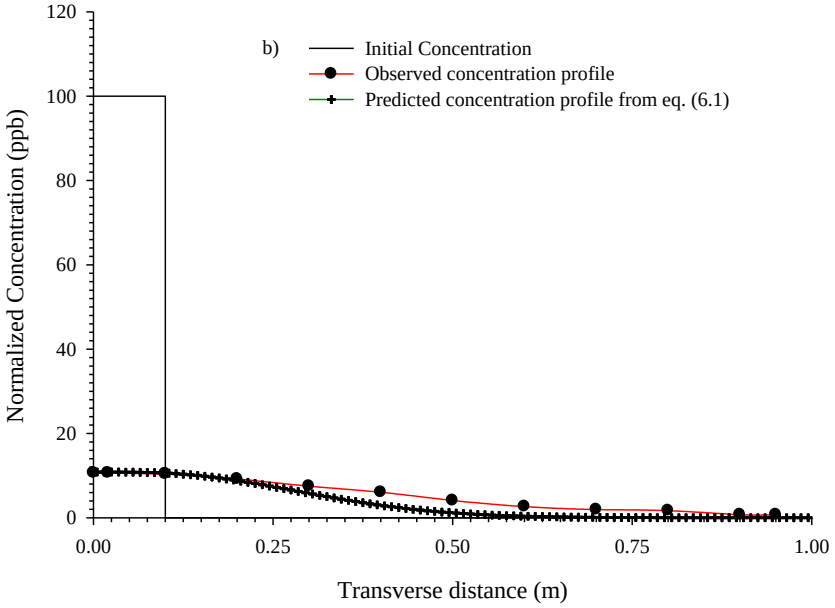
b)
Initial Concentration
Observed concentration profile
Predicted concentration profile from eq. (6.1)
Normalized Concentration (ppb)
120
100
80
60
40
20
0
0.00
0.25
0.50
0.75
1.00
Transverse distance (m)

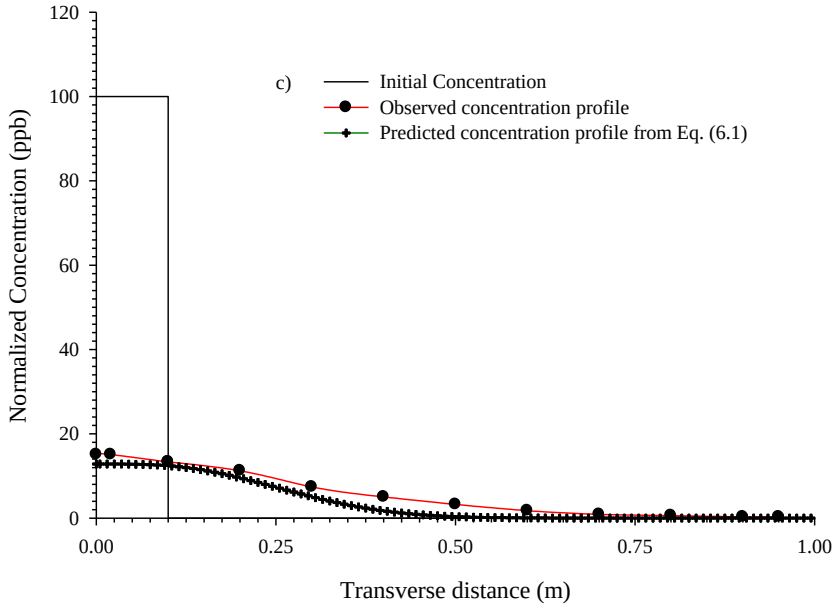

Fig. 6.13 Comparison of observed and predicted concentration profiles for 4 vane rows for depth of flow a) 0.1241 m; b) 0.1025 m and c) 0.09 m.

Transverse mixing length is an important parameter in the establishment of longitudinal movement of pollutants because it is assumed that after transverse mixing is completed then only the mixing in longitudinal direction will start prominently (Fischer, 1979; Rutherford, 1994). Transverse mixing length is given by following formula (Ahmad, 2009):

$$L_m = K\frac{UB^2}{E_y} \tag{6.2}$$

Here, K = a constant whose value is 0.44 for the discharge of pollutants from either of the bank for 95% mixing and 0.54 for the discharge of pollutants from either of the bank for 98% mixing. From Eq. (6.2) it can be observed that transverse mixing length is in inverse proportion with the transverse mixing coefficient, i.e. more will be the transverse mixing coefficient less will be the length of transverse mixing and less will be the movement of pollutants in the longitudinal direction. Transverse mixing length was calculated for three graphs shown above for 98% mixing case and it was observed that for 0.06 m vane and depth of flow = 0.1241 m, tracer mixes 11 times faster than its absence. In case of 0.04 m vane and depth of flow = 0.1025 m, this mixing length in presence of vane was around 3.5 times shorter

than what it has to be without vane. For 0.02 m vane and depth of flow = 0.09 m, tracer was observed to mix 2 times faster than without vanes. Hence, mixing length also shows the effect of submerged vanes in enhancing the tracer transverse mixing.

6.6 CONCLUDING REMARKS

Following conclusions can be drawn from present chapter:

- In the presence of submerged vanes turbulence parameters like turbulent kinetic energy, turbulent intensities and Reynolds stress were observed to increase drastically due to the vortices formed due to separation from trailing edge.
- It was observed that the point of origin of vortices was observed to be 0.85 times vane height in each case, which was in accordance with the observation of Odgaard and Wang (1991 a) who suggested that vortices originated just below the tip of trailing edge and position of the point of vortices is 0.8 times vane height.
- It can be seen that as the number of vane rows were increased, the transverse mixing was also observed to increase. The reason for this increase in the rate of transverse mixing was that the vane rows generated a complex but a large field of circulation, in which secondary currents dominates the flow.
- Transverse mixing coefficient was observed to be a strong function of number and size of vanes, i.e., as the size and number of vanes were increased, an increase in the transverse mixing coefficient was observed.
- A predictor of transverse mixing was proposed here which will predict the transverse mixing coefficient in the presence of submerged vanes by taking into account the relative height of vane (i.e. non-dimensionalized height of vane with depth of flow) and number of vane rows and value of R^2 of the predictor was 0.75.
- It was observed that plotting the degree of agreement of observed and predicted value of non-dimensionalized transverse mixing coefficient with vane rows, a good agreement was obtained around line of agreement.
- By plotting the concentration profiles using the values of transverse mixing coefficient calculated from Eq. (6.1), it was observed that predicted concentration profiles were in accordance with the variation of concentration profiles obtained experimentally.

- It was observed that tracer mixes 11 times, 3.5 times and 2 times faster for 0.06 m high vane and 0.1241 m deep flow, 0.04 m high vane and 0.1025 m deep flow and 0.02 m high vane and 0.09 m deep flow, respectively.

Chapter

7

CONCLUSIONS

The following conclusions have been drawn from the present study:

1. The governing equation for the transient transverse mixing in a prismatic channel is solved by finite volume method using upwind and central difference schemes. The model takes care of variation of transverse mixing coefficient across the width. Satisfactory agreement is found between concentration profiles computed using the proposed finite volume model and the analytical model for constant mixing coefficient and continuous pollutant injection.

2. A computational fluid dynamics model to simulate flow pattern and turbulence characteristics around and downstream of a submerged vane and a series of vane rows containing multiple vanes in a single row is developed on ANSYS-CFX platform. *K*-ω turbulence model is used herein.

3. For the single vane, the developed CFD model was validated for simulated transverse velocity profile with the observed transverse velocity profile of Wang and Odgaard (1993). It was observed that for each of the transects the simulated transverse velocity profile matches with the observed transverse velocity profile in a satisfactory manner. For the multiple vane arrays system, the developed CFD model is validated by comparing simulated longitudinal velocity at three sections *viz.* x = 3H, 8H and 20H with the measured values in the present study. Good agreement between the simulated and observed velocity profiles were observed. Such validation was also done for measured transverse velocity with the simulated transverse velocity profile.

4. In order to optimize vane parameters using the CFD, model for various vane configurations and depth of flow were created and used to optimize so as to generate circulation of maximum intensity. It was observed that when angle of attack of vane was 28.7^{o} and height of vane was 0.4 times depth of flow, circulations of maximum intensity were generated. For optimizing the length of vane, it was observed that as length of vane was increased, vorticity of vane was also increased. This increase is attributed to high drag force due to increase in contact area.

5. Longitudinal spacing of vane arrays and lateral spacing between vanes were the two main components that were optimized to obtain maximum circulations from multiple vane rows (in present study it varied from one vane row to four vane rows). It was observed that for multiple vane arrays when lateral spacing was 3H, circulations of maximum intensity were generated. In order to optimize longitudinal spacing, a method was recommended in which to acquire vorticity of a given strength (say 50 % of the strength of the vorticity generated by pre-installed vane row) in the downstream of a pre-installed vane row, the distance, x/H, is can be read from the graph.

6. Flow around the single vane was simulated using CFD and it was observed that leading edge of vane was responsible for the generation of tip vortices downstream of the vane. A sheet of separated vortices was also observed downstream of the single vane. In the suction side of the vane, the separated vortex was observed to break into two counter-rotating vortices due to low pressure. The turbulent kinetic energy of flow also varies on the same pattern. Simulated flow pattern around multiple array of vanes indicate that near to the submerged vanes a large vortical field exists. A large field of turbulence was observed near distance, however, at further downstream, it was observed that vortices interacted with each other to make a large vortical field with a less effective vorticity. It was further observed that going further downstream, vorticity was reduced and subsequently effects of submerged vanes were reduced. Due to reduction in effective vorticity and simultaneous effect of viscosity on the generated vortices, they were completely diminished in the flow.

7. Analysis of measured instantaneous velocity downstream of the zero, one, two, three and four arrays of submerged vanes indicates that in the presence of vanes, flow near to the vane is highly unstable and chaotic. The turbulence is clearly having heterogeneity as going up in the vertical direction. The variation of all turbulence characteristics was same in all directions and

was nearly overlapping to each other for measured instantaneous velocity at three transects in case of plane shear flow.

8. Variation of transverse velocity along the depth for zero, one, two, three and four array of vanes was studied experimentally. It was observed that the extent of field of secondary current is in proportion with the number of vane arrays, i.e. more will be the number of vane arrays larger will be the extent of secondary current region. Thus, larger area was observed to be available for the tracer for its mixing. It was also observed that more and more fluid was advected to the transverse direction when the multiple vane arrays were present.

9. Effect of the submerged vanes on tracer concentration profiles was studied experimentally. For this purpose, variation of tracer concentration across the width of the channel at distance x = 5 m and 15 m for the depth of flow = 0.09 m, 0.1025 m and 0.1241 m, vane height = 0.02 m, 0.04 m, and 0.06 m and vane rows = 0, 1, 2, 3, and 4 was studied. It was seen that in the case of 4 vane rows, generation of circulation field was large and was extended to a greater distance; hence the mixing was highest in the case of 4 vane rows. As the numbers of vanes were reduced, the mixing was also reduced.

10. Transverse mixing coefficients were obtained from the measured concentration profiles for three vane dimensions *viz.* 0.02 m $\times$0.05 m, 0.04 m $\times$ 0.1 m and 0.06 m $\times$ 0.12 m for four, three, two, one and no vane row arrays for three different depths of flow *viz*. 0.09 m, 0.1025 m and 0.1241 m. It was found that as the vane size increases there is a drastic increase in the transverse mixing coefficient. This is due to the fact that a high magnitude of transverse circulations is generated in the flow as vane size increases.

11. Further, the transverse mixing coefficient for higher arrays/rows of vanes is high. For an example, for the depth of flow of 0.1241 m, the transverse mixing coefficient for four, three, two and one array of vanes are 23, 17, 13, and 7.5 times, respectively higher than the transverse mixing coefficients with no vane condition. However, such order of increase in the transverse mixing coefficient with vane for lower depth of flow is low. Flow with vane height/depth of flow of the order of 0.25 is not significant for the enhancement in the transverse mixing.

12. A predictor has been proposed to estimate the transverse mixing coefficient in presence of vane. It was observed that the proposed predictor estimates the transverse mixing coefficient in satisfactory manner.

13. Transverse mixing length was studied and it is observed that tracer mixes 11 times, 3.5 times and 2 times faster for 0.06 m high vane and 0.1241 m depth of flow, 0.04 m high vane and 0.1025 m depth of flow and 0.02 m high vane and 0.09 m depth of flow, respectively.

REFERENCES

1. Ahmad, Z. (2007) *Two-dimensional mixing of pollutants in open channels*. A technical report submitted to DST, New Delhi.

2. Ahmad, Z. (2008) "Finite volume model for steady-state transverse mixing in streams.", Journal of Hydraulic Research, Vol. 46/Issue: extra, 72-80.

3. Ahmad, Z. (2009) "Mixing length for establishment of longitudinal dispersion in streams.", International Journal of Modelling & Simulation, 29(2**)**, 1-10.

4. Ahmad, Z. and Kothyari, U.C. (2001) "Time-line cubic spline interpolation scheme for solution of advection equation.", Journal of Computers and Fluids, 30, 737–752.

5. Ahmad, Z., Kothyari, U. C., and Ranga Raju, K. G. (1999) "Finite difference scheme for longitudinal dispersion.", Journal of Hydraulic Research, 37 (3), 389-406.

6. Ahmad, Z., Azmathulla, M.H., and Zakaria, N.A. (2011) "ANFIS based approach for estimation of transverse mixing coefficient.", Water Science and Technology, 63, 1005-1010.

7. Albers, C., and Steffler, P. (2007) "Estimating transverse mixing in open channels due to secondary currents induced shear dispersion.", Journal of Hydraulic Engineering, 133, 186–196.

8. Allahyonesi, H., Omid M.H., and Haghiabi, A.M. (2008) "A study of effects of longitudinal arrangement sediment behavior near intake structures.", Journal of Hydraulic Research, 46(6), 814-819.

9. Ansys CFX (2011) *Ansys ICEM CFD User's Manual.* Ansys Inc., USA.

10. Aware, R., Ahmad, Z., and Asawa, G.L. (2005) "Scour control by submerged vanes in a curved channel.", ISH Journal of Hydraulic Engineering, 11(3), 81-90.

11. Azmathulla, H.M., and Ghani, A.A. (2011) "Genetic programming for predicting longitudinal dispersion coefficients in streams.", Water Resources Management, 25, 1537-1544.

12. Azmathulla, H.M., and Ahmad, Z. (2012) "Gene-expression programming for transverse mixing coefficient.", Journal of Hydrology, 434-435, 142-148.

13. Azizi, R., Bejestan, M.S., and Ghomeshi, M. (2012) "Scour depth at the edge of different submerged vanes shapes.", Journal of Applied Sciences, 12, 362-368.

14. Baek, K.O., and Seo, I.W. (2010) “Routing procedures for observed dispersion coefficients in two dimensional river mixing.”, Advances in Water Resources, 33, 1551–1559.

15. Barkdoll, B.D., Ettema, R., and Odgaard, A.J. (1999) “Sediment control at lateral diversions: limits and enhancements to vane use.”, Journal of Hydraulic Engineering, 125(8), 862-870.

16. Beltaos, S, and Day, T.J. (1976) *Longitudinal dispersion in a natural stream: Lesser Slave River.* Alberta Report No.REH/76/1 Alberta Co-operative Research Program in Highway and River Engineering Edmonton Alberta.

17. Beltaos, S. (1980) “Transverse mixing tests in natural streams.”, Journal of Hydraulic Division, 106(HY10), 1607-1625.

18. Bertin, J.J., and Smith, M.L. (1979) *Aerodynamics for engineers,* First edition, Prentice Hall, New Jersey, USA.

19. Bhuyian, F., Hey, R.D., and Wormleaton P.R. (2010) “Bank attached vanes for bank erosion control and restoration of river meanders.”, Journal of Hydraulic Engineering, 136(9), 583-596.

20. Biron, P.M., Ramamurthy, A.S., and Han, S. (2004) “Three dimensional numerical modeling of mixing at river confluences.”, Journal of Hydraulic Engineering, 130(3), 243–253.

21. Blinco, P.H., and Partheniades, E. (1971) “Turbulence characteristics in free surface flows over smooth and rough boundaries.” Journal of Hydraulic Research, 9, 43-69.

22. Boxall, J.B., and Guymer, I. (2001) “Estimating transverse mixing coefficients.”, Water Management, 148(4), 263-275.

23. Boxall, J.B., and Guymer, I. (2002) “Locating outfalls on meandering channels to optimize transverse mixing.”, Journal of the Charted Institution of Water and Environment Management, 16(3), 194-198.

24. Boxall, J.B., and Guymer, I. (2003 a) “Analysis and prediction of transverse mixing coefficients in natural channels.”, Journal of Hydraulic Engineering, 129(2), 129-139.

25. Boxall, J.B., and Guymer, I. (2003 b) “Transverse mixing in natural open channels.”, XXX IAHR Congress Greece, 309-315.

26. Boxall, J.B., Guymer, I., and Marion, A. (2003) “Transverse mixing in natural sinuous natural open channel flows.”, Journal of Hydraulic Research, 41(2), 153–165.

27. Bradford, S.F., and Sanders, B.F. (2002) “Finite volume model for shallow water flooding of arbitrary topography.”, Journal of Hydraulic Engineering, 128(3), 289-298.

28. Bruno, M.S., Muntisov, M., and Fischer, H.B. (1990) “Effect of buoyancy on transverse mixing in streams.”, Journal of Hydraulic Engineering, 116(12), 1484–1494.

29. Brusseau, M.L., Hu, Q., and Srivastava, R. (1997) "Using flow interruption to identify factors causing non-ideal contaminant transport.", Journal of Contaminant Transport, 24(4), 205-219.

30. Capart, H., Eldho, T.I., Huang, S.Y., Young, D.L., and Zech, Y. (2003) "Treatment of natural geometry in finite volume river flow computations.", Journal of Hydraulic Engineering, 129(3), 385-393.

31. Chang, Y.C. (1971) *Lateral mixing in meandering channels.* Ph.D. thesis, University of Iowa, Iowa City, Iowa.

32. Chau, K.W. (2000) "Transverse mixing coefficient measurements in an open rectangular channel.", Advances in Environmental Research, 4, 287-294.

33. Chaudhuri, A., and Sekhar, M. (2005) "Probabilistic analysis of pollutant migration from landfills using stochastic finite element method.", Journal of Geotechnical and Geo-environmental Engineering, 131(8), 1042-1049.

34. Chaudhuri, A., and Sekhar, M. (2008) "Modeling of solute transport in a mild heterogeneous porous medium using stochastic finite element method: effect of random source conditions.", International Journal for Numerical Methods in Fluids, 56(5), 557-586.

35. Cotton, A.P., and West, J. (1980) "Field measurement of transverse diffusion in unidirectional flow in wide straight channel.", Water Research, 14(11), 1597-1604.

36. Demetracopoulos, A.C. (1994) "Computation of transverse mixing in streams.", Journal of Environmental Engineering, 120(3), 699–706.

37. Demetracopoulos, A.C., and Stefan, H.G. (1983) "Transverse mixing in wide and shallow river: case study.", Journal of Environmental Engineering, 109(3), 685–699.

38. Demuren, A.O., and Rodi, W. (1986) "Calculation of flow and pollutant dispersion in meandering channels.", Journal of Fluid Mechanics, 172, 63–92.

39. Dow, K.E., Steffler, P.M., and Zhu, D.Z. (2009) "Case study: Intermediate field mixing for a bank discharge in a natural river.", Journal of Hydraulic Engineering, 135(1), 1–12.

40. Elder, J.W. (1959) "The dispersion of marked fluid in turbulent shear flow.", Journal of Fluid Mechanics, 5, 544-560.

41. Eldho, T.I., and Rao, B.V. (1997) "Simulation of two-dimensional contaminant transport with dual reciprocity boundary elements.", International Journal of Engineering Analysis with Boundary Elements, 20(3), 213-228.

42. Eldho, T.I., Young, D.L., and Rao, B.V. (1999) "Use of the dual reciprocity boundary elements for simulation of groundwater flow and pollutant transport.", Journal of the Chinese Institute of Engineers, 22(6), 795-803.

43. Elhadi, N., Harrington, A., Lau, Y.L., and Krishnappan, B.G. (1984) "River mixing: a-state-of-the-art report.", Canadian Journal of Civil Engineering, 11(3), 585–609.

44. Engelund, F. (1969) "Dispersion of floating particles in uniform channel flow.", Journal of Hydraulic Division, 95, 1149-1162.

45. Engmann, J.E.O. (1974) *Transverse mixing characteristics of an ice-covered open channel flows*. PhD Thesis, University of Alberta.

46. Engmann, J.E.O., and Kellerhals, R. (1974) "Transverse mixing in an ice covered river.", Water Resources Research, 10(4), 775–784.

47. Ferziger, J. H., and Peric, M. (2002) *Computational Methods for Fluid Dynamics.* Springer, USA.

48. Fischer, H.B. (1969) "The effect of bends on dispersion in streams.", Water Resources Research, 5(2), 496–506.

49. Fischer, H.B., List, E.J., Koh, R.C.Y., Imberger, J., and Brooks, N.H. (1979) *Mixing in inland and coastal waters*. Academic Press, New York.

50. Flokstra, C. (2002) "Modelling of submerged vanes.", Journal of Hydraulic Research, 44(5), 591-602.

51. Ghorbani, B., and Kells, J.A. (2008) "Effect of submerged vanes on scour occurring at cylindrical pier.", Journal of Hydraulic Research, 46(5), 610-619.

52. Guan Y, Altinakar M.S., and Krishnappan B.G. (2002) "Two-dimensional simulation of advection-dispersion in open channel flows.", Proc. Fifth International Conference on Hydro-informatics Cardiff, UK, 226-231.

53. Gupta, U.P., Sharma, N., and Ojha, C.S.P. (2005) "Modelling of local scour around rectangular submerged vane.", ISH Journal of Hydraulic Engineering, 11(1), 57-66.

54. Gupta, U.P., Sharma, N., and Ojha, C.S.P. (2006 a) "Vorticity with different shapes of submerged vanes.", ISH Journal of Hydraulic Engineering, 12(1), 13-26.

55. Gupta, U.P., Sharma, N., and Ojha, C.S.P. (2006 b) "Decay of vortex downstream of submerged vane.", ISH Journal of Hydraulic Engineering, 12(2), 37-48.

56. Gupta, U.P., Sharma, N., and Ojha, C.S.P. (2007) "Performance evaluation of tapered vane.", Journal of Hydraulic Research, 45(4), 472-477.

57. Gupta, U.P., Sharma, N.,and Ojha, C.S.P. (2010) "Enhancing utility of submerged vanes with collar.", Journal of Hydraulic Engineering, 136(9), 651-655.

58. Han, S.S., Biron, P.M., and Ramamurthy, A.S. (2011) "Three dimensional modeling of flow in sharp bends with vanes.", Journal of Hydraulic Research, 49(1), 64-72.

59. Ho, J., Coonrod J., Gill, T., and Mefford, B. (2010) “Case study: Movable bed model scaling for bed load sediment exclusion at intake structure on Rio Grande.”, Journal of Hydraulic Engineering, 136(4), 247-250.

60. Holley, E.R. and Abraham, G. (1973 a) “Field tests on transverse mixing in rivers.”, Journal of Hydraulic Division, 99(HY12), 2313-2331.

61. Holley, E.R., and Abraham, G. (1973 b) “Laboratory studies on transverse mixing in rivers.”, Journal of Hydraulic Research, 11(3), 219–253.

62. Holley, E.R., Simons, J., and Abraham, G. (1972) “Some aspects of analyzing transverse diffusion in rivers.”, Journal of Hydraulic Research, 10(1), 27–57.

63. Holley, F.M., Jr., and Nerat, G. (1983) “Field calibration of stream tube dispersion model.”, Journal of Hydraulic Engineering, 109(11), 1455–1470.

64. Jobson, H.E. (1997) “Predicting travel time and dispersion in rivers and streams.”, Journal of Hydraulic Engineering, 123(11), 971-978.

65. Johnson, P.A., Hey, R.D., Tessier, M., and Rosgen, D.L. (2001) “Use of vanes for control of scour hole for vertical wall abutments.”, Journal of Hydraulic Engineering, 127(9), 772-778.

66. Kalinske, A.A., and Pien, C.L. (1944) “Eddy diffusion.”, Industrial Engineering Chemistry, 36, 220-223.

67. Kartha, S., and Srivastava, R. (2008 a) “Effect of immobile water content on contaminant transport in unsaturated zone.”, Journal of Hydro-environment Research, 1(3-4), 206-215.

68. Kartha, S., and Srivastava, R. (2008 b) “Effect of slow and fast moving liquid zones on solute transport in porous media.”, Transport in Porous Media, 75(2), 227-247.

69. Krishnappan, B.G., and Lau, Y.L. (1977) “Transverse mixing in meandering channels with varying bottom topography.”, Journal of Hydraulic Research, 15(4), 351–370.

70. Kumar, J., Jain, A., and Srivasatava, R. (2006) “Neural network based solutions for locating groundwater pollution sources.”, Hydrology Journal, 29(1/2), 55-66.

71. Lau, Y.L. (1981) *Dispersion coefficient for natural streams*. National Water Research Institute, Canada Centre for Inland Waters, October.

72. Lau, Y.L. (1985) “Mixing coefficients for ice covered and free surface flows.”, Canadian Journal of Civil Engineering, 12(3), 521–526.

73. Lau Y.L., and Krishnappan G. (1977) “Transverse dispersion in rectangular channels.”, Journal of Hydraulic Division, 103(HY10), 1173-1189.

74. Lau Y.L., and Krishnappan G. (1981) “Modelling transverse mixing in natural streams.”, Journal of Hydraulic Division, 107(HY2), 209-226.

75. Lee, M.E., and Seo, I.W. (2013) “Spatially variable dispersion coefficients in meandering channels.”, Journal of Hydraulic Engineering, 139(2), 141-153.

76. Lipsett, A.W., and Beltaos, S. (1978) *Tributary mixing characteristics using water quality parameters.* Open report 1978-7, Transportation and Surface Water Engineering Division, Research Council of Alberta, Alberta, Canada.

77. Luk, G.K.Y., Lau, Y.L., and Watt, W.E. (1990) “Two-dimensional mixing in rivers with unsteady pollutant source.”, Journal of Environmental Engineering Division, 116(2), 125-143.

78. Marelius, F., and Sinha, S.K. (1998) “Experimental analysis of flow past submerged vanes.”, Journal of Hydraulic Engineering, 124(5), 542-545.

79. Marion, A., and Zaramella, M. (2006) “Effect of velocity gradients and secondary flow on the dispersion of solute in meandering channel.”, Journal of Hydraulic Engineering, 132(12), 1295-1302.

80. Menter, F.R. (1992 a) “Performance of popular turbulence models for attached and separated adverse pressure gradient flow.”, AIAA Journal, 30, 2066-2072.

81. Menter, F.R. (1992 b) *Improved two-equation K-ω turbulence models for aerodynamic flow*. NASA Technical Memorandum (TM-103975), NASA, Ames, CA.

82. Menter, F.R. (1994) “Two-equation eddy viscosity turbulence model for engineering applications.”, AIAA Journal, 32, 1598-1605.

83. Menter, F.R. (1997) “Eddy viscosity transport equation and their relation to *k*-ε turbulence model.”, Journal of Fluids Engineering, 119, 876-884.

84. Menter, F.R., Kuntz, M., and Langtry, R. (2003) “Ten years industrial experience with the SST turbulence model.”, Proceedings of Fourth International Symposium on Turbulence, Heat and Mass Transfer, Begell house, Redding, CT.

85. Miller, A.C., and Richardson, E.V. (1974) “Diffusion and dispersion in open channel flow.”, Journal of Hydraulic Division, 100, 159-171.

86. Mingham, C.G., and Causon, D.M. (1998) “High resolution finite volume method for shallow water flows.”, Journal of Hydraulic Engineering, 124(6), 605-614.

87. Nakato, T., Kennedy, J.F., and Bauerly, D. (1990) “Pump-station intake-shoaling control by submerged vanes.”, Journal of Hydraulic Engineering, 116(1), 119-128.

88. Nezu, I., and Nakagawa, N. (1993) *Turbulence in open channel flows.* AA Balkema, Delft, Netherlands.

89. Nezu, I., and Rodi, W. (1986) “Open channel flow measurements with laser Doppler anemometer.”, Journal of Hydraulic Engineering, 112 (5), 335-355.

90. Nokes, R.I. (1986) *Problems in turbulent dispersion*. Ph.D. Thesis, University of Canterbury, Christchurch.

91. Odgaard, A.J., and Kennedy, J.F. (1983) “River bend bank protection by submerged vanes.”, Journal of Hydraulic Engineering, 109(8), 1161-1173.

92. Odgaard, A.J., and Mosconi, C.E. (1987) “Streambank protection by submerged vanes.”, Journal of Hydraulic Engineering, 113(4), 520-536.

93. Odgaard, A.J., and Spoljaric, A. (1986) “Sediment control by submerged vanes.”, Journal of Hydraulic Engineering, 112(12), 1164-1181.

94. Odgaard, A.J., and Wang, Y. (1991 a.) “Sediment management with submerged vanes. Theory: I.”, Journal of Hydraulic Engineering, 117(3), 267-283.

95. Odgaard, A.J., and Wang, Y. (1991 b) “Sediment management with submerged vanes. Applications: II.”, Journal of Hydraulic Engineering, 117(3), 284-302.

96. Okoye, J.K. (1970) *Characteristics of Transverse Mixing in Open Channel Flows.* Report no. KH-R-23, California Institute of Technology, Pasadena, CA.

97. Orlob, G.T. (1983) *Mathematical modelling of water quality: streams, lakes and reservoirs.* Chichester, Wiley.

98. Ouyang, H.T., Weber, L., and Odgaard, A.J. (2006) “Design optimization of two-dimensional hydrofoil by applying a genetic algorithm.”, Engineering Optimization, 38(5), 529-540.

99. Ouyang, H.T., Lai, J.S., Yu, H., and Lu, C.H. (2008) “Interaction between submerged vanes for sediment management.”, Journal of Hydraulic research, 46(5), 620-627.

100. Ouyang, H.T. (2009) “Investigation on the dimensions and shape of a submerged vane for sediment management in alluvial channels.”, Journal of Hydraulic Engineering, 135(3), 209-217.

101. Ouyang, H.T., and Lai, J.S. (2013) “Design optimization of a submerged vane with streamlined profile for sediment management in rivers.”, Journal of Marine Science and Technology, 21(3), 325-332.

102. Pilechi, A., Rennie C.D., Mohammadian, M., and Zhu, D.Z. (2015) “In situ spatially distributed field measurements of transverse dispersion of waste-water effluent in an extended natural meandering river.”, Journal of Hydraulic Research, 53(1), 20-35.

103. Pope, S.B. (2000) *Turbulent flows.* Cambridge University Press, Cambridge, UK.

104. Prych, E.A. (1970) *Effect of density difference on lateral mixing in open channel flows.* Report no. KH-R-21, California Institute of Technology, Pasadena, CA.

105. Rodi, W. (1980) *Turbulence models and their applications in hydraulics, a-state-of-the-art report.* AA Balkema, Delft, Netherlands.

106. Rutherford, J.C. (1994) *River mixing.* John Wiley and Sons, Chichester, UK.

107. Sanders, B. F., Green, C. L., Chu, A. K., and Grant, S. B. (2001) "Case study: Modeling tidal transport of urban runoff in channels using the finite volume method.", Journal of Hydraulic Engineering, 127 (10), 795-804.

108. Sayre, W.W. (1968) *Dispersion of mass in open channel flow.* Hydraulics Papers No. 3, Colorado State Univ. Fort Collins, Co.

109. Sayre, W.W. (1979) *Shore-attached thermal plumes in river*. In *Modeling in Rivers*. *Edited by* H.W. Shen. Wiley-Interscience, London. pp. 15.1–15.44.

110. Sayre, W.W., and Chamberlin, A.R. (1964) *Exploratory laboratory study of lateral turbulent diffusion at the surface of an alluvial channel.* US Geol. Surv. Circ. No. 484.

111. Sayre, W.W., and Chang, F.M. (1968) *A Laboratory Investigation of the Open Channel Dispersion Process of Dissolved, Suspended and Floating Dispersants.* US Geological Survey, Professional Paper 433-E.

112. Seo, I.W., Baek, K.O., and Jeon, T.M. (2006) "Analysis of transverse mixing in natural streams under slug tests.", Journal of Hydraulic Research, 44(3), 350-362.

113. Sharma, P.K., Sekhar, M., Srivastava, R., and Ojha, C.S.P. (2012) "Temporal moments of reactive transport through fractured impermeable/permeable formations.", Journal of Hydrologic Engineering, 17(12), 1302-1314.

114. Shen H.T. (1978) "Transient dispersion in river channels.", Journal of Environmental Engineering Division, 104(3), 445-459.

115. Singh, S. (2005) *Two dimensional mixing of pollutants in open channels*. PhD thesis, IIT Roorkee, Roorkeee, India.

116. Singh, S., Ahmad, Z., and Kothyari, U.C. (2009) "Two-dimensional mixing of pollutants with transverse line source.", Journal of Hydraulic Research, 47(1), 90-99.

117. Singh, S., Ahmad, Z., and Kothyari, U.C. (2010) "Mixing coefficients for longitudinal and vertical mixing in near field of a surface pollutant discharge.", Journal of Hydraulic Research, 48(1), 91-99.

118. Sinha, S.K., and Marelius, F. (2000) "Analysis of flow past submerged vanes.", Journal of Hydraulic Research, 38(1), 65-71.

119. Stone, H.L., and Brian, P.T. (1963) "Numerical solution of convective transport problems.", Journal of American Institute of Chemical Engineering, 9, 681–688.

120. Sullivan, P.J. (1968) *Dispersion in a Turbulent Shear Flow*. PhD thesis, University of Cambridge, Cambridge, England.

121. Tan, S.K., Guoliang, Y., Lim, S.Y., and Ong, M.C. (2005) "Flow structure and sediment motion around submerged vanes in open channel.", Journal of Waterway, Port, Coastal and Ocean Engineering, 131(3), 132-136.

122. Tennekes, H., and Lumley, J.L. (1972) *A first course in turbulence*. MIT Press, USA.

123. Versteeg H.K., and Malalasekera W. (1995) *An introduction to computational fluid dynamics: The finite volume method.* Longman.

124. Voisin, A., and Townsend, R.D. (2002) "Model testing of submerged vanes in strongly curved narrow channel bends.", Canadian Journal of Civil Engineering, 29, 37-49.

125. Wang, Y., and Odgaard, A.J. (1993) "Flow control with vorticity.", Journal of Hydraulic Research, 31(4), 549-562.

126. Ward, P.B.R. (1974) "Transverse dispersion in oscillatory channel flow.", Journal of Hydraulic Division, 106(HY6), 755–772.

127. Webel, G., and Schatzmann, M. (1984) "Transverse mixing in open channel flow.", Journal of Hydraulic Engineering, 110(4), 423–435.

128. Wilcox, D.C. (1988) "Reassessment of scale determining equation for turbulence models.", AIAA Journal, 26(11), 1299-1310.

129. Wilcox, D.C. (1993 a) "Comparison of two-equation turbulence models for boundary layers with pressure gradients.", AIAA Journal, 31(8), 1414-1421.

130. Wilcox, D.C. (1993 b) *Turbulence modelling for CFD*. DCW Industries Inc., La Canada, CA.

131. Wilcox, D.C. (1994) "Simulating transition with a two-equation turbulence model.", AIAA Journal, 32, 247-255.

132. Yotsokoura, N., Fischer, H.B., and Sayre, W.W. (1970) *Measurement of mixing characteristics of Missouri river between Sioux City, Iowa and Plattsmouth, Nebraska*. US Geological Survey, Water Supply paper No. 1899-G.

133. Yotsoukura, N., and Cobb, E.D. (1972) *Transverse diffusion of solutes in natural streams.* United States Geological Society Professional Paper 582-C.

134. Yotsoukura, N., and Sayre, W.W. (1976) "Transverse mixing in natural streams.", Water Resources Research, 12(4), 695–704.

135. Young, D.L., Her, B.C., and Eldho, T.I. (2000 a) "Boundary integral modeling of three dimensional pollutant-transport in stratified estuaries.", Journal of Engineering Mechanics, 126(10), 1083-1092.

136. Young, D.L., Her, B.C., and Eldho, T.I. (2000 b) "Solution of advection-diffusion equation using Eulerian-Langragian boundary element method.", International Journal of Engineering Analysis with Boundary Elements, 24(6), 449-457.

137. Zhang, W., and Zhu, D.Z. (2011 a) "Near-field mixing downstream of a multiport diffuser in shallow river.", Journal of Hydraulic Engineering, 137(4), 230–240.

138. Zhang, W., and Zhu, D.Z. (2011 b) "Transverse Mixing in an Unregulated Northern River.", Journal of Hydraulic Engineering, 137(11), 1426–1440.

139. Zhao, D. H., Shen, H. W., Tabios III, G. Q., Lai, J. S., and Tan, W. Y. (1994) “Finite volume two dimensional unsteady model for river basins.”, Journal of Hydraulic Engineering, 120 (7), 863-883.

140. Zheng, Y., Huai, W., and Guymer, I. (2008) “Transverse mixing in trapezoidal compound open channel.”, Journal of Hydrodynamics, 20(5), 645-649.

APPENDIX-I

In the colum having title as “Run no.” h represents the depth of flow and R represents the number of rows. Therefore, h1 = 0.1241m, h2 = 0.1025 m and h3 = 0.09 m while R1 = 4, R2 = 3, R3 = 2 and R4 = 1.

S. No.	Run No.	Transverse Distance (m)	Concentration Profile (ppb)								
			Vane Size = 0.06 m			Vane Size = 0.04 m			Vane Size = 0.02 m		
			Initial Concentration	Concentration at distance x = 5 m	Concentration at distance x = 15 m	Initial Concentration	Concentration at distance x = 5 m	Concentration at distance x = 15 m	Initial Concentration	Concentration at distance x = 5 m	Concentration at distance x = 15 m
1	h1R1	0.0	100	9.42	9.17	100	14.61	14.43	100	74.59	27.20
2		0.1	100	9.14	8.86	100	14.61	13.90	100	31.26	19.24
3		0.10001	0	9.14	8.86	0	14.61	13.90	0	31.26	19.24
4		0.2	0	8.31	8.25	0	13.72	13.57	0	7.10	13.91
5		0.3	0	6.65	7.64	0	13.65	12.91	0	4.62	7.10

6		0.4	0	5.54	7.03	0	12.07	12.58	0	3.91	5.33
7		0.5	0	4.71	6.42	0	11.05	10.92	0	2.84	2.96
8		0.6	0	3.88	5.50	0	8.26	10.59	0	1.78	2.66
9		0.7	0	3.60	4.89	0	6.67	9.27	0	1.07	2.66
10		0.8	0	3.05	3.97	0	6.41	9.27	0	0.71	2.66
11		0.9	0	1.66	3.36	0	6.35	7.15	0	0.71	2.37
12		0.95	0	1.38	3.06	0	3.18	6.29	0	0.71	2.07
13	h1R2	0.0	100	10.86	10.24	100	26.74	18.42	100	78.91	29.24
14		0.1	100	10.57	9.63	100	19.50	18.42	100	17.90	25.44
15		0.10001	0	10.57	9.63	0	19.50	18.42	0	17.90	25.44
16		0.2	0	9.69	9.03	0	16.72	16.80	0	6.24	16.71
17		0.3	0	7.63	7.83	0	16.16	15.17	0	5.83	6.83

18		0.4	0	5.28	6.62	0	12.82	13.00	0	5.41	5.32
19		0.5	0	4.70	5.42	0	11.70	11.65	0	4.99	4.18
20		0.6	0	3.82	4.52	0	6.69	8.13	0	2.50	3.80
21		0.7	0	3.52	4.21	0	5.57	7.04	0	1.66	3.80
22		0.8	0	3.23	2.71	0	4.46	3.79	0	1.66	3.80
23		0.9	0	1.76	2.41	0	2.79	2.37	0	1.66	3.04
24		0.95	0	1.47	2.11	0	1.67	2.37	0	1.66	2.66
25	h1R3	0.0	100	14.71	13.40	100	33.03	23.56	100	82.24	34.21
26		0.1	100	11.95	12.34	100	22.60	22.11	100	33.47	26.55
27		0.10001	0	11.95	12.34	0	22.60	22.11	0	33.47	26.55
28		0.2	0	10.42	11.64	0	19.29	19.69	0	7.65	17.51
29		0.3	0	7.97	10.23	0	13.13	15.82	0	6.06	8.48

30		0.4	0	4.60	7.76	0	10.41	12.19	0	3.83	3.56
31		0.5	0	3.68	6.35	0	6.97	9.63	0	2.23	2.19
32		0.6	0	2.15	4.58	0	5.07	6.39	0	0.96	1.37
33		0.7	0	1.84	2.82	0	2.94	4.84	0	0.96	1.09
34		0.8	0	1.23	1.76	0	1.75	3.10	0	0.96	1.09
35		0.9	0	0.61	1.41	0	0.09	2.03	0	0.96	1.09
36		0.95	0	0.61	1.41	0	0.00	1.69	0	0.96	1.09
37	h1R4	0.0	100	18.06	17.07	100	46.80	33.69	100	87.93	45.58
38		0.1	100	15.05	15.56	100	29.75	28.24	100	38.79	25.11
39		0.10001	0	15.05	15.56	0	29.75	28.24	0	38.79	25.11
40		0.2	0	12.04	13.66	0	16.72	22.98	0	10.02	14.65
41		0.3	0	7.69	11.00	0	11.51	15.52	0	3.56	7.06

42		0.4	0	4.68	7.59	0	8.43	9.46	0	1.94	2.88
43		0.5	0	3.01	6.07	0	5.83	6.20	0	1.29	2.09
44		0.6	0	1.67	3.04	0	2.98	3.22	0	0.97	1.31
45		0.7	0	1.00	1.52	0	2.27	1.40	0	0.97	1.05
46		0.8	0	0.33	0.38	0	2.04	0.61	0	0.97	1.05
47		0.9	0	0.00	0.00	0	1.80	0.19	0	0.97	1.05
48		0.95	0	0.00	0.00	0	1.80	0.00	0	0.97	1.05
49	h2R1	0.0	100	10.65	9.36	100	11.13	9.65	100	32.31	19.48
50		0.1	100	10.40	9.17	100	9.91	8.63	100	9.69	15.58
51		0.10001	0	10.40	9.17	0	9.91	8.63	0	9.69	15.58
52		0.2	0	9.19	8.20	0	8.99	8.26	0	5.65	9.21
53		0.3	0	7.50	7.00	0	6.98	6.98	0	4.85	4.96

54		0.4	0	6.05	6.03	0	5.51	5.69	0	2.83	3.54
55		0.5	0	4.11	5.07	0	3.85	4.59	0	2.02	2.48
56		0.6	0	2.66	3.86	0	2.75	3.85	0	0.81	1.06
57		0.7	0	1.94	2.41	0	2.20	3.30	0	0.40	1.06
58		0.8	0	1.69	1.93	0	2.02	2.20	0	0.40	0.71
59		0.9	0	0.73	0.97	0	1.10	1.65	0	0.40	0.35
60		0.95	0	0.73	0.97	0	1.10	1.65	0	0.40	0.35
61	h2R2	0.0	100	13.43	12.36	100	14.65	13.28	100	36.62	21.72
62		0.1	100	12.97	11.90	100	14.09	12.70	100	18.31	16.52
63		0.10001	0	12.97	11.90	0	14.09	12.70	0	18.31	16.52
64		0.2	0	9.79	10.03	0	12.58	10.55	0	3.95	9.12
65		0.3	0	6.60	7.70	0	6.57	9.18	0	2.51	4.78

66		0.4	0	4.78	5.37	0	3.38	5.08	0	2.15	3.48
67		0.5	0	2.73	4.20	0	2.07	3.71	0	1.08	2.61
68		0.6	0	1.59	2.80	0	1.13	1.76	0	0.36	1.74
69		0.7	0	1.37	1.17	0	0.56	0.98	0	0.36	1.74
70		0.8	0	1.14	0.93	0	0.38	0.78	0	0.36	1.30
71		0.9	0	1.14	0.70	0	0.19	0.39	0	0.36	0.87
72		0.95	0	1.14	0.70	0	0.19	0.39	0	0.36	0.87
73	h2R3	0.0	100	15.98	14.61	100	16.26	15.08	100	38.20	22.36
74		0.1	100	15.34	13.66	100	15.03	14.58	100	16.55	16.15
75		0.10001	0	15.34	13.66	0	15.03	14.58	0	16.55	16.15
76		0.2	0	14.06	12.07	0	14.29	12.61	0	4.14	9.63
77		0.3	0	11.51	9.85	0	10.84	10.63	0	2.87	4.35

78		0.4	0	8.63	8.58	0	7.39	8.40	0	1.59	2.48
79		0.5	0	5.43	6.67	0	5.17	5.93	0	0.96	1.24
80		0.6	0	2.88	4.13	0	2.96	4.70	0	0.96	0.93
81		0.7	0	2.24	3.49	0	2.71	2.72	0	0.64	0.93
82		0.8	0	1.60	2.22	0	2.22	1.98	0	0.64	0.62
83		0.9	0	0.96	1.59	0	1.48	1.24	0	0.64	0.62
84		0.95	0	0.96	1.59	0	1.48	1.24	0	0.64	0.62
85	h2R4	0.0	100	16.83	15.50	100	19.97	17.27	100	39.71	26.65
86		0.1	100	13.09	10.35	100	17.06	15.88	100	18.28	17.57
87		0.10001	0	13.09	10.35	0	17.06	15.88	0	18.28	17.57
88		0.2	0	11.05	8.91	0	11.44	12.11	0	3.71	9.37
89		0.3	0	7.27	7.46	0	5.24	6.75	0	1.43	4.69

90		0.4	0	4.94	5.46	0	2.52	4.17	0	0.86	1.76
91		0.5	0	3.20	3.74	0	0.97	1.99	0	0.29	1.17
92		0.6	0	1.75	2.87	0	0.39	0.79	0	0.29	0.59
93		0.7	0	0.87	1.72	0	0.39	0.40	0	0.29	0.59
94		0.8	0	0.58	1.15	0	0.39	0.20	0	0.29	0.59
95		0.9	0	0.29	0.86	0	0.39	0.20	0	0.29	0.59
96		0.95	0	0.29	0.86	0	0.39	0.20	0	0.29	0.59
97	h3R1	0.0	100	15.08	11.55	100	12.19	11.58	100	31.71	18.67
98		0.1	100	13.31	10.39	100	11.03	11.19	100	6.50	15.04
99		0.10001	0	13.31	10.39	0	11.03	11.19	0	6.50	15.04
100		0.2	0	11.24	8.95	0	9.10	10.28	0	5.28	9.96
101		0.3	0	7.39	7.79	0	6.00	9.10	0	3.46	6.10

102		0.4	0	5.03	5.48	0	3.87	7.18	0	2.64	4.47
103		0.5	0	3.25	3.75	0	1.74	5.03	0	0.81	2.64
104		0.6	0	1.77	2.89	0	0.97	3.59	0	0.41	1.83
105		0.7	0	0.89	1.73	0	0.77	1.92	0	0.41	1.22
106		0.8	0	0.59	1.15	0	0.58	1.20	0	0.41	1.02
107		0.9	0	0.30	0.87	0	0.39	0.72	0	0.41	0.81
108		0.95	0	0.30	0.87	0	0.39	0.72	0	0.41	0.81
109	h3R2	0.0	100	15.86	11.90	100	13.45	12.92	100	32.80	20.08
110		0.1	100	14.58	10.68	100	12.35	12.64	100	7.41	18.31
111		0.10001	0	14.58	10.68	0	12.35	12.64	0	7.41	18.31
112		0.2	0	12.02	8.74	0	11.25	11.17	0	5.29	13.24
113		0.3	0	7.67	7.53	0	7.56	8.85	0	4.06	7.28

114		0.4	0	4.60	5.34	0	2.58	6.53	0	2.12	5.08
115		0.5	0	2.81	3.64	0	1.84	4.42	0	1.06	3.31
116		0.6	0	1.53	2.19	0	1.11	2.32	0	0.35	1.99
117		0.7	0	1.02	1.21	0	0.55	1.47	0	0.35	1.54
118		0.8	0	0.77	0.73	0	0.37	0.84	0	0.35	1.32
119		0.9	0	0.26	0.49	0	0.37	0.63	0	0.35	1.10
120		0.95	0	0.26	0.49	0	0.37	0.63	0	0.35	1.10
121	h3R3	0.0	100	17.77	14.55	100	14.78	14.57	100	38.69	21.46
122		0.1	100	16.25	13.23	100	14.39	13.29	100	13.08	19.76
1231		0.10001	0	16.25	13.23	0	14.39	13.29	0	13.08	19.76
124		0.2	0	11.93	10.85	0	13.01	11.79	0	5.31	12.75
125		0.3	0	6.09	7.67	0	7.29	9.43	0	3.41	6.59

126		0.4	0	3.05	4.76	0	2.56	5.79	0	1.52	3.61
127		0.5	0	1.52	3.17	0	1.18	3.00	0	0.57	2.34
128		0.6	0	0.76	2.38	0	0.79	2.14	0	0.19	0.84
129		0.7	0	0.51	1.32	0	0.59	0.64	0	0.19	0.42
130		0.8	0	0.51	0.79	0	0.39	0.21	0	0.19	0.42
131		0.9	0	0.51	0.79	0	0.39	0.21	0	0.19	0.42
132		0.95	0	0.51	0.79	0	0.39	0.21	0	0.19	0.42
133	h3R4	0.0	100	21.22	16.16	100	24.21	18.32	100	43.53	27.04
134		0.1	100	19.25	14.90	100	15.89	15.80	100	15.13	23.68
135		0.10001	0	19.25	14.90	0	15.89	15.80	0	15.13	23.68
136		0.2	0	12.09	11.36	0	9.98	12.36	0	3.50	12.37
137		0.3	0	4.94	7.07	0	4.89	8.24	0	2.03	5.45

138		0.4	0	1.48	4.80	0	2.04	4.35	0	0.92	2.72
139		0.5	0	0.99	2.78	0	0.81	3.21	0	0.18	1.26
140		0.6	0	0.74	1.26	0	0.41	1.60	0	0.00	0.42
141		0.7	0	0.74	0.51	0	0.41	0.92	0	0.00	0.21
142		0.8	0	0.74	0.51	0	0.41	0.46	0	0.00	0.00
143		0.9	0	0.74	0.51	0	0.41	0.46	0	0.00	0.00
144		0.95	0	0.74	0.51	0	0.41	0.46	0	0.00	0.00

APPENDIX-II

In the present appendix data of discharge and velocity is given as follows:

S. No.	Depth of flow (m)	Discharge (m^3/s)	Transverse distance from left wall (m)	Velocity (m/s)
1	0.1241	0.056	0.00	0.000
2	0.1241	0.056	0.02	0.442
3	0.1241	0.056	0.10	0.442
4	0.1241	0.056	0.20	0.442
5	0.1241	0.056	0.30	0.459
6	0.1241	0.056	0.40	0.451
7	0.1241	0.056	0.50	0.459

8	0.1241	0.056	0.60	0.467
9	0.1241	0.056	0.70	0.459
10	0.1241	0.056	0.80	0.442
11	0.1241	0.056	0.90	0.434
12	0.1241	0.056	0.95	0.434
13	0.1025	0.040	0.00	0.000
14	0.1025	0.040	0.02	0.368
15	0.1025	0.040	0.10	0.368
16	0.1025	0.040	0.20	0.378
17	0.1025	0.040	0.30	0.388
18	0.1025	0.040	0.40	0.397
19	0.1025	0.040	0.50	0.425

20	0.1025	0.040	0.60	0.416
21	0.1025	0.040	0.70	0.397
22	0.1025	0.040	0.80	0.378
23	0.1025	0.040	0.90	0.368
24	0.1025	0.040	0.95	0.368
25	0.09	0.024	0.00	0.000
26	0.09	0.024	0.02	0.274
27	0.09	0.024	0.10	0.274
28	0.09	0.024	0.20	0.288
29	0.09	0.024	0.30	0.324
30	0.09	0.024	0.40	0.347
31	0.09	0.024	0.50	0.358

32	0.09	0.024	0.60	0.347
33	0.09	0.024	0.70	0.324
34	0.09	0.024	0.80	0.300
35	0.09	0.024	0.90	0.260
36	0.09	0.024	0.95	0.260